A Glance into the Future of Particle Physics with Effective Field Theories

Dissertation

zur Erlangung des akademischen Grades

doctor rerum naturalium

(Dr. rer. nat.)

im Fach Physik

Spezialisierung: Theoretische-Physik

eingereicht an der

Mathematisch-Naturwissenschaftlichen Fakultät der Humboldt-Universität zu Berlin

von

Herrn **Alejo Nahuel Rossia**

Präsidentin der Humboldt-Universität zu Berlin

Prof. Dr.-Ing. Dr. Sabine Kunst

Dekan der Mathematisch-Naturwissenschaftlichen Fakultät

Prof. Dr. Elmar Kulke

Gutacther/innen:

1. Prof. Dr. Agostino Patella
2. Prof. Dr. Christophe Grojean
3. Prof. Dr. Eleni Vryonidou

Tag der mündlichen Prüfung: 08.09.2021

This page is intentionally left blank.

To my grandfather Cachi, in memoriam.
To my grandmother Chiculi.
To my parents Mario and Susana.

A la memoria de mi abuelo Cachi.
A mi abuela Chiculi.
A mis padres Susana y Mario.

This page is intentionally left blank.

Acknowledgements

I am deeply grateful to my supervisor, Prof. Dr. Christophe Grojean, for his guidance and support throughout these years. This space is not enough to list all that I have learned from him, but I wish to highlight his relentless push towards a deeper understanding and his perseverance in not losing perspective. I also thank his commitment and ability to gather physicists from different backgrounds in a freedom-imbued environment where no knowledge frontier is safe from scrutiny. And above all, I will always be grateful for having trusted me with this position. A career opportunity like this is an enormous privilege that I could never take for granted.

Research, though sometimes lonely, reaches its peak in the interaction among different people. That is why I thank all my collaborators over these years, either in projects that were included here or not. They are Fady Bishara, Quentin Bonnefoy, Leandro Da Rold, Stefania De Curtis, Luigi Delle Rose, Di Liu, Luca Di Luzio, Philipp Englert, Emanuele Gendy, Christophe Grojean, Yann Gouttenaire, Camila Machado, Oleksii Matsedonskyi, Marc Montull, Giuliano Panico, Ayan Paul, and Thibaud Vantalon.

Writing a thorough list of all the people I have interacted meaningfully with over this time period is a task bound to fail. I would surely forget someone who deserves to be mentioned. Hence, I thank all the DESY staff, secretaries, PhD students, postdoctoral fellows and senior scientists. Among them, I highlight my office mates and fellow PhD students in Prof. Grojean's group, who had to bear me during the longest periods without much choice: Ibrahim Akal, Philipp Englert, Aleix Gimenez, Emanuele Gendy, Riccardo Nagar, Marc Riembau, Jasper Roosmale Nepveu, and Thibaud Vantalon. In addition, I am extremely grateful to Philipp Englert for helping me to translate to German the summary of this thesis.

The knowledge I acquired during my Bachelor and Master was essential not only to begin this PhD but also to finish it. Then, I am grateful to all my professors at Instituto Balseiro and Universidad Nacional de Río Cuarto. I must single out my Master's thesis advisor, Dr. Leandro Da Rold, especially for his guidance and support while I was searching and applying for a PhD position. I will never forget the moment when he asked me "Did you send an email to Christophe Grojean?". Without that question, this thesis would not have happened.

My time in Bariloche gave me not only a lot of knowledge, but also a group of very valuable friends. Having kept in touch with them, even if just via Internet, has been extremely helpful during these years and, particularly, since the COVID-19 pandemic struck. Hence, I am grateful to Alan Arsen, Federico Lamagna, Francisco Riberi, Franco Piñán, Iván Fernández Aguirre, Jeffrey Paredes, Livio Leiva, Martín Marchioni, Mauricio Toribio, Mauro Forlino, and Yasuo Oda.

Finally, and not less any important, I am grateful to my parents and grandparents, for their support and encouragement over all these years.

Finalmente, y no por ello menos importante, sino más bien el agradecimiento más especial. Muchas gracias a mis padres y abuelos por todo el apoyo y ánimo, por haber soportado mis quejas cada semana, por todos los consejos, por darme tranquilidad cuando la necesité y por haberme brindado todo.

This page is intentionally left blank.

Declaration of Independent work

I declare that I have completed the thesis independently using only the aids and tools specified. I have not applied for a doctor's degree in the doctoral subject elsewhere and do not hold a corresponding doctor's degree. I have taken due note of the Faculty of Mathematics and Natural Sciences PhD Regulations, published in the Official Gazette of Humboldt-Universität zu Berlin no. 42/2018 on 11/07/2018.

Hamburg, 05.07.2021 Alejo Nahuel Rossia

This page is intentionally left blank.

Zusamenfassung

Die am LHC gewonnen experimentellen Ergebnisse stimmen überwiegend mit den Vorhersagen des Standardmodells der Teilchenphysik (SM) überein. Dennoch bleibt die Notwendigkeit von Physik jenseits des Standardmodells (BSM) bestehen. Es ist allerdings kein klarer Weg zu einem Nachfolger des Standardmodells bekannt. Daher muss das Werkzeug bereitet werden, das nötig ist, um die Grenzen der Physik gründlich zu erkunden. In dieser Arbeit wird eines der zentralsten theoretischen Werkzeuge studiert, das für diese Untersuchung benutzt werden kann, die Effektiven Feldtheorien (EFTs). Es wird gezeigt, wie sie zu benutzen sind, einige ihrer formalen Aspekte werden studiert und die Konstruktion eines verbesserten Frameworks wird untersucht.

In dieser Arbeit wird die Standard Model Effective Field Theory (SMEFT) verwendet, um das Entdeckungspotential eines zukünftigen experimentellen Werkzeugs, des Hadronenbeschleunigers FCC-hh, zu beurteilen. Hierfür wird der Vh Produktionsprozess mit $V = W, Z$ untersucht. Es werden die Kanäle, in denen das Higgs Boson zu einem Photon-Paar und die Eichbosonen leptonisch zerfallen, betrachtet. Diese werden nur durch die hohen Energien, die vom FCC-hh erreicht werden, zugänglich. Die Sensitivität dieser Kanäle für BSM-Effekte wird durch die Messung von doppelt differenziellen Wirkungsquerschnitten möglich. Es werden projizierte Schranken auf SMEFT Wilson-Koeffizienten (WCs) der Massendimension 6 berechnet und diese werden mit Projektionen für andere zukünftige Beschleuniger und andere Prozesse am FCC-hh verglichen. Die Ergebnisse werden auch im Kontext der Triple Gauge Couplings und einfacher UV-Modelle interpretiert.

Die Abwesenheit von Eich-Anomalien ist nötig, um die Konsistenz einer Quantenfeldtheorie zu bewahren. Wenn Parameter, wie z.B. die WCs einer EFT, für bestimmte Werte Eich-Anomalien generieren würden, würden für sie theoretische Einschränkungen gelten. Es wird gezeigt, dass die SMEFT bis zur Massendimension 6 für beliebige Werte seiner WCs frei von Eich-Anomalien ist, die durch Dreiecks-Diagramme produziert werden. Überprüft wird dies durch die innovative Nutzung bosnischer EFT-Techniken.

Die bosonischen EFT-Techniken werden auch benutzt, um die Beziehung zwischen gemischten globalen Eich-Anomalien und Axion-Kopplungen zu Vektorbosonen in Axion-EFTs zu analysieren. Es stellt sich heraus, dass diese in keiner Beziehung zueinander stehen, wenn schwere chirale Fermionen ausintegriert werden. Dieser Fakt verknüpft Axion-EFTs mit chiralen Erweiterungen des Standardmodells. Für nichtabelsche Eichbosonen werden IR-Summenregeln gefunden, deren Verletzung die Anwesenheit chiraler Felder im UV-Bereich anzeigen. Es wird eine minimale phänomenologisch relevante Erweiterung des Standardmodells mit einem Axion und einem chiralen schweren Fermion als Beispiel präsentiert und seine hauptsächlichen Einschränkungen bewertet.

Letztlich wird gezeigt, wie das Zurückgreifen auf alte Formalismen zu neuen Einsichten führen kann. Der Formalismus der masselosen Helizitäts-Spinoren und masselosen Streuamplituden wird eingeführt und es wird gezeigt, wie er die Berechnung der Amplituden des Vh-Produktionsprozesses erleichtert. Dann wird die Erweiterung jenes Formalismus auf den massiven Fall präsentiert und diskutiert, inwiefern es eine Alternative zu EFTs als Parametrisierung von BSM-Effekten darstellt. Die VVh- und $VVhh$-Amplituden werden studiert, deren Hoch-Energie-Grenzwert einschließlich verschiedener BSM-Beiträge berechnet wird.

This page is intentionally left blank.

Summary

The experimental results obtained at the LHC mostly agree with the predictions made by the Standard Model of particle physics (SM). However, the need for Beyond the Standard Model (BSM) physics remains solid. But there is no clear path towards a successor for the SM. Hence, we must prepare the tools needed to explore the frontiers of physics thoroughly. In this work, we study one of the main theoretical tools that can be used for such an exploration, Effective Field Theories (EFTs). We show how to use them, study some of their formal aspects and explore the construction of an improved framework.

We use the Standard Model Effective Field Theory (SMEFT) to assess the discovery potential of a future experimental tool, the hadron collider FCC-hh. We study the Vh production process, with $V = W, Z$. We consider the channels where the Higgs boson decays to a photon pair and the gauge bosons decay leptonically, which will become available only at the high energies achieved by FCC-hh. The sensitivity of these channels to BSM effects is improved via the measurement of doubly-differential cross-sections. We obtain projected bounds on SMEFT dimension-6 Wilson Coefficients (WCs) and compare them with projections for other future colliders and other processes at FCC-hh. We also interpret our results in terms of anomalous Triple Gauge Couplings and simple UV models.

The absence of gauge anomalies is required to preserve the consistency of a Quantum Field Theory. If parameters, such as the WCs in an EFT, generated gauge anomalies for certain values, they would be affected by theoretical constraints. We prove that SMEFT at dimension 6 is free from gauge anomalies coming from triangle diagrams for any value of its WCs. We checked this via the innovative use of bosonic EFT techniques.

The bosonic EFT techniques are also used to analyse the relationship in axion EFTs between mixed global-gauge anomalies and axion couplings to vector bosons. They turn out to be unrelated when heavy chiral fermions are integrated out. This fact links axion EFTs to chiral extensions of the SM. For non-abelian gauge bosons, we find IR sum rules whose violation indicate the presence of chiral fields in the UV. We show a minimal phenomenologically relevant extension of the SM with an axion and chiral heavy fermions as an example and evaluate its main constraints.

Finally, we explore how revisiting old formalisms can lead to new insights. We introduce the massless helicity spinor and massless scattering amplitudes formalisms and show how they facilitate the computation of the Vh production process helicity amplitudes. Then, we present the extension of that formalism to the massive case and discuss how it constitutes an alternative to EFTs as a parametrisation of BSM effects. We study the VVh and $VVhh$ amplitudes, of which we compute the high-energy limit including different BSM contributions.

This page is intentionally left blank.

List of Publications

[1] F. Bishara, P. Englert, C. Grojean, M. Montull, G. Panico, and A. N. Rossia, *A New Precision Process at FCC-hh: the diphoton leptonic Wh channel*, *JHEP* **07** (2020) 075, [arXiv:2004.06122].

[2] F. Bishara, S. De Curtis, L. Delle Rose, P. Englert, C. Grojean, M. Montull, G. Panico, and A. N. Rossia, *Precision from the diphoton Zh channel at FCC-hh*, *JHEP* **04** (2021) 154, [arXiv:2011.13941].

[3] Q. Bonnefoy, L. Di Luzio, C. Grojean, A. Paul, and A. N. Rossia, *The Anomalous Case of Axion EFTs and Massive Chiral Gauge Fields*, arXiv:2011.10025. Accepted for publication in JHEP.

[4] Q. Bonnefoy, L. Di Luzio, C. Grojean, A. Paul, and A. N. Rossia, *Comments on gauge anomalies at dimension-six in the Standard Model Effective Field Theory*, *JHEP* **05** (2021) 153, [arXiv:2012.07740].

Chapter 3 contains all the results published in [1] and [2] plus some non-published results. Chapter 4 is based mostly on [4] and partially on [3]. The results published in [3] are contained in Chapter 5. Chapter 6 is based on computations made for [1] and [2], and unpublished results obtained in collaboration with Philipp Englert, Emanuele Gendy, and Prof. Dr. Christophe Grojean.

This page is intentionally left blank.

Contents

This page is intentionally left blank.

List of Figures

This page is intentionally left blank.

Chapter 1

Introduction

> *“It is wrong to think that the task of physics is to find out how nature is. Physics concerns what we can say about nature.”*
>
> — Niels Bohr, as quoted by A. Peteresen in “The Philosophy of Niels Bohr”, Bulletin of the Atomic Scientists, Vol. 19, No. 7 (Sept. 1963).

Science might be rightly considered as the most ambitious, comprehensive, satisfactory and useful endeavour ever undertaken by humankind. The deep understanding of how nature works is stimulating and rewarding in the broadest sense, and sets our species apart from any other on Earth. The fact that science has been developed systematically at large scale over only the last few hundred years magnifies even more its achievements. The big and abrupt change in human life over the last 200 years, unrivalled by any other period in human history, cannot be understood without science and its applications through technology. In fact, those years saw the birth of most sciences in their current form and more technological developments than what a person can count, leading to a very different relationship with nature. Our minds are now able to comprehend, scrutinize and marvel with the truths of nature at extents that were unimaginable before the Enlightenment. However, there are still several unexplained mysteries and large portions of the Universe remain unexplored. How this could affect our understanding of nature and reshape our lives is beyond imagination. Hence, the need of a continuous effort to pursue the gain of knowledge about our Universe is clearly established.

Among all the branches of science, physics has always enjoyed a unique position. As the science that tries to understand the fundamental laws that govern the Universe at all scales, physics covers the widest scope of knowledge. This has opened uncountable opportunities to influence other sciences and different aspects of our lives since the early days of modern physics with Galileo Galilei. Thus, the interest in researching fundamental physics is two-fold. On one hand, its reward in terms of understanding nature and the Universe at the deepest and most general level. On the other hand, its potential influence on many other areas, which is impossible to predict and often goes beyond the mere application of the fundamental laws of nature.

The development of physics between the beginning of the 19th and late 20th century altered our picture of the Universe more deeply than anything else. In just over 150 years, physics went from Newtonian mechanics and rudiments of optics, electromagnetism and thermodynamics, to a complex and wonderful amalgam of several branches that cover almost all scales. Even more, they are intertwined in such a way that one can transition smoothly from one to the other. This picture of physics is rather accurate and clear when one thinks in terms of length, from Quantum Field Theory at the smallest distances to General Relativity on the other extreme.

In this thesis, we will focus on the bottom of this ladder, i.e. on Quantum Field Theories that attempt to describe the smallest and most elementary components of nature and their interactions. Our interest in this area is not justified so much by its essentialness and possible influence in all the other physical branches, but because it is one where many fundamental mysteries still remain, where the questions are not how but what.

The remaining shortcomings can not be accurately identified without first acknowledging the achievements of the currently valid theory. The best model of fundamental particles and interactions to date is the Standard Model (SM) [1–5]. Contrary to what its name might suggest, the SM is not short of theoretical wonders. Some of its most remarkable features are the unification of electro-weak forces, the pleasant symmetry in its fermionic particle content and the prediction of the Higgs boson, a particle that is the only of its kind and controls the masses of all the others and give a peculiar structure to the vacuum through the Electroweak Symmetry Breaking (EWSB) mechanism [6–11]. Moreover, the SM is theoretically consistent up to infinitely high energies [4].

A marvellous physical model is nevertheless just peripheral if it does not describe nature. On that front, the success of the SM has little comparison in the history of physics. All of its particle content has been observed and their properties are mostly measured. A plethora of experiments across different energy scales, either Earth-based or cosmological, have rendered results that confirm the predictions of the SM with astonishing precision. Not in vain, some people consider it the most precise description of nature ever made by humankind [12].

The SM and its accomplishments are old news by now. Its theoretical foundations were fully laid almost 50 years ago. The last piece of the puzzle, the Higgs boson, was discovered 9 years ago. Thus, our model of fundamental particles and interactions has remained largely unaltered over the last half century. This contrasts starkly with the period of relentless revolutions that preceded it. Nevertheless, as new measurements at colliders agree with the SM prediction, our certainty about the need for a more fundamental theory remains intact thanks to the robustness of other (mostly cosmological) observations. Evidence of this need has been piling up over the last 20 years [12].

From an experimental point of view, the measurement of neutrino oscillations[1], the existence of Dark Matter (DM), the high asymmetry between matter and anti-matter, the accelerated expansion of the Universe that signals the existence of Dark Energy (DE), and the homogeneity and isotropy of the Universe are phenomena that can not be explained with the SM [12, 13]. Additionally, several small deviations from the SM predictions have a appeared at different experiments but none of them is statistically significant enough to claim that the SM is not a valid description of that process (see e.g Ref. [14–18]).

Despite its minimalism, the SM leaves several questions unanswered that strengthen the case against its candidacy for the ultimate model of nature [19–21]. Some of them are: what is the cause of EWSB? Why does the Higgs field has such an specific vacuum expectation value (VEV)? Is the Higgs an elementary particle? What stabilizes the SM vacuum? Why do the strong interactions respect the CP symmetry? Why are there only 3 families of fermions? What explains the mass hierarchy of quarks and leptons? And finally, the elephant in the room, how can we reconcile the SM with gravity? It becomes clear that we are not allowed to rest on the laurel wreaths of the SM.

The current situation of fundamental theoretical physics can then be summarised as follows: we have a very successful model and however we need Beyond the Standard Model (BSM) physics in order to account for unexplained phenomena and answer fundamental questions. At the same time, all the experimental results that justify the search of BSM physics are vague enough to

[1]They can not be explained with the SM considering only operators of dimension up to 4. The addition of higher-dimensional operators to the SM allows to describe these oscillations.

not indicate clearly any path forward, while the theoretical possibilities to build new models are very broad. Although the present seems clear, the future is highly intriguing and exciting. It is as we were standing at the peak of a mountain, barely above a shroud of dense clouds, without knowing certainly towards where we should go.

The particle physics community is then faced with the difficult conundrum of what to do next. On one hand, we should make sure to extract every piece of information out of the available results, which comprises several specific tasks. First, building new BSM models with novel signatures or new analysis techniques is a clear way to extract more from the same data by looking at it with a different lens. Second, a clear and solid understanding of the whole set of available results and their correlations in a more model independent language has the potential to provide insights on the most promising paths to explore in the future. Third, and not less important, we must review critically the formalism we have used so far and look for new tools and paradigms that can help us to understand better what we know and how we can increase our knowledge [22, 23].

On the other hand, we should guarantee the exploration of the frontiers of nature in the mid- and long-term. This can only mean ensuring that there will be new trailblazing experiments that test our predictions and hypothesis in conditions never seen before. In fact, this is clearly connected to the previous point, because only a precise determination of our current knowledge can ensure that we build and optimise the experiments with the biggest potential. Hence, both tasks could be seen as two faces of the same coin, one with a theoretical focus while the other is mostly experimental. We shall never forget that the heart of physics lies just in between theory and experiment.

The focus of this work will be almost exclusively on the theoretical face of the aforementioned coin. However, we insist on the link between both sides and dedicate a chapter to show how theoretical physics can help to estimate the reach of future experiments, collaborating in this way to assess the motivation to build them. Additionally, in two other chapters we will show how a careful use of theoretical tools can help to make experimental results more meaningful. The back and forth relation between theory and experiment is deeply rooted in the spirit of this work. Staying closer to measured quantities is one of the guiding principles in our revisit to the tools and paradigms that we use, with the hope of finding new trails to follow.

This thesis is organized as follows. In Chapter 2, we summarise the current efforts of the theoretical and experimental communities, outlining what we might expect in the near future of particle physics. In particular, we introduce two tools that can be used to find BSM physics, Effective Field Theories (EFTs) and future colliders. The first one is a theoretical tool that will play a central role in each of the following chapters and constitutes the most transversal topic of this thesis. The second one is an experimental tool, the proposed future proton collider FCC-hh, which will be a central piece of Chapter 3. In said Chapter 3, we will use EFTs to assess the capabilities of FCC-hh, showing how new processes and novel ideas for observables can improve the reach of this collider. Then, in Chapter 4, we will focus on more formal properties of EFTs, in particular their relation with the anomalous breaking of gauge symmetries. Chapter 5 revisits the connection between EFTs and global symmetries, showing how its study can lead to insights about the field content of the UV model and how this can be inferred from low-energy observables. Chapter 6 explores how the use of a different formalism can bring us two advantages: one, easier computation of cross-sections, and two, a different way to parametrize BSM effects with certain advantages over EFTs. Finally, we summarize our findings and give some closing remarks in Chapter 7.

This page is intentionally left blank.

Chapter 2

Tools for tomorrow

> *“‘Data! Data! Data!’ he cried impatiently. ‘I can’t make bricks without clay.’ ”*
>
> — Arthur Conan Doyle, “The Adventure of the Copper Beeches”, The Adventures of Sherlock Holmes (1892)

2.1 The future that lies ahead

The future of particle physics lies in the wake of the LHC, whose legacy has some already clear features. First, the Higgs boson has been discovered and its couplings to some SM particles have already been measured, notably to the third-generation quarks and the EW gauge bosons. Although its main role in EWSB is out of question, there are still several questions regarding the Higgs boson yet to be answered. Second, there is no clear signal of BSM Physics around the TeV scale and, in particular, in the range of $\sim 200 - 1000$ GeV. Finally, the performance of LHC/ATLAS/CMS has exceeded expectations and there is a rapid progress of theoretical computations to support future precision measurements [24].

The next era of particle physics will combine several facets: the accurate understanding of the meaning of LHC results, the pursuit of precision measurements, the thorough study of the Higgs boson and the need of new BSM-model-building paradigms. We now review briefly the main theoretical and experimental efforts to develop the tools that we will need in the future to unveil BSM Physics.

The negative results from searches of new particles at Run-1 and Run-2 of LHC have constrained severely various well-motivated and popular BSM models such as Supersymmetry (SUSY), Composite Higgs (CHM), and large/warped extra dimensions. Hence, the theoretical community has actively looked for new model-building paradigms and classes of models that can avoid such constraints, e.g. clockwork/linear dilaton [25, 26] and relaxion models [27]. Additionally, the theoretical efforts on DM and axion-like particles (ALPs) have increased over the last decade and motivated new experiments and collider searches.

A key step in the interpretation of the LHC results and the building of its legacy is the comparison between theoretical predictions and the experimental measurements. The high precision achieved by LHC and the even higher expected at HL-LHC have made the need of precise theoretical predictions more pressing. In turn, there is a growing effort in computing higher-order corrections to collider observables, helped by the appearance of new techniques (see Ref. [28] for a short review).

Furthermore, we are also constantly finding new and non-trivial observables and searches that can probe NP in unprecedented ways, prompting innovative analyses of current data (see e.g. Ref. [29]). Chapter 3 will show an example of such kind of observables, although for future colliders. In the last decade, the development of analysis based on artificial intelligence (AI) and more precisely Machine Learning (ML) has increased significantly and is already one of the main tools used by experimental collaborations [30–33]. ML techniques are also being applied to improve the Monte-Carlo simulation of collider events, which is another topic of great relevance for the future [34–37]. There are also incipient efforts to apply quantum computing techniques [38–41].

An important part of the LHC legacy will be formed by global fits of all the experimental measurements and there are currently growing efforts to improve and produce them [42, 43]. They help to identify interesting sectors where the agreement between SM prediction and the data is poorer and analyse the interplay between different sectors. The preferred framework to parametrise NP effects in such global fits are EFTs, which are very well motivated by the no discovery of new particles at the scale of the TeV. We will cover EFTs in detail from Section 2.3 onwards.

Let us stress here that EFTs have established themselves as the preferred framework not only for global fits, but for any kind of indirect search of BSM Physics, as it will be done in Chapter 3. This has led to a increasingly more intense study of formal aspects of EFTs. Chapters 4 and 5 are, in fact, aligned with this trend. A parallel effort is the computation of higher-order corrections in EFTs and observables computed with them, which establishes a clear connection with the aforementioned high-precision computation of collider observables [44–46].

While EFTs do not present any major flaw as a parametrisation of NP, it is unavoidable and, in fact, healthy to think about possibly better frameworks or other theoretical tools that can help us to constrain the BSM parameter space. The latter is what lies in the foundation of the positivity constraints program [47–53], while the former has led to the rise of the Scattering Amplitudes for BSM program [54–56], which we will cover extensively in Chapter 6.

Given the lack of clear guidance towards the model that succeeds the SM, we are entering an epoch in which the exploration must be led by experiments. The variety and scope of the experiments planned for the mid and long-term future is remarkable and encouraging. Let us start highlighting that over the next decade, several new results are expected from flavour experiments such as LHCb [57], Belle-II [58], NA-62 [59], and KOTO [60]. Their results will be key to either confirm or wipe out the several tensions with the SM present in flavour observables.

In the same period of time, we will see big improvements in high-precision observables such as $(g-2)_\mu$ being measured at Fermilab [61] and also at J-PARC in the future [62], and the electron EDM measured by ACME [63]. Several new groundbreaking experiments in the intensity and precision frontiers have been proposed recently, e.g. LUXE [64]. The searches for DM candidates and axion-like particles (ALPs) will continue strongly in the next decade and the vastness of related experiments is beyond the scope of this work (see e.g Ref. [65] for a recent review). In the field of neutrino physics, the promising experiment KATRIN has already published its first results [66], and in the near future we will have new results from Hyper-Kamiokande [67]. All these experiments might discover new phenomena and/or give clear hints about the right BSM model.

One area that receives increasing attention and has entered its own precision era is astroparticle physics. Its results are becoming more relevant to particle physics by the day, strengthening the connection with cosmology and making big contributions in searches for DM, axions, and neutrino physics. Some present and near future experiments of high relevance [68] are H.E.S.S [69], Antares [70], IceCube [71], and CTA [72].

When speaking about connections between astrophysics and particle physics, there is one

event that can not be left aside: the first detection of gravitational waves (GWs) made by LIGO and Virgo five years ago [73]. GWs have opened a completely new way to survey the skies and is a fundamental piece in the future multimessenger astronomy [74]. LIGO and sister observatories scattered around the world will continue detecting GWs in the next decade [75]. However, from the particle physics point of view, the next generation of GWs observatories is the most interesting. Observatories such as Einstein Telescope (ET) [76] and the Laser Interferometer Space Antenna (LISA) [77–80] among others will be able to detect GWs in different ranges of the spectrum and hence be sensitive to different phenomena. They could give further insights on the nature of DM and DE and will probe the structure of Black Holes (BHs). Through the latter, we will be able to look for scalar fields (like axions) which might be surrounding BHs [81–83]. Also, they could detect stochastic background GWs produced by a first-order phase transition in the early Universe [84], which in turn provides a probe to the scalar potential [85]. There is no clear time schedule for ET, while LISA is expected to be launched in 2034 and operate during 4 years [77, 78].

Colliders stand out among as our main exploration tool thanks to their breadth of capabilities, their ability to measure many different processes that can probe several physics scenarios. Differently to most of the experiments mentioned before, colliders are not designed to measure a particular coupling, to study a specific phenomenon, to look for a certain hypothetical model, but to explore beyond our knowledge frontiers. They are truly discovery machines that take us to uncharted territory and give a broad scope of opportunities to find NP. We build them to chart the unknown, not to confirm our knowledge [86]. Thus, building a new one should be an ambitious project that goes well beyond the current frontier. Even more, colliders are rather modular machines whose capabilities can be expanded with the addition of new experiments, which usually can be mounted a posteriori with a minimal amount of additional effort. Particle colliders can also be counted as some of the most complex and biggest machines conceived by mankind, comprising an enormous span of technologies from vacuum and magnets to big data management and communications. The recent past is filled with examples of how colliders development could generate technological progress that benefited to the whole society and that is another strong reason to keep building them.

The next decade of collider physics will be marked by the running of HL-LHC [87], which is expected to operate until 2036. In parallel, part of the community has pushed to enhance the capabilities of HL-LHC on the lifetime frontier, i.e. in searches of long-lived particles, with the addition of detectors like MATHUSLA [88, 89]. Due to the lack of clear deviations from the SM at LHC, it is uncertain if HL-LHC will make any disruptive discovery. However, the reliable and precise analysis of all its data will greatly mould the legacy of the LHC and unexpected surprises might always appear.

In the mid and long-term future, we will have a next generation of colliders that includes a rich landscape of complementary possibilities [90]. The question, instead of whether we should build one, is rather which one to choose [86]. The International Linear Collider (ILC) is a proposed linear e^+e^- collider to be built in Japan with the goal of making precise measurements of the Higgs boson [91]. Since there are no big technological challenges involved, it is the one that could start operating the soonest but a clear commitment to build it has not been made yet. An alternative, very similar in concept, is the Compact Linear Collider (CLIC) projected at CERN [92]. CLIC features a three-stage program, with $\sqrt{s} \sim 380$ GeV, ~ 1.5 GeV and ~ 3 GeV in each of them. The first stage would start measuring not before 2036 and the full program would extend for around 30 years (see Fig. 2.1).

A muon collider, despite being also a lepton collider, is a very different proposal to ILC and CLIC. Muon colliders are seen as an almost ideal middle ground between electron-positron and proton colliders [86]. Thanks to the fundamental nature of the muon, its full energy is available

in the collision and the final states are cleaner than in proton colliders. The higher muon mass permits to achieve higher centre of mass energies than with electrons, combining the benefits of high energy and precision. However, the short lifetime of the muon poses several technological challenges to be solved. The physics case for this kind of collider is strong since it combines benefits from lepton and hadron colliders, and because it can also be seen as a vector boson collider [86]. Hence, it is one of the most challenging but also potentially rewarding possibilities for the future.

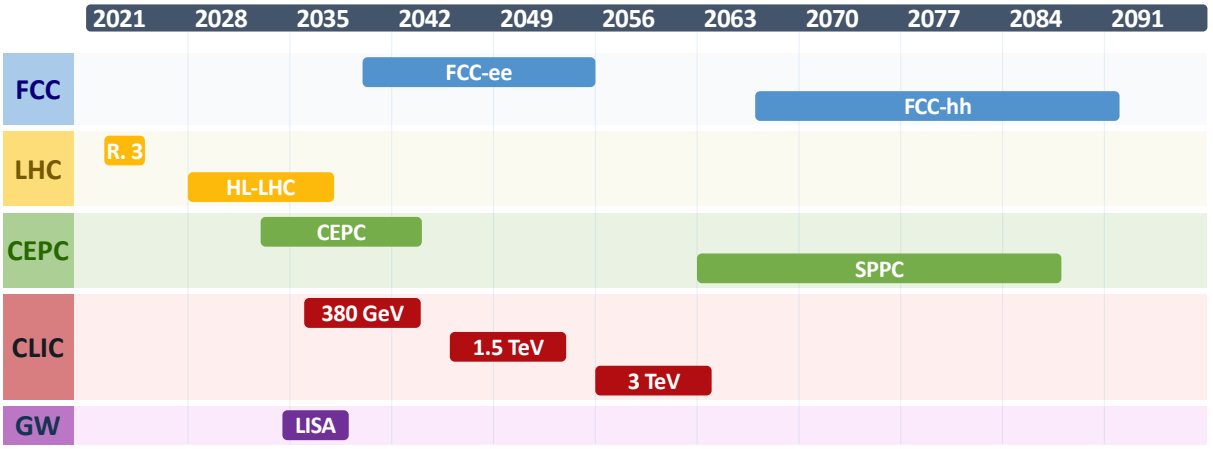

Figure 2.1: Estimated operation timeline of future colliders and GW observatories. We include the current Run 3 of LHC, HL-LHC [93], FCC-ee and FCC-hh [94], CEPC and SPPC [95], three stages of CLIC [96, 97] and the LISA GW observatory [77, 78].

And finally, future circular lepton and hadron colliders. The spirit of going beyond our knowledge frontiers and defy our limits drives large projects as the Future Circular Collider (FCC) proposed by CERN as a replacement of LHC [24, 94, 98]. This program would include a circular e^+e^- collider (FCC-ee) followed by a proton collider (FCC-hh) in the same 100 km circular tunnel. The latter would reach centre-of-mass energies of at least 100 TeV. While the focus of the lepton collider would be measuring EW processes with astonishing precision, the hadron collider would focus on searching new heavy particles and measuring the Higgs self couplings. FCC-ee could start operating by the early 2040s, with FCC-hh starting around 20 years later and running until around 2090 [94]. A very similar project called CEPC-SPPC is under study in China and it would have a slightly smaller tunnel and could start operating nearly a decade earlier [99].

We show the tentative timeline for operation of different future colliders and GW observatories in Fig. 2.1. Let us stress the complementarity of the different kinds of experiments presented here. The combination of their results is the only way that guarantees exploring all the BSM physics models thoroughly. In the next section, we summarize the Physics case for FCC, in particular FCC-hh, since Chapter 3 is dedicated to projections for FCC-hh.

2.2 Digging more than ever before: FCC

As said before, there are several experiments planned in the near to mid-term future with huge potential to explore BSM Physics. Here, we will review briefly the main technical features and Physics opportunities of the FCC project [24]. The FCC project is an integrated circular collider programme, in full similarity to the LEP/LHC program, planned to be built at CERN. It includes a luminosity-frontier highest-energy lepton collider, FCC-ee, as first step, and an

energy-frontier hadron collider to be installed in the same tunnel afterwards. It constitutes the most ambitious and far-reaching particle physics programme with foreseeable technology, although the technological R&D challenges are sizeable [90].

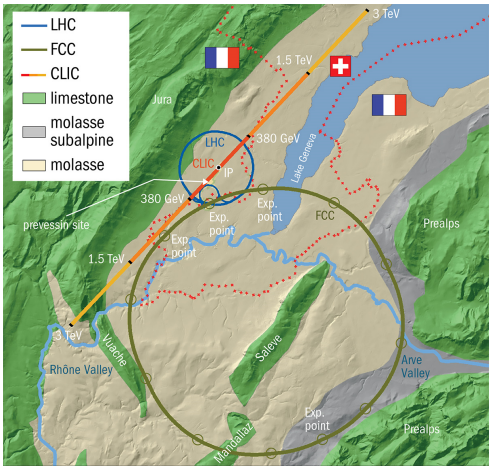

Figure 2.2: Map showing the location of CERN, the LHC tunnel and the proposed location of the CLIC and FCC tunnels. Credit: CERN, extracted from Ref. [100].

The FCC program implies digging a 100 km circular tunnel, which would surround the city of Geneva, going through Swiss and French territory and below Lake Geneva, as depicted in Fig. 2.2, where its scale can be compared with the current LHC and the proposed CLIC. The current LHC would be used as part of the feeding and acceleration chain of the beam. The lepton collider FCC-ee would consist of a double ring, with electrons and positrons circulating in separate vacuum chambers, crossing each other only at the interaction points of the different detectors. This e^+e^- collider would operate at several centre-of-mass energies: $\sqrt{\hat{s}} \sim 91$ GeV, $\sqrt{\hat{s}} \sim 160$ GeV, $\sqrt{\hat{s}} \sim 240$ GeV, and $\sqrt{\hat{s}} \sim 350 - 365$ GeV, in order to produce $\sim 5 \times 10^{12}$ Z bosons, 10^8 WW pairs, $\gtrsim 10^6$ Higgses and $\gtrsim 10^6$ $t\bar{t}$ pairs respectively.

The hadron collider, FCC-hh, is designed to be a pp collider that reaches at least 100 TeV centre-of-mass energy with a goal integrated luminosity of 30 ab^{-1}. For reference, this collider would produce more than 10^{10} Higgs bosons. In comparison with LHC, FCC-hh would operate at an energy seven times bigger, and collect about 10 times more data in its planned 25 years of operation. FCC-hh should have two main interaction points (IPs) for general-purpose experiments, like CMS and ATLAS at LHC. Details about the baseline detector for such experiments can be found in Ref. [94]. Moreover, those general-purpose detectors should be complemented by dedicated experiments, focused for example in flavour, forward physics or long-lived particles. The detailed exploration of these additional detectors is still to be done.

Two further possibilities are available. First, FCC-hh could also be operated with heavy ions thanks to two additional IPs. Second, FCC-hh could be combined with a 60 GeV electron beam coming from an energy recovery linac to form FCC-eh, which indeed can be run simultaneously with FCC-hh. FCC-eh would produce ~ 2 ab^{-1} of 3.5 TeV ep collisions. In the rest of this section, we focus on FCC-hh because it is the collider that we have done projections for, as shown in Chapter 3. However, we will highlight complementarities with the other colliders in the FCC program.

The combined FCC program has ambitious goals in several areas. In particular, the precise understanding of the Higgs boson is a cornerstone of the Physics motivation of the FCC program. Thanks to the precise measurement of its couplings, the Higgs will become an exploration tool and also a showcase for the synergies within the FCC program. While FCC-ee would measure

leading Higgs couplings to SM particles with sub-percent precision, FCC-hh could carry out a complementary program. The ability of FCC-ee to measure the Higgs coupling to the Z is the starting point of a model-independent determination of the Higgs total width, opening doors to many other measurements via branching ratios. In particular, FCC-hh could measure rare and invisible Higgs decays [101]. The enormous sample of Higgs bosons produced at FCC-hh would allow us to establish (or disprove) firmly the Higgs coupling to the second generation of fermions. The fact that new channels will become available thanks to better statistics plays a crucial role in this, and we will see a concrete example in Chapter 3.

FCC-hh would be able to measure directly the cubic Higgs self coupling, particularly via the gluon-fusion production process. The projected model-independent precision for this coupling is $5-10\%$. A big part of this improved precision is due to the increase by a factor of 40 w.r.t. LHC of the rate of Higgs pair production events, which partially occur through Higgs self-interactions. The measurement of the quartic self-coupling is also possible, but with a precision $\sim 30\%$. This unique ability to measure the Higgs self-couplings stresses the need for high-energy hadron colliders to study the Higgs boson.

Beyond the large statistics, another characteristic element of the Higgs production at FCC-hh is the large kinematic range, which, for several production channels, probes p_T in the multi-TeV region. In fact, the p_T spectrum can be measured with a precision $\lesssim 10\%$ thanks to very clean final states such as $\gamma\gamma$ and 4ℓ, up to p_T values well in excess of 1 TeV. This big range helps the measurement of possible higher-dimension operators affecting Higgs dynamics, as we will show in Chapter 3. Another important parameter in Higgs dynamics and EWSB is its coupling to vector bosons. There, the scattering of longitudinal components of vector bosons can lead to a precision of $\sim 3\%$ and, additionally, measurements with FCC-eh can improve those constraints.

Then, FCC-hh would change drastically the results of Higgs global fits from FCC-ee, thanks to its higher-energy reach and showing their complementarity. The differential measurements performed at FCC-hh will not only reduce uncertainties, but also remove correlations. The FCC program, through a combination of indirect and direct searches, would comprehensively assess whether the Higgs is elementary or composite. In few words, the combined FCC program would allow us to know the Higgs better than any other experiment and could help enormously to solve the EW hierarchy problem.

The determination of Higgs properties includes the measurement of its potential, which has a key role on the Electroweak Phase Transition (EWPT). The interest in EWPT is partially motivated by the fact that a first-order EWPT is a necessary condition to induce baryogenesis and explain the matter-antimatter asymmetry. However, in the SM the EWPT is of second order. Searching for evidence of a first-order EWPT at colliders is a two-fold endeavour. On one hand, a large deviation of the cubic Higgs self-coupling w.r.t. its SM value could lead to first-order EWPT, and thus the precision measurement commented in a previous paragraph becomes crucial. On the other hand, first-order EWPT appears in several models with additional scalar particles. FCC-hh would have the power to conclusively discover or exclude several of such models, in particular for singlet or EW multiplet scalars.

Electroweak Precision Observables (EWPOs) have been of utmost importance in particle physics in the last 30 years, since they were first measured at LEP. LHC has improved partially those measurements, but only FCC-ee would be able to measure them with unprecedented precision. However, FCC-hh would also improve them through indirect measurements at high energy, just as LHC has done. The focus on the measurement of high-energy tails is a key in this complementarity and we will show it explicitly in Chapter 3. A particular process where that strategy is very successful is Drell-Yan (DY) production, which has been already used at LHC for such purpose [29] and where FCC-hh could show fully its potential. Moreover, the interplay between EW and Higgs measurements gives another handle to explore Higgs dynamics.

And measuring the running of EW couplings with higher precision would reduce systematic uncertainties in global fits at the same time that probes indirectly the existence of new EW-charged states.

The heaviest particle in the SM, the top quark, enjoys a rather particular position. Its high mass makes it look like an outlier in the quark spectrum. It also means that interacts with the Higgs boson more strongly and hence it generates the main loop-level corrections to the Higgs couplings. As a consequence, the study of the top quark and the Higgs boson are inextricably intertwined. FCC-hh would produce top quark pairs at a rate around 30 times larger than the LHC and it would offer good sensitivity particularly at high invariant masses ($m_{t\bar{t}} > 10$ TeV). Single top and top production associated to EW bosons offer additional handles to study EW and Higgs properties. Finally, the sensitivity to rare top decays should improve by a factor of 10 w.r.t. LHC.

The high energies that FCC-hh would reach make it a very fertile place to perform direct searches of BSM particles. These searches are heavily model dependent and therefore we will discuss a few popular classes of models. In supersymmetric scenarios, FCC-hh would be able to discover (or exclude) stops with masses up to $8-10$ TeV and neutralinos up to $3-4$ TeV. This represents an improvement w.r.t. LHC of a factor 5 to 7. For Composite Higgs scenarios, the combination of direct searches of coloured top partners or massive vector bosons with indirect searches would allow us to probe the whole theoretically motivated parameter space, leading to either their discovery or exclusion. The situation is even more interesting in models of Neutral Naturalness, which usually evade all constraints from LHC. The measurement of the Higgs BR at FCC would probe most of the relevant parameter space for those models. And those searches can be complemented with direct searches of displaced vertices or light top partners.

Another area where FCC-hh promises a great potential is in the search of DM particles at colliders. No collider could probe entirely the enormous landscape of DM candidates, but there is a very broad class of DM models for which the theory motivates particles with masses in the range 1 GeV-10 TeV, being then in the scope of FCC-hh. These are the models with weakly interacting massive particles (WIMPs), and projections indicate that FCC would cover their full mass range. Additionally, models of composite DM also motivate the search of DM particles in the same mass range $\sim 1-10$ TeV [102–104].

Finally, FCC-hh is the ideal machine to look for new and unexpected phenomena, given its big energy reach. It can explore most of the parameter space of popular models motivated by flavour anomalies, it can find indirect evidence of BSM Physics by measuring W-bosons scattering or far off-shell Z bosons. The simultaneous running of FCC-eh could determine the parton structure of the proton with high precision, which in turn could be an important input for such precision measurements.

2.3 Across the scales of knowledge: introduction to EFTs

Effective Field Theories are based on a simple but powerful idea: when trying to describe some phenomena at a certain (length or energy) scale, consider only the degrees of freedom relevant and dynamical at that scale. Any other more fundamental degree of freedom will enter the description as an effective modification of the interactions among the relevant ones. This effective description can then be matched onto a more fundamental one and the corrections induced by the neglected degrees of freedom can be computed in a systematic way. In fact, this idea is rooted in the systematic reductionism of Natural Sciences and is applied in one way or another in every branch of Science.

A clear example from elementary Physics is the friction force between two sliding surfaces. The ultimate origin of this force is the exchange of (mainly) photons between a pair of electrons,

one bounded to an atom of each surface. Those degrees of freedom are completely irrelevant (out of scale) to the macroscopic problem and however their effect is relevant and is parametrized by an effective parameter, the coefficient of friction. The extension of this idea to BSM Physics is straightforward: the interaction among the particles that we can measure might be modified by heavier particles, out of reach for our direct probes.

Formally, and in the framework of Quantum Field Theories, this is known as an Effective Field Theory (EFT). The basic recipe to build an EFT is to define the fields that describe the degrees of freedom that matter at the energy scale of your interest. Then, select the local and global symmetries that the EFT must respect. Finally, build the Lagrangian as a series in energy dimension of all the operators that can be written with the selected fields and that respect the chosen symmetries [105].

Any EFT is valid only up to a maximum energy scale called cutoff and generically noted Λ. The operators of energy dimension higher than 4, called irrelevant operators, will cause effects that are suppressed by a scale and will be negligible at low energies. The series of higher dimensional operators is expressed as a series in powers of $1/\Lambda$, and then the Lagrangian is generally written as

$$\mathcal{L}_{EFT} = \mathcal{L}_{d\leqslant 4} + \sum_{d=5}^{\infty} \sum_{i} \frac{c_i^{(d)}}{\Lambda^{d-4}} \mathcal{O}_i^{(d)}, \tag{2.1}$$

where $\mathcal{O}_i^{(d)}$ are all the operators of dimension d allowed by the symmetries. The Wilson Coefficients (WCs) $c_i^{(d)}$ encode the effects of the heavy fields in the UV model on the interactions between the particles included in the EFT. In QFTs, interactions mediated by heavy massive fields are generically suppressed by inverse powers of the intermediate particle mass and hence they decouple at low energies. This result is known as the decoupling theorem by Appelquist and Carazzone [106]. It justifies why EFTs are adequate low-energy descriptions of a more general UV theory.

EFTs provide us with a systematic way of computing corrections to the renormalisable part of the theory from a bottom-up approach [105]. Corrections to observables can be computed systematically at increasing order in $1/\Lambda$. Notice also that any possible interaction, in the sense of allowed by symmetries, is included. If it is not forbidden, then it is compulsory [107].

EFTs have been used in particle Physics with great success over the last century. The clearest example is also the oldest: Fermi's theory of weak interactions is an EFT of the weak interaction contained in the SM. Furthermore, it showcases several main features of an EFT and how it can be matched onto an UV model. For those reasons, we will revisit it briefly here.

In order to explain the beta decay of atoms, Enrico Fermi proposed in 1933 that a neutron could, at one point in space, transform into a proton, an electron and a neutrino, giving place to a four-fermion interaction [108]. In modern language, his proposal means the existence of an operator with 2 quarks of different flavour, one electron and a neutrino, i.e.

$$\mathcal{L}_{\text{Fermi}} = \mathcal{G}_F \overline{d}_L \gamma^\mu u_L \overline{\nu}_L \gamma_\mu e_L. \tag{2.2}$$

This 4-fermion operator has energy dimension 6 and therefore the coupling constant must have an energy dimension $[\mathcal{G}_F] = -2$. It is convenient to rewrite it as

$$\mathcal{G}_F = \frac{g_F^2}{M^2}, \tag{2.3}$$

where M has dimensions of mass. Let us notice that is this mass the one that determines the actual cutoff of the theory, i.e. the energy at which new degrees of freedom will appear. For

$E \gtrsim M$, the EFT should be replaced by the UV theory. On the other hand, $\mathcal{G}_F^{-\frac{1}{2}}$ defines the scale of the interaction. Since the theory loses perturbative unitarity at $E \simeq 4\pi\mathcal{G}_F^{-\frac{1}{2}}$, it is expected that some new physics appears at energies below that value, either to tame the energy growth of the amplitude generated by the operator or to describe the non-perturbative regime. This is what is known as a no-lose theorem [20]. Let us stress again that new physics will be found at $M \sim g\mathcal{G}_F^{-\frac{1}{2}}$, which could (and turns out to) be much smaller than $4\pi\mathcal{G}_F^{-\frac{1}{2}}$ [20, 109]. The distinction between cutoff and scale is even clearer when $\hbar$ is not set to 1, since that makes evident that masses and scales are incommensurable [20, 109].

From an UV point of view, we know that this interaction is mediated by a W boson. When the centre-of-mass energy of the process is low, one can neglect the propagation of the W, its propagator being approximated by $1/m_W^2$. In this regime, the decay is well described by $\mathcal{L}_{\text{Fermi}}$ if

$$\mathcal{G}_F = \frac{g_F^2}{M^2} = \frac{g^2}{2m_W^2}V_{ud} = \frac{4}{\sqrt{2}}G_F V_{ud}, \tag{2.4}$$

where g is the $\text{SU}(2)_L$ gauge coupling of the SM, V_{ud} is the element of the CKM matrix and G_F is the so-called Fermi's constant. What is this matching telling us? The unknown Physics in Fermi's times was the weak interaction and the existence of the W boson. And the mass of the latter is the physical scale that suppresses the dimension-6 operator in Fermi's theory. The operator in Fermi's theory, Eq. (2.2), properly generalized for all quarks and leptons represent the leading correction to renormalisable QED. Together, they constitute the low energy EFT of the electroweak sector of the SM at order $(p/m_W)^2$. Higher-order terms in p/m_W can be added consistently [110].

Clearly, from only the measurement of Fermi's constant one can not determine the mass of the intermediate particle because of the unknown gauge coupling. However, one might assume that the intermediate vector boson receives its mass via a Higgs mechanism and then $g/m_W = 2/v$, and then one can say that the measurement of Fermi's constant is a measurement of a scalar VEV. But such conclusion comes at the expense of an additional theoretical assumption.

This simple example leaves several interesting lessons. First, how a low energy measurement tells us about the existence of New Physics (NP) at higher energies and how it constraints the possible UV models. Second, how with the addition of theoretical assumptions one might change the interpretation of the measurement. Third, it is important to notice that Fermi's 4-fermion operator generates cross-sections that grow with energy like E^2/m_W^2. That is also a usual sign of NP effects affecting a process and, as we will see in Chapter 3, it can be leveraged to improve the sensitivity of an experiment.

Fourth, let us come back to the distinction between the cutoff and the scale of the interaction. Fermi's theory breaks down and is replaced by its UV completion, the EW sector of the SM, at $E \simeq m_W \cong 80$ GeV, much smaller than $G_F^{-\frac{1}{2}} \sim 300$ GeV or even $4\pi\mathcal{G}_F \simeq 4\pi v \simeq 3$ TeV. This is a consequence of the smallness of the EW gauge coupling.

2.4 Parametrizing our current ignorance: SMEFT and HEFT

The discovery of all the particles contained in the SM and the absence of hints about the existence of further states just above the EW scale lead to a sharp hypothesis: the SM is a valid description of nature up to a cutoff $\Lambda \lesssim$ TeV. Current data does not show a clear preference for any particular class of BSM models. Then, how can we parametrise our ignorance about BSM?

An EFT that has the SM as low-energy limit and can be matched to any BSM model

afterwards could clearly perform this task. In particular, it offers the ability to compute systematically higher-order corrections without further assumptions about the UV model. Efforts to develop this EFT started over 35 years ago [111], though an intense and thorough development only happened over the last decade. At the same time, this development has laid the ground for the systematic program of indirect BSM searches that has blossomed in the last years. In terms of the EFT, this program can be seen as simply the effort to measure as many WCs as precisely as possible, hoping that deviations w.r.t. to the SM or particularly large allowed values will point towards a preferred BSM model [112].

The choice of symmetries and field content for an EFT built upon the SM might look obvious: just like in the SM. However, there is a subtlety in the fact that we have not measured precisely enough all the interactions predicted by the latter. Hence, we can not guarantee that the observed particles fit in the gauge group representations exactly as predicted by the SM. This is partially the dichotomy that leads to two possible non-exclusive EFTs that we will discuss in the following subsections.

2.4.1 SMEFT

Given the success of the SM, it is straightforward to assume that the observed Higgs boson belongs in the UV theory to a scalar $\mathrm{SU}(2)_L$ doublet. This doublet transforms linearly under the SM gauge group and is the one that triggers SSB. Then, EWSB is linearly realized in this EFT.

The choice of keeping the Higgs doublet defines the SM Effective Field Theory (SMEFT). Its field content and renormalisable Lagrangian are exactly equal to the SM, then the matching to the SM at low energies is achieved by simply setting to zero all higher-dimensional WCs. The higher-dimensional operators are built with SM fields, including the full Higgs doublet. In other words, SMEFT is constructed in the unbroken phase. This is consistent with assuming $\Lambda \gg v$ and that only the Higgs doublet breaks spontaneously the EW gauge symmetry.

The expansion parameter of the higher-dimensional operator series is, naturally, $1/\Lambda$. When computing an amplitude, this leads to the power-counting parameter $(E/\Lambda)^n$, where E is the typical energy of a process. The SMEFT is renormalisable order by order in $1/\Lambda$, independently of the number of loops. The higher-dimensional operators can be further ordered and classified with additional assumptions that impose other power-counting formulas, like the one we will use in Chapter 3 [113]. Some of them concern the flavour structure of operators involving fermions, like Flavour Universality and Minimal Flavour Violation [114].

At a given dimension, not all the operators allowed by symmetries are independent. Some of them might be related by equations of motion, Fierz identities, integration by parts, and other constraints. Related operators are equivalent from a physical point of view and then, only one of them should be included in SMEFT. This makes the determination of a basis of higher-dimensional operators, i.e. a set of non-redundant operators, cumbersome. There is only one exception: operators of dimension 5. At such dimension, only the lepton-number violating Weinberg's operator (and its flavour variants) is allowed by the SM gauge symmetries [115]. The upper bound on neutrino masses and constraints from lepton-number violating processes justify to consider the WC of this dimension-5 operator as small.

The situation changes greatly at dimension 6. Only 11 years passed since the first full determination of a basis of dimension-6 operators for SMEFT [116], despite early efforts 35 years ago [111]. The basis developed in Ref. [116] has become known as the "Warsaw basis". Alternative dimension-6 bases have appeared in subsequent years and the selection among them usually is based on the sector of most interest or the preferred BSM scenario [117]. Neglecting the flavour structure and assuming baryon-number conservation, there are 59 independent

dimension-6 operators [116]. Allowing for a fully generic flavour structure, that number grows to 2499 [118].

The number of non-redundant operators grows quickly with the dimension. Beyond dimension 6, full non-redundant basis are known only for dimension 7 [119, 120], 8 [44, 45, 120, 121], and 9 [122, 123]. The operators of dimension 5, 7 and 9 are often excluded from phenomenological analysis because they all violate lepton-number or baryon-number or $B-L$ conservation respectively.

As a consequence, the leading deviations from the SM should be caused by dimension-6 operators. Dimension-8 operators are naively expected to generically produce effects suppressed by $1/\Lambda^2$ w.r.t. the dimension-6 operators. However, recent studies indicate that in certain processes such as DY, the interference of dimension-8 operators with the SM can lead to deviations of similar size than the ones coming from the squared amplitude containing a dimension-6 operator [124–129]. Other processes are affected by non-interference theorems, i.e. dimension-6 operators do not interfere with the SM contribution to an observable and then the leading SMEFT term $\mathcal{O}\left(\Lambda^{-4}\right)$ [130, 131]. Contributions of that order can be produced by the interference of dimension-8 operators with the SM or the squared amplitude generated by dimension-6 operators. As we will show explicitly in Chapter 3, the use of certain observables can recover the interference [131, 132].

2.4.2 HEFT

The SMEFT is built upon the assumption than the Higgs boson belongs into an $\mathrm{SU}(2)_L$ doublet, whose other components are the NGBs absorbed by the massive EW bosons as their longitudinal components, and that all the massive particles acquire their mass via the Higgs VEV[1]. This constrains several parameters, linking tightly for example the triple and quartic self-interactions of the Higgs boson, relating the fermion masses to the fermion-Higgs boson coupling, and the EW gauge couplings to the EW gauge boson masses. All the measurements performed so far agree with this hypothesis, although there is room for doubt since the heavy quark Yukawa couplings have not yet been measured precisely enough and the Higgs self-interactions have not been observed. The observation of any deviation w.r.t. the predicted correlations among couplings and masses would be a clear sign of BSM physics.

Then, dropping the Higgs doublet assumption is still allowed yet several experimental constraints should be fulfilled by tuning accordingly certain parameters. This opens the possibility of building a more general EFT where the EW gauge bosons are massive, with longitudinal components described by NGBs, and there is a singlet Higgs-like scalar boson, but no relation is presumed among them. This is the so-called Higgs Effective Field Theory (HEFT).

We begin the discussion of HEFT revisiting the Higgs sector of the SM and reminding that it has a global $\mathrm{SU}(2)_L{\times}\mathrm{SU}(2)_R$ symmetry, known as custodial symmetry, which is broken spontaneously by the Higgs VEV to its diagonal subgroup,

$$\mathrm{SU}(2)_L \times \mathrm{SU}(2)_R \to \mathrm{SU}(2)_{L+R}, \tag{2.5}$$

under which the Higgs is a singlet[2]. This spontaneous symmetry breaking (SSB) pattern generates NGBs with the right properties to become the longitudinal degrees of freedom of the W and Z bosons. Once the SSB pattern is fixed, the EFT of the NGBs can always be built via the Callan-Coleman-Wess-Zumino (CCWZ) formalism [134, 135].

[1] For short, we will refer to this set of assumptions as the Higgs doublet structure assumption from now on.

[2] There is disagreement in the literature on whether to call custodial group to $\mathrm{SU}(2)_L{\times}\mathrm{SU}(2)_R$ or its diagonal subgroup. See Section 3 of Ref. [133].

HEFT is built upon the EFT for the NGBs from the SSB pattern (2.5) by adding the SM fermions, SM gauge bosons, and a singlet scalar boson h. This EFT is constructed in the broken phase and therefore its only manifest gauge symmetry is $\mathrm{SU}(3)_c{\times}\mathrm{U}(1)_{em}$ while $\mathrm{SU}(2)_L{\times}\mathrm{U}(1)_Y$ is non-linearly realised. For complete descriptions of HEFT, see Ref. [136–139], here we will only highlight some of its features that set it apart from SMEFT.

We begin by noting that with the NGBs, commonly denoted $\boldsymbol{\pi} = \left(\pi^1, \pi^2, \pi^3\right)$, one builds the Goldstone matrix,

$$U\left(\boldsymbol{\pi}\right) = \exp(i\tau^a\pi^a/(2v)), \tag{2.6}$$

where τ^a are the Pauli matrices [134, 135, 140]. The Goldstone matrix depends only on the SSB pattern. In HEFT, the covariant derivative acting on U reads [140],

$$D_\mu U\left(\boldsymbol{\pi}\right) \equiv \partial_\mu U\left(\boldsymbol{\pi}\right) + igW_\mu^a \frac{\tau^a}{2} U\left(\boldsymbol{\pi}\right) - ig' B_\mu U\left(\boldsymbol{\pi}\right) \frac{\tau^3}{2}. \tag{2.7}$$

The scalar sector of HEFT is complemented with the singlet scalar h, which plays the role of the observed Higgs boson, but it has, as said before, no relation with the NGBs. The lack of link between h and the NGBs might be seen as something dangerous because it threatens perturbative unitarity in the scattering of longitudinally polarised vector bosons. However, this is allowed because an EFT has to be unitary only up to its cut-off scale [141]. HEFT contains SMEFT and then, in certain limits, the relations imposed by the Higgs doublet structure can be recovered.

The HEFT Lagrangian, often called Electroweak Chiral Lagrangian (EWχL), contains operators invariant under the linearly realised gauge symmetry $\mathrm{SU}(3)_c{\times}\mathrm{U}(1)_{em}$ [140, 141]. The lagrangian includes higher-order custodial-violating terms [136], as expected from the fact that custodial symmetry is already broken in the SM by the gauging of the EW group and the difference between the top and bottom quark masses. Nevertheless, the approximate custodial symmetry remains an useful explanation for measured quantities such as the ρ parameter and hence the custodial-violating operators might face stringent constraints [142, 143].

The systematic expansion of the EWχL is done in orders of the momentum and power-counting rules can be consistently defined [144]. However, these power-counting rules may fail in ordering the contribution of different operators and alternative rules based on a "primary dimension" have been proposed [145]. The EWχL is conventionally written as

$$\mathcal{L}_{HEFT} = \mathcal{L}_0 + \Delta\mathcal{L}, \tag{2.8}$$

where $\mathcal{L}_0$ is LO in the chiral derivative expansion and essentially reproduces the SM Lagrangian [140]. $\Delta\mathcal{L}$ contains the new interactions and the main deviations w.r.t. the SM. The basis of NLO HEFT was constructed recently in Ref. [137, 139]. It is not easier to build than the analogous dimension-6 operator basis of SMEFT and, in fact, it has approximately the double of linearly-independent operators [141].

The scalar sector of the LO piece is already different from the SM, as it can be expected from the absence of the doublet structure [140]. More explicitly, the scalar sector of $\mathcal{L}_0$ is

$$\mathcal{L}_0 \supset \frac{1}{2}\partial_\mu h \partial^\mu h - \frac{m_h^2}{2}h^2 - \frac{v^2}{4}\,\mathrm{Tr}\left[V_\mu V^\mu\right]\mathcal{F}_C\left(\frac{h}{v}\right) - V\left(\frac{h}{v}\right), \tag{2.9}$$

where we used the generalised Maurer-Cartan form,

$$V_\mu \equiv \left(D_\mu U\left(\boldsymbol{\pi}\right)\right) U^\dagger\left(\boldsymbol{\pi}\right), \tag{2.10}$$

and the general function $\mathcal{F}_C\left(\frac{h}{v}\right)$ is

$$\mathcal{F}_C\left(\frac{h}{v}\right) = 1 + 2\,a_C\,\frac{h}{v} + b_C\left(\frac{h}{v}\right)^2 + \sum_{i=3}^{\infty} a_C^{(i)}\left(\frac{h}{v}\right)^i . \tag{2.11}$$

Notice that every invariant term, in particular the h kinetic term, could be multiplied with an arbitrary function of h/v, since h is invariant under all the symmetries. However, such function can be reabsorbed via a h field redefinition [113, 146].

Finally, the HEFT scalar potential is,

$$V\left(\frac{h}{v}\right) = v^4 \sum_{n=3}^{\infty} c_V^{(n)}\left(\frac{h}{v}\right)^n , \tag{2.12}$$

with $c_V^{(n)}$ all dimensionless arbitrary coefficients. Let us stress that $\langle h \rangle = 0$. If we wanted to match this scalar sector to the SM (and leading-order SMEFT in consequence), we should fix,

$$a_C = b_C = 1, \quad a_C^{(i\geq 3)} = 0, \quad c_V^{(3)} = \frac{m_h^2}{2v^2}, \quad c_V^{(4)} = \frac{m_h^2}{8v^2}, \quad c_V^{(n>4)} = 0. \tag{2.13}$$

This is a clear evidence of the greater generality of HEFT with respect to SMEFT. In the following subsection, we will delve into the differences between SMEFT and HEFT and when one is preferred over the other.

2.4.3 To be, or not to be in a doublet, is that the question?

How to differentiate HEFT from SMEFT and, crucially, how to know when one or the other should be used according to the UV model under consideration has been the topic of intense recent work [146–148]. There is a naive assumption on this distinction that is actually wrong: that is a matter of whether the NGBs and the Higgs-like scalar can be arranged into a multiplet that transforms linearly under $\mathrm{SU}(2)_L$ as a doublet. The simplest version of this assumption can be disproven easily since any SMEFT Lagrangian can be rewritten in terms of the non-linearly transforming Goldstone matrix and the singlet scalar h, and the field redefinition can be inverted to convert a HEFT lagrangian into one with a Higgs doublet [141, 146, 148].

The existence of such field redefinitions has historically caused confusion on whether HEFT and SMEFT can be differentiated with measurements, since the field reparametrisation equivalence theorem establishes that scattering matrix elements are independent of the basis used for scalar fields [141, 149]. However, as it was said earlier, SMEFT predicts certain correlations among couplings that are the signature of the Higgs doublet structure absent from HEFT. Clear examples are the relation between the fermion masses and Yukawa couplings, Higgs couplings to EW gauge bosons and the relation between the Higgs cubic and quartic self couplings.

Those relations influence processes such as double Higgs production, $\bar{t}th$, vector boson fusion (VBF) and others. Hence, the precise measurement of triple gauge couplings (TGCs), gauge-Higgs interactions, Yukawa couplings and testing correlations among them is a clear way to probe which EFT is realised in nature. For example, any statistically-significant deviation from the SM expectation in the Yukawa couplings would favour the use of HEFT. On the other hand, the confirmation of some of these correlations would strengthen the case of SMEFT but would not fully discard HEFT since they could appear accidentally. The selection of a set of observables which could conclusively decide between HEFT and SMEFT is a matter of ongoing discussion in the community.

In parallel, the community has devoted substantial efforts to the search of a clear theoretical discriminant between HEFT and SMEFT. This problem has been tackled with the tools provided

by geometric interpretations, analyticity and a combination of them. The geometric approach was pioneered in Ref. [147] and relies on seeing the real scalar fields as the Cartesian coordinates of a manifold of field configurations with a metric defined from the kinetic term in the lagrangian [146, 147]. Then, curvature invariants, which are independent of field redefinitions, can distinguish between HEFT and SMEFT.

The analyticity approach pursued in Ref. [148] is based on the observation that even if any HEFT Lagrangian can be written in terms of a Higgs doublet, in general it will lead to a Lagrangian that is not analytic at the origin $|H| = 0$ and hence it is not SMEFT [146, 148]. The caveat of this approach is its lack of invariance under field redefinitions, which can induce some un-physical (and irrelevant) non-analyticities [146]. In fact, an EFT is SMEFT-like if there is at least one field redefinition that makes its lagrangian analytic at $H = 0$, while it is HEFT-like if its lagrangian is non-analytic for any field definition [148]. A third approach combines both the geometric interpretation and the analyticity requirement and, perhaps more importantly, yields further insight into which kind of UV models require one or the other EFT [146].

Whether a BSM model must be matched onto HEFT or SMEFT is ultimately a question of decoupling [136–138,146]. HEFT is the right description when the UV model includes additional sources of EWSB, i.e. BSM states that break EW symmetry, or when there are integrated-out BSM states that acquire all their mass from EWSB. A pragmatic criterion is that HEFT should be used when states near the EW scale have been integrated out [146].

Chapter 3

Diboson processes at future hadron colliders

" We have to remember that what we observe is not nature herself, but nature exposed to our method of questioning. "

—Werner Heisenberg, Physics and Philosophy: The Revolution in Modern Science (1958)

Diboson production processes, such as Vh, offer a great opportunity to perform precise measurements that probe the high-energy dynamic of the electroweak and Higgs sector and are expected to become more relevant at future colliders.

3.1 Introduction

High-energy hadron colliders play a dominant role in the landscape of future accelerators due to the broad range of new-physics probes they would enable, as discussed in Chapter 2. Although their primary target is undoubtedly the direct search of new massive particles, their possible contribution to precision measurements should not be overlooked. Indirect probes of new physics at hadron colliders have already attested to be a successful strategy at the LHC, where some indirect electroweak (EW) measurements surpassed the accuracy achieved at LEP [29, 150].

Precision measurements at hadron colliders are achieved thanks to the interplay between a clever selection of channels with low uncertainties and the large accessible energy range. The latter exploits what might be considered the key ingredient for this enhanced precision: new-physics effects tend to grow with the centre of mass energy. If we parametrize those effects within an effective field theory (EFT) formalism (see Chapter 2), the leading SM deformations, which generically correspond to dimension-six operators, give rise to amplitudes that can grow with the process energy up to quadratically. In such a situation, having access to the high-energy tails of kinematic distributions can significantly increase the precision reach.

The sensitivity to the energy growth in the distribution tails is usually achieved via a binning of the events in their centre-of-mass energy or some correlated observable. This strategy ensures that deviations from the SM in the high-energy tails, which might represent just a small change in the inclusive cross section, are assigned statistical significance. Additionally, and not less importantly, binning the events helps to overcome one of the main disadvantages of hadron colliders: their systematic uncertainties.

Over the last decade, it has been shown that several simple production channels can be exploited to obtain precision measurements at the LHC. Some examples are the charged and

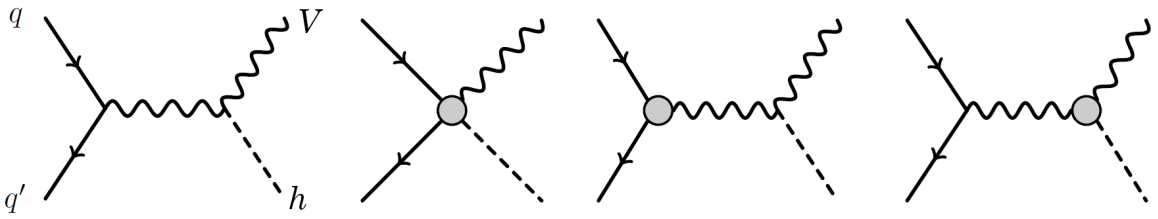

Figure 3.1: Representative Feynman diagrams for $q\,q' \to Wh$ at leading order. The leftmost diagram shows the SM process while the grey circles in the other diagrams represent one insertion of a dimension-6 SMEFT operator. The related process $q\,q \to Zh$ is described by analogous diagrams.

neutral Drell-Yann process [29, 150–153], di-jets and multi-jets [154, 155], di-tops [156], and diboson [126, 128, 131, 132, 157–180]. The latter, diboson production processes, are particularly interesting since they probe SM gauge bosons couplings and the high-energy dynamics of the Higgs boson. Hence, they provide a new window to the UV nature of the Higgs boson and the EW sector. Moreover, related processes have shown potential to constrain Higgs coupling modifications without a Higgs boson in the final state [161].

One of the main limiting factors in carrying on the EW precision program at the LHC is the modest number of events in many clean channels, which forces us to focus only on final states with high cross section. In particular, for the Higgs, this means that the analysis is essentially limited to the $h \to b\bar{b}$ decay mode, which implies coping with large backgrounds and a relatively complicated final state. Future high-energy hadron colliders have a big advantage from this point of view, since they provide significantly larger cross sections and a much higher integrated luminosity. This broadens the set of decay channels suitable for high-energy precision probes.

To see how significant that advantage is, let us focus for a moment on the Wh diboson channel, where the W decays leptonically. Figure 3.1 shows the leading order SM Feynman diagram (leftmost diagram). At the LHC, this channel can be exploited [160, 162, 172, 181, 182] for precision measurements by only considering decays of the Higgs into a pair of bottom quarks, especially thanks to jet substructure analysis [183]. We show in Table 3.1 the approximate number of Wh events expected in the SM for different Higgs decay channels at the LHC and future hadron colliders. These results correspond to the leading order SM prediction for the number of events with high Higgs transverse momentum ($p_T^h > 550\,\text{GeV}$). The W is assumed to decay to first and second generation leptons and only detector acceptance cuts were applied (see upper part of Table 3.6). We consider three benchmark colliders: the high-luminosity LHC (HL-LHC), at 14 TeV and $3\,\text{ab}^{-1}$, the high-energy LHC (HE-LHC), at 27 TeV and $15\,\text{ab}^{-1}$, and the FCC-hh at 100 TeV and $30\,\text{ab}^{-1}$.

One can see that rare channels, such as the ones where the Higgs decays into two photons or two muons, have branching ratios that are too small to populate the high-energy tail at HL-LHC. At future hadron colliders, instead, the situation will improve drastically thanks to a big increase in the production cross section ($\sim 30\times$) and in the integrated luminosity ($\sim 10\times$). For instance, at FCC-hh, the $\gamma\gamma$ channel is expected to provide ~ 700 events, which can allow one to probe new physics effects at the 5–10% level. Let us notice that the $\tau\tau$ channel offers a bigger number of events but the partially hadronic decay channels of the τ increase the backgrounds and hinder the final-state reconstruction.

This simple comparison already singles out the $h \to \gamma\gamma$ channel as the preferred one to study at FCC-hh, given that provides a large enough number of events and it usually has low backgrounds. The combination with a leptonic decay channel for the W boson allows for an easy reconstruction of the final state and reduces the backgrounds. Additionally, the penalty of

Higgs decay	Higgs BR	$n_{\text{HL-LHC}}$	$n_{\text{HE-LHC}}$	$n_{\text{FCC-hh}}$
$\bar{b}b$	0.6	600	$1 \cdot 10^4$	$2 \cdot 10^5$
$\tau\tau$	$6 \cdot 10^{-2}$	60	$1 \cdot 10^3$	$2 \cdot 10^4$
$\gamma\gamma$	$2 \cdot 10^{-3}$	2	40	700
$\mu\mu$	$2 \cdot 10^{-4}$	0.2	4	70
4ℓ	$1 \cdot 10^{-4}$	0.1	2	40

Table 3.1: Number of $Wh \to \ell\nu\, XX$ events predicted by the SM at LO for different Higgs decay channels and with a cut $p_T^h > 550\,\text{GeV}$. The results correspond to $3\,\text{ab}^{-1}$, $|\eta| < 2.5$ for the HL-LHC, $15\,\text{ab}^{-1}$, $|\eta| < 6$ for the HE-LHC and $30\,\text{ab}^{-1}$, $|\eta| < 6$ for the FCC-hh.

using only leptonic decays is small because the BR of massive gauge bosons, like the W and Z, to leptons is $\gtrsim 0.2$.

A process closely related to Wh is the Zh production process. Although the cross section of Zh is lower than for Wh, the Z boson has two fully leptonic decay channels, $Z \to \ell^+\ell^-$ and $Z \to \nu\bar{\nu}$, whose combination can partially compensate the cross section disadvantage. The Wh and Zh processes constitute the two channels of the more general Vh production process. During the rest of this chapter, we will explore how to use the Vh process, with the Higgs boson decaying to a pair of photons and the gauge boson decaying to leptons, to probe new physics at FCC-hh.

3.2 Effective Field Theory parametrization

We focus on small deviations from the SM that could be detected through precision measurements. Hence, it is sensible to parametrize the new-physics effects within an EFT formalism. We use the Standard Model Effective Field Theory as described in Chapter 2 and keep only dimension-6 operators in the Warsaw basis [116]. We assume that all the experiments previous to FCC-hh will not find any new particle that could modify the Vh production process. We also assume that the WCs follow the Minimal Flavour Violation (MFV) counting rules in order to fulfil automatically several flavour constraints [114]. We will dedicate part of Section 3.6 to analyse how our results depend on the cutoff of the EFT (see Fig. 3.10 and 3.12).

Table 3.2 shows all the dimension-6 operators that can modify the Vh diboson production process. The bosonic operators on the left column modify the VVh coupling, i.e. they enter the leading-order Vh amplitude as seen in the rightmost diagram in Figure 3.1. Hence, they induce effects that grow at most linearly with the energy[1], which reduces our possible sensitivity to them.

The operators in the middle column of Table 3.2 combine chiral quark, Higgs and gauge boson fields and, consequently, generate a contact interaction of the type $\bar{q}'qVh$, like the one depicted in the second-from-left diagram in Figure 3.1. The effect of this contact interaction on the Vh amplitude grows quadratically with the centre-of-mass energy of the process, improving our possible sensitivity[2]. Additionally, these operators also enter the Vh amplitude at leading order as shown by the second-from-right diagram in Figure 3.1. Nevertheless, we do not expect those five operators to have similar relevance in our analysis since $\mathcal{O}_{\varphi ud}$ is doubly suppressed by Yukawa couplings according to the MFV counting rules[3] and does not interfere with the SM

[1] Accordingly, these operators will be called sub-leading operators.

[2] From now on, we will call them leading operators.

[3] One expects this suppression to be $\sim y_u y_d$ and for the first two generations this number is $\sim 10^{-10}$ and $\sim 10^{-6}$ respectively.

Bosonic operators	$\psi^2\varphi^2 D$ operators	Dipole operators
$\mathcal{O}_{\varphi D} = \left(H^\dagger D^\mu H\right)^* \left(H^\dagger D_\mu H\right)$	$\mathcal{O}_{\varphi q}^{(3)} = \left(\bar{Q}_L \sigma^a \gamma^\mu Q_L\right)\left(iH^\dagger \sigma^a \overleftrightarrow{D}_\mu H\right)$	$\mathcal{O}_{u\mathrm{W}} = \left(\bar{q}_L \sigma^{\mu\nu} u_R\right)\tau^I \tilde{H} W^I_{\mu\nu}$
$\mathcal{O}_{\varphi \mathrm{W}} = H^\dagger H\, W^{a,\mu\nu} W^a_{\mu\nu}$	$\mathcal{O}_{\varphi q}^{(1)} = \left(\bar{Q}_L \gamma^\mu Q_L\right)\left(iH^\dagger \overleftrightarrow{D}_\mu H\right)$	$\mathcal{O}_{d\mathrm{W}} = \left(\bar{q}_L \sigma^{\mu\nu} d_R\right)\tau^I H W^I_{\mu\nu}$
$\mathcal{O}_{\varphi \widetilde{\mathrm{W}}} = H^\dagger H\, W^{a,\mu\nu} \widetilde{W}^a_{\mu\nu}$	$\mathcal{O}_{\varphi u} = \left(\bar{u}_R \gamma^\mu u_R\right)\left(iH^\dagger \overleftrightarrow{D}_\mu H\right)$	$\mathcal{O}_{u\mathrm{B}} = \left(\bar{q}_L \sigma^{\mu\nu} u_R\right)\tilde{H} B_{\mu\nu}$
$\mathcal{O}_{\varphi \mathrm{B}} = H^\dagger H\, B^{\mu\nu} B_{\mu\nu}$	$\mathcal{O}_{\varphi d} = \left(\bar{d}_R \gamma^\mu d_R\right)\left(iH^\dagger \overleftrightarrow{D}_\mu H\right)$	$\mathcal{O}_{d\mathrm{B}} = \left(\bar{q}_L \sigma^{\mu\nu} d_R\right) H B_{\mu\nu}$
$\mathcal{O}_{\varphi \widetilde{\mathrm{B}}} = H^\dagger H\, B^{\mu\nu} \widetilde{B}_{\mu\nu}$	$\mathcal{O}_{\varphi ud} = \left(\bar{u}_R \gamma^\mu d_R\right)\left(iH^\dagger \overleftrightarrow{D}_\mu H\right)$	Yukawa-like operators
$\mathcal{O}_{\varphi \mathrm{WB}} = H^\dagger \sigma^a H\, B^{\mu\nu} W^a_{\mu\nu}$		$\mathcal{O}_{u\varphi} = H^\dagger H \left(\bar{q}_L \tilde{H} u_R\right)$
$\mathcal{O}_{\varphi \widetilde{\mathrm{WB}}} = H^\dagger \sigma^a H\, B^{\mu\nu} \widetilde{W}^a_{\mu\nu}$		$\mathcal{O}_{d\varphi} = H^\dagger H \left(\bar{q}_L H d_R\right)$

Table 3.2: Dimension-6 operators of the SMEFT in the Warsaw basis that can modify the Vh diboson production process. Flavour indices are omitted.

amplitude in the massless quark limit. Therefore, its effect would be much smaller than the ones generated by the other operators of the same class and we will not include this operator in our analysis.

The right column in Table 3.2 shows dipole and Yukawa-like operators. The first ones also generate contact interactions, although with a distinctive Lorentz structure. They are MFV suppressed and do not interfere with the SM amplitude for massless quarks and hence, as with $\mathcal{O}_{\varphi ud}$, we will not include them in our analysis. Finally, the Yukawa-like operators can only modify the Yukawa coupling of the quarks and enter the Vh process via diagrams where a quark is exchanged in the t or u channels. This means they can not generate a growth with the square of the centre-of-mass energy. Moreover, they are also MFV suppressed and do not interfere with the SM for massless quarks. Those reasons justify their exclusion from our analysis.

In summary, there are only 4 linearly-independent leading operators that we will consider in our analysis:

$$\mathcal{O}_{\varphi q}^{(1)} = \left(\overline{Q}_L \gamma^\mu Q_L\right)\left(iH^\dagger \overleftrightarrow{D}_\mu H\right), \tag{3.1}$$

$$\mathcal{O}_{\varphi q}^{(3)} = \left(\overline{Q}_L \sigma^a \gamma^\mu Q_L\right)\left(iH^\dagger \sigma^a \overleftrightarrow{D}_\mu H\right), \tag{3.2}$$

$$\mathcal{O}_{\varphi u} = \left(\overline{u}_R \gamma^\mu u_R\right)\left(iH^\dagger \overleftrightarrow{D}_\mu H\right), \tag{3.3}$$

$$\mathcal{O}_{\varphi d} = \left(\overline{d}_R \gamma^\mu d_R\right)\left(iH^\dagger \overleftrightarrow{D}_\mu H\right), \tag{3.4}$$

where σ^a are the Pauli matrices. While the four of them contribute to the Zh channel, only $\mathcal{O}_{\varphi q}^{(3)}$ affects Wh. This is because, to be able to generate a vertex $\bar{q}' q W^\pm h$, the fermionic and bosonic pieces of the operator can not be gauge invariant separately. We assume flavour-universality in addition to the MFV counting. Further comments about the impact of this assumption on our results will be made at the end of this Section.

Among the sub-leading bosonic operators, only two of them can modify the Wh channel:

$$\mathcal{O}_{\varphi \mathrm{W}} = H^\dagger H\, W^{a,\mu\nu} W^a_{\mu\nu}\,, \tag{3.5}$$

$$\mathcal{O}_{\varphi \widetilde{\mathrm{W}}} = H^\dagger H\, W^{a,\mu\nu} \widetilde{W}^a_{\mu\nu} \tag{3.6}$$

where $\widetilde{W}^{a,\mu\nu} \equiv 1/2\, \epsilon^{\mu\nu\rho\sigma} W^a_{\rho\sigma}$. We include them in our analysis because we studied how being differential in angular variables allows you to be sensitive to additional sub-leading operators.

We desisted from including the bosonic operators that contribute to the Zh process. This is justified because the angular binning needed to be sensitive to them would require using only the $Z \to \ell^+\ell^-$ channel, which has a too low cross section to render a statistically significant number of events after the angular binning. Additionally, ambiguities related to the chirality of the leptons would harm the sensitivity to some of those operators [131].

It is useful to put these operators in perspective by looking at how they are generated in some common UV-completions of SMEFT. The operators in Eq. (3.1)-(3.4) can be generated at tree-level via exchange of fermionic resonances in the t or u-channels or EW-charged vector resonances in the s-channel. In accordance with the SILH power counting [113], it is expected that:

$$c_{\varphi q}^{(1),(3)} \sim c_{\varphi u,\, d} \sim g_*^2, \tag{3.7}$$

where g_* is the typical coupling of the new particles with the SM degrees of freedom. For models where the BSM sector is weakly or not directly coupled to the SM, one expects $g_* \sim g$, where g is the SM EW gauge coupling. In the fully strongly-coupled case, one expects $g_* \sim 4\pi$. The bosonic operators $\mathcal{O}_{\varphi \mathrm{W}}$ and $\mathcal{O}_{\varphi \widetilde{\mathrm{W}}}$ tend to be suppressed with respect to the other ones because they are often generated at loop level. In this case, the estimate becomes:

$$c_{\varphi \mathrm{W}} \sim c_{\varphi \widetilde{\mathrm{W}}} \sim \frac{g^2 g_*^2}{16\pi^2}. \tag{3.8}$$

In subsection 3.6.4, we will match explicitly two simple UV models onto SMEFT which follow this power-counting estimates.

However, some unusual models, generically called "remedios"-like, in which the transverse degrees of freedom of the gauge fields couple strongly to new physics, could lead to larger effects on these operators. Furthermore, $\mathcal{O}_{\varphi \mathrm{W}}$ and $\mathcal{O}_{\varphi \widetilde{\mathrm{W}}}$ could be generated at tree-level by massive vector fields $\mathcal{L}_1$ in the $\mathbf{2}_{-1/2}$ irrep of $\mathrm{SU}(2)_L \times \mathrm{U}(1)_Y$, via mixing with the Higgs $\mathcal{L}^\dagger_{1,\mu} D^\mu H$ + *h.c.* [184]. If $\mathcal{L}_1$ is the lightest new physics particle, the operators $\mathcal{O}_{\varphi \mathrm{W}}$ and $\mathcal{O}_{\varphi \widetilde{\mathrm{W}}}$ could have larger Wilson Coefficients than $\mathcal{O}^{(3)}_{\varphi q}$. However, this situation does not occur in the most common BSM scenarios. As an additional remark regarding these purely bosonic operators, let us note that whenever they are parametrically enhanced with respect to Eq. (3.8), minimal coupling imposes structural cancellations in the contributions to $h \to \gamma\gamma$ [113]. Hence, one must be careful when deriving bounds on them from Higgs precision data.

All the operators presented in this section can modify the branching-ratio of decay channels that either we will use in our analysis, as mentioned in the previous paragraph, or that have been measured with high-precision. The latter is the case of $Z \to$ hadrons, which has been determined with less than per-mille precision and is affected by the operators in Eq. (3.1)-(3.4). However, it is well justified to take the SM value of those BRs for two main reasons. First, all these BRs, even the Higgs ones, are expected to be measured with at most $\mathcal{O}(1\%)$ precision by the time FCC-hh runs [185]. Second, the effects of the operators included in our analysis can be erased via structural cancellations with other dimension-6 operators.

The additional operators needed to perform the aforementioned structural cancellations, such as $\mathcal{O}_{ll}$, $\mathcal{O}_{\varphi D}$, and $\mathcal{O}_{\varphi u}$, do not need to be considered in our study [186]. The reason for this

is that our analysis obtains its sensitivity from the shape of the p_T and angular distributions, not from the inclusive cross section value, which would represent an overall normalization in the distribution. And none of those additional operators can generate an effect that grows with the energy or changes the angular distribution.

We conclude this section with a discussion of our flavour universality assumption. The signal channels Wh and Zh are dominated by the production through initial states containing first-generation quarks. Contributions from second-generation quarks and from the bottom are suppressed by the proton parton distribution functions, and together give $\sim 20\%$ of the whole cross section[4]. Our analysis, in consequence, captures approximately the cases in which new-physics couples only to the first generation, or the case with an U(2) flavour symmetry in the first two generations.

On the other hand, the situation is potentially different for the $gg \to Zh$ process. In this case, new-physics corrections to the top-quark couplings might affect strongly the dominant loop diagrams. In the flavour universal scenario, the corrections to the top couplings are related to the ones of the light flavours and therefore they are relatively small. We checked that, for values of the Wilson coefficients of the order of our bounds ($|c^{(3)}_{\varphi q}| \sim 3\times10^{-3}$; $|c^{(1)}_{\varphi q}|, |c_{\varphi u}|, |c_{\varphi d}| \sim 2\times10^{-2}$), the corrections to the $gg \to Zh$ cross section are below 5% for $p_{T,\text{min}} = \min\{p_T^h, p_T^Z\} < 800$ GeV bins and increase to $\sim 30\%$ and $\sim 60\%$ for $p_{T,\text{min}} \in [800, 1200]$ GeV and $[1200, \infty)$ GeV respectively[5]. The impact of these corrections on the fit is negligible because this channel renders a very small number of events at FCC-hh (see subsection 3.5.2).

If the flavour universality assumption is relaxed and the top coupling modifications are allowed to be bigger, the situation could change. In that case, a dedicated analysis exploiting other processes sensitive to the top couplings, in addition to the $gg \to Zh$ channel, would be required. However, one must be aware of the fact that relaxing flavour universality could easily induce large flavour-violating effects, unless flavour symmetries or alignment assumptions are imposed.

3.3 Amplitudes and interference patterns

3.3.1 The importance of interference

Before delving into the specifics of the Vh process, let us remark some generalities about how to maximize our sensitivity to NP effects. Given a certain process with SM amplitude $\mathcal{M}_{SM}$ and a BSM contribution $\mathcal{M}_{BSM}$, its cross section will take the general shape:

$$\sigma = |\mathcal{M}_{SM}|^2 + 2\,\text{Re}\,(\mathcal{M}_{SM}\mathcal{M}^*_{BSM}) + |\mathcal{M}_{BSM}|^2, \tag{3.9}$$

where the second term on the right hand side is known as interference term. Crucially, the interference term is the only one linear on the BSM parameters, e.g. the Wilson coefficients if an EFT is used, and therefore it will tend to be the leading modification to the SM cross section for small deviations. Hence, ensuring and maximizing our sensitivity to the interference term is key to perform precision measurements.

When the BSM effects are parametrized with an EFT, the relevance of the interference term can be phrased in terms of series expansion order. Assuming one keeps in the EFT operators of dimension up to $d = 4 + n$, the interference term will be proportional to $1/\Lambda^n$, while the BSM squared piece will go as $1/\Lambda^{2n}$. This means that the BSM squared piece will be of the same order

[4]The relative contribution of each $q\bar{q}$ initial state to the total Zh cross section at LO after our selection cuts in the regime 400 GeV $< p_{T,h} <$ 600 GeV is: $u(42\%)$, $d(38\%)$, $s(9.2\%)$, $c(5.7\%)$, $b(4.7\%)$.

[5]These $p_{T,\text{min}}$ ranges correspond to the different bins that will be used in our analysis.

V polarization	SM	$\mathcal{O}_{\varphi f}$	$\mathcal{O}_{\varphi \mathrm{W}}$	$\mathcal{O}_{\varphi \widetilde{\mathrm{W}}}$
$\lambda = 0$	1	$\frac{\hat{s}}{\Lambda^2}$	$\frac{M_W^2}{\Lambda^2}$	0
$\lambda = \pm$	$\frac{M_W}{\sqrt{\hat{s}}}$	$\frac{\sqrt{\hat{s}}\, M_W}{\Lambda^2}$	$\frac{\sqrt{\hat{s}}\, M_W}{\Lambda^2}$	$\frac{\sqrt{\hat{s}}\, M_W}{\Lambda^2}$

Table 3.3: High energy behaviour of the SM and BSM helicity amplitudes for $pp \to Vh$, with $V = W, Z$. $\mathcal{O}_{\varphi f}$ stands for $\mathcal{O}_{\varphi q}^{(1)}$, $\mathcal{O}_{\varphi q}^{(3)}$, $\mathcal{O}_{\varphi u}$ and $\mathcal{O}_{\varphi d}$.

than the interference generated by operators of a higher order in the series expansion, whose exclusion should then be justified with additional UV assumptions. Those assumptions become unnecessary if the sensitivity comes mainly from the interference term.

However, the presence of the interference term should not be taken for granted, particularly in diboson processes [130]. Indeed, these processes are affected by a so-called "non-interference theorem", which states the following. In the high energy regime, $E \gg m_V$, where the amplitudes can be well characterized by the final particles helicity, $2 \to 2$ tree level amplitudes involving transversely polarized vector bosons exhibit different helicity in the SM and BSM. This implies that the interference term vanishes in inclusive analyses. Fortunately, this caveat can be overcome thanks to the use of observables that are differential in the vector boson decay angles [131]. We will discuss at extent how to use this idea in the processes of our concern in the following subsections.

3.3.2 High-energy behaviour

The first step in the discussion is to analyse how the amplitudes generated by SM and BSM operators behave at high-energies for different polarizations of the gauge boson. This is conveniently done in the helicity amplitudes formalism [187]. The leading high-energy behaviour of each helicity amplitude is shown in Table 3.3. The leading SM amplitude corresponds to a longitudinally polarized gauge boson and behaves as a constant at high centre-of-mass energy of the process, $\sqrt{\hat{s}}$, whereas the transverse polarization channels are suppressed at high energy by $1/\sqrt{\hat{s}}$.

All the dimension-6 operators that involve quarks, namely $\mathcal{O}_{\varphi q}^{(1)}$, $\mathcal{O}_{\varphi q}^{(3)}$, $\mathcal{O}_{\varphi u}$ and $\mathcal{O}_{\varphi d}$, induce a quadratic growth with the energy, i.e. of order $\hat{s}/\Lambda^2$, and the leading amplitude is the one with a longitudinally polarized gauge boson. On the other hand, the purely bosonic operators $\mathcal{O}_{\varphi \mathrm{W}}$ and $\mathcal{O}_{\varphi \widetilde{\mathrm{W}}}$ have amplitudes that grow at most with $\sqrt{\hat{s}}/\Lambda$, i.e. linearly with the energy. Furthermore, the leading amplitude for the purely bosonic operators is the one with a transversely polarized gauge boson.

As explained in Section 3.1, we want to seize on the energy growth to increase our sensitivity to the interference term between the SM and new physics amplitudes. The analysis of the high-energy behaviour of the different amplitudes performed in the previous paragraphs is not enough to determine the existence or not of a growth with energy in the interference term because the interference pattern depends on the observables.

If the observable is inclusive in the gauge boson decay products, the interference occurs only between amplitudes with the same polarization. Hence, only the operators $\mathcal{O}_{\varphi q}^{(1)}$, $\mathcal{O}_{\varphi q}^{(3)}$, $\mathcal{O}_{\varphi u}$ and $\mathcal{O}_{\varphi d}$ can generate an interference term that grows with energy. The operator $\mathcal{O}_{\varphi \mathrm{W}}$ would generate an interference term that is at most constant, and the operator $\mathcal{O}_{\varphi \widetilde{\mathrm{W}}}$ would not even

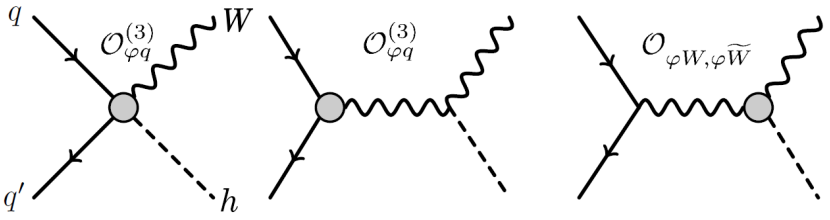

Figure 3.2: Representative Feynman diagrams for $q\,q' \to Wh$ at leading order with one insertion of dimension-6 SMEFT operators.

interfere with the SM for being CP-odd. What can be done to maximize or recover sensitivity to each of those operators is process dependent and therefore, we will discuss the Wh and Zh channels separately in the next subsections.

3.3.3 Wh channel

This channel is sensitive to the operators $\mathcal{O}_{\varphi q}^{(3)}$, $\mathcal{O}_{\varphi \mathrm{W}}$ and $\mathcal{O}_{\varphi \widetilde{\mathrm{W}}}$, which modify the amplitudes at leading order as depicted in Fig. 3.2. In consequence of what was discussed in the previous subsection, a simple binning in $\hat{s}$ is a good enough observable to make use of the growth with energy of the interference term generated by $\mathcal{O}_{\varphi q}^{(3)}$. On the other hand, the same observable is expected to probe poorly $\mathcal{O}_{\varphi \mathrm{W}}$ and $\mathcal{O}_{\varphi \widetilde{\mathrm{W}}}$ because they generate either constant or vanishing interference terms. More precisely, the leading high-energy behaviour of the SM squared amplitude and the interference terms for an analysis that bins only in $\hat{s}$ is:

$$\begin{aligned} |\mathcal{M}_{SM}|^2 &\sim \sin^2\theta\,, & \mathrm{Re}\,\mathcal{M}_{SM}\,\mathcal{M}_{\varphi \mathrm{W}}^{*} &\sim \frac{M_W^2}{\Lambda^2}\,, \\ \mathrm{Re}\,\mathcal{M}_{SM}\,\mathcal{M}_{\varphi q}^{(3)\,*} &\sim \frac{\hat{s}}{\Lambda^2}\sin^2\theta\,, & \mathrm{Re}\,\mathcal{M}_{SM}\,\mathcal{M}_{\varphi \widetilde{\mathrm{W}}}^{*} &= 0\,, \end{aligned} \tag{3.10}$$

where θ is the scattering angle of the W boson (see Fig. 3.3). We provide the full expressions for the helicity amplitudes in Appendix 3.A.1. The interference term for $\mathcal{O}_{\varphi q}^{(3)}$ above shows that most of the events will be generated in the central region, $\theta \sim \pi/2$ and, therefore it is convenient to perform the binning in p_T^h, which is correlated to $\hat{s}$.

A possible way to probe better the bosonic operators is adding a second binning in the decay angles of the W boson products. This restores the interference between different helicity and CP parity channels [131,132,169,171]. We checked the interference resurgence by computing the helicity amplitudes for $pp \to Wh \to \ell\nu h$. We provide the expressions of the interference terms and SM amplitude squared in full in Appendix 3.A.2.

Here, we present only the leading pieces in the expansion on $M_W/\sqrt{\hat{s}}$ that depend on the W decay angles:

$$\begin{aligned} |\mathcal{M}_{SM}|^2 &\sim \frac{1}{4}\sin^2\theta\sin^2\theta_W \;+\frac{M_W}{\sqrt{\hat{s}}}\mathcal{F}(\theta,\theta_W)\cos\phi_W\,, \\ \mathrm{Re}\,\mathcal{M}_{SM}\,\mathcal{M}_{\varphi q}^{(3)*} &\sim \frac{\hat{s}}{\Lambda^2}\left[\frac{1}{4}\sin^2\theta\sin^2\theta_W + \frac{M_W}{\sqrt{\hat{s}}}\mathcal{F}(\theta,\theta_W)\cos\phi_W\right], \\ \mathrm{Re}\,\mathcal{M}_{SM}\,\mathcal{M}_{\varphi \mathrm{W}}^{*} &\sim \frac{\sqrt{\hat{s}}\,M_W}{\Lambda^2}\mathcal{F}(\theta,\theta_W)\cos\phi_W\,, \\ \mathrm{Re}\,\mathcal{M}_{SM}\,\mathcal{M}_{\varphi \widetilde{\mathrm{W}}}^{*} &\sim \frac{\sqrt{\hat{s}}\,M_W}{\Lambda^2}\mathcal{F}(\theta,\theta_W)\sin\phi_W\,, \end{aligned} \tag{3.11}$$

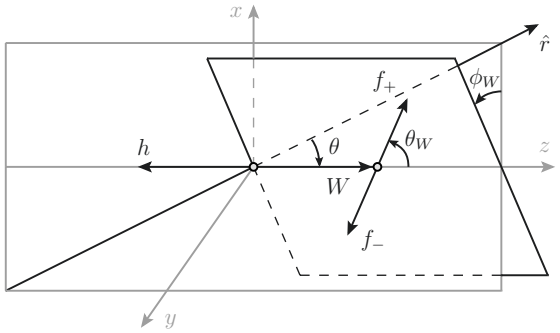

Figure 3.3: Scattering and decay angles that describe the process $pp \to Wh \to \ell\nu h$. $f_\pm$ denotes the $\pm$ helicity lepton from the W decay.

where we have defined:

$$\mathcal{F}(\theta, \theta_W) = (1 - \cos\theta\cos\theta_W)\sin\theta\sin\theta_W. \tag{3.12}$$

The scattering and decay angles involved in the previous equations are defined according to the diagram in Figure 3.3, where the reference vector $\hat{r}$ is defined as the direction of the boost of the Wh system in the lab frame. For a $2 \to 2$ scattering process, $\hat{r}$ is parallel to the beam axis. The scattering angle θ is defined as the angle between the W boson momentum and $\hat{r}$. The decay angles θ_W and ϕ_W are defined in the W rest frame and with respect to the positive helicity lepton. Due to the W coupling exclusively to left-handed fermions, the helicity of the lepton is unambiguously related to the charge sign of the charged lepton. Indeed, the charge sign agrees with the helicity sign [131].

From Equation (3.11), it is clear that the interference term between the SM and the $\mathcal{O}_{\varphi q}^{(3)}$ operator grows with energy as $\hat{s}$, even after integrating over all the decay and scattering angles. On the other hand, the interference terms generated by $\mathcal{O}_{\varphi \mathrm{W}}$ and $\mathcal{O}_{\varphi \widetilde{\mathrm{W}}}$ grow only as $\sqrt{\hat{s}}$ and provided we do not integrate over the azimuthal angle ϕ_W. The decay angle θ_W has a less profound influence and integrating over it does not change the leading energy dependence of any of these interference terms.

The interference terms from $\mathcal{O}_{\varphi \mathrm{W}}$ and $\mathcal{O}_{\varphi \widetilde{\mathrm{W}}}$ also behave differently after integrating over ϕ_W, as anticipated in the previous section. In the case of $\mathcal{O}_{\varphi \mathrm{W}}$, the remaining leading piece is constant with energy:

$$\mathrm{Re}\,\mathcal{M}_{\mathrm{SM}}\mathcal{M}^*_{\varphi \mathrm{W}} \sim \frac{g^4 c_{\varphi \mathrm{W}}}{6}\frac{M_W^2}{\Lambda^2}\left[2\,(1 - \cos\theta\cos\theta_W)^2 + \sin^2\theta\sin^2\theta_W\right], \tag{3.13}$$

where g is the $\mathrm{SU}(2)_L$ gauge coupling. On the other hand, the interference term generated by $\mathcal{O}_{\varphi \widetilde{\mathrm{W}}}$ vanishes exactly after the integration over ϕ_W. Therefore, a double binning in p_T^h and ϕ_W should allow us to be sensitive to the interference terms generated for the three studied operators and seize on their growth with energy.

However, there is a subtlety that affects this conclusion. The neutrino momentum can be reconstructed from the missing transverse momentum, the kinematics of the charged lepton and the invariant mass of their mother, but only up to a two-fold ambiguity. In the limit of high neutrino p_T, i.e. for large missing transverse momentum, this ambiguity is equivalent to the phase shift $\phi_W \to \pi - \phi_W$. This implies that, at high energies, all the terms proportional to $\cos\phi_W$ in Equation (3.11) vanish.

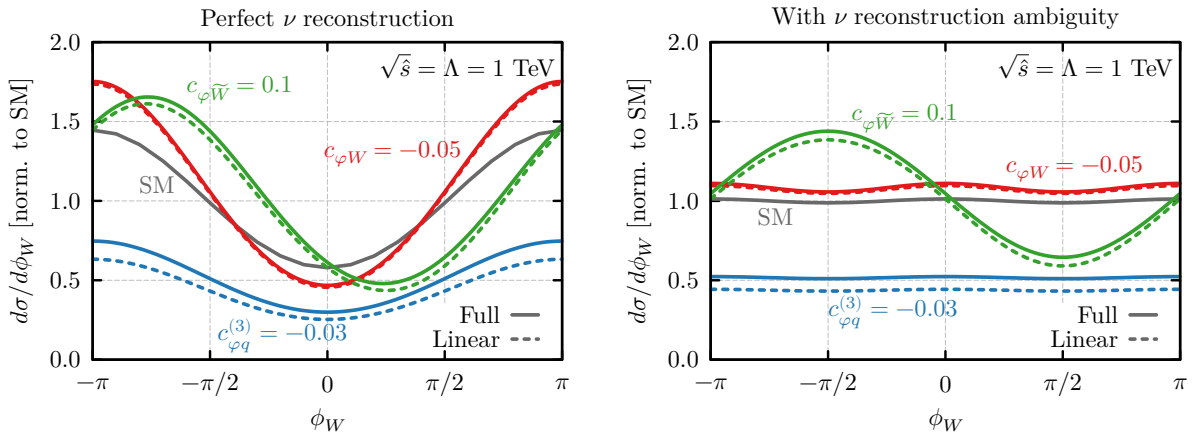

Figure 3.4: Distributions in the azimuthal angle of the W, $\sqrt{\hat{s}} = 1$ TeV and integrated over θ and θ_W. Gray lines correspond to the SM distribution, blue to $c^{(3)}_{\varphi q} = -0.03$, red to $c_{\varphi \mathrm{W}} = -0.05$, and green to $c_{\varphi \widetilde{\mathrm{W}}} = 0.1$ and we set $\Lambda = 1$ TeV. Dotted lines do not include the squared BSM terms, whereas solid lines correspond to the full amplitude. The values of the Wilson coefficients were chosen to make the figure legible and are not necessarily within the bounds reported later. **Left:** distribution with perfect neutrino reconstruction. **Right:** distribution taking into account the ambiguity in the neutrino reconstruction ($\phi_W \to \pi - \phi_W$).

Hence, the subleading terms in the squared and interference term for the SM and $\mathcal{O}^{(3)}_{\varphi q}$, and, most notably, the leading interference term between $\mathcal{O}_{\varphi \mathrm{W}}$ and the SM average to zero. On the other hand, the leading interference term for $\mathcal{O}_{\varphi \widetilde{\mathrm{W}}}$ and $\mathcal{O}^{(3)}_{\varphi q}$ are unaffected by this ambiguity. The lost sensitivity to $\mathcal{O}_{\varphi \mathrm{W}}$ could be recovered by considering the hadronic W decay channels, which allow to determine the decay angles up to an ambiguity $(\theta_W, \phi_W) \to (\pi - \theta_W, \pi - \phi_W)$ [131]. As discussed before, those channels have much larger backgrounds and require more sophisticated analysis techniques and will not be considered here.

Even if the neutrino ambiguity erases the growth with energy from the interference between $\mathcal{O}_{\varphi \mathrm{W}}$ and the SM, the situation is different from having integrated over ϕ_W. After accounting for the neutrino ambiguity, the leading piece in the $\mathcal{O}_{\varphi \mathrm{W}}$ interference is:

$$\mathrm{Re}\,\mathcal{M}_{SM}\,\mathcal{M}^{*}_{\varphi \mathrm{W}} \sim \frac{M_W^2}{\Lambda^2}\left[(1 - \cos\theta\cos\theta_W)^2 + \sin^2\theta \sin^2\theta_W \frac{(1 + \cos 2\phi_W)}{2}\right]. \tag{3.14}$$

which shows two different contributions. First, there is a term that possesses no ϕ_W dependence and comes from the interference of amplitudes with equal helicity, which can be checked by comparison with Equation (3.13). Secondly, there is an additional term proportional to $\cos 2\phi_W$ which comes from the interference between opposite transverse W polarizations. This is what generates the observed modulation in the azimuthal angle, which vanishes upon integration over it. The same effect can be observed in the interference between the SM and $\mathcal{O}^{(3)}_{\varphi q}$ by taking the part of Equation (3.43) that is constant with energy and averaging it over the neutrino ambiguity.

The effect of the neutrino ambiguity on the differential distributions with respect to ϕ_W can be seen graphically in Figure 3.4, where we have set $\hat{s} = 1$ (TeV)^2 and integrated over all the other kinematic variables, namely θ and θ_W. On the left panel, we show the distributions without taking into account the neutrino ambiguity, while on the right we plot the same distributions after averaging over ϕ_W and $\pi - \phi_W$. Full lines correspond to the full amplitude and dotted lines

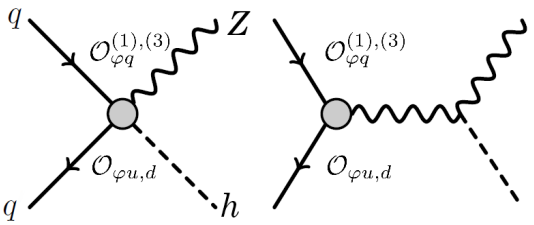

Figure 3.5: Representative Feynman diagrams for $q\,q \to Zh$ at leading order with one insertion of dimension-6 SMEFT operators.

include only the SM squared and interference pieces. From comparing them, it is clear that the squared BSM terms do not change the differential distribution sizeably in any case for the chosen values of the Wilson coefficients, which are of the same order or larger than the bounds reported in Section 3.6.5. Therefore, the effects discussed here concern mainly to the interference terms. As discussed above, the SM, $\mathcal{O}_{\varphi q}^{(3)}$ and $\mathcal{O}_{\varphi \mathrm{W}}$ distributions are almost flat when considering the neutrino ambiguity, while the $\mathcal{O}_{\varphi \widetilde{\mathrm{W}}}$ distribution is not affected by the aforementioned ambiguity and is proportional to $\sin\phi_W$.

3.3.4 Zh channel

The 4 linearly-independent dimension-6 operators that we study in the Zh channel, $\mathcal{O}_{\varphi q}^{(1)}$, $\mathcal{O}_{\varphi q}^{(3)}$, $\mathcal{O}_{\varphi u}$ and $\mathcal{O}_{\varphi d}$, modify the amplitudes at leading order as depict in Fig. 3.5. All these operators generate an effect that grows quadratically with the centre-of-mass energy. As can be seen in Table 3.3, such growth appears in the longitudinal Z polarization channel, which is also the leading one in the SM amplitude, for all those operators. The high-energy behaviour of the squared SM amplitude and the interference terms generated by the operators of our interest is:

$$\begin{aligned} |\mathcal{M}_{SM}|^2 &\sim \sin^2\theta\,, \\ \mathrm{Re}\,\mathcal{M}_{SM}\,\mathcal{M}_{\mathrm{BSM}}^{*} &\sim \frac{\hat{s}}{\Lambda^2}\sin^2\theta\,, \end{aligned} \tag{3.15}$$

where $\mathcal{M}_{\mathrm{BSM}} \in \{\mathcal{M}_{\varphi q}^{(3)}, \mathcal{M}_{\varphi q}^{(1)}, \mathcal{M}_{\varphi u}, \mathcal{M}_{\varphi d}\}$ and θ is the scattering angle of the Z boson, which is defined with the same convention used for the scattering angle of the Wh process (see Fig. 3.3). We provide the full expressions of the helicity amplitudes, the squared SM and interference terms in Appendix 3.A. Due to the growth with energy, the main BSM effects are expected to be captured by exploiting the transverse-momentum distribution which is closely related to the $\hat{s}$ distribution. An analysis that is inclusive in the decay products would yield similar sensitivity to all the considered operators.

However, stark differences in the size of the interference terms are present even though the behaviour of the BSM amplitudes is the same for all effective operators (3.1)–(3.4). This can be seen by direct inspection of the analytic expressions (see Appendix 3.A), or our numerical results, see Tables 3.C.2 and 3.C.3. To be concise, we collect the non-shared prefactors of the different interference terms in Table 3.4. From there, it is clear that the only operator that leads to a sizeable interference is $\mathcal{O}_{\varphi q}^{(3)}$, while all others suffer suppressions or cancellations.

For the right-handed operators, $\mathcal{O}_{\varphi u}$ and $\mathcal{O}_{\varphi d}$, the interference terms are suppressed since they are proportional to the coupling between the Z boson and right-handed quarks, which is significantly smaller than the one with left-handed quarks. BSM effects linear in the Wilson coefficients are therefore suppressed with respect to the SM contributions and to the quadratic BSM terms, degrading the sensitivity. In fact, with our analysis we find that, for values of the

Operator	Pre-factor	u-type quark	d-type quark
$\mathcal{O}_{\varphi q}^{(3)}$	$(-1)^{1+3Q}\dfrac{T_{3,f}-s_{\rm W}^2 Q_f}{s_{\rm W}c_{\rm W}}$	$\dfrac{\frac{2}{3}s_W^2-\frac{1}{2}}{s_W c_W}$ [−0.82]	$\dfrac{\frac{1}{3}s_{\rm W}^2-\frac{1}{2}}{s_{\rm W}c_{\rm W}}$ [−1.00]
$\mathcal{O}_{\varphi q}^{(1)}$	$\dfrac{T_{3,f}-s_W^2 Q_f}{s_W c_W}$	$\dfrac{\frac{1}{2}-\frac{2}{3}s_W^2}{s_W c_W}$ [0.82]	$-\dfrac{\frac{1}{2}-\frac{1}{3}s_W^2}{s_W c_W}$ [−1.00]
$\mathcal{O}_{\varphi u}$	$-\dfrac{s_W}{c_W}Q_f$	$-\dfrac{s_W}{c_W}\dfrac{2}{3}$ [−0.37]	-
$\mathcal{O}_{\varphi d}$	$-\dfrac{s_W}{c_W}Q_f$	-	$\dfrac{s_W}{c_W}\dfrac{1}{3}$ [0.18]

Table 3.4: Non-shared prefactors of the interference terms between the SM and the operators $\mathcal{O}_{\varphi q}^{(3)}$, $\mathcal{O}_{\varphi q}^{(1)}$, $\mathcal{O}_{\varphi u}$ and $\mathcal{O}_{\varphi u}$ in the process $q\bar{q} \to Zh$. Besides the pre-factors shown here, the interference terms have identical kinematic and parametric dependence as can be checked in Appendix 3.A. In the third and fourth columns, we show the pre-factor evaluated for up-type and down-type quarks respectively. We indicate the approximate numerical value in those cases between square brackets. The operators $\mathcal{O}_{\varphi u}$ and $\mathcal{O}_{\varphi d}$ generate interference terms where the initial state can be given by only one type of quark.

Wilson coefficients of order of the expected bounds ($c_{\varphi u} \sim c_{\varphi d} \sim 2 \times 10^{-2}$), linear and quadratic BSM corrections are roughly of the same order.

The weak isospin singlet operator, $\mathcal{O}_{\varphi q}^{(1)}$, is affected by an accidental partial cancellation between the up-type and down-type quark contributions, as can be deduced easily from Table 3.4. This cancellation arises because the SM-BSM interference term is linear in the SM coupling of the left-handed quarks to the Z. That coupling is proportional to $T_3 - s_{\rm W}^2 Q$, where T_3 is the weak isospin charge, Q the electric charge and $s_{\rm W}$ is the sine of the weak mixing angle, and has opposite sign for up-type and down-type quarks. On the other hand, the leading BSM amplitudes (see Eq. (3.51)) coming from $\mathcal{O}_{\varphi q}^{(1)}$ have the same sign for all quarks, leading to opposite-sign interference contributions for up-type and down-type quarks. The suppression is further exacerbated by the relative weight of the valence-quark content of the proton. As a result, the sensitivity to $\mathcal{O}_{\varphi q}^{(1)}$ is deeply degraded and dominated by the terms that are quadratic in the Wilson coefficients.

It is worth of mention that the operator $\mathcal{O}_{\varphi q}^{(3)}$ is not affected by the same cancellation than $\mathcal{O}_{\varphi q}^{(1)}$ due to the way its SU(2) invariance is obtained. This causes that its amplitudes with up-type and down-type quarks have opposite sign (see Eq. (3.50)), which compensates the sign change in the SM coupling.

A possible way to partially lift the cancellation that affects $\mathcal{O}_{\varphi q}^{(1)}$ is to consider the differential distribution in the rapidity of the Zh system or a correlated quantity, such as the Higgs rapidity. The rapidity distribution coming from up-type and down-type quark initiated processes is slightly different. In particular, the $u\bar{u}$ parton luminosity is peaked at larger rapidity than the $d\bar{d}$ one [188]. Hence, the cancellation can be partially undone by separating the small and large rapidity regions.

The potential of the rapidity binning to lift the cancellation is shown in Fig. 3.6, where we plot the differential cross section of the SM-$\mathcal{O}_{\varphi q}^{(1)}$ interference term with respect to the Zh rapidity (normalized to the total SM cross section) for different flavour assumptions. The solid, dash-dotted, double-dashed, and dashed curves correspond to the sum over the lightest 2, 3, 4, and 5 quarks respectively. This term changes sign around $y_{Zh} \sim 2$ because the relative contribution

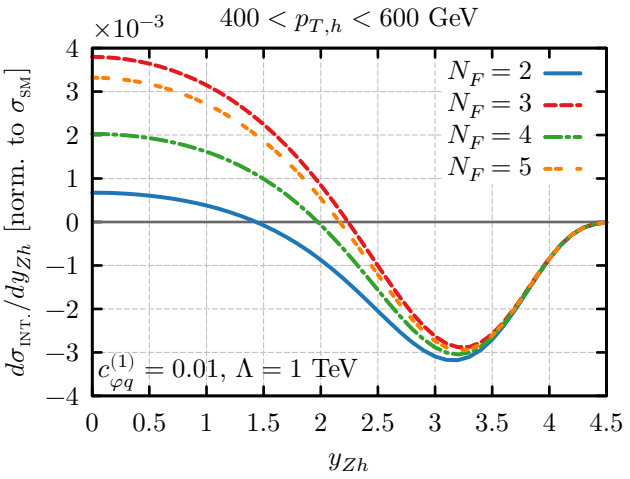

Figure 3.6: Differential distribution of the interference term, $\propto c_{\varphi q}^{(1)}$, w.r.t. the rapidity of the Zh system, y_{Zh}. The value of N_F indicates the number of initial-state flavours summed over (in PDG order). The distribution is integrated over the $p_{T,h}$ range of $[400, 600]$ GeV and $\sqrt{\hat{s}}$ over the appropriate range. The normalization factor is the SM only distribution further integrated over y_{Zh}.

between the u- and d-quark initial states depends on y_{Zh} as discussed above. The choice of N_F depends on the flavour assumption imposed on the Wilson coefficient $c_{\varphi q}^{(1)}$. The solid, $N_F = 2$, curve sums over first-generation quarks which comprise the valence quarks. For any $N_F > 2$, each down-type quark contributes positively in the central region ($|y_{Zh}| < 2$) and each up-type quark contributes negatively. The size of the contribution progressively decreases for heavier flavours. The resulting differences in the distributions could, in principle, be exploited to disentangle the flavour assumption given a clean decay channel with large statistics to sufficiently suppress the quadratic terms.

It is important to notice that performing an analysis that is differential in the Z decay angles, like the one presented in the previous section for the Wh channel, would have little to no effect in our sensitivity to the leading operators. This is because the restoration of interference between different polarization channels does not remove the discussed suppression and cancellation effects. Although an analysis differential in the Z decay angles would give sensitivity to new sub-leading operators, just like it did in the Wh channel, it would be heavily limited by statistics because of the smaller cross section of the leptonic diphotonic Zh channels. Nevertheless, they are worth considering when studying partly or fully hadronic decay channels.

To conclude this discussion, we would like to mention that, in the high energy limit, there is only one non-zero BSM-BSM interference term. This is the one between $\mathcal{O}_{\varphi q}^{(1)}$ and $\mathcal{O}_{\varphi q}^{(3)}$. All the other possible terms cancel because of different initial quark states. Therefore, we only expect sizeable correlations between $c_{\varphi q}^{(1)}$ and $c_{\varphi q}^{(3)}$.

3.3.5 Additional contributions to the signal

So far, we have discussed only the tree-level amplitudes of the Vh production channels. However, there could be additional contributions with different features arising at 1-loop level. In the case of Wh production, there are no loop-induced processes that can contribute in a sizeable way at the precision to be explored at FCC-hh. This process can be affected at EW NLO level by top operators [189], but as said before considering top-specific effects would require a dedicated

analysis that is left for future work.

On the other hand, the Zh process, thanks to the neutralness of the involved bosons, receives a non-negligible contribution from the $gg \to Zh$ process, depicted at leading order in Fig. 3.7. A sizeable dependence of this channel on the effective operators of our interest might be present, even when it is known that new-physics contributions to this channel do not grow with energy [164]. Furthermore, the SM contribution to the $gg \to Zh$ channel is suppressed, especially at high-energy, by a cancellation between the contributions from triangle-type and box-type diagrams, as shown in Ref. [190]. This cancellation could be partially removed by new-physics effects, leading to sizeable deviations in the $\hat{s}$ distributions which grow at high-energy. In fact, we checked that corrections by the operator $\mathcal{O}_{\varphi q}^{(1)}$ with a Wilson coefficient value of $c_{\varphi q}^{(1)} = 1.5 \times 10^{-2}$, which is close to the bounds we derived, range from $\sim 4\%$ in the low-energy bins up to $\sim 60\%$ in the high-energy tail.

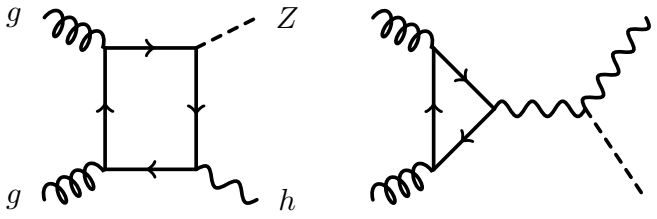

Figure 3.7: Representative Feynman diagrams for $g\,g \to Zh$ at leading order.

However, the extraction of useful information from this gluon-initiated channel can be cumbersome for several reasons. First of all, its cross section is much smaller than the leading $q\bar{q} \to Zh$ process and, in the high-energy bins, where the corrections are stronger, it contributes to less than one event at the end of the FCC-hh operation, as we will see in Section 3.5.3. Hence, special cuts would be needed to enhance its visibility. Second, the $gg \to Zh$ process depends strongly on additional dimension-6 operators, whose measurement could be not precise enough to neglect their effects. In particular, there is a strong dependence on deviations in the top Yukawa coupling. An uncertainty on its determination at $\sim 1\%$ level could easily overshadow the effects of the operators we considered. Consequently, in our analysis we will not exploit the new-physics dependence of the $gg \to Zh$ channel and we will treat it as a background, ignoring its dependence on the Wilson coefficients. Notice that there is no technical difficulty behind this choice, since this process can be properly simulated with the same tools we used for the other ones.

Finally, and beyond loop-induced processes, there is an interesting additional contribution to the Zh signal that intertwines it with the Wh channel. We characterize the final state of the $Z \to \bar{\nu}\nu$ channel by requiring a pair of photons within a certain acceptance region and missing transverse momentum. A non-negligible fraction of the events with this signature is produced by the Wh channel with a leptonically-decaying W boson, in which the charged lepton is not detected. More specifically, this happens quite often when the W boson decays into τ-leptons, while electrons and muons escape detection more rarely (see Section 3.5.3). And, as discussed previously, the Wh process depends on the operator $\mathcal{O}_{\varphi q}^{(3)}$ in such a way that its corrections grow with the energy. Hence, this will enhance the sensitivity of the Zh channel to the aforementioned operator and increase the difference in sensitivity with respect to $\mathcal{O}_{\varphi q}^{(1)}$, $\mathcal{O}_{\varphi u}$, and $\mathcal{O}_{\varphi d}$.

	Wh channel	Zh channel
MadGraph5_aMC@NLO	v.2.6.5	v.2.7.3
Pythia	v.8.2	v.8.24
Delphes	v.3.4.1	
UFO model	Built in-house	SMEFTatNLO

Table 3.5: Simulation software used for the processes involved in the Wh and Zh channels.

3.4 Collider event simulation

3.4.1 General considerations

The collider events were simulated with MadGraph5_aMC@NLO [191] using NNPDF23 parton distribution functions [192]. The parton shower and the Higgs boson decay to photons were modelled with Pythia8 [193]. Finally, the detector simulation was performed with Delphes v.3.4.1 [194–199] configured according to its FCC-hh card. In Table 3.5, we specify the version of each software we used, given that they differed slightly between the Wh and Zh channels. Performed cross-checks indicate that those differences do not generate any variation in the final results.

In the Wh channel, we used an extension of the SM UFO model [200] with the dimension-6 operators of our interest. The CP-even operators there included, $\mathcal{O}_{\varphi q}^{(3)}$ and $\mathcal{O}_{\varphi \mathrm{W}}$, were cross-checked against the LO results obtained with SMEFTatNLO [46] UFO. This latter model was used in all the simulations performed for the Zh channel. Given the different peculiarities of the two studied channels, a deeper discussion on the details of the simulations will be carried out separately in the next subsections.

3.4.2 Wh channel

Our signal process is $pp \to W(\to \ell\nu)h(\to \gamma\gamma)$. The main backgrounds for this process are $W\gamma\gamma$, $W\gamma j$, Wjj, with the jets faking a photon. The envisaged rapidity coverage of the FCC-hh detectors for charged leptons, according to its Delphes card, is $|\eta_\ell| < 6$ [24, 94]. This is large enough to consider the process $Z(\to \ell\ell)h(\to \gamma\gamma)$ with a missing lepton as a negligible background. We take the rate for a jet to fake a photon to be $P_{j\to\gamma} = 10^{-3}$. The projections for this rate are $P_{j\to\gamma} = 0.01 \exp\left(-p_T^\gamma/(30\text{ GeV})\right)$ [101] or $P_{j\to\gamma} = 0.002 \exp\left(-p_T^\gamma/(30\text{ GeV})\right)$ [24], and therefore our assumption is conservative. As we will discuss below, assuming a lower rate would not modify significantly our results.

The event samples of the processes Wh and $W\gamma\gamma$ were generated inclusively with one additional hard jet. The 0– and 1– jet samples were matched in the MLM scheme as implemented in MadGraph. The $k_\perp$-cutoff scale was set to $(1/3)\, p_{T,\,\min\{\text{bin}\}}^{\gamma\gamma}$ when generating the background and to $(1/2)\, p_{T,\,\min\{\text{bin}\}}^{h}$ for the signal process, where $\min\{\text{bin}\}$ is the lower edge of the generation bin. The main reason for this was to account for new production channels with initial gluons, which are the main responsible of non-negligible differences between LO and NLO. On the other hand, the backgrounds with at least one jet at generation level already have those channels open without the need for an additional hard jet and do not receive relevant corrections at NLO.

	Wh	$W\gamma\gamma$	$Wj\gamma$ and Wjj
$p_{T,\min}^{\ell}$ [GeV]		30 (all samples)	
$p_{T,\min}^{\gamma,j}$ [GeV]		50 (all samples)	
$\not{E}_{T,\min}$ [GeV]		100 (all samples)	
$\lvert\eta_{\max}^{j,\ell}\rvert$		6.1 (all samples)	
$\Delta R_{\min}^{\gamma\gamma,\gamma j,\gamma\ell}$	–	0.01	0.01
$\Delta R_{\max}^{\gamma\gamma,\gamma j,jj}$	–	2.5	2
$m^{\gamma\gamma,\gamma j,jj}$ [GeV]	–	[50,300]	[50,250]
$p_{T,\min}^{h,\gamma\gamma}$ [GeV]	{150,350,550,750}	{100,300,500,700}	–
$p_{T,\min}^{\ell\nu}$ [GeV]	–	–	{100,300,500,700}

Table 3.6: Parton level generation cuts for the signal and background processes in the Wh channel. Each element in the list of values for $p_T^{h,\gamma\gamma}$ and $p_T^{\ell\nu}$ corresponds to the cut used in 4 different generation runs. Each run was used in the analysis of the corresponding p_T^h bin. The last generation bin is used for both the fourth and fifth (overflow) bin.

Regarding the signal process, fully differential corrections to Wh production have been computed previously, including mass effects and matched to a parton shower [201–205]. Generically, the NNLO/NLO k-factors as a function of p_T^h are small ($< 10\%$). The same is also true of the NLO/LO k-factors if the LO is showered. In our case, with the $0+1j$ matched sample, the NLO/$0+1j$ k-factor is $25-50\%$ but this difference comes mainly from the choice of PDFs. As mentioned above, we used `NNPDF23LO` for the $0+1j$ sample. However, at NLO, we used the `NNPDF23NLO` PDFs for consistency. The NLO/$0+1j$ k-factor becomes $\leq 10\%$ if one generates the $0+1j$ sample using the NLO PDFs.

The inclusive electroweak (EW) corrections to the Wh process were computed in [206] and the fully-differential corrections, in [207, 208]. They were included in `MG5_aMC@NLO` in [209]. While EW corrections are known to be large for large p_T^h, their effect on our analysis is $\lesssim 20\%$; nevertheless, we applied the k-factors extracted from [209] to the signal process. The recomputed k-factors in our first four p_T^h bins defined in Eq. (3.16) are $\{0.92, 0.85, 0.79, 0.73\}$ while we applied an estimated k-factor of 0.6 in the overflow ($p_T^h > 1$ TeV) bin. As we will see in Section 3.6, the overflow bin does not contribute to the bound and therefore does not warrant a more careful estimate.

In order to increase the number of Monte Carlo events that survive the selection cuts in our analysis, we imposed several basic cuts at generation level which we list in Table 3.6. On the upper part of Table 3.6, we show the cuts common to all the processes and bins. Those cuts that are specific to each process and bin are shown on the lower part of the table. The bin-specific cuts are done in order to increase the number of Monte Carlo events falling in each p_T^h bin of our analysis, without cutting any events that could pass the detector simulation and subsequent selection cuts. The generation cuts are not one to one with the p_T^h bins, because this quantity is shifted due to showering.

For illustration, we show in Table 3.7 the cross section before and after the generation cuts

	$h \to \gamma\gamma$	$\gamma\gamma$	$j\gamma$	jj
$\sigma_{\text{(loose)}}$ [fb]	7.5	$4.8 \cdot 10^3$	10^6	$6.2 \cdot 10^7$
$\sigma_{(3^{\text{rd}} \text{ bin gen. cuts})}$ [fb]	0.026	2.9	$3.0 \cdot 10^2$	$5.2 \cdot 10^3$

Table 3.7: Parton level cross sections for signal and backgrounds in the Wh channel, before and after imposing the generation level cuts defined in Table 3.6. Signal and $\gamma\gamma$ were generated at $(0{+}1j)$, while $j\gamma$ and jj are LO. We only show the cross section after generation cuts for the third bin. See text for more details. The subscript 'loose' refers to the mild cuts we had to impose to regulate infrared divergences. We employed the cuts $p_T^{j,\gamma} > 20\,\text{GeV}$ for all the four processes, $m_X > 20\,\text{GeV}$ for the process $pp \to \ell\nu X$, $\Delta R_{\text{min}}^{\gamma j,\gamma\ell} = 0.01$ for $X = \gamma\gamma$ and $\Delta R_{\text{min}}^{\gamma\ell} = 0.01$ for $X = \gamma j$.

described in Table 3.6. After the generation cuts, we only give the results for the events in the third generation bin, since it is the most sensitive one as a showcase example. Notice that the generation cuts are slightly different for each process, therefore the interpretation of the relative size of the cross sections before and after generation cuts must be made carefully.

3.4.3 Zh channel

The signal process is $pp \to Z(h \to \gamma\gamma)$, with the Z boson decaying either into a pair of charged leptons, $Z \to \ell^+\ell^-$ (with $\ell = e, \mu$), or into neutrinos, $Z \to \nu\bar{\nu}$. The channel in which the Z boson decays hadronically suffers from a much larger background and requires a more sophisticated analysis strategy that we leave for future work. Given the similarities between the studied decay channels, we will discuss their generation altogether, specifying their differences when needed.

The signature given by the signal process in the $Z \to \nu\bar{\nu}$ decay channel is a pair of photons and sizeable missing transverse momentum. As we mentioned in Section 3.3.5, the additional process $q\bar{q} \to W(\to \ell\nu)\, h(\to \gamma\gamma)$ where the charged lepton is not reconstructed contributes to the same final state and must be considered as part of the signal, since it depends on the $\mathcal{O}_{\varphi q}^{(3)}$ operator. In particular, the main contribution comes from events where $W \to \tau\nu_\tau$, see Section 3.5.3 for details. On the other hand, the signature of the signal in the $Z \to \ell\ell$ channel is a pair of photons and a pair of charged leptons. There are no additional contributions to the signal beyond Zh production in this channel.

All the processes contributing to the signal in both decay channels were simulated at LO in QCD. NLO QCD and EW corrections were taken into account through k-factors. NLO corrections turn out to be sizeable, but with a weak dependence on new-physics. It is thus a good approximation to rescale the cross section in each bin by the SM NLO k-factors. We give more details on the computation of these k-factors in Appendix 3.B and their value is given in Table 3.B.1. As expected, they follow a very similar pattern for both Z decay channels and for the Wh process. Notice that this procedure to generate the signal could not be performed in the Wh channel because the operator $\mathcal{O}_{\varphi\widetilde{W}}$ is not implemented at NLO and therefore we could not check its influence on the QCD k-factors.

We also take into account the $gg \to Zh(\to \gamma\gamma)$ production channel at LO in both Z decay channels. According to the discussion in Section 3.3.5, we neglect new-physics contributions and treat this process as a background.

The main backgrounds for the neutrino channel come from the processes $Z(\to \nu\bar{\nu})\,\gamma\gamma$ and $W(\to \ell\nu)\,\gamma\gamma$, where the charged lepton is missed and the photon pair is non-resonantly produced. We checked that the $j\gamma\gamma$ process in which missing transverse momentum comes from showering

	$Z \to \nu\bar{\nu}$	$Z \to \ell^+\ell^-$
$p^{\ell}_{T,\min}$	0	30^a
$\lvert\eta^{\ell}_{max}\rvert$	∞	6.1
$p^{\gamma}_{T,\min}$ [GeV]	50^b	
$\lvert\eta^{\gamma}_{max}\rvert$	6.1^c	
$\Delta R^{\ell\ell,\gamma\ell}_{\min}$	0.01	
$\Delta R^{\gamma\gamma}_{\min}$	0.25^d	
p^{V}_{T}	$\{0, 200, 400, 600, 800, 1200, \infty\}$	

Table 3.8: Parton level generation cuts for signal and background processes in the Zh channel. p^V_T denotes the gauge boson p_T. ^{a}: only applied to QCD LO runs. ^{b}: not applied to the photons produced by a Higgs decay. ^{c}: not applied to the photons coming from a Higgs boson. ^{d}: set to 0.01 in QCD LO runs.

and detector effects, constitutes a huge background at low energy, but becomes negligible when a 200 GeV cut on the missing transverse momentum is imposed.

For the leptonic channel, the main background process is $Z(\to \ell^+\ell^-)\gamma\gamma$, with a small additional contribution from processes in which the lepton pair arises from the splitting of a virtual photon. This contribution can be suppressed by restricting the di-lepton invariant mass to be around the Z-pole.

While processes where a gauge boson decays to τ-leptons play an important role in the $Z \to \nu\bar{\nu}$ channel as discussed above, they are mostly irrelevant in the $Z \to \ell\ell$ channel. We estimate that the $Z \to \tau\tau$ decay channel contribution would increase both the signal and background cross sections of the $Z \to \ell\ell$ channel in at most 5%. The impact of such change on our results would be negligible, therefore we do not include the τ- decay channel in our simulations.

Regardless the Z decay channel, additional contributions from events in which one or two jets fake a photon are negligible if we assume a $P_{j\to\gamma} = 10^{-3}$ jet-to-photon fake rate [24, 101] (see discussion in Section 3.4.2). Consequently, we do not consider processes with less than 2 photons as part of the background.

All the backgrounds were generated at NLO in QCD. This is particularly important for the $W(\to \ell\nu)\gamma\gamma$ and $Z\gamma\gamma$ channels. In the former, the cross section is fully dominated by the NLO contribution with a real emission (which is a factor ~ 17 larger than the LO contribution). Similarly, the NLO contributions for the $Z\gamma\gamma$ channel are a factor ~ 2 larger than the LO ones. The enhancement is partly due to the fact that at NLO an additional channel with an initial gluon instead of a sea quark opens up, as also discussed in Section 3.4.2. As we will see in Section 3.5.3, the presence of a large component of events with an additional jet significantly modifies the kinematic configuration of the events, providing efficient handles to distinguish the background processes from the signal.

As we did with the Wh process, we applied a set of generation level cuts to increase the number of Monte Carlo events after the selection cuts in our analysis. The generation cuts used for the different processes involved in the Zh channel are shown in Table 3.8. There, the second (third) column shows the values used for all the processes relevant for the $Z \to \nu\bar{\nu}$ ($Z \to \ell^+\ell^-$) decay channel. Furthermore, we generated the events in 6 exclusive bins in the p_T of the gauge boson. We notice that, due to initial state radiation effects, a sizeable migration of events between generation and $p_{T\,\min}$ bins is present.

3.5 Event selection and analysis

3.5.1 Selection cuts

We have to consider three processes with distinguishable final states: $W(\to \ell\nu)h$, $Z(\to \ell\ell)h$ and $Z(\to \nu\bar{\nu})h$, with $h \to \gamma\gamma$ in all of them. Due to their similarity, there are several selection cuts which are shared among them.

In particular, the Higgs boson reconstruction was performed exactly in the same way. We require the event to have at least 2 photons with $p_T^\gamma > 50$ GeV and $|\eta^\gamma| < 6$. Furthermore, the photon pair must have an invariant mass within the range $[120, 130]$ GeV. If there is more than one pair of photons that fulfils the previous conditions, we select the pair with the smallest angular separation, $\Delta R^{\gamma\gamma} = \sqrt{(\Delta\phi_{\gamma\gamma})^2 + (\Delta\eta_{\gamma\gamma})^2}$. We checked that the effect of radiated photons on this reconstruction procedure is negligible. We also verified that the alternative criteria of choosing the pair of hardest photons[6] gives almost equal results.

Electrons and muons are accepted if they have $p_T^{e,\mu} > 30$ GeV and $|\eta^{e,\mu}| < 6$. The required number of accepted leptons depends on the process. For Wh, we required 1 charged lepton within the acceptance region; for $Z(\to \nu\bar{\nu})h$, we ask for 0 charged leptons in such a region; and for $Z(\to \ell\ell)h$, we ask for exactly 2 leptons with opposite charges. Accordingly, the reconstruction of the gauge boson is different in each case.

In the $Z \to \ell\ell$ case, the Z momentum is directly reconstructed from the charged lepton pair and we require its invariant mass to fulfil 81 GeV $\leqslant m^{\ell\ell} \leqslant$ 101 GeV to suppress the photon-mediated background, as discussed in Section 3.4.3. The $Z \to \nu\bar{\nu}$ decay channel allows us to only reconstruct the transverse momentum of the Z boson by assigning it to the total missing transverse momentum.

On a middle ground, the W boson in the Wh process is reconstructed from both the charged lepton and the missing transverse energy, which is interpreted as coming completely from the neutrino. Imposing the reconstruction of the W invariant mass allows us to reconstruct the neutrino four-momentum up to a two-fold ambiguity previously discussed in Section 3.3.3. Only for the Wh process, we also require the events to have $\not{E}_T > 100$ GeV.

In order to further reduce the backgrounds, we impose a maximum cut on the transverse momentum of the reconstructed Vh system, $p_T^{Vh} < p_{T,\max}^{Vh}$. This is motivated by the fact that a large transverse momentum is typically due to the recoil against a hard QCD jet instead of the energy growth produced by BSM physics effects. Events with this signature are more likely to come from background processes than from the signal. The value of $p_{T,\max}^{Vh}$ depends on the process and on the p_T binning, which will be described in the next section, such that the efficiency of this cut is maximized. The chosen values can be found in Table 3.9.

Finally, in the Wh process we imposed a maximum angular separation cut on the photon pair, $\Delta R^{\gamma\gamma} < \Delta R_{\max}^{\gamma\gamma}$. This cut is justified on the fact that the background photon pair is non-resonant and hence it tends to have a larger $\Delta R^{\gamma\gamma}$ than the one that originates from the boosted Higgs. The value of $\Delta R_{\max}^{\gamma\gamma}$ depends on the bin of p_T^h to improve the efficiency of the cut and the specific values can be found in Table 3.9. We checked the usefulness of this cut and its analogous for leptons, $\Delta R^{\ell\ell} < \Delta R_{\max}^{\ell\ell}$ for the Zh process. We found that, after the cuts on the invariant masses, the ΔR distributions for signal and backgrounds were very similar and as a result, they did not improve the bounds. Hence, they were discarded for the analysis of the Zh process. We summarize all the selection cuts for all processes in Table 3.9.

[6] By hardest, we mean highest p_T.

	Wh	$Z(\to \nu\bar{\nu})h$	$Z(\to \ell\ell)h$
$p^{\ell}_{T,\text{min}}$[GeV]	30		
# of leptons	1	0	2
$p^{\gamma}_{T,\text{min}}$ [GeV]	50		
$\not{E}_{T,\text{min}}$[GeV]	100	-	
$m^{\gamma\gamma}$ [GeV]	$[120, 130]$		
$m^{\ell\ell}$ [GeV]	-		$[81, 101]$
$\Delta R^{\gamma\gamma}_{\text{max}}$	$\{1.3, 0.9, 0.75, 0.6, 0.6\}$	-	
$p^{Vh}_{T,\text{max}}$ [GeV]	$\{300, 500, 700, 900, 900\}$	$\{200, 600, 1100, 1500, 1900\}$	

Table 3.9: Summary of selection cuts. The entries for $\Delta R^{\gamma\gamma}_{\text{max}}$ and $p^{Vh}_{T,\text{max}}$ in the Wh channel correspond to the different p^h_T bins defined in Eq. (3.16). The entries for $p^{Vh}_{T,\text{max}}$ in the Zh channel correspond to the $p_{T,\text{min}}$ bins defined in Eq. (3.18).

3.5.2 Binning

The detailed analysis of interference patterns in Section 3.3 showed the need of different binning strategies for the Wh and Zh channels. This need is reinforced by the fact that in the Wh channel we are interested in two sub-leading dimension-6 operators and our sensitivity to them depends crucially on the binning in an angular variable. However, both channels share an underlying binning on the transverse momentum, that is correlated with the centre-of-mass energy of the process and yields most of the sensitivity to the leading operators. We detail the different chosen binning strategies in the next subsections.

The Wh channel

As discussed in Section 3.3.3, to maximize the sensitivity to the three operators of interest we need to select events with large Wh invariant mass and be differential in the azimuthal angle of the leptons, ϕ_W, in order to have linear sensitivity to the CP-odd operator. Since BSM physics effects are largely in the central scattering region, it is convenient to perform a binning in the p^h_T variable, which is correlated with $\sqrt{\hat{s}}$, and is easier to reconstruct accurately. In our analysis we use bins with their borders given by,

$$\begin{aligned} p^h_T &\in \{200, 400, 600, 800, 1000, \infty\}\,\text{GeV}\,, \\ \phi_W &\in [-\pi, 0]\,,\ [0, \pi]\,. \end{aligned} \tag{3.16}$$

With this choice, the overflow p^h_T bin contains $\mathcal{O}(10)$ SM events for $30\,\text{ab}^{-1}$ of integrated luminosity. The number of SM events per p^h_T bin after all the selection cuts is shown in Fig. 3.8 for both the signal and the backgrounds. A detailed discussion of that figure is postponed until subsection 3.5.3. To efficiently populate the five p^h_T bins in Eq. (3.16), we generated four runs with a cut on p^h_T or a proxy for it in the case of backgrounds, see discussion in Section 3.4.2.

The binning in ϕ_W is chosen to enhance the sensitivity to $\mathcal{O}_{\varphi\widetilde{\text{W}}}$ by recovering its interference with the leading SM amplitude. On the other hand, no sizeable improvement is possible for $\mathcal{O}_{\varphi\text{W}}$

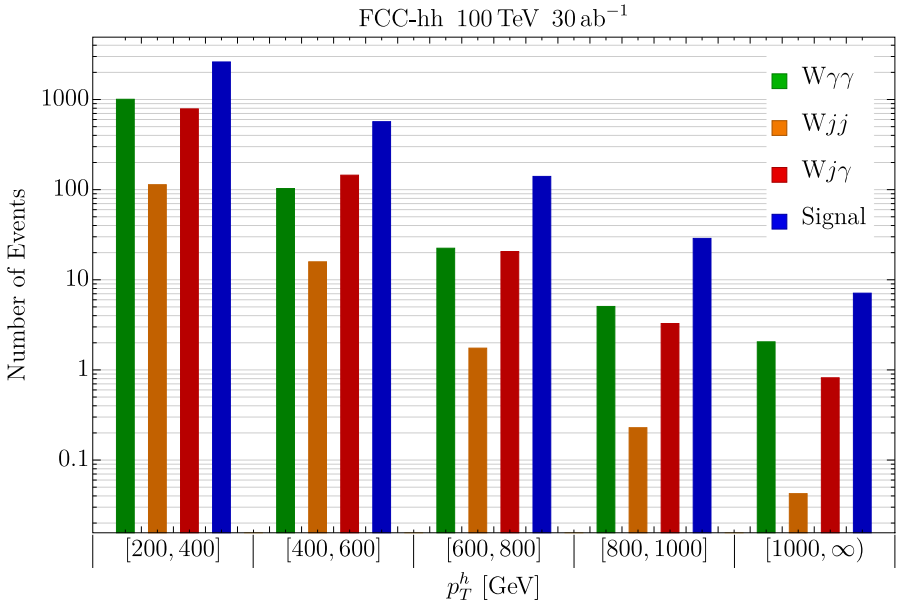

Figure 3.8: Number of SM events per p_T^h bin after selection cuts for the signal and backgrounds in the Wh channel at the FCC-hh assuming 30 ab^{-1}.

because of the neutrino ambiguity, as discussed in Section 3.3.3.

The Zh channels

In the Zh channels, we consider the double-differential distribution in the centre-of-mass partonic-energy and in the rapidity of the events, in accordance to the discussion in Section 3.3.4. As can be seen from Eq. (3.15), the signal events are mostly emitted in the central scattering region. We can therefore approximately trade the event energy for the transverse momentum of the Z or Higgs. Both of these can be reconstructed in the two decay channels we consider. We choose to bin in the minimum p_T of the two bosons:

$$p_{T,\text{min}} = \min\{p_T^h, p_T^Z\}\,, \tag{3.17}$$

where, in the neutrino channel, p_T^Z is identified with the missing transverse momentum. This choice is useful to select hard events in the Zh centre-of-mass frame and, simultaneously, to remove the $j\gamma\gamma$ background where the missing energy comes from soft radiation. We use five bins in $p_{T,\text{min}}$, whose boundaries are given by

$$p_{T,\text{min}} \in \{200, 400, 600, 800, 1000, \infty\}\ \text{GeV}\,. \tag{3.18}$$

The number of events at FCC-hh in each $p_{T,\text{min}}$ for the SM signal and background processes in each Z decay channel is shown in Fig. 3.9, which will be discussed in detail in subsection 3.5.3.

In the $Z \to \ell^+\ell^-$ channel, we also use a simple binning in the rapidity of the Zh system y_{Zh}, namely

$$|y_{Zh}| \in [0, 2], [2, 6]. \tag{3.19}$$

We can not use such binning in the $Z \to \nu\bar{\nu}$ channel because the rapidity of the Zh system can not be determined. Instead, we bin in the rapidity of the Higgs y_h, which is strongly correlated

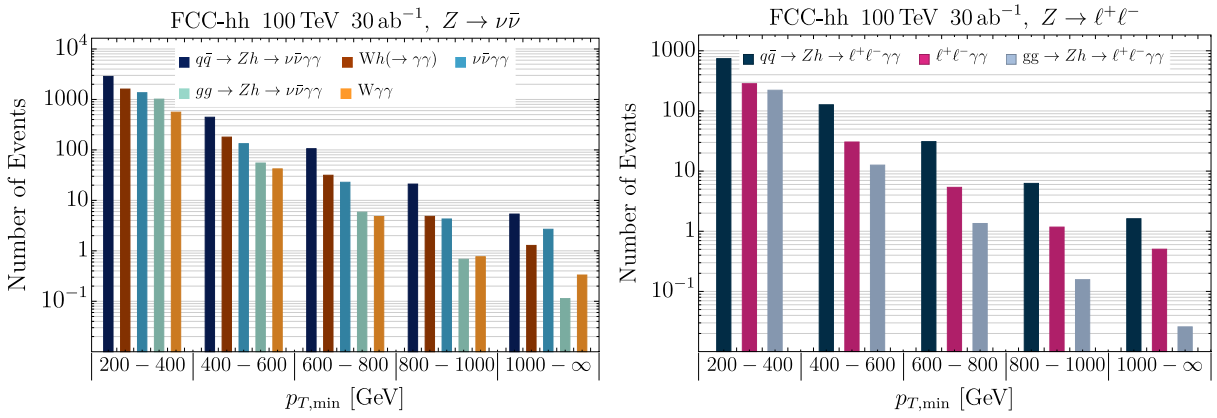

Figure 3.9: Number of SM events per $p_{T,\min}$ bin after selection cuts for the signal and backgrounds in the Zh channel at the FCC-hh assuming $\mathcal{L} = 30$ ab^{-1} integrated luminosity. Left (right) panel: for the decay channel $Z \to \nu\bar{\nu}$ ($Z \to \ell^+\ell^-$). The bins are defined according to $p_{T,\min}$.

Selection cuts / efficiency	Wh	$W\gamma\gamma$	$Wj\gamma$	Wjj
$\geq 1\ell^{\pm}$ with $p_T > 30$ GeV	0.86	0.46	0.94	0.94
$\geq 2\gamma$ each with $p_T > 50$ GeV	0.50	0.18	$5.7 \cdot 10^{-3}$	$8.7 \cdot 10^{-7}$
$\not{E}_T > 100$ GeV	0.49	0.16	$5.1 \cdot 10^{-3}$	$8.5 \cdot 10^{-7}$
120 GeV $< m_{\gamma\gamma} <$ 130 GeV	0.46	$6 \cdot 10^{-3}$	$2 \cdot 10^{-4}$	$8.2 \cdot 10^{-8}$
$\Delta R^{\gamma\gamma} < \Delta R_{max}$	0.45	$4 \cdot 10^{-3}$	$3.1 \cdot 10^{-5}$	$6.4 \cdot 10^{-8}$
$p_T^{Wh} < p_{T,max}^{Wh}$	0.41	$7 \cdot 10^{-4}$	$1.1 \cdot 10^{-5}$	$4.7 \cdot 10^{-8}$

Table 3.10: Cutflow efficiency of the selection cuts for the processes in the Wh channel. This table was computed using only the third p_T^h bin at generation level to focus on the events most sensitive to BSM effects.

with y_{Zh}. The bin definitions depend on $p_{T,\min}$ as follows:

$$|y_h| \in \begin{cases} [0,2],\,[2,6] & \text{for} \quad 200 < p_{T,\min} < 600\ [\text{GeV}]\,, \\ [0,1.5]\,,[1.5,6] & \text{for} \quad 600 < p_{T,\min} < 800\ [\text{GeV}]\,, \\ [0,1]\,,[1,6] & \text{for} \quad p_{T,\min} > 800\ [\text{GeV}]. \end{cases} \tag{3.20}$$

3.5.3 Cut efficiencies

In this section, we evaluate the effectiveness in suppressing the backgrounds of the selection cuts described in Section 3.5.1. We analyse how the different topologies present in the background processes required the use of complementary cuts. Due to small differences in the generation-level cuts of the different processes (see Section 3.4 and in particular Tables 3.6 and 3.8), the starting phase volumes differ slightly. Nevertheless, this analysis provides a good idea of the effect of the different cuts.

We start analysing the Wh channel. In Table 3.10, we show the cutflow analysis for the third p_T^h bin and all the processes considered in the Wh channel. From Table 3.10, it is clear that the

Cuts / Efficiency	$q\bar{q} \to Zh$	Wh	$W\gamma\gamma$	$Z\gamma\gamma$	$gg \to Zh$
0 $\ell^\pm$ in acc. region	1	0.30	0.44	1	0.97
$\geq 2\,\gamma$ in acc. region	0.60	0.19	0.30	0.72	0.60
$m_{\gamma\gamma} \in [120, 130]\,\text{GeV}$	0.58	0.17	7.7×10^{-3}	1.3×10^{-2}	0.59
$p_{T,\text{min}} \geq 400$ GeV	0.42	0.061	6.9×10^{-4}	2.9×10^{-3}	0.37
$p_T^{Zh} \leq p_{T,max}^{Zh}$	0.40	0.057	1.1×10^{-4}	2.8×10^{-3}	0.33

Table 3.11: Cutflow efficiency of the selection cuts for the processes in the $Z \to \nu\bar{\nu}$ channel. The acceptance region for charged leptons and photons is defined in the text. This table was computed using only events with $p_T^V > 400$ GeV at generation level to focus on the events most sensitive to BSM effects.

Cuts / Efficiency	$q\bar{q} \to Zh \to \ell^+\ell^-\gamma\gamma$	$Z\gamma\gamma \to \ell^+\ell^-\gamma\gamma$	$gg \to Zh \to \ell^+\ell^-\gamma\gamma$
2 $\ell^\pm$ in acc. region	0.85	0.74	0.75
$\geq 2\,\gamma$ in acc. region	0.51	0.54	0.46
$m_{\gamma\gamma} \in [120, 130]$ GeV	0.50	9.4×10^{-3}	0.45
$m_{l^+l^-} \in [81, 101]$ GeV	0.47	8.8×10^{-3}	0.42
$p_{T,\text{min}} \geq 400$ GeV	0.35	2.2×10^{-3}	0.26
$p_T^{Zh} \leq p_{T,max}^{Zh}$	0.33	2.1×10^{-3}	0.23

Table 3.12: Cutflow efficiency of the selection cuts for the processes in the $Z \to \ell^+\ell^-$ channel. The acceptance region for charged leptons and photons is defined in the text. This table was computed using only events with $p_T^V > 400$ GeV at generation level to focus on the events most sensitive to BSM effects.

cut on the photon pair invariant mass, $m^{\gamma\gamma}$ is highly effective and reduces the backgrounds in at least one order of magnitude. The cut on p_T^{Wh} also shows a great effectiveness and reduces the $W\gamma\gamma$ ($Wj\gamma$) process by a factor of 5 (3) respectively. In the case of the $W\gamma\gamma$ channel, this is a direct consequence of the big contribution given by the QCD correction with a real emission.

Figure 3.8 shows the expected number of SM events in each p_T^h bin for the signal and background processes after applying all the selection cuts. From there, it is clear that $W\gamma\gamma$ and $Wj\gamma$ are the dominant backgrounds. Their size is roughly a third of the signal in the first bin and gradually decreases to around 10% of the signal in the last bin. The Wjj background is at least one to two orders of magnitude smaller than the signal and, therefore, it can be safely neglected. We stress that the overall background is very low, especially in the higher p_T^h bins, and hence the selection cuts are highly effective.

We also remark that the exact background projections for $Wj\gamma$ and Wjj depend crucially on the jet fake rate into photons and therefore is highly sensitive to the detector performance. The importance of this fake rate in suppressing these backgrounds can be seen in the second line of Table 3.10, where the photon-acceptance cut reduces these backgrounds by several orders of magnitude. Nonetheless, given that even after taking a very conservative estimate for the fake rate, as previously discussed in Section 3.4.2, the backgrounds are much smaller that the signal; we do not expect our bounds to change noticeably even if the fake rate is further reduced.

Focusing now on the Zh channel, we show in Tables 3.11 and 3.12 the cutflow analysis for the $Z \to \nu\bar{\nu}$ and $Z \to \ell^+\ell^-$ decay channels respectively. For this analysis, we only considered events that satisfy the generation-level cut $p_T^V > 400$ GeV and that populate all but the first $p_{T,\text{min}}$ bins in order to focus on those events that show a good sensitivity to BSM physics effects.

The cut on the invariant mass of the photon pair is as effective as it was in the Wh channel in reducing the contribution from channels with non-resonant photon pairs, i.e. $W\gamma\gamma$ and $Z\gamma\gamma$. Analogously, the cut on the lepton-pair invariant mass $m^{\ell^+\ell^-}$ is useful to reduce the $\ell^+\ell^-\gamma\gamma$ background component in which the lepton pair is generated by an off-shell photon. Such channel becomes completely negligible after the selection cuts, so we did not include it in Table 3.12, where only the $Z\gamma\gamma \to \ell^+\ell^-\gamma\gamma$ channel is listed.

In the neutrino channel, the charged-lepton veto reduces the cross section of the Wh and $W\gamma\gamma$ channels by only $60-70\%$. This behaviour, which might seem surprising at first sight, is mainly due to the $W \to \tau\,\nu_\tau$ decay channel, in which the τ decays hadronically. On the other hand, when the W decays to light leptons, the cut is much more effective, with a reduction of the events of 96% for decays with an electron and 98% for decays with a muon.

However, a large fraction of the events with hadronically decaying taus is removed by the cuts on $p_{T,\text{min}}$ and p_T^{Zh}. The reason for this is twofold. First, the jets from the τ decay carry sizeable fraction of the τ momentum, thus creating an unbalance between the missing transverse momentum and the photon pair p_T. And, second, in the $W\gamma\gamma$ channel, a vast majority of the events come from the NLO contribution with an additional extra jet. In such events, a large transverse momentum p_T^{Zh} is present. This phenomenon was already observed in the analysis of the Wh channel.

Finally, the $p_{T,\text{min}}$ cut is highly effective in suppressing the $Z\gamma\gamma$ background in both decay channels. The underlying reason is the same one that explains the effectiveness of p_T^{Zh} with $W\gamma\gamma$: most of the events ($\sim 65\%$) come from the NLO contribution with an additional hard jet.

The number of expected SM events at the FCC-hh in each $p_{T,\text{min}}$ bin for the signal and background processes in the Zh channels are shown in Figure 3.9. The figure shows the number of events after summing over the rapidity bins. The number of signal and background events in all bins used in the analysis can be found in Tables 3.C.2 and 3.C.3 in Appendix 3.C, together with the signal cross-section dependence on the Wilson coefficients.

In the neutrino channel, the Wh process gives remarkably a significant contribution to the signal with a number of events of the same order of magnitude than the Zh process. This happens despite the much lower efficiency of the Wh process to pass the selection cuts with respect to Zh, as can be seen from Table 3.11. The suppression is, nevertheless, partially compensated by the significantly higher initial cross section. Moreover, the dependence on $c_{\varphi q}^{(3)}$ of the Wh process is stronger than in Zh, due to accidental numerical factors in the new-physics amplitude. For this reason, the Wh channel can enhance, up to $\sim 50\%$, the dependence of the signal cross section on $c_{\varphi q}^{(3)}$, as can be seen by comparing the results in Tables 3.C.2 and 3.C.3.

The main background in the neutrino channel is $Z\gamma\gamma \to \nu\bar{\nu}\gamma\gamma$, followed by $W\gamma\gamma$. In most of the $p_{T,\text{min}}$ bins, the backgrounds are much smaller than the signal, making the analysis almost background free. The only exceptions are the first bin, where however the dependence on new physics is small, and the last one, where the number of events is quite limited. Finally, the $gg \to Zh$ process contributes with a quite small number of events, so that its dependence on new physics can be safely neglected.

In the $Z \to \ell^+\ell^-$ decay channel, the main background is the $Z\gamma\gamma \to \ell^+\ell^-\gamma\gamma$ process and is much smaller than the signal in all bins. Analogously to the neutrino channel, the $gg \to Zh$ has an almost negligible impact especially in the higher $p_{T,\text{min}}$ bins.

3.6 Results

In this section, we present our projection of the bounds on the Wilson coefficients. For our statistical analysis, we assume that the likelihood function is Gaussian and do a χ^2 analysis. The Gaussian assumption is justified since we do not have any bin with less than $\mathcal{O}(10)$ events,

for which the Gaussian approximation is already very good. This also allows us to compute 95% C.L. bounds by solving $\Delta\chi^2 = 3.84$.

The χ^2 function is constructed with the number of signal and background events, the former as a function of the Wilson coefficients. The fits of the signal events as a polynomial in the Wilson coefficients and the number of total background events in each bin for each channel can be found in Tables 3.C.1, 3.C.2, and 3.C.3 in Appendix 3.C.

Since the systematic errors at FCC-hh are unknown at the time of writing, we consider three benchmark scenarios: 1%, 5% and 10%. The 1% benchmark is meant to give an estimate of the maximal sensitivity achievable by removing all possible sources of systematic uncertainty. Meanwhile, the 5% one should represent a more realistic scenario, being roughly comparable with the present LHC systematics for diboson production processes with leptonic final states [162]. The 10% benchmark should be considered as a worst-case scenario.

We performed several analyses according to different UV assumptions. First, in Section 3.6.1, we focus on the $\mathcal{O}_{\varphi q}^{(3)}$ operator and consider both the Wh and the Zh channels. Afterwards, we perform a global analysis of all the leading operators, namely $\mathcal{O}_{\varphi q}^{(1)}$, $\mathcal{O}_{\varphi q}^{(3)}$, $\mathcal{O}_{\varphi u}$ and $\mathcal{O}_{\varphi d}$, in Section 3.6.2. There, we consider the contribution of both Wh and Zh channels, which exacerbates the difference in the sensitivity to $\mathcal{O}_{\varphi q}^{(3)}$ with respect to the rest. In Section 3.6.3, we translate our results into the popular anomalous Triple Gauge Couplings (aTGC) framework and analyse how they could improve the bounds obtained from future lepton colliders. We put our results into an UV context by recasting them into the parameter space of two simple UV models in Section 3.6.4. Finally, the ability of the Wh channel to constrain the sub-leading operators $\mathcal{O}_{\varphi \mathrm{W}}$ and $\mathcal{O}_{\varphi \widetilde{\mathrm{W}}}$ is explored in Section 3.6.5.

3.6.1 Single-operator analysis for $\mathcal{O}_{\varphi q}^{(3)}$

The decision of doing a single-operator analysis for $\mathcal{O}_{\varphi q}^{(3)}$ is justified by several reasons. The first one is that $\mathcal{O}_{\varphi q}^{(3)}$ is the only common leading operator between the Wh and Zh channels that generates a quadratic growth with energy and, therefore, via the combination of both channels, we expect a more stringent bound than to any other. Second, any of the two channels on its own is more sensitive to $\mathcal{O}_{\varphi q}^{(3)}$ than to the other operators, as discussed in Section 3.3. Third, in many new-physics scenarios we expect $c_{\varphi q}^{(3)}$, $c_{\varphi q}^{(1)}$, $c_{\varphi u}$ and $c_{\varphi d}$ to be of roughly the same size, and $c_{\varphi \mathrm{W}}$ and $c_{\varphi \widetilde{\mathrm{W}}}$ to be loop-suppressed with respect to them. This justifies excluding $c_{\varphi \mathrm{W}}$ and $c_{\varphi \widetilde{\mathrm{W}}}$ from the analysis, and the bigger sensitivity to $c_{\varphi q}^{(3)}$ over similarly sized coefficients legitimises the exclusion of the remaining three.

According to the discussion in Section 3.3, the sensitivity of our analysis to $\mathcal{O}_{\varphi q}^{(3)}$ comes almost exclusively from the binning in p_T^h or $p_{T,\mathrm{min}}$ in both channels. Nevertheless, the results we present in this section were obtained using the double-binning, either in azimuthal angle or rapidity, described in Section 3.5.2. Notice that a double binning can improve the sensitivity in high-systematic uncertainty scenarios even when it does not distinguish between SM and BSM contributions.

We show in Table 3.13 the 95% C.L. bounds on $c_{\varphi q}^{(3)}$ for the different systematics and using either the Wh or Zh channel, or combining them. The bounds coming from each channel on its own are very similar, with the ones from Zh just slightly better than the ones from Wh. Thus, a combination of both channels allows for a significant improvement in the $c_{\varphi q}^{(3)}$ bounds, as seen in the fourth column of the aforementioned table. In both channels, the bounds for positive and negative values of the Wilson coefficient are quite similar. This is because the new-physics contributions are dominated by the linear interference terms with the SM, as can be checked from the fits in Appendix 3.C.

Syst.	Wh	Zh	Combined
1%	$[-2.7, 2.5] \times 10^{-3}$	$[-2.1, 2.0] \times 10^{-3}$	$[-1.6, 1.6] \times 10^{-3}$
5%	$[-3.3, 2.9] \times 10^{-3}$	$[-2.6, 2.4] \times 10^{-3}$	$[-2.0, 1.9] \times 10^{-3}$
10%	$[-4.0, 3.4] \times 10^{-3}$	$[-3.2, 2.8] \times 10^{-3}$	$[-2.4, 2.2] \times 10^{-3}$

Table 3.13: 95% C.L. bounds on $c_{\varphi q}^{(3)}$ from a one-operator fit for the different assumptions on the systematic uncertainties. The second (third) column gives the bounds obtained from the Wh (Zh) channel. The fourth column shows the bounds obtained from the combination of both channels.

We present our bounds for $c_{\varphi q}^{(3)}$ as a function of the cutoff of the EFT, M, for the different systematics in Figure 3.10. The cutoff is enforced by selecting events with $m_{Vh} \leqslant M$ for each value of M, where m_{Vh} is the invariant mass of the Vh system[7]. On the left panel, we present the result obtained with the Wh channel, and on the right panel, the one obtained from the combination of the Wh and Zh channels. The respective plot obtained with only the Zh channel can be found in Fig. 3.12. These plots give an idea of the dependence of the bound on the cutoff of the EFT, since we can roughly identify Λ with M, which allows us to test the validity of the EFT description and understand the kind of models we can probe with these operators.

In the Wh channel, the bounds saturate for $M \sim 4$ TeV and there is only a mild degradation for $M \simeq 2$ TeV, energy below which it rapidly becomes worse. Then, the bounds reported in Table 3.13 for the Wh channel are valid for $M \geqslant 4$ TeV. This behaviour is inherited by the results obtained with the combination of both channels, although they have a gentler slope. The latter feature comes from the Zh channel, where the bounds saturate for slightly larger cutoffs, $M \sim 5$ TeV.

The diagonal dashed and solid grey lines in Figure 3.10 show the values of $c_{\varphi q}^{(3)}$ expected in weakly-coupled new-physics models (labelled "Weak" in the plot), $c_{\varphi q}^{(3)} \sim g^2/(4M^2)$; and strongly-coupled ones (labelled "Strong"), where $c_{\varphi q}^{(3)} \sim (4\pi)^2/(4M^2)$ (see discussion in Section 3.2) [8]. These lines allow us to interpret our bounds as follows: the diphotonic Vh channels at FCC-hh will probe weakly-coupled theories with cutoffs of up to $M \sim 5-7$ TeV, and strongly coupled ones with cutoffs above 50 TeV.

Our bounds must be compared with results obtained from current data and other projections at future colliders. The most direct comparison is with the leptonic WZ channel, whose projected bound at FCC-hh, assuming 5% systematics, is [162]:

$$\text{FCC-hh} \;\; (20\,\text{ab}^{-1}) \qquad c_{\varphi q}^{(3)} \in [-1.8, 1.4] \times 10^{-3} \qquad 5\%\ \text{syst.}, \tag{3.21}$$

for $M \geqslant 5$ TeV. This is only slightly more stringent than the bound we find combining the Wh and Zh channels. Further combination with the WZ bounds can therefore lead to a significant improvement in the sensitivity.

[7] In the Wh channel, to reconstruct the invariant mass we randomly chose one of the two neutrino solutions. We checked that this procedure gives the same bound as always choosing the solution that maximizes $\sqrt{\hat{s}}$, i.e. the conservative choice where we would reject more events. In the Zh channel, when $Z \to \nu\bar{\nu}$, we can not reconstruct p_z^Z. We choose always $p_z^Z = -p_z^h$, which maximizes $\sqrt{\hat{s}}$ over the option $p_z^Z = 0$ and it is, therefore, the conservative option.

[8] The extra factor of 1/4 is included to match the conventions of Ref. [162]; it also arises in the matching of vector-like quark extensions of the SM, see Ref. [184]

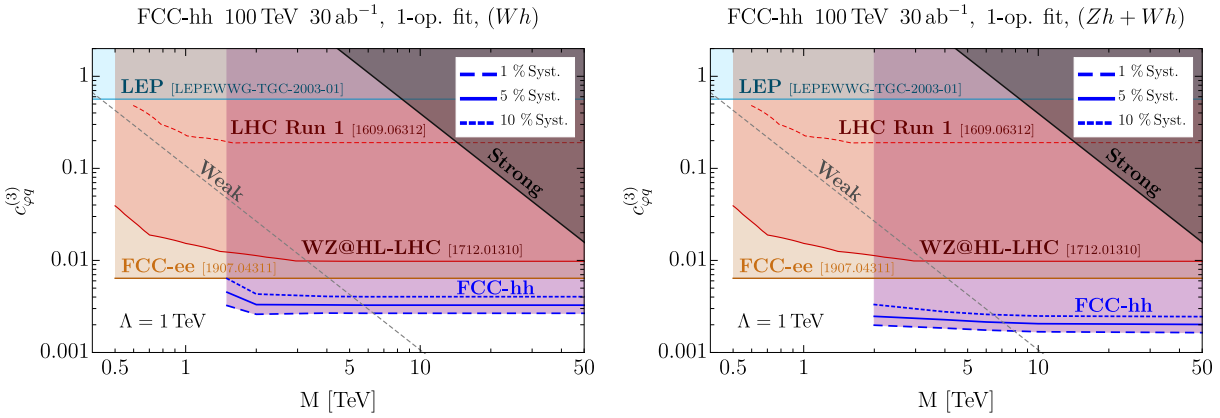

Figure 3.10: Bounds at 95% C.L. on $c^{(3)}_{\varphi q}$ from one-operator fits as functions of the maximal-invariant-mass cut M. The dashed, solid and dotted lines show the bounds for 1%, 5% and 10% systematic errors. For comparison, we show the current bounds from LEP [210] and LHC Run 1 [211] and the projected bounds from the WZ channel at HL-LHC from Ref. [162] and from a global fit at FCC-ee [212]. The dashed grey and solid black lines show the values of the Wilson coefficient expected in weakly-coupled ($c \sim g^2/(4M^2)$) and strongly-coupled ($c \sim (2\pi)^2/(M^2)$) new physics models [162]. **Left:** results derived from the Wh channel. **Right:** results derived from the combination of Wh and Zh channels.

Other current and projected bounds at 95% C.L. on $c^{(3)}_{\varphi q}$ are[9]:

$$
\begin{array}{lll}
\text{LEP [210]} & & [-5.7, 5.7] \times 10^{-1} \,, \\
\text{HL-LHC [185, 212]} & (3\ \text{ab}^{-1}) & [-3.9, 3.9] \times 10^{-2}\ ([-0.01, 0.01]) \,, \\
\text{HE-LHC [162]} & (27\ \text{TeV},\ 10\ \text{ab}^{-1}) & [-4.0, 3.3] \times 10^{-3} \quad \text{w/5\% syst.}, \\
\text{FCC-ee [212]} & & [-6.3, 6.3] \times 10^{-3}\ ([-4.8, 4.8] \times 10^{-4}) \,, \\
\text{CLIC/ILC [212]} & & [-7.8, 7.8] \times 10^{-3}\ ([-6.3, 6.3] \times 10^{-3}) \,, \\
\text{CEPC [212]} & & [-9.2, 9.2] \times 10^{-3}\ ([-1.1, 1.1] \times 10^{-3}) \,.
\end{array}
\tag{3.22}
$$

We also quote in parentheses the bound from one-operator fits. All these bounds are much weaker than the ones from the Wh, Zh and WZ channels, with the exception of the FCC-ee and CEPC one-operator fits.

3.6.2 Global analysis of leading operators

In this section, we perform a four-operator global fit with the leading operators that affect the Vh process, i.e $\mathcal{O}^{(1)}_{\varphi q}$, $\mathcal{O}^{(3)}_{\varphi q}$, $\mathcal{O}_{\varphi u}$, and $\mathcal{O}_{\varphi d}$. The bounds obtained on each of those operators after profiling over the other three operators at a time are reported in the column "Profiled Fit" in Table 3.14. The bounds in the first four rows come from the analysis of the Zh channel, since it is the only one capable of probing the four operators at the same time.

The last row in Table 3.14, labelled $c^{(3)}_{\varphi q}$ ($+Wh$), shows the impact of combining the four-operator fit from the Zh channel with a one-operator fit $c^{(3)}_{\varphi q}$ from the Wh channel. This combination leads to an improvement of the bound by a factor of ~ 2. The combination with the Wh channel has a negligible impact on the bounds for the other operators. The reason behind

[9]The quoted projection for HL-LHC is compatible with the results of Ref. [42]. The comparison with Ref. [43] is misleading due to different flavour assumptions and how the LEP bounds were taken into account.

Coefficient	Profiled Fit		One-Operator Fit	
$c_{\varphi q}^{(1)}$	$[-1.3, 1.4] \times 10^{-2}$	1% syst.	$[-1.1, 1.2] \times 10^{-2}$	1% syst.
	$[-1.5, 1.5] \times 10^{-2}$	5% syst.	$[-1.2, 1.2] \times 10^{-2}$	5% syst.
	$[-1.6, 1.5] \times 10^{-2}$	10% syst.	$[-1.2, 1.2] \times 10^{-2}$	10% syst.
$c_{\varphi u}$	$[-2.0, 1.6] \times 10^{-2}$	1% syst.	$[-1.9, 0.89] \times 10^{-2}$	1% syst.
	$[-2.1, 1.7] \times 10^{-2}$	5% syst.	$[-2.1, 0.96] \times 10^{-2}$	5% syst.
	$[-2.3, 1.8] \times 10^{-2}$	10% syst.	$[-2.2, 1.0] \times 10^{-2}$	10% syst.
$c_{\varphi d}$	$[-2.1, 2.3] \times 10^{-2}$	1% syst.	$[-1.4, 2.2] \times 10^{-2}$	1% syst.
	$[-2.2, 2.4] \times 10^{-2}$	5% syst.	$[-1.5, 2.2] \times 10^{-2}$	5% syst.
	$[-2.3, 2.5] \times 10^{-2}$	10% syst.	$[-1.5, 2.2] \times 10^{-2}$	10% syst.
$c_{\varphi q}^{(3)}$	$[-5.2, 3.1] \times 10^{-3}$	1% syst.	$[-2.1, 2.0] \times 10^{-3}$	1% syst.
	$[-6.7, 3.3] \times 10^{-3}$	5% syst.	$[-2.6, 2.4] \times 10^{-3}$	5% syst.
	$[-8.2, 3.7] \times 10^{-3}$	10% syst.	$[-3.2, 2.8] \times 10^{-3}$	10% syst.
$c_{\varphi q}^{(3)}$ $(+Wh)$	$[-2.5, 2.1] \times 10^{-3}$	1% syst.	$[-1.6, 1.6] \times 10^{-3}$	1% syst.
	$[-3.0, 2.4] \times 10^{-3}$	5% syst.	$[-2.0, 1.9] \times 10^{-3}$	5% syst.
	$[-3.7, 2.7] \times 10^{-3}$	10% syst.	$[-2.4, 2.2] \times 10^{-3}$	10% syst.

Table 3.14: Bounds at 95% C.L. on the coefficients of the $\mathcal{O}_{\varphi q}^{(1)}$, $\mathcal{O}_{\varphi u}$, $\mathcal{O}_{\varphi d}$ and $\mathcal{O}_{\varphi q}^{(3)}$ operators (with normalization $\Lambda = 1\,\text{TeV}$) using the Zh channel. The row labelled as $c_{\varphi q}^{(3)}$ $(+Wh)$ provides the bounds on that coefficient obtained from the combination of the Zh and Wh channels. Such combination does not have any sizeable impact on the other operators. **Left column:** Bounds from a global fit, profiled over the other coefficients. **Right column:** Bounds from a one-operator fit (i.e. setting the other coefficients to zero).

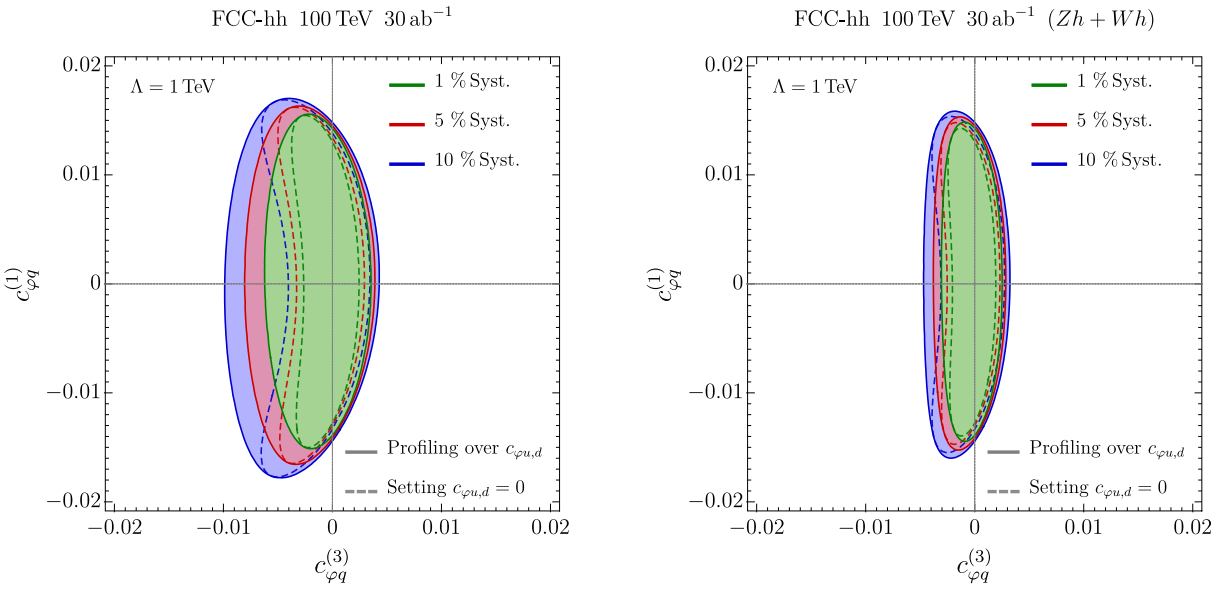

Figure 3.11: Expected 95% C.L. bounds on $c^{(1)}_{\varphi q}$ and $c^{(3)}_{\varphi q}$ at the FCC-hh. Bounds in green, red, blue, assume 1%, 5% and 10% systematic error respectively. Solid (dashed) lines correspond to the bounds when profiling over (setting to zero) the Wilson coefficients not appearing in the plot. **Left panel:** Bounds obtained from the Zh channel analysis. **Right panel:** Bounds obtained from the combination of the Wh and Zh channels.

this is that the bounds on the various operators in the fit are nearly uncorrelated. Such feature is confirmed by the fact that the bounds from single-operator fits on $c^{(1)}_{\varphi q}$, $c_{\varphi u}$ and $c_{\varphi d}$, shown in the column called "One-Operator Fit" of Table 3.14, are nearly equal to the ones coming from the global fit. On the contrary, the bound on $c^{(3)}_{\varphi q}$ in the global fit becomes significantly weaker than in the single-operator analysis, since large values of the other Wilson coefficients can easily compensate the linear corrections in $c^{(3)}_{\varphi q}$.

In Figure 3.11, we show the fits from the Zh channel in the $(c^{(3)}_{\varphi q}, c^{(1)}_{\varphi q})$ plane, obtained either by profiling (solid lines) or by setting to zero (dashed lines) the $c_{\varphi u}$ and $c_{\varphi d}$ Wilson coefficients. In the latter case, some correlation in the fit can be seen, as expected from the $c^{(3)}_{\varphi q} - c^{(1)}_{\varphi q}$ interference (see discussion at the end of Section 3.3.4). This correlation, however, disappears in the profiled fit. In the right panel, we show how the fit is modified by the combination of the Zh and Wh channels. The main impact of such combination is an improvement of the bounds on $c^{(3)}_{\varphi q}$, whereas the bound along the $c^{(1)}_{\varphi q}$ direction is roughly unaffected.

We show in Figure 3.12 the bounds from single-operator fits as functions of the maximal invariant mass cut M. In this Figure, we only consider the fits from the Zh channel. We see that, for all the operators, the bounds saturate for $M \sim 5$ TeV, signalling that our bounds are valid for a cut-off $\Lambda \gtrsim 5$ TeV. Also, the bounds on $c^{(1)}_{\varphi q}$, $c_{\varphi u}$ and $c_{\varphi d}$ are not strong enough to test the region of weakly-coupled new-physics, although they can mostly probe theories with strongly-coupled new dynamics. Only the bounds on $c^{(3)}_{\varphi q}$ can probe significantly weakly-coupled theories.

Finally, we can compare the bounds we obtained with the expected sensitivity at the LHC and other proposed future colliders (our fits always implicitly also rely on LEP measurements that are crucial in particular to size the SM input parameters). The current and projected 95%

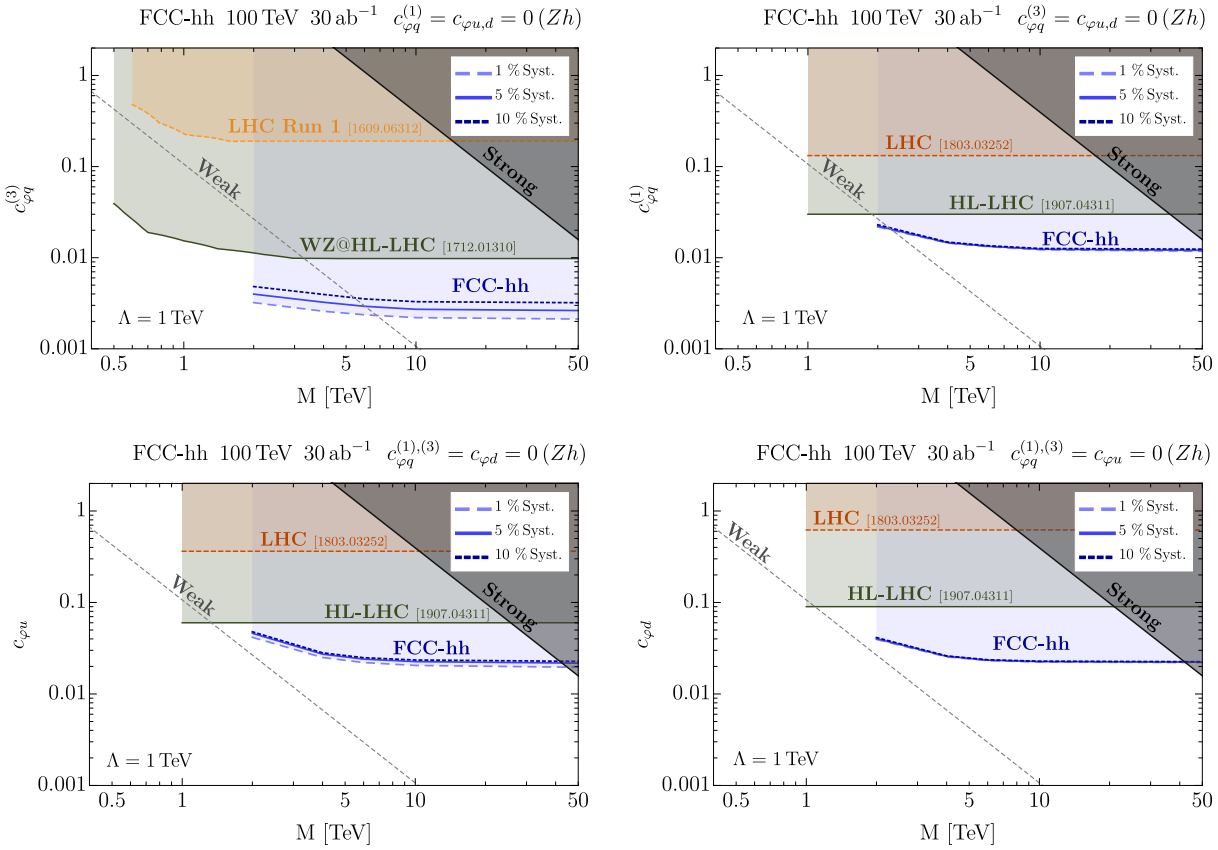

Figure 3.12: Bounds on $c^{(3)}_{\varphi q}$, $c^{(1)}_{\varphi q}$, $c_{\varphi u}$ and $c_{\varphi d}$ from one-operator fits as functions of the maximal-invariant-mass cut M. The bounds correspond to 95% C.L. ($\Delta\chi^2 = 3.84$). The dashed, solid and dotted lines show the bounds for 1%, 5% and 10% systematic errors. The current bounds and the projections for some future hadron colliders are also shown. For $c^{(3)}_{\varphi q}$, we show the LHC Run 1 bound from Ref. [211] and the projections from the WZ channel at HL-LHC from Ref. [162]. For the rest of operators, we show the global LHC data fit bound from Ref. [213] and the 1-operator fit at HL-LHC from Ref. [212]. LHC bounds are shown in orange and HL-LHC ones are shown in dark green. The dashed grey and solid black lines show the values of the Wilson coefficient expected in weakly-coupled ($c \sim g^2/(4M^2)$) and strongly-coupled ($c \sim (2\pi)^2/(M^2)$) new physics models [162].

C.L. bounds on $c^{(1)}_{\varphi q}$ from a global analysis are [185, 212, 213]:

LHC	Run 2 data	$[-0.132, 0.066]$,
HL-LHC	(3 ab^{-1})	$[-0.085, 0.085]$ ($[-0.03, 0.03]$) ,
CLIC/ILC		$[-0.07, 0.07]$ ($[-0.03, 0.03]$) ,
CEPC		$[-0.008, 0.008]$ ($[-0.003, 0.003]$) ,
FCC-ee		$[-0.018, 0.018]$ ($[-0.0017, 0.0017]$) ,

(3.23)

for $\Lambda = 1$ TeV. The current and projected bounds on $c_{\varphi u}$ are [185, 212, 213]:

LHC	Run 2 data	$[-0.36, 0.36]$,
HL-LHC	$(3\,\text{ab}^{-1})$	$[-0.24, 0.24]$ $([-0.06, 0.06])$,
CLIC/ILC		$[-0.17, 0.17]$ $([-0.07, 0.07])$,
CEPC		$[-0.02, 0.02]$ $([-0.007, 0.007])$,
FCC-ee		$[-0.04, 0.04]$ $([-0.003, 0.003])$.

(3.24)

Finally the bounds on $c_{\varphi d}$ are [185, 212, 213]:

LHC	Run 2 data	$[-0.62, 0.50]$,
HL-LHC	$(3\,\text{ab}^{-1})$	$[-0.45, 0.45]$ $([-0.09, 0.09])$,
CLIC/ILC		$[-0.4, 0.4]$ $([-0.1, 0.1])$,
CEPC		$[-0.04, 0.04]$ $([-0.009, 0.009])$,
FCC-ee		$[-0.095, 0.095]$ $([-0.004, 0.004])$.

(3.25)

We see that, for all operators, our analysis provides bounds that are competitive with the ones expected from global fits at other future colliders. On the other hand, if one-operator fits are considered, FCC-ee and CEPC will surpass our bounds on all four operators by roughly one order of magnitude.

3.6.3 Connection to aTGCs and Universal Theories

It might be convenient to interpret the bounds in terms of anomalous Triple Gauge Couplings (aTGCs). The $\mathcal{O}_{\varphi q}^{(3)}$, $\mathcal{O}_{\varphi q}^{(1)}$, $\mathcal{O}_{\varphi u}$ and $\mathcal{O}_{\varphi d}$ operators can be rewritten in terms of vertex corrections, $\delta g_{L,R}^{Zq}$, and aTGCs, δg_{1z} and $\delta\kappa_\gamma$ by adopting the Higgs basis [214, 215]:

$$\begin{aligned}
c_{\varphi q}^{(3)} &= +\frac{\Lambda^2}{4m_W^2} g^2 \left(\delta g_L^{Zu} - \delta g_L^{Zd} - c_{\rm w}^2\, \delta g_{1z}\right) \\
c_{\varphi q}^{(1)} &= -\frac{\Lambda^2}{4m_W^2} g^2 \left(\delta g_L^{Zu} + \delta g_L^{Zd} + \frac{1}{3}\left(t_{\rm w}^2 \delta\kappa_\gamma - s_{\rm w}^2 \delta g_{1z}\right)\right) \\
c_{\varphi u} &= -\frac{\Lambda^2}{2m_W^2} g^2 \left(\delta g_R^{Zu} + \frac{2}{3}\left(t_{\rm w}^2 \delta\kappa_\gamma - s_{\rm w}^2 \delta g_{1z}\right)\right) \\
c_{\varphi d} &= -\frac{\Lambda^2}{2m_W^2} g^2 \left(\delta g_R^{Zd} - \frac{1}{3}\left(t_{\rm w}^2 \delta\kappa_\gamma - s_{\rm w}^2 \delta g_{1z}\right)\right)
\end{aligned} \tag{3.26}$$

where $c_{\rm w}$, $s_{\rm w}$ and $t_{\rm w}$ are the cosine, sine and tangent of the weak mixing angle respectively.

One way to estimate the impact of diboson searches at FCC-hh is to compare their reach with the sensitivity at future lepton colliders. As an illustrative example we show, in Fig. 3.13, the expected bounds on the aTGC parameters δg_{1z} and $\delta\kappa_\gamma$ for CEPC and FCC-ee. These bounds are obtained through a global fit, which takes into account 18 effective operators in flavour-universal theories [212].[10] We also show in the same plot the impact of the combination of the CEPC and FCC-ee constraints with the FCC-hh fit of diboson channels. For the FCC-hh fit we combine the projections for $WZ \to \ell\nu\ell^+\ell^-$ [162] with the analysis of the Wh and Zh channels exposed in this work, and we assume 5% systematic uncertainty.

We find that, once the diboson channels at FCC-hh are included, the projected bounds on

[10] When flavour-universal theories are mapped into the 18 operators used in the fit, an ambiguity in the choice of the 4-lepton effective interactions is present. To obtain the results shown in Fig. 3.13 we used the choice $[c_{\ell\ell}]_{1221} = 0$. We however checked that the choice of $[c_{\ell\ell}]_{1221}$ only has a mild impact on the bounds.

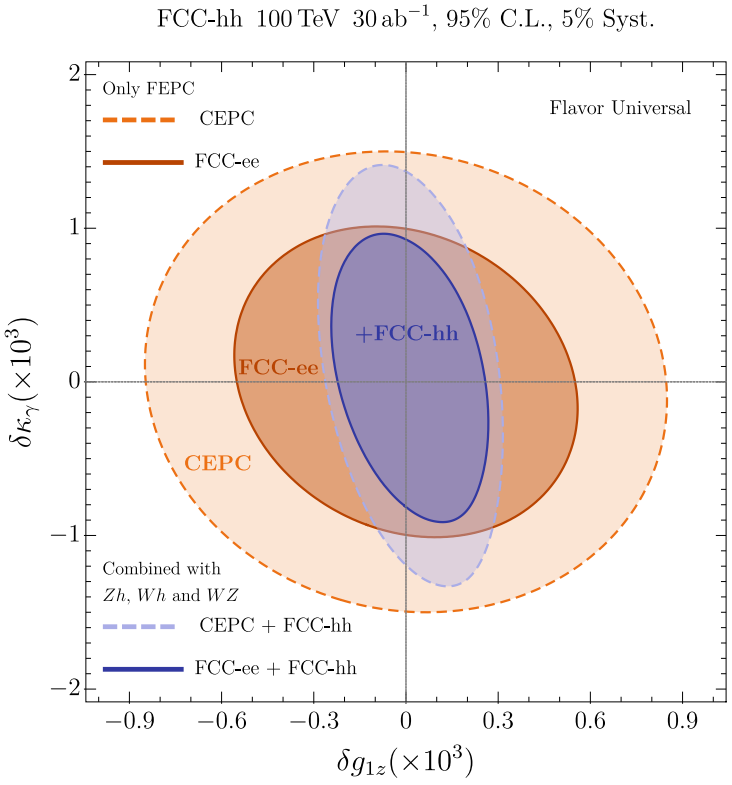

Figure 3.13: Projected 95% C.L. bounds on the anomalous Triple Gauge Couplings $\delta\kappa_\gamma\,, \delta g_{1z}$ for flavour universal theories at future colliders. In dark and light orange, we show the expected bounds at FCC-ee and CEPC [212]. In dark (light) blue, we show the combination of the FCC-ee (CEPC) fit with the projections at FCC-hh for the diboson channels $WZ \to \ell\nu\ell^+\ell^-$ [162], $Wh \to \ell\nu\gamma\gamma$ and the combined $Zh \to \ell^+\ell^-\gamma\gamma$ and $Zh \to \nu\bar{\nu}\gamma\gamma$. In the FCC-hh projections we assume 5% systematic uncertainty.

δg_{1z} improve by a factor ~ 2 (3) with respect to the bounds at FCC-ee (CEPC). On the other hand the bounds on $\delta\kappa_\gamma$ are only marginally affected. This behaviour is due to the fact that diboson channels have a very good sensitivity to $c^{(3)}_{\varphi q}$, which only depends on δg_{1z} (see Eq. (3.26)), while information on $\delta\kappa_\gamma$ can only be extracted from $c^{(1)}_{\varphi q}$, $c_{\varphi u}$ and $c_{\varphi d}$, whose expected bounds are much weaker.

For completeness, we report in the following the allowed 95% C.L. regions for δg_{1z},

$$\begin{aligned} &\text{FCC-ee} && [-4.5, 4.5]\times 10^{-4}\,,\\ &\text{FCC-ee + Diboson at FCC-hh} && [-2.0, 2.2]\times 10^{-4}\,,\\ &\text{CEPC} && [-6.8, 6.8]\times 10^{-4}\,,\\ &\text{CEPC + Diboson at FCC-hh} && [-2.3, 2.5]\times 10^{-4}\,, \end{aligned} \tag{3.27}$$

and for $\delta\kappa_\gamma$,

$$\begin{aligned} &\text{FCC-ee} && [-8.1, 8.1]\times 10^{-4}\,,\\ &\text{FCC-ee + Diboson at FCC-hh} && [-7.4, 7.7]\times 10^{-4}\,,\\ &\text{CEPC} && [-1.2, 1.2]\times 10^{-3}\,,\\ &\text{CEPC + Diboson at FCC-hh} && [-1.1, 1.1]\times 10^{-3}\,. \end{aligned} \tag{3.28}$$

These bounds are obtained from the global fit profiling over all the other parameters.

Another way to analyse the impact of these diboson measurements on aTGCs is via their connection with Universal Theories. Those theories are the only ones where it is fully valid to parametrise BSM effects via the oblique Peskin-Takeuchi parameters [142, 216–218]. They also impose correlations among the vertex corrections or, equivalently, WCs, as it is explained in Appendix 3.D. For the WCs that enter in our analysis, the relevant relations are

$$c_{\varphi q}^{(1)} = \frac{1}{4} c_{\varphi u} = -\frac{1}{2} c_{\varphi d}. \tag{3.29}$$

This leaves only two independent WCs, that we choose as $c_{\varphi q}^{(1)}$ and $c_{\varphi q}^{(3)}$.

The vertex corrections $\delta g_{L,R}^{Zq}$ in Universal Theories are completely parametrized by oblique parameters (see Eq. (3.58) in Appendix 3.D), which will be highly constrained through various measurements at FCC-ee and FCC-hh [212]. Then, one can safely assume $\delta g_{L,R}^{Zq} \simeq 0$ and recast our diboson bounds on $c_{\varphi q}^{(3)}$, $c_{\varphi q}^{(1)}$, $c_{\varphi u}$, $c_{\varphi d}$ as constraints on δg_{1z} and $\delta\kappa_\gamma$. With these assumptions, the combined analysis of the Zh and Wh channels gives the following constraints (for 5% systematic uncertainty):

$$\delta g_{1z} \in [-1.8, 2.4] \times 10^{-4} \quad ([-1.5, 1.7] \times 10^{-4}), \tag{3.30}$$

$$\delta\kappa_\gamma \in [-1.5, 2.8] \times 10^{-3} \quad ([-1.2, 2.8] \times 10^{-3}), \tag{3.31}$$

where the bounds in parenthesis are obtained through one-operator fits. Let us repeat that they are valid only for Universal Theories with negligible vertex corrections. Notice that the bound on δg_{1z} is very similar to the one obtained after combination with FCC-ee under the flavour-universal hypothesis, while the bound on $\delta\kappa_\gamma$ is significantly worse. This stresses that our analysis can constrain well only the first one and the second is better constrained by lepton colliders.

3.6.4 Interpretation in terms of simple UV models

In this subsection, we revisit the results presented in the previous sections with the help of two simple UV completions of the SM. The goal behind this is two-fold. On one hand, it allows us to compare our results with other kinds of probes that are heavily model-dependent, e.g. resonance searches. On the other hand, it allows us to study how our bounds are translated to UV parameters when either a single parameter enters into several WCs or a few UV parameters into the same WC.

A model of spin-1 triplets

The first model that we consider adds to the SM a massive vector boson that is a weak triplet, $L_\mu \sim (1,3)_0$. We will neglect any possible kinetic mixing and interaction of this resonance with the electroweak gauge bosons and remain agnostic about the ultimate origin of its mass m_L. The Lagrangian that must be added to the SM is

$$\mathcal{L}_{BSM} = \frac{1}{4} F_{L,\mu\nu}^a F_L^{a,\mu\nu} + \frac{m_L^2}{2} L_\mu L^\mu + \gamma_H L_\mu^a J_H^{a,\mu} + \sum_f \gamma_f L_\mu^a J_f^{a,\mu}, \tag{3.32}$$

where $F_{L,\mu\nu}^a$ is the usual non-abelian field strength tensor, the sum over f runs over all the SM fermion fields, and the triplet L_μ interacts with the SM currents defined as

$$J_H^{a,\mu} = \frac{i}{2} H^\dagger \sigma^a \overleftrightarrow{D}^\mu H, \quad J_f^{a,\mu} = \overline{f} \gamma^\mu \sigma^a f. \tag{3.33}$$

In principle, the coupling γ_f carries flavour indices, but we assume flavour universality to be consistent with our assumptions at EFT level (see discussion in Section 3.2). This reduces the number of new couplings introduced by this model to 3: γ_H, γ_q, and γ_ℓ. This model was used in Ref. [166], from where we borrow the notation, and is a simplification of the custodial symmetric model presented in Ref. [157, 219, 220].

For a high enough mass of the vector resonance, one can integrate it out and match this model onto SMEFT. At tree-level, it generates several dimension-6 operators in the Warsaw basis [184][11], but only to one of the operators considered in our analysis: $\mathcal{O}^{(3)}_{\varphi q}$. The matching to its WC renders

$$c^{(3)}_{\varphi q} = -\frac{\gamma_H \gamma_q}{2 m_L^2}. \tag{3.34}$$

Notice that this UV model exemplifies perfectly the power-counting explained in subsection 3.2 and justifies setting to zero all the other WCs that enter in the Vh channel, instead of profiling over them.

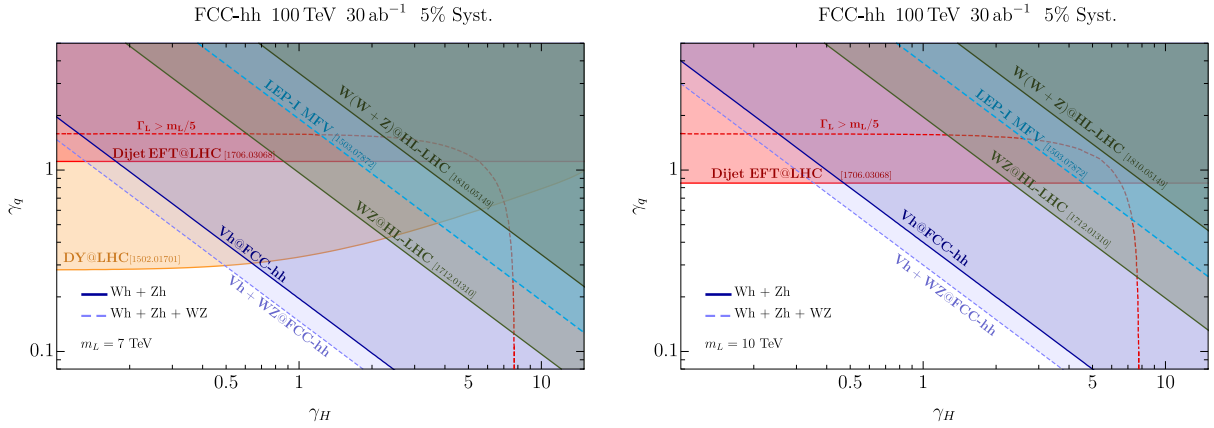

Figure 3.14: Projected 95% C.L. bounds on the couplings of a spin-1 triplet resonance, L_μ, with mass m_L. γ_H and γ_q are its couplings to the Higgs and quark currents, the latter is flavour universal. We show the bounds for m_L = 7 TeV (left panel) and m_L = 10 TeV (right panel). The continuous dark blue line is the projected bound from the combination of the Wh and Zh channels. The dashed light blue line is the bound obtained combining the former with the WZ channel analysed in Ref. [162]. The orange curve is the bound obtained from the analysis of the Drell-Yann process at LHC in Ref. [221]. The red curve represents the bound from a dijet EFT analysis at LHC from Ref. [155]. The bright red dashed curve indicates the value of the couplings above which the width of the resonance is bigger than 20% of its mass, regime in which direct searches like the former two lose sensitivity [166]. The dark green curve is the bound from the diboson channels WW and WZ projected for HL-LHC in Ref. [166], while the green line is the result obtained in Ref. [162] via a refined analysis of the WZ channel. The dashed cyan curve is the bound from LEP-I assuming MFV [222]. In the FCC-hh projections we assume 5% systematic uncertainty.

Our results recast in the parameter space of this UV model are shown in Fig. 3.14 for two different values of the mass m_L, 7 and 10 TeV. In that Figure, we also include several other bounds on the same model from LEP-I measurements, direct searches and diboson processes at LHC or HL-LHC [155, 162, 166, 221, 222]. We show our projection for FCC-hh combining the Wh channel with both Zh channels and also show the result of a further combination with the WZ channel analysed in Ref. [162]. Our projections improve significantly the ones for the

[11] In the notation of Ref. [184], the resonance we are considering is $\mathcal{W}$.

diboson channels WW and WZ at HL-LHC, as well as the LEP-I bound. It must be noticed that the LEP bound and the diboson bound from Ref. [162] were obtained with a different flavour assumption, namely MFV. As discussed in Section 3.2, that flavour hypothesis would weaken our bound by around 20%.

For $m_L = 7$ TeV, the projected bound from diboson channels at FCC-hh overlaps almost completely with the bounds from Drell-Yann[12] and dijet processes at LHC. Moreover, it improves them significantly for large γ_H. However, it is expected that the repetition of those direct searches at FCC-hh will render stronger bounds that our diboson analysis for small γ_H, just as it happens at LHC.

Interestingly, for $\gamma_H > \gamma_\ell$, our simple UV model describes approximately the vector resonances of a composite model that couples strongly to the Higgs boson but weakly to light quarks[13], where one expects $\gamma_H\gamma_f \sim 1$ and $\gamma_H/\gamma_f \sim (g_*/g)^2$ with $g_* >> g$ [166, 220]. From our results, it is clear that such class of models might be better probed by diboson processes than with direct probes. This highlights the importance of performing both kinds of analysis, since they complement each other and probe different regions of the parameter space. Finally, let us point out that the inclusion of the WZ channel improves the diboson projection at FCC-hh noticeably.

A model of vector-like quarks

The second model that we will use consists of two vector-like heavy quarks, T_1 and T_2, that are triplets of both colour and weak isospin but have different hypercharges, namely $T_1 \sim (3,3)_{-1/3}$ and $T_2 \sim (3,3)_{2/3}$. The BSM part of the Lagrangian is [184]

$$\mathcal{L} = \sum_{i=1}^{2} \overline{T}_i \left(i\not{D} - m_{T_i}\right) T_i - \frac{\lambda_1}{2}\overline{T}^a_{1,R} H^\dagger \sigma^a q_L - \frac{\lambda_2}{2}\overline{T}^a_{2,R} \tilde{H}^\dagger \sigma^a q_L + h.c., \tag{3.35}$$

where we assume that the couplings to SM fields are flavour universal in accord with our previous analyses. We assume $\lambda_i \in \mathbb{R}$ for $i = 1, 2$ for simplicity.

Upon integration of both vector-like fermions, this model generates at tree-level non-vanishing contributions to the WCs $c^{(1)}_{\varphi q}$ and $c^{(3)}_{\varphi q}$ among several others that do not affect diboson processes at leading order [184]. Matching gives the following values for $c^{(1)}_{\varphi q}$ and $c^{(3)}_{\varphi q}$:

$$\begin{aligned} c^{(1)}_{\varphi q} &= \frac{3}{16}\left(\frac{\lambda_2^2}{m_{T_2}^2} - \frac{\lambda_1^2}{m_{T_1}^2}\right), \\ c^{(3)}_{\varphi q} &= \frac{1}{16}\left(\frac{\lambda_1^2}{m_{T_1}^2} + \frac{\lambda_2^2}{m_{T_2}^2}\right). \end{aligned} \tag{3.36}$$

We notice the opposite sign in the contribution to $c^{(1)}_{\varphi q}$, which resembles the change in sign of the interference term of $\mathcal{O}^{(1)}_{\varphi q}$ for up and down-type quarks.

Figure 3.15 shows our results recast into the parameter space of this simple model. In the plot, we assume an equal mass of 10 TeV for both vector-like fermion resonances. We include in the plot also the bounds from a global fit of Run 2 LHC data [42]. Our projections are significantly better than the current bounds. The weakening of our constraints along the $\lambda_1 = \lambda_2$ axis is due to the fact that such condition forces $c^{(1)}_{\varphi q}$ to vanish and hence all the constraining

[12] The Drell-Yann bound was recast under the assumption $\gamma_\ell = \gamma_q$ [166].

[13] This might cast doubt on the validity of the flavour-universal assumption and, in fact, makes MFV preferable. However, our results are safe from big corrections since partial compositeness predicts that the vector resonance will couple strongly mainly to the top quark, and particularly to its RH component. Hence, one could free $c_{\varphi t} = (c_{\varphi u})_{33}$ without modifying our results.

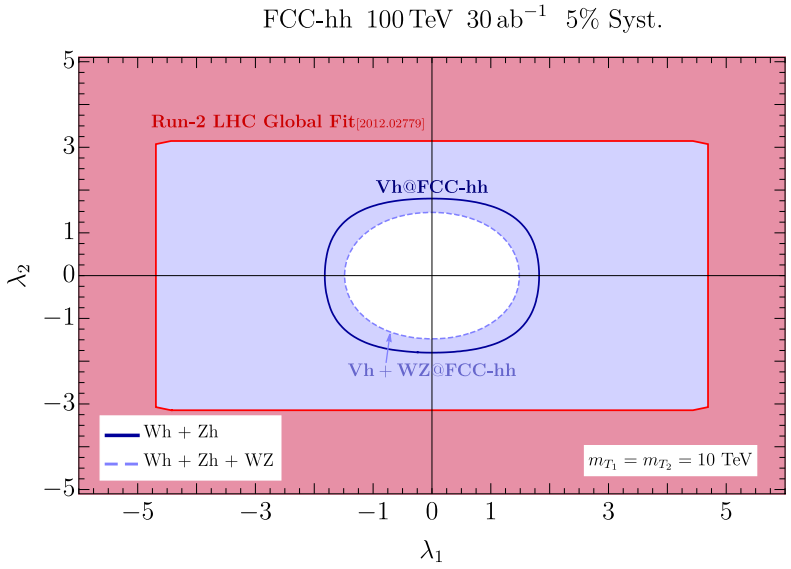

Figure 3.15: Projected 95% C.L. bounds on the couplings of two vector-like weak-isospin-triplet quarks, T_1 and T_2, with mass $m_{T_1} = m_{T_2} = 10$ TeV. λ_1 and λ_2 are their Yukawa couplings to SM quark doublets. The continuous dark blue line is the projected bound from the combination of the Wh and Zh channels. The dashed light blue line is the bound obtained combining the former with the WZ channel analysed in Ref. [162]. In both projections, a 5% systematic uncertainty is assumed. The red curve indicates the bound obtained from a global fit of LHC Run 2 data in Ref. [42].

power comes from our bound on $c^{(3)}_{\varphi q}$. Fortunately, $\mathcal{O}^{(3)}_{\varphi q}$ is the operator shared by both Vh processes and also the WZ channel, hence the inclusion of the latter improves our projection, particularly along the aforementioned direction. Nevertheless, given the coloured nature of these resonances, direct searches at FCC-hh should improve our bounds.

3.6.5 The sub-leading operators in the Wh channel

In this subsection, we focus exclusively on the Wh channel and, more specifically, on its sensitivity to the sub-leading operators $\mathcal{O}_{\varphi \mathrm{W}}$ and $\mathcal{O}_{\varphi \widetilde{\mathrm{W}}}$. We still have to consider the $\mathcal{O}^{(3)}_{\varphi q}$ in our analysis and therefore we perform a three-operator global fit. The 95% C.L. constraints in the $(c^{(3)}_{\varphi q} - c_{\varphi \mathrm{W}})$, $(c^{(3)}_{\varphi q} - c_{\varphi \widetilde{\mathrm{W}}})$, and $(c_{\varphi \mathrm{W}} - c_{\varphi \widetilde{\mathrm{W}}})$ planes are shown in Fig. 3.16 in the top-left, top-right, and bottom-left panels respectively. In the aforementioned figure, we present two sets of results. The first one is obtained by profiling over the additional Wilson coefficient and delineated by solid contours in the plots. The second set of results, delineated by dashed contours, is obtained by setting the remaining Wilson coefficient to zero. All the results are given for the three systematic uncertainty scenarios we consider. The bottom-right panel of the figure shows the effect of binning in ϕ_W on the bound on $c_{\varphi \widetilde{\mathrm{W}}}$.

The constraints on $c^{(3)}_{\varphi q}$ are stronger, by roughly one order of magnitude, than the ones on $c_{\varphi \mathrm{W}}$, $c_{\varphi \widetilde{\mathrm{W}}}$, as expected from our discussion in Section 3.3. This also confirms that a one-operator analysis for $c^{(3)}_{\varphi q}$ is fully justified even in BSM scenarios in which the contributions to all three effective operators are of the same order. Figure 3.16 is also useful to assess correlations among the different operators. Its top left panel shows clearly that $c^{(3)}_{\varphi q}$ and $c_{\varphi \mathrm{W}}$ are correlated, mainly due to the fact that both operators can only be distinguished by a different growth in the p^h_T distribution. On the other hand, $c_{\varphi \widetilde{\mathrm{W}}}$ is essentially uncorrelated with the other two Wilson

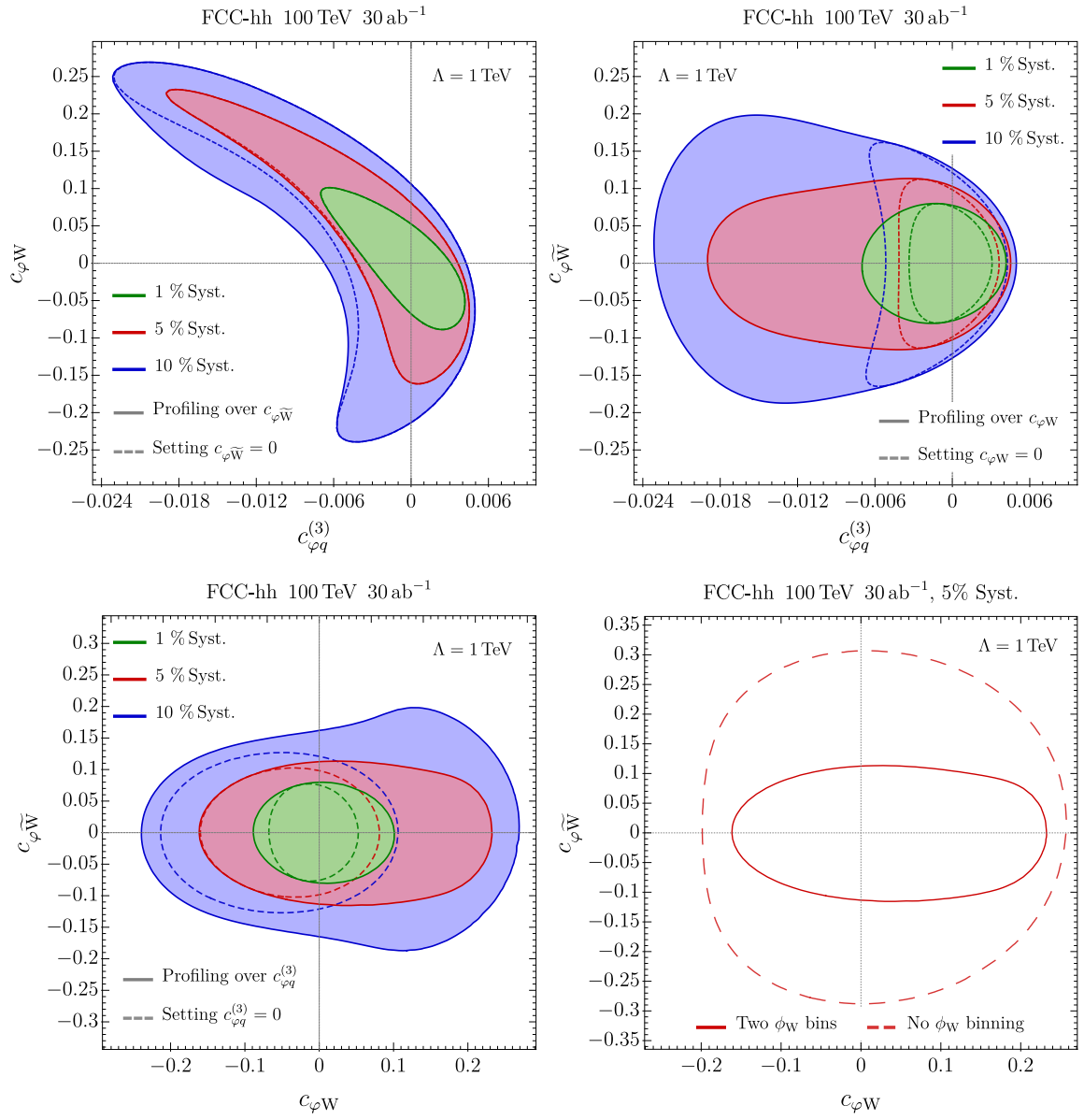

Figure 3.16: Expected 95% C.L. bounds on $c_{\varphi W}$, $c_{\varphi\widetilde{W}}$, $c^{(3)}_{\varphi q}$ at the FCC-hh for 30 ab^{-1} obtained using the Wh channel. Bounds in green, red, blue, assume 1%, 5% and 10% systematic error. Solid (dashed) lines in top and bottom left panels correspond to the bounds when profiling over (setting to zero) the Wilson coefficient not appearing in the plot **Top Left:** Bounds on the $c_{\varphi W}$, $c^{(3)}_{\varphi q}$ plane. **Top Right:** Bounds on the $c_{\varphi\widetilde{W}}$, $c^{(3)}_{\varphi q}$ plane. **Bottom Left:** Bounds on the $c_{\varphi W}$, $c_{\varphi\widetilde{W}}$ plane. **Bottom Right:** In solid red (dashed red) the bounds when using (not using) the double differential binning in ϕ_W assuming 5% systematics in the plane $c_{\varphi W}$, $c_{\varphi\widetilde{W}}$.

coefficients. This is because the linear sensitivity to $c_{\varphi\widetilde{W}}$ derives from the ϕ_W binning, instead of the p_T^h one. The effect of the ϕ_W binning can be clearly seen in the bottom right panel of Figure 3.16. For the 5% systematics scenario, the bound on $c_{\varphi\widetilde{W}}$ with two ϕ_W bins is ~ 3 times stronger than without ϕ_W binning.

The impact of the systematic error on the fits is also significant. For 1% systematics, the bounds are mainly driven by the linear SM-BSM interference terms in the cross section for all three operators. However, for the 5% and 10% benchmarks, quadratic terms clearly play an

Coefficient	Profiled Fit		One Operator Fit	
$c_{\varphi \mathrm{W}}$	$[-7.1, 7.9] \times 10^{-2}$	1% syst.	$[-5.3, 4.3] \times 10^{-2}$	1% syst.
	$[-13.0, 17.5] \times 10^{-2}$	5% syst.	$[-12.1, 6.8] \times 10^{-2}$	5% syst.
	$[-20.0, 25.2] \times 10^{-2}$	10% syst.	$[-18.8, 9.0] \times 10^{-2}$	10% syst.
$c_{\varphi \widetilde{\mathrm{W}}}$	$[-6.4, 6.4] \times 10^{-2}$	1% syst.	$[-6.1, 6.1] \times 10^{-2}$	1% syst.
	$[-9.0, 8.8] \times 10^{-2}$	5% syst.	$[-8.1, 8.1] \times 10^{-2}$	5% syst.
	$[-13.5, 14.2] \times 10^{-2}$	10% syst.	$[-10.1, 10.1] \times 10^{-2}$	10% syst.
$c_{\varphi q}^{(3)}$	$[-5.1, 3.4] \times 10^{-3}$	1% syst.	$[-2.7, 2.5] \times 10^{-3}$	1% syst.
	$[-11.6, 3.8] \times 10^{-3}$	5% syst.	$[-3.3, 2.9] \times 10^{-3}$	5% syst.
	$[-20.6, 4.1] \times 10^{-3}$	10% syst.	$[-4.0, 3.5] \times 10^{-3}$	10% syst.

Table 3.15: Bounds at 95% C.L. on the coefficients of the $\mathcal{O}_{\varphi q}^{(3)}$, $\mathcal{O}_{\varphi \mathrm{W}}$ and $\mathcal{O}_{\varphi \widetilde{\mathrm{W}}}$ operators setting $\Lambda = 1\,\mathrm{TeV}$. **Left column:** bounds profiling over the other two coefficients. **Right column:** bounds with a one operator fit, i.e. setting the other two coefficients to zero.

important role, significantly worsening and distorting the constraints.

Another relevant comparison to make is the one between profiling and setting to zero the remaining Wilson coefficient. The upper left panel in Figure 3.16 shows that the constraints in the $(c_{\varphi q}^{(3)} - c_{\varphi \mathrm{W}})$ plane remain largely unchanged. This is expected, since the correlation between these Wilson coefficients and $c_{\varphi \widetilde{\mathrm{W}}}$ is small. On the contrary, the correlation between $c_{\varphi q}^{(3)}$ and $c_{\varphi \mathrm{W}}$ leads to a very sizeable weakening of the bounds on each of these coefficients when we profile over the other one. Instead, profiling over $c_{\varphi q}^{(3)}$ or $c_{\varphi \mathrm{W}}$ has a minor effect on the determination of $c_{\varphi \widetilde{\mathrm{W}}}$.

In Table 3.15, we report our 95% C.L. bounds on $c_{\varphi \mathrm{W}}$, $c_{\varphi \widetilde{\mathrm{W}}}$ and $c_{\varphi q}^{(3)}$ obtained from the Wh channel at FCC-hh with 30 ab^{-1}. We list in the second column the results obtained after profiling over the other two coefficients, and in the third column, the ones obtained from a one-operator fit. The comparison between both set of results reaffirms our conclusions regarding correlations drawn before from Figure 3.16. We only add that the bounds on $c_{\varphi q}^{(3)}$ from a profiled fit are significantly worse than the ones obtained in the previous subsection (see Table 3.14) also from a profiled fit. This is due to the strong correlation with $c_{\varphi \mathrm{W}}$ and the poor sensitivity to the latter in comparison with $c_{\varphi q}^{(1)}$.

To conclude this section, we compare our constraints on $c_{\varphi \mathrm{W}}$ and $c_{\varphi \widetilde{\mathrm{W}}}$ with other projected and current bounds. We compare our constraints on $c_{\varphi \mathrm{W}}$ with the projections at the HL-LHC, future lepton colliders and FCC-hh. At 95% C.L., those bounds are expected to be [185, 212]:

$$\begin{array}{lll} \text{HL-LHC} & (3\,\mathrm{ab}^{-1}) & c_{\varphi \mathrm{W}} \in [-0.4, 0.4]\,, \\ \text{FCC-ee / CEPC / ILC} & & c_{\varphi \mathrm{W}} \in [-0.02, 0.02]\,, \\ \text{CLIC} & & c_{\varphi \mathrm{W}} \in [-0.01, 0.01]\,, \\ \text{FCC-hh} & (30\,\mathrm{ab}^{-1}) & c_{\varphi \mathrm{W}} \in [-0.01, 0.01]\,, \end{array} \tag{3.37}$$

for $\Lambda = 1$ TeV, which for future lepton colliders and FCC-hh are significantly stronger than our results.[14]

The situation is very different for $\mathcal{O}_{\varphi \widetilde{\mathrm{W}}}$, which can be indirectly tested through its contribu-

[14] Recall that in minimally coupled models, large single-operator contributions to $h \to \gamma\gamma$ are structurally correlated, cancelling their effects.

tions to the electric dipole moment of the electron. Excluding accidental cancellations with the contributions from other CP-violating operators, the current experimental results give a constraint $c_{\varphi\widetilde{\mathrm{W}}} \lesssim 2 \cdot 10^{-5}$(with $\Lambda = 1$ TeV) [223], which is three orders of magnitudes stronger than our bound. The current direct bounds on $\mathcal{O}_{\varphi\widetilde{\mathrm{W}}}$ at the LHC (with 36 fb^{-1}) are $|c_{\varphi\widetilde{\mathrm{W}}}| \lesssim 11$ and are expected to reach the level $|c_{\varphi\widetilde{\mathrm{W}}}| \lesssim 1$ (with $\Lambda = 1$ TeV) at the HL-LHC [224, 225], which is worse than the bound we obtain. Nonetheless, we expect that the extrapolation of this differential analysis to FCC-hh will overpass the bound derived from our Wh analysis.

3.7 Summary and conclusions

The next generation of hadron colliders will take our efforts to explore nature to uncharted territory, as discussed in Chapter 2. The associated increases in energy, cross section and luminosity will allow us to revisit several electroweak processes in a cleaner environment, bringing advantages for precision measurements. Here, we have studied the interesting example of Vh production, which can only be studied at HL-LHC through the $h \to b\bar{b}$ decay, but becomes accessible at FCC-hh also in the very clean $h \to \gamma\gamma$ channel.

It is interesting to notice the interplay between the two channels of Vh production, i.e. Wh and Zh production. On one hand, Wh has a bigger cross section and it probes fewer dimension-6 operators, which in turns allows it to probe sub-leading operators and break degeneracies. On the other hand, Zh compensates its smaller cross section with the presence of two useful fully-leptonic Z decay channels that can be combined to give a similar sensitivity than Wh. And it probes more equally growing operators, which makes it useful to evaluate correlations.

We found that a binning in the transverse momentum allowed us to obtain, with either Wh or Zh on their own, a sensitivity to $\mathcal{O}_{\varphi q}^{(3)}$ that is competitive with other processes and experiments. Our estimates show that the bounds at FCC-hh can significantly surpass the precision achievable at HL-LHC and at FCC-ee. Furthermore, the combination of the Zh and Wh channels improves the bound by roughly 20% and further improvement could be achieved via a combination with the WZ channel. This shows the importance of a comprehensive study of all processes available at future colliders in order to correctly assess their potential.

The sensitivity to the $\mathcal{O}_{\varphi q}^{(1)}$ operator via the Zh channel turns out to be significantly worse than to $\mathcal{O}_{\varphi q}^{(3)}$, due to a (partially accidental) cancellation between the contributions from up-type and down-type quarks. We showed that this cancellation can be partially overcome by implementing a second binning in the rapidity of the Zh system (or the rapidity of the Higgs boson when the former cannot be computed). This double binning exploits the different rapidity distributions of the parton distribution functions for the several quark flavours. Although the improvement is limited by the small cross section of the final state we considered in this thesis, the obtained sensitivity is one order of magnitude better than the one at HL-LHC and is competitive with the one achievable at future lepton colliders (CLIC/ILC, CEPC and FCC-ee).

Furthermore, the rapidity binning strategy used to improve our bound on $\mathcal{O}_{\varphi q}^{(1)}$ could be useful for final states with higher cross section (for instance the $h \to b\bar{b}$ channel) or for analogous processes. We also stress that the pattern of deviations in the rapidity distribution depends on the flavour structure of the new-physics effects (see Fig. 3.6), thus it could potentially be a way to disentangle different flavour hypotheses.

Our sensitivity to $\mathcal{O}_{\varphi u}$ and $\mathcal{O}_{\varphi d}$ is limited by inherent characteristics of the operators, whose contributions only interfere with the SM amplitudes due to the relatively small couplings of the right-handed quarks with the Z boson. The expected bounds are more than one order of magnitude better than the ones at HL-LHC and competitive with the ones from global fits at future lepton colliders. Regarding the bounds on $\mathcal{O}_{\varphi u}$ and $\mathcal{O}_{\varphi d}$, we note that, due to the

suppression of the interference with the SM amplitudes, the constraints are mostly driven by the square of the BSM contributions. This might cause some limitation in their interpretability within the EFT formalism.

Regarding the sub-leading operators studied via the Wh channel, they do not interfere with the leading SM amplitude if we simply use a p_T binning. We found, nonetheless, that a double differential distribution which also takes into account the azimuthal decay angle of the lepton, ϕ_W, can be used to recover the interference for $\mathcal{O}_{\varphi\widetilde{\mathrm{W}}}$ and significantly strengthen the bounds.

More precisely, our results for the $\mathcal{O}_{\varphi\widetilde{\mathrm{W}}}$ determination are one order of magnitude stronger than the ones achievable at the HL-LHC obtained using CP-sensitive observables from VBF and gluon fusion [224, 225]. One feature of those observables is that they are linearly sensitive to CP-odd operators, as opposed to inclusive Higgs data. This is also true for the observable we constructed in our analysis. Nevertheless, indirect constraints coming from the current electron EDM bounds are already three orders of magnitude stronger than the expected bound we find.

On the other hand, the double binning in p_T^h and ϕ_W has only a minor impact on the determination of $\mathcal{O}_{\varphi\mathrm{W}}$. Consequently, our bounds on $\mathcal{O}_{\varphi\mathrm{W}}$ are competitive with a projected global fit to Higgs data anticipated by the end of the HL-LHC but not at FCC-ee nor FCC-hh.

A summary of the projected 95% C.L. bounds on all the considered operators is shown in Fig. 3.17. The blue bars correspond to the constraints derived from the profiling of a global fit. For the leading operators, this global fit is the four-operators one from Section 3.6.2, and for the sub-leading operators, it corresponds to the three-operators fit from Section 3.6.5. On the other hand, the horizontal bars with a triangle indicate the bound obtained from one-operator fits. For $c_{\varphi q}^{(3)}$, we used the combination of the Wh and Zh channels in both kind of fits. We considered three possible values for the systematic uncertainties: 1% (lighter shading), 5% (medium shading), and 10% (darker shading). The systematic uncertainty has a sizeable effect only on the bound for $\mathcal{O}_{\varphi q}^{(3)}$. The 5% scenario is comparable to the present LHC systematics for similar processes, therefore it could be considered as a conservative estimate, while the 10% benchmark is most probably a pessimistic one.

Another interesting feature of our results is the impact of a global fit instead of a single-operator one. We find that only the bound on $c_{\varphi q}^{(3)}$ is strongly affected. This feature comes from its correlation with $c_{\varphi q}^{(1)}$. A similar effect is found when considering the bound on $c_{\varphi q}^{(3)}$ from the global fit in Section 3.6.5, but due to a correlation with $c_{\varphi\mathrm{W}}$ (result not shown in the plot, see Table 3.15 instead). It is important to stress that, in a majority of BSM scenarios, the deformations parametrised by $\mathcal{O}_{\varphi\mathrm{W}}$ and $\mathcal{O}_{\varphi\widetilde{\mathrm{W}}}$ are expected to be subleading with respect to the other ones. In this class of theories, the correct bound on $c_{\varphi q}^{(3)}$ is the one shown in Figure 3.17.

Finally, let us comment on the complementarity between diboson processes like the ones we have studied and vector boson scattering (VBS). VBS processes also probe the EW sector of the SM, both its gauge structure and the dynamics of the Higgs boson. Differently from diboson, VBS is sensitive to quartic gauge couplings. Recent studies on its interplay with diboson at LHC indicate that VBS can not improve significantly the bound on $c_{\varphi q}^{(3)}$ but it enhances the sensitivity to $c_{\varphi q}^{(1)}$, $c_{\varphi d}$, and purely bosonic operators [179]. This complementarity highlights the need of a combined projection of VBS and diboson at FCC-hh to fully assess the potential of said future collider. Since the analysis techniques required for VBS are similar to the ones used in vector-boson-fusion (VBF) Higgs production, this latter topology could also be included in such analysis [179, 226, 227]. We leave this direction to be explored in future work.

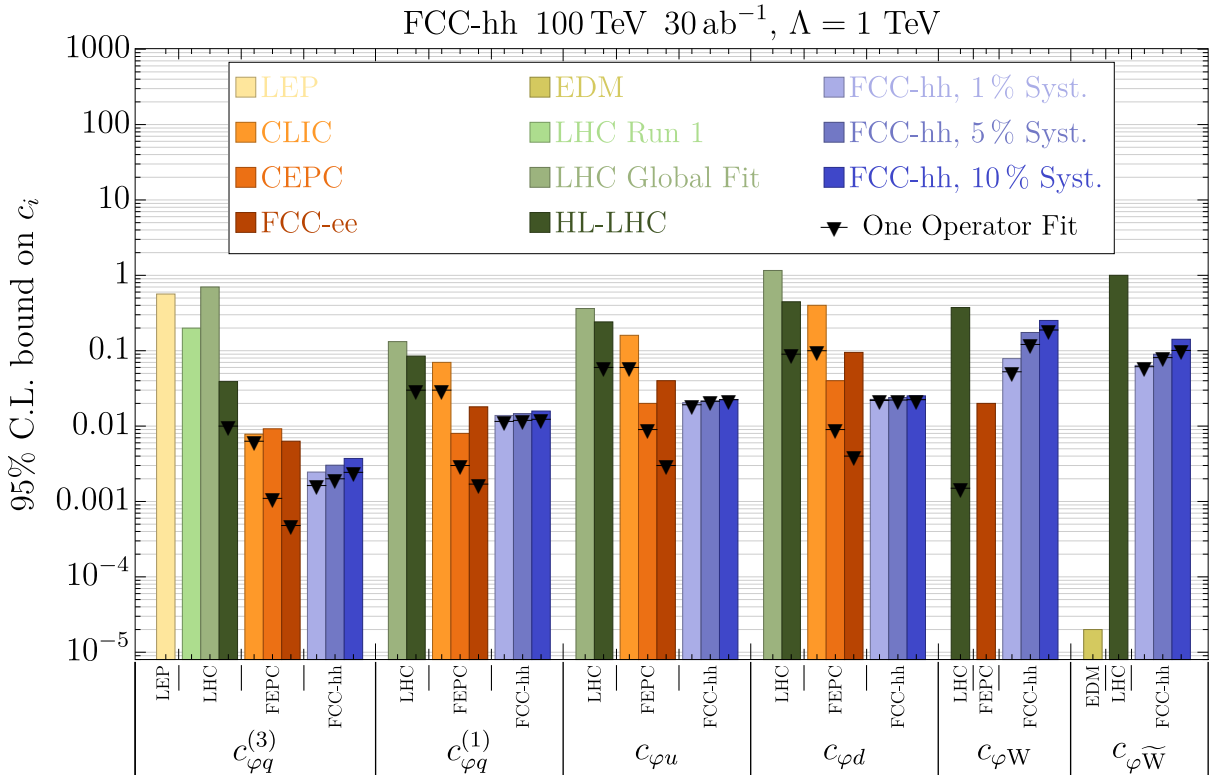

Figure 3.17: 95% C.L. bounds on $c^{(3)}_{\varphi q}$, $c^{(1)}_{\varphi q}$, $c_{\varphi u}$ and $c_{\varphi d}$. In blue, our combined bounds from $Zh \to (\nu\bar{\nu}/\ell^+\ell^-)\gamma\gamma$ and $Wh \to \ell\nu\gamma\gamma$ at FCC-hh with 30 ab^{-1} for different systematics and computed from a global fit (see text for details). In all cases, the black lines with a triangle on top represent the bound from a one-operator fit instead. In light yellow, the current LEP [210] bound for $c^{(3)}_{\varphi q}$. In medium yellow, the current EDM bound on $c_{\varphi\widetilde{\mathrm{W}}}$ [223]. In light green for $c^{(3)}_{\varphi q}$, the run-1 LHC [211] bounds. In medium green, the current bound on all the operators from a global fit [213]. In dark green, the projections from a global fit at HL-LHC [185, 212] for the CP-even operators and from dedicated measurements [223, 224] for $c_{\varphi\widetilde{\mathrm{W}}}$. In light, medium and dark orange, the projected bounds on the operators from a global fit at CLIC, CEPC and FCC-ee respectively [212]. FEPC stands for Future Electron-Positron Colliders.

Appendix to Chapter 3

3.A Helicity amplitudes for diboson processes

In this appendix, we compute the helicity amplitudes of the processes $pp \to Vh$, where $V = W,\ Z$, at leading order in the SM and when generated by the dimension-6 SMEFT operators $\mathcal{O}_{\varphi q}^{(1)}$, $\mathcal{O}_{\varphi q}^{(3)}$, $\mathcal{O}_{\varphi u}$, $\mathcal{O}_{\varphi d}$, $\mathcal{O}_{\varphi \mathrm{W}}$ or $\mathcal{O}_{\varphi \widetilde{\mathrm{W}}}$. We define $\varepsilon_V \equiv M_V/\sqrt{\hat{s}}$ and $\varepsilon_H \equiv M_h/\sqrt{\hat{s}}$. The scattering angle θ is defined in Section 3.3.3, see Fig. 3.3. The V boson polarization vectors are defined with respect to the null reference momentum $(|\boldsymbol{p}_V|, -\boldsymbol{p}_V)$, where $\boldsymbol{p}_V$ is the V momentum in the Vh centre of mass frame.

3.A.1 $pp \to Wh$

In this subsection, we give the exact helicity amplitudes of the process $pp \to Wh$ at LO in the SM and when generated by the dimension-6 operators $\mathcal{O}_{\varphi q}^{(3)}$, $\mathcal{O}_{\varphi \mathrm{W}}$ and $\mathcal{O}_{\varphi \widetilde{\mathrm{W}}}$. We follow the conventions defined before.

$$\begin{aligned} \mathcal{M}_{\mathrm{SM},\pm} &= \frac{i g_2^2}{2} \frac{M_W}{\sqrt{\hat{s}}} (1 \mp \cos\theta) \frac{1}{1-\varepsilon_W^2} \\ \mathcal{M}_{\mathrm{SM},0} &= \frac{i g_2^2}{2\sqrt{2}} \sin\theta \frac{1+\varepsilon_W^2-\varepsilon_H^2}{1-\varepsilon_W^2} \end{aligned} \tag{3.38}$$

$$\begin{aligned} \mathcal{M}^{(3)}_{\varphi q,\pm} &= 2i\, c^{(3)}_{\varphi q} \frac{\sqrt{\hat{s}} M_W}{\Lambda^2} (1 \mp \cos\theta) \frac{1}{1-\varepsilon_W^2} \\ \mathcal{M}^{(3)}_{\varphi q,0} &= i\sqrt{2}\, c^{(3)}_{\varphi q} \frac{\hat{s}}{\Lambda^2} \sin\theta \frac{1+\varepsilon_W^2-\varepsilon_H^2}{1-\varepsilon_W^2} \end{aligned} \tag{3.39}$$

$$\begin{aligned} \mathcal{M}_{\varphi \mathrm{W},\pm} &= 2i\, c_{\varphi \mathrm{W}} \frac{\sqrt{\hat{s}} M_W}{\Lambda^2} (1 \mp \cos\theta) \frac{1+\varepsilon_W^2-\varepsilon_H^2}{1-\varepsilon_W^2} \\ \mathcal{M}_{\varphi \mathrm{W},0} &= 4i\sqrt{2}\, c_{\varphi \mathrm{W}} \frac{M_W^2}{\Lambda^2} \sin\theta \frac{1}{1-\varepsilon_W^2} \end{aligned} \tag{3.40}$$

$$\begin{aligned} \mathcal{M}_{\varphi \widetilde{\mathrm{W}},\pm} &= 2\, c_{\varphi \widetilde{\mathrm{W}}} \frac{\sqrt{\hat{s}} M_W}{\Lambda^2} (1 \mp \cos\theta) \frac{\lambda(\varepsilon_W, \varepsilon_H)}{1-\varepsilon_W^2} \\ \mathcal{M}_{\varphi \widetilde{\mathrm{W}},0} &= 0\,, \end{aligned} \tag{3.41}$$

where $\lambda(\varepsilon_W, \varepsilon_H) \equiv \sqrt{(1+\varepsilon_W+\varepsilon_H)(1+\varepsilon_W-\varepsilon_H)(1-\varepsilon_W+\varepsilon_H)(1-\varepsilon_W-\varepsilon_H)}$ is sometimes referred to as the triangle function.

3.A.2 $pp \to Wh \to \ell\nu h$

Here, we write the full squared amplitudes for Wh production with $W \to \ell\nu$. The expressions are expanded in $M_W/\sqrt{\hat{s}}$ up to the order where even functions of ϕ_W appear in order to capture the dependence on ϕ_W in the presence of the neutrino momentum reconstruction ambiguity discussed in section 3.3.3.

The squared amplitudes and the interference terms between one BSM amplitude and the SM are given separately. The three BSM-BSM interference amplitudes are omitted for brevity since we are mainly interested in the regime where the dependence on the Wilson coefficients is linear. For convenience, we define the square of the W propagator denominator as $|\mathcal{D}_W|^2 \equiv (M_{\ell\nu}^2 - M_W^2)^2 + M_W^2\Gamma_W^2$.

$$|\mathcal{M}_{\mathrm{SM}}|^2 = \frac{g_2^6}{48}\Bigg[\frac{1}{4}\sin^2\theta\sin^2\theta_W + \frac{M_W}{\sqrt{\hat{s}}}\left(1-\cos\theta\cos\theta_W\right)\sin\theta\sin\theta_W\cos\phi_W + \frac{M_W^2}{\hat{s}}\left(1-\cos\theta\cos\theta_W\right)^2\cos^2\phi_W\Bigg]\frac{M_W^2}{|\mathcal{D}_W|^2} \tag{3.42}$$

$$2\,\mathrm{Re}\,\mathcal{M}_{\mathrm{SM}}\mathcal{M}_{\varphi q}^{(3)*} = \frac{c_{\varphi q}^{(3)}g_2^4}{6}\frac{\hat{s}}{\Lambda^2}\Bigg[\frac{1}{4}\sin^2\theta\sin^2\theta_W + \frac{M_W}{\sqrt{\hat{s}}}\left(1-\cos\theta\cos\theta_W\right)\sin\theta\sin\theta_W\cos\phi_W + \frac{M_W^2}{\hat{s}}\left\{\left(1-\cos\theta\cos\theta_W\right)^2 + \sin^2\theta\sin^2\theta_W\cos^2\phi_W\right\} - \frac{M_H^2}{2\hat{s}}\sin^2\theta\sin^2\theta_W\Bigg]\frac{M_W^2}{|\mathcal{D}_W|^2} \tag{3.43}$$

$$2\,\mathrm{Re}\,\mathcal{M}_{\mathrm{SM}}\mathcal{M}_{\varphi\mathrm{W}}^{*} = -\frac{g_2^4 c_{\varphi\mathrm{W}}}{6}\frac{M_W^2}{\Lambda^2}\Bigg[\left(1-\cos\theta\cos\theta_W\right)^2 + \sin^2\theta\sin^2\theta_W\cos^2\phi_W + \frac{1}{2}\frac{\sqrt{\hat{s}}}{M_W}\left(1-\cos\theta\cos\theta_W\right)\sin\theta\sin\theta_W\cos\phi_W\Bigg]\frac{M_W^2}{|\mathcal{D}_W|^2} \tag{3.44}$$

$$2\,\mathrm{Re}\,\mathcal{M}_{\mathrm{SM}}\mathcal{M}_{\varphi\widetilde{\mathrm{W}}}^{*} = \frac{g_2^4 c_{\varphi\widetilde{\mathrm{W}}}}{12}\frac{\sqrt{\hat{s}}M_W}{\Lambda^2}\Bigg[\left(1-\cos\theta\cos\theta_W\right)\sin\theta\sin\theta_W\sin\phi_W\Bigg]\frac{M_W^2}{|\mathcal{D}_W|^2} \tag{3.45}$$

$$\left|\mathcal{M}_{\varphi q}^{(3)}\right|^2 = \frac{g_2^2 c_{\varphi q}^{(3)2}}{3}\frac{\hat{s}^2}{\Lambda^4}\Bigg[\frac{1}{4}\sin^2\theta\sin^2\theta_W + \frac{M_W}{\sqrt{\hat{s}}}\left(1-\cos\theta\cos\theta_W\right)\sin\theta\sin\theta_W\cos\phi_W + \frac{M_W^2}{\hat{s}}\left(\sin^2\theta\sin^2\theta_W\cos^2\phi_W + \left(\cos\theta-\cos\theta_W\right)^2\right)\Bigg]\frac{M_W^2}{|\mathcal{D}_W|^2} \tag{3.46}$$

$$|\mathcal{M}_{\varphi \mathrm{W}}|^2 = \frac{g_2^2\, c_{\varphi \mathrm{W}}^2}{3} \frac{\hat{s} M_W^2}{\Lambda^4} \Bigg[\sin^2\theta \sin^2\theta_W \cos^2\phi_W + (\cos\theta - \cos\theta_W)^2 + \frac{M_W}{\sqrt{\hat{s}}} \sin\theta \sin\theta_W \left(1 - \cos\theta \cos\theta_W\right) \cos\left(\phi_W\right) \Bigg] \frac{M_W^2}{|\mathcal{D}_W|^2} \quad (3.47)$$

$$\left|\mathcal{M}_{\varphi \widetilde{\mathrm{W}}}\right|^2 = \frac{g_2^2\, c_{\varphi \widetilde{\mathrm{W}}}^2}{3} \frac{\hat{s} M_W^2}{\Lambda^4} \Bigg[(1 - \cos\theta \cos\theta_W)^2 - \sin^2\theta \sin^2\theta_W \cos^2\phi_W \Bigg] \frac{M_W^2}{|\mathcal{D}_W|^2} \quad (3.48)$$

3.A.3 $q\bar{q} \to Zh$

In this section, we report the exact $q\bar{q} \to Zh$ helicity amplitudes at tree level. The helicity of the fermion is denoted by $h = -1(+1)$ for a left- (right-) handed fermion and its electric charge by Q. The coupling of the SM Z-boson to the fermions is denoted by $g_{Z,f}^h$ where $g_{Z,f}^- = (T_{3,f} - s_{\mathrm{W}}^2 Q_f)/(s_{\mathrm{W}} c_{\mathrm{W}})$ and $g_{Z,f}^+ = -s_{\mathrm{W}} Q_f / c_{\mathrm{W}}$. Note that a common phase between any given SM and BSM helicity amplitude is not physical (we stress that it must be a common and not a relative phase) – all such phases have been removed for clarity.

$$\begin{aligned} \mathcal{M}_{\mathrm{SM},\pm} &= -\frac{4\pi\alpha\, g_{Z,f}^h}{\sqrt{2} c_{\mathrm{W}} s_{\mathrm{W}}} \frac{M_Z}{\sqrt{\hat{s}}} \frac{1 \pm h\cos\theta}{1 - \varepsilon_Z^2} \\ \mathcal{M}_{\mathrm{SM},0} &= -\frac{2\pi\alpha\, g_{Z,f}^h}{c_{\mathrm{W}} s_{\mathrm{W}}} \sin\theta \frac{1 - \varepsilon_H^2 + \varepsilon_Z^2}{1 - \varepsilon_Z^2} \end{aligned} \quad (3.49)$$

$$\begin{aligned} \mathcal{M}_{\varphi q,\pm}^{(3)} &= -(-1)^{3Q} \frac{1-h}{2} \sqrt{2}\, c_{\varphi q}^{(3)} \frac{M_Z \sqrt{\hat{s}}}{\Lambda^2} \frac{1 \pm h\cos\theta}{1 - \varepsilon_Z^2} \\ \mathcal{M}_{\varphi q,0}^{(3)} &= -(-1)^{3Q} \frac{1-h}{2} c_{\varphi q}^{(3)} \frac{\hat{s}}{\Lambda^2} \sin\theta \frac{1 - \varepsilon_H^2 + \varepsilon_Z^2}{1 - \varepsilon_Z^2} \end{aligned} \quad (3.50)$$

$$\begin{aligned} \mathcal{M}_{\varphi q,\pm}^{(1)} &= \frac{1-h}{2} \sqrt{2}\, c_{\varphi q}^{(1)} \frac{M_Z \sqrt{\hat{s}}}{\Lambda^2} \frac{1 \pm h\cos\theta}{1 - \varepsilon_Z^2} \\ \mathcal{M}_{\varphi q,0}^{(1)} &= \frac{1-h}{2} c_{\varphi q}^{(1)} \frac{\hat{s}}{\Lambda^2} \sin\theta \frac{1 - \varepsilon_H^2 + \varepsilon_Z^2}{1 - \varepsilon_Z^2} \end{aligned} \quad (3.51)$$

$$\begin{aligned} \mathcal{M}_{\varphi u,\pm} &= \frac{1+h}{2} \sqrt{2}\, c_{\varphi u} \frac{M_Z \sqrt{\hat{s}}}{\Lambda^2} \frac{1 \pm h\cos\theta}{1 - \varepsilon_Z^2} \\ \mathcal{M}_{\varphi u,0} &= \frac{1+h}{2} c_{\varphi u} \frac{\hat{s}}{\Lambda^2} \sin\theta \frac{1 - \varepsilon_H^2 + \varepsilon_Z^2}{1 - \varepsilon_Z^2} \end{aligned} \quad (3.52)$$

$$\begin{aligned}\mathcal{M}_{\varphi d,\pm} &= \frac{1+h}{2}\sqrt{2}\,c_{\varphi d}\,\frac{M_Z\sqrt{\hat{s}}}{\Lambda^2}\,\frac{1\pm h\cos\theta}{1-\varepsilon_Z^2}\\ \mathcal{M}_{\varphi d,0} &= \frac{1+h}{2}c_{\varphi d}\,\frac{\hat{s}}{\Lambda^2}\,\sin\theta\,\frac{1-\varepsilon_H^2+\varepsilon_Z^2}{1-\varepsilon_Z^2}\end{aligned} \tag{3.53}$$

3.A.4 Squared amplitudes and interference terms for $q\bar{q}\to Zh$

The squared SM amplitude and the SM-BSM interference terms for the process $q\bar{q}\to Zh$ are given below. Notice that we do not need to compute separately the cases where $Z\to\bar{\nu}\nu$ and $Z\to\ell^+\ell^-$ because our analysis is inclusive in the decay variables, differently from what was done in the Wh channel. For convenience, we define a function that depends on the scattering angle and is common among all squared and interference terms,

$$f(\hat{s},\theta) = (1-\varepsilon_H^2+\varepsilon_Z^2)^2\sin^2\theta + \frac{2M_Z^2}{\hat{s}}\,(3+\cos 2\theta)\ . \tag{3.54}$$

With this definition, the squared and interference terms are,

$$\begin{aligned}|\mathcal{M}_{\rm SM}|^2 &= \left(\frac{2\pi\alpha}{c_{\rm W}s_{\rm W}}\right)^2\frac{{g^-_{Z,q}}^2+{g^+_{Z,q}}^2}{(1-\varepsilon_Z^2)^2}\,f(\hat{s},\theta)\,,\\ 2\,\mathrm{Re}\,\mathcal{M}_{\rm SM}\mathcal{M}^{(3)*}_{\varphi q} &= \frac{4\pi\alpha}{c_{\rm W}s_{\rm W}}\frac{(-1)^{3Q}g^-_{Z,f}\,c^{(3)}_{\varphi q}}{(1-\varepsilon_Z^2)^2}\,\frac{\hat{s}}{\Lambda^2}\,f(\hat{s},\theta)\,,\\ 2\,\mathrm{Re}\,\mathcal{M}_{\rm SM}\mathcal{M}^{(1)*}_{\varphi q} &= -\frac{4\pi\alpha}{c_{\rm W}s_{\rm W}}\frac{g^-_{Z,f}\,c^{(1)}_{\varphi q}}{(1-\varepsilon_Z^2)^2}\,\frac{\hat{s}}{\Lambda^2}\,f(\hat{s},\theta)\,,\\ 2\,\mathrm{Re}\,\mathcal{M}_{\rm SM}\mathcal{M}^{*}_{\varphi u} &= -\frac{4\pi\alpha}{c_{\rm W}s_{\rm W}}\frac{g^+_{Z,u}\,c_{\varphi u}}{(1-\varepsilon_Z^2)^2}\,\frac{\hat{s}}{\Lambda^2}\,f(\hat{s},\theta)\,,\\ 2\,\mathrm{Re}\,\mathcal{M}_{\rm SM}\mathcal{M}^{*}_{\varphi d} &= -\frac{4\pi\alpha}{c_{\rm W}s_{\rm W}}\frac{g^+_{Z,d}\,c_{\varphi d}}{(1-\varepsilon_Z^2)^2}\,\frac{\hat{s}}{\Lambda^2}\,f(\hat{s},\theta)\,.\end{aligned} \tag{3.55}$$

3.B QCD and QED k-factors for diboson processes

The main processes contributing to the signal of the Zh channel ($q\bar{q}\to Zh$ and $q\bar{q}\to Wh$) were simulated at LO and we took into account QCD and QED NLO effects via k-factors. We computed the QCD k-factors with MadGraph5_aMC@NLO, while the QED ones were extracted from Ref. [209]. We verified that, in our bins, NLO QCD corrections have a negligible dependence on the Wilson coefficients $c^{(1)}_{\varphi q}$, $c^{(3)}_{\varphi q}$, $c_{\varphi u}$, and $c_{\varphi d}$. Thus, we rescaled the LO cross-sections by the SM k-factors. The NLO QED k-factors in Ref. [209] are given as a function of p_T^h. To compute them in our $p_{T\,\rm min}$ bins, we used an event-by-event rescaling.

The k-factors in the various $p_{T,min}$ bins are listed in Table 3.B.1 in the format $1+(k_{\rm QCD}-1)+(k_{\rm QED}-1)$. As one can see, they give an enhancement of the cross-section of up to 50%. QCD corrections, which enhance the cross-section, typically dominate. On the other hand, QED effects, which tend to lower the cross-section, are subleading in the low-energy bins, whereas they become comparable to the QCD ones at high energy.

$p_{T\,\mathrm{min}}$ bin [GeV]	$Zh \to \ell\ell\gamma\gamma$	$Zh \to \nu\bar{\nu}\gamma\gamma$	$Wh \to \nu\ell\gamma\gamma$
200 – 400	1 + 0.52 – 0.09 = 1.43	1 + 0.31 – 0.09 = 1.22	1 + 0.28 – 0.08 = 1.20
400 – 600	1 + 0.64 – 0.14 = 1.50	1 + 0.37 – 0.14 = 1.23	1 + 0.29 – 0.17 = 1.12
600 – 800	1 + 0.69 – 0.18 = 1.51	1 + 0.40 – 0.18 = 1.22	1 + 0.36 – 0.24 = 1.12
800 – 1000	1 + 0.70 – 0.24 = 1.46	1 + 0.40 – 0.24 = 1.16	1 + 0.37 – 0.32 = 1.05
1000 – ∞	1 + 0.69 – 0.32 = 1.37	1 + 0.40 – 0.32 = 1.08	1 + 0.37 – 0.40 = 0.97

Table 3.B.1: NLO k-factors for the main signal processes. Each entry shows separately the QCD and QED contributions to the k-factors. The accuracy on the determination of the k-factors is of order $few \times 10^{-2}$.

3.C Signal and background cross-sections in Vh diboson processes

In this appendix, we present the number of events per bin of the signal and background in each channel of $pp \to Vh$. This is valid for FCC-hh with c.o.m. energy of 100 TeV and integrated luminosity of 30 ab^{-1}. The number of events for the signal is presented as a quadratic function of the Wilson coefficients studied in each channel.

3.C.1 The Wh channel

In Table 3.C.1, we show the fits of the $Wh \to \ell\nu\gamma\gamma$ cross section as a function of the $c_{\varphi q}^{(3)}$, $c_{\varphi \mathrm{W}}$ and $c_{\varphi \widetilde{\mathrm{W}}}$ Wilson coefficients for the bins used in the global analysis of Section 3.6.5. The one-operator fit used in Sections 3.6.1-3.6.3 can be derived from this by setting $c_{\varphi \mathrm{W}} = c_{\varphi \widetilde{\mathrm{W}}} = 0$. We also present the total number of background events expected in each bin.

p_T^h bin	ϕ_W bin	Number of expected events	
		Signal	Background
$[200-400]\,\text{GeV}$	$[-\pi,0]$	$1310 + 10380\,c_{\varphi q}^{(3)} + 1290\,c_{\varphi \text{W}} + 641\,c_{\varphi\widetilde{\text{W}}} + 25700\left(c_{\varphi q}^{(3)}\right)^2 + 1510\,\left(c_{\varphi \text{W}}\right)^2 + 1350\left(c_{\varphi\widetilde{\text{W}}}\right)^2 + 5912\,c_{\varphi q}^{(3)}\,c_{\varphi \text{W}} + 3402\,c_{\varphi\widetilde{\text{W}}}\,c_{\varphi q}^{(3)} + 234\,c_{\varphi \text{W}}\,c_{\varphi\widetilde{\text{W}}}$	830
	$[0,\pi]$	$1310 + 10480\,c_{\varphi q}^{(3)} + 1250\,c_{\varphi \text{W}} - 651\,c_{\varphi\widetilde{\text{W}}} + 27000\left(c_{\varphi q}^{(3)}\right)^2 + 1470\,\left(c_{\varphi \text{W}}\right)^2 + 1400\left(c_{\varphi\widetilde{\text{W}}}\right)^2 + 5770\,c_{\varphi q}^{(3)}\,c_{\varphi \text{W}} - 2390\,c_{\varphi\widetilde{\text{W}}}\,c_{\varphi q}^{(3)} - 153\,c_{\varphi \text{W}}\,c_{\varphi\widetilde{\text{W}}}$	960
$[400-600]\,\text{GeV}$	$[-\pi,0]$	$284 + 5820\,c_{\varphi q}^{(3)} + 288\,c_{\varphi \text{W}} + 262\,c_{\varphi\widetilde{\text{W}}} + 35800\left(c_{\varphi q}^{(3)}\right)^2 + 872\,\left(c_{\varphi \text{W}}\right)^2 + 834\left(c_{\varphi\widetilde{\text{W}}}\right)^2 + 2900\,c_{\varphi q}^{(3)}\,c_{\varphi \text{W}} + 3400\,c_{\varphi\widetilde{\text{W}}}\,c_{\varphi q}^{(3)} + 72.3\,c_{\varphi \text{W}}\,c_{\varphi\widetilde{\text{W}}}$	119
	$[0,\pi]$	$283 + 5860\,c_{\varphi q}^{(3)} + 287\,c_{\varphi \text{W}} - 255\,c_{\varphi\widetilde{\text{W}}} + 36000\left(c_{\varphi q}^{(3)}\right)^2 + 876\,\left(c_{\varphi \text{W}}\right)^2 + 835\left(c_{\varphi\widetilde{\text{W}}}\right)^2 + 3260\,c_{\varphi q}^{(3)}\,c_{\varphi \text{W}} - 3760\,c_{\varphi\widetilde{\text{W}}}\,c_{\varphi q}^{(3)} - 75.7\,c_{\varphi \text{W}}\,c_{\varphi\widetilde{\text{W}}}$	129
$[600-800]\,\text{GeV}$	$[-\pi,0]$	$70 + 2760\,c_{\varphi q}^{(3)} + 69.4\,c_{\varphi \text{W}} + 98.9\,c_{\varphi\widetilde{\text{W}}} + 33500\left(c_{\varphi q}^{(3)}\right)^2 + 446\,\left(c_{\varphi \text{W}}\right)^2 + 439\left(c_{\varphi\widetilde{\text{W}}}\right)^2 + 1830\,c_{\varphi q}^{(3)}\,c_{\varphi \text{W}} + 2660\,c_{\varphi\widetilde{\text{W}}}\,c_{\varphi q}^{(3)} + 28.2\,c_{\varphi \text{W}}\,c_{\varphi\widetilde{\text{W}}}$	21
	$[0,\pi]$	$70 + 2850\,c_{\varphi q}^{(3)} + 74.1\,c_{\varphi \text{W}} - 102\,c_{\varphi\widetilde{\text{W}}} + 33800\left(c_{\varphi q}^{(3)}\right)^2 + 452\,\left(c_{\varphi \text{W}}\right)^2 + 427\left(c_{\varphi\widetilde{\text{W}}}\right)^2 + 1380\,c_{\varphi q}^{(3)}\,c_{\varphi \text{W}} - 2520\,c_{\varphi\widetilde{\text{W}}}\,c_{\varphi q}^{(3)} - 24.3\,c_{\varphi \text{W}}\,c_{\varphi\widetilde{\text{W}}}$	22
$[800-1000]\,\text{GeV}$	$[-\pi,0]$	$15 + 947\,c_{\varphi q}^{(3)} + 15.2\,c_{\varphi \text{W}} + 27.8\,c_{\varphi\widetilde{\text{W}}} + 17900\left(c_{\varphi q}^{(3)}\right)^2 + 159\,\left(c_{\varphi \text{W}}\right)^2 + 147\left(c_{\varphi\widetilde{\text{W}}}\right)^2 + 653\,c_{\varphi q}^{(3)}\,c_{\varphi \text{W}} + 864\,c_{\varphi\widetilde{\text{W}}}\,c_{\varphi q}^{(3)} + 5.54\,c_{\varphi \text{W}}\,c_{\varphi\widetilde{\text{W}}}$	3
	$[0,\pi]$	$15 + 947\,c_{\varphi q}^{(3)} + 15.3\,c_{\varphi \text{W}} - 28.8\,c_{\varphi\widetilde{\text{W}}} + 18200\left(c_{\varphi q}^{(3)}\right)^2 + 156\,\left(c_{\varphi \text{W}}\right)^2 + 149\left(c_{\varphi\widetilde{\text{W}}}\right)^2 + 541\,c_{\varphi q}^{(3)}\,c_{\varphi \text{W}} - 1150\,c_{\varphi\widetilde{\text{W}}}\,c_{\varphi q}^{(3)} - 10.3\,c_{\varphi \text{W}}\,c_{\varphi\widetilde{\text{W}}}$	5
$[1000-\infty]\,\text{GeV}$	$[-\pi,0]$	$4 + 426\,c_{\varphi q}^{(3)} + 4.12\,c_{\varphi \text{W}} + 9.72\,c_{\varphi\widetilde{\text{W}}} + 16400\left(c_{\varphi q}^{(3)}\right)^2 + 73.2\,\left(c_{\varphi \text{W}}\right)^2 + 69.7\left(c_{\varphi\widetilde{\text{W}}}\right)^2 + 281\,c_{\varphi q}^{(3)}\,c_{\varphi \text{W}} + 955\,c_{\varphi\widetilde{\text{W}}}\,c_{\varphi q}^{(3)} + 1.56\,c_{\varphi \text{W}}\,c_{\varphi\widetilde{\text{W}}}$	2
	$[0,\pi]$	$4 + 428\,c_{\varphi q}^{(3)} + 4.23\,c_{\varphi \text{W}} - 10.6\,c_{\varphi\widetilde{\text{W}}} + 16600\left(c_{\varphi q}^{(3)}\right)^2 + 71.4\,\left(c_{\varphi \text{W}}\right)^2 + 69.7\left(c_{\varphi\widetilde{\text{W}}}\right)^2 + 226\,c_{\varphi q}^{(3)}\,c_{\varphi \text{W}} - 740\,c_{\varphi\widetilde{\text{W}}}\,c_{\varphi q}^{(3)} - 3.13\,c_{\varphi \text{W}}\,c_{\varphi\widetilde{\text{W}}}$	1

Table 3.C.1: Number of expected signal and background events in the Wh channel at FCC-hh with $30\,\text{ab}^{-1}$. For the signal, it is given as a function of the Wilson coefficients (with $\Lambda = 1\,\text{TeV}$). Notice that the coefficients have errors of order *few* percent due to statistical fluctuations. The contribution of Wjj to the background events is neglected.

3.C.2 The Zh channel

In Tables 3.C.2 and 3.C.3, we show the fits of the signal and background cross-section in the various bins as a function of the $c_{\varphi q}^{(3)}$, $c_{\varphi q}^{(1)}$, $c_{\varphi u}$ and $c_{\varphi d}$ Wilson coefficients.

$p_{T,min}$ bin	$\lvert y_h\rvert$ bin	Number of expected events	
		Signal	Background
$[200-400]$ GeV	$[0,2]$	$2574 + 21600\,c_{\varphi q}^{(3)} + 1620\,c_{\varphi q}^{(1)} + 2430\,c_{\varphi u} - 1370\,c_{\varphi d} + 61900\left(c_{\varphi q}^{(3)}\right)^2 + 32600\left(c_{\varphi q}^{(1)}\right)^2 + 15930\left(c_{\varphi u}\right)^2 + 16620\left(c_{\varphi d}\right)^2 + (1500\pm600)\,c_{\varphi q}^{(3)}\,c_{\varphi q}^{(1)}$	1860
	$[2,6]$	$1928 + 15540\,c_{\varphi q}^{(3)} - (610\pm32)\,c_{\varphi q}^{(1)} + 2160\,c_{\varphi u} - 790\,c_{\varphi d} + 42500\left(c_{\varphi q}^{(3)}\right)^2 + 22600\left(c_{\varphi q}^{(1)}\right)^2 + 13240\left(c_{\varphi u}\right)^2 + 9280\left(c_{\varphi d}\right)^2 - (7500\pm500)\,c_{\varphi q}^{(3)}\,c_{\varphi q}^{(1)}$	1150
$[400-600]$ GeV	$[0,2]$	$406 + 9870\,c_{\varphi q}^{(3)} + 600\,c_{\varphi q}^{(1)} + 1250\,c_{\varphi u} - 620\,c_{\varphi d} + 79700\left(c_{\varphi q}^{(3)}\right)^2 + 42710\left(c_{\varphi q}^{(1)}\right)^2 + 21870\left(c_{\varphi u}\right)^2 + 21020\left(c_{\varphi d}\right)^2 - (1400\pm400)\,c_{\varphi q}^{(3)}\,c_{\varphi q}^{(1)}$	157
	$[2,6]$	$217 + 5050\,c_{\varphi q}^{(3)} - 400\,c_{\varphi q}^{(1)} + 821\,c_{\varphi u} - 262\,c_{\varphi d} + 38780\left(c_{\varphi q}^{(3)}\right)^2 + 21950\left(c_{\varphi q}^{(1)}\right)^2 + 13320\left(c_{\varphi u}\right)^2 + 8550\left(c_{\varphi d}\right)^2 - 9600\,c_{\varphi q}^{(3)}\,c_{\varphi q}^{(1)}$	78 ± 6
$[600-800]$ GeV	$[0,1.5]$	$75 + 3385\,c_{\varphi q}^{(3)} + 215\,c_{\varphi q}^{(1)} + 496\,c_{\varphi u} - 243\,c_{\varphi d} + 49020\left(c_{\varphi q}^{(3)}\right)^2 + 31340\left(c_{\varphi q}^{(1)}\right)^2 + 16130\left(c_{\varphi u}\right)^2 + 15200\left(c_{\varphi d}\right)^2 - (1800\pm200)\,c_{\varphi q}^{(3)}\,c_{\varphi q}^{(1)}$	17 ± 1
	$[1.5,6]$	$63 + 2796\,c_{\varphi q}^{(3)} - 206\,c_{\varphi q}^{(1)} + 487\,c_{\varphi u} - 169\,c_{\varphi d} + 39130\left(c_{\varphi q}^{(3)}\right)^2 + 25570\left(c_{\varphi q}^{(1)}\right)^2 + 15380\left(c_{\varphi u}\right)^2 + 10250\left(c_{\varphi d}\right)^2 - 10100\,c_{\varphi q}^{(3)}\,c_{\varphi q}^{(1)}$	17 ± 1
$[800-1000]$ GeV	$[0,1]$	$10 + 728\,c_{\varphi q}^{(3)} + (45\pm7)\,c_{\varphi q}^{(1)} + 111\,c_{\varphi u} - (50\pm4)\,c_{\varphi d} + 16510\left(c_{\varphi q}^{(3)}\right)^2 + 11320\left(c_{\varphi q}^{(1)}\right)^2 + 5790\left(c_{\varphi u}\right)^2 + 5460\left(c_{\varphi d}\right)^2 - (400\pm200)\,c_{\varphi q}^{(3)}\,c_{\varphi q}^{(1)}$	2.4 ± 0.4
	$[1,6]$	$16 + 1116\,c_{\varphi q}^{(3)} - (68\pm6)\,c_{\varphi q}^{(1)} + 210\,c_{\varphi u} - 71\,c_{\varphi d} + 24920\left(c_{\varphi q}^{(3)}\right)^2 + 17460\left(c_{\varphi q}^{(1)}\right)^2 + 10330\left(c_{\varphi u}\right)^2 + 7180\left(c_{\varphi d}\right)^2 - 6500\,c_{\varphi q}^{(3)}\,c_{\varphi q}^{(1)}$	3 ± 1
$[1000-\infty]$ GeV	$[0,1]$	$3 + 373\,c_{\varphi q}^{(3)} + (20\pm10)\,c_{\varphi q}^{(1)} + (63\pm4)\,c_{\varphi u} - (20\pm5)\,c_{\varphi d} + 17600\left(c_{\varphi q}^{(3)}\right)^2 + 12550\left(c_{\varphi q}^{(1)}\right)^2 + 6700\left(c_{\varphi u}\right)^2 + 5800\left(c_{\varphi d}\right)^2 - (1700\pm300)\,c_{\varphi q}^{(3)}\,c_{\varphi q}^{(1)}$	1.3 ± 0.3
	$[1,6]$	$4 + 498\,c_{\varphi q}^{(3)} - (30\pm10)\,c_{\varphi q}^{(1)} + (88\pm5)\,c_{\varphi u} - (44\pm5)\,c_{\varphi d} + 22250\left(c_{\varphi q}^{(3)}\right)^2 + 15800\left(c_{\varphi q}^{(1)}\right)^2 + 9670\left(c_{\varphi u}\right)^2 + 6270\left(c_{\varphi d}\right)^2 - (7500\pm300)\,c_{\varphi q}^{(3)}\,c_{\varphi q}^{(1)}$	1.9 ± 0.3

Table 3.C.2: Number of expected signal events as a function of the Wilson coefficients (with $\Lambda = 1$ TeV) and background events in the $Zh \to \nu\bar{\nu}\gamma\gamma$ channel at FCC-hh with $30\,\text{ab}^{-1}$ integrated luminosity. The Monte Carlo errors on the fitted coefficients, when not explicitly specified, are at most of order *few* %.

$p_{T,min}$ bin	$\lvert y_{Zh}\rvert$ bin	Number of expected events	
		Signal	Background
$[200-400]$ GeV	$[0,2]$	$433 + 3330\,c_{\varphi q}^{(3)} + 480\,c_{\varphi q}^{(1)} + 651\,c_{\varphi u} - 355\,c_{\varphi d}$ $+ 8800\left(c_{\varphi q}^{(3)}\right)^2 + 8780\left(c_{\varphi q}^{(1)}\right)^2$ $+ 4270\,\left(c_{\varphi u}\right)^2 + 4550\left(c_{\varphi d}\right)^2 + (600\pm 140)\,c_{\varphi q}^{(3)}\,c_{\varphi q}^{(1)}$	339
	$[2,6]$	$306 + 2270\,c_{\varphi q}^{(3)} - (164\pm 9)\,c_{\varphi q}^{(1)} + 548\,c_{\varphi u} - 185\,c_{\varphi d}$ $+ 5740\left(c_{\varphi q}^{(3)}\right)^2 + 5680\left(c_{\varphi q}^{(1)}\right)^2$ $+ 3370\,\left(c_{\varphi u}\right)^2 + 2320\left(c_{\varphi d}\right)^2 - (2270\pm 130)\,c_{\varphi q}^{(3)}\,c_{\varphi q}^{(1)}$	177
$[400-600]$ GeV	$[0,2]$	$84 + 1810\,c_{\varphi q}^{(3)} + 198\,c_{\varphi q}^{(1)} + 360\,c_{\varphi u} - 185\,c_{\varphi d}$ $+ 12650\left(c_{\varphi q}^{(3)}\right)^2 + 12610\left(c_{\varphi q}^{(1)}\right)^2$ $+ 6340\,\left(c_{\varphi u}\right)^2 + 6280\left(c_{\varphi d}\right)^2 - (240\pm 90)\,c_{\varphi q}^{(3)}\,c_{\varphi q}^{(1)}$	31
	$[2,6]$	$43 + 892\,c_{\varphi q}^{(3)} - 130\,c_{\varphi q}^{(1)} + 230\,c_{\varphi u} - 71\,c_{\varphi d}$ $+ 5940\left(c_{\varphi q}^{(3)}\right)^2 + 5980\left(c_{\varphi q}^{(1)}\right)^2$ $+ 3710\,\left(c_{\varphi u}\right)^2 + 2250\left(c_{\varphi d}\right)^2 - 2960\,c_{\varphi q}^{(3)}\,c_{\varphi q}^{(1)}$	13
$[600-800]$ GeV	$[0,2]$	$22 + 936\,c_{\varphi q}^{(3)} + (67\pm 4)\,c_{\varphi q}^{(1)} + 201\,c_{\varphi u} - 97\,c_{\varphi d}$ $+ 12390\left(c_{\varphi q}^{(3)}\right)^2 + 12350\left(c_{\varphi q}^{(1)}\right)^2$ $+ 6430\,\left(c_{\varphi u}\right)^2 + 5930\left(c_{\varphi d}\right)^2 - (950\pm 90)\,c_{\varphi q}^{(3)}\,c_{\varphi q}^{(1)}$	5
	$[2,6]$	$9 + 346\,c_{\varphi q}^{(3)} - 64\,c_{\varphi q}^{(1)} + 91\,c_{\varphi u} - 26\,c_{\varphi d}$ $+ 4370\left(c_{\varphi q}^{(3)}\right)^2 + 4380\left(c_{\varphi q}^{(1)}\right)^2$ $+ 2830\,\left(c_{\varphi u}\right)^2 + 1560\left(c_{\varphi d}\right)^2 - 2540\,c_{\varphi q}^{(3)}\,c_{\varphi q}^{(1)}$	2
$[800-1000]$ GeV	$[0,2]$	$4.7 + 318\,c_{\varphi q}^{(3)} + (14\pm 3)\,c_{\varphi q}^{(1)} + 69\,c_{\varphi u} - (30\pm 2)\,c_{\varphi d}$ $+ 6690\left(c_{\varphi q}^{(3)}\right)^2 + 6720\left(c_{\varphi q}^{(1)}\right)^2$ $+ 3560\,\left(c_{\varphi u}\right)^2 + 3130\left(c_{\varphi d}\right)^2 - (830\pm 70)\,c_{\varphi q}^{(3)}\,c_{\varphi q}^{(1)}$	1.1 ± 0.08
	$[2,6]$	$1.48 + 95\,c_{\varphi q}^{(3)} - (23\pm 2)\,c_{\varphi q}^{(1)} + 25\,c_{\varphi u}$ $- (7.6\pm 0.8)\,c_{\varphi d} + 1890\left(c_{\varphi q}^{(3)}\right)^2 + 1910\left(c_{\varphi q}^{(1)}\right)^2$ $+ 1252\,\left(c_{\varphi u}\right)^2 + 645\left(c_{\varphi d}\right)^2 - (1240\pm 40)\,c_{\varphi q}^{(3)}\,c_{\varphi q}^{(1)}$	0.29 ± 0.04
$[1000-\infty]$ GeV	$[0,2]$	$1.31 + 163\,c_{\varphi q}^{(3)} - (0.4\pm 4.7)\,c_{\varphi q}^{(1)} + 41\,c_{\varphi u}$ $- (14\pm 2)\,c_{\varphi d} + 7280\left(c_{\varphi q}^{(3)}\right)^2 + 7310\left(c_{\varphi q}^{(1)}\right)^2$ $+ 4120\,\left(c_{\varphi u}\right)^2 + 3240\left(c_{\varphi d}\right)^2 - (1780\pm 100)\,c_{\varphi q}^{(3)}\,c_{\varphi q}^{(1)}$	0.44 ± 0.04
	$[2,6]$	$0.29 + 32\,c_{\varphi q}^{(3)} - (9\pm 2)\,c_{\varphi q}^{(1)} + (10.5\pm 0.9)\,c_{\varphi u}$ $- (1.7\pm 0.8)\,c_{\varphi d} + 1230\left(c_{\varphi q}^{(3)}\right)^2 + 1240\left(c_{\varphi q}^{(1)}\right)^2$ $+ 842\,\left(c_{\varphi u}\right)^2 + 379\left(c_{\varphi d}\right)^2 - (940\pm 40)\,c_{\varphi q}^{(3)}\,c_{\varphi q}^{(1)}$	0.12 ± 0.03

Table 3.C.3: Number of expected signal events as a function of the Wilson coefficients (with $\Lambda = 1$ TeV) and background events in the $Zh \to \ell^+\ell^-\gamma\gamma$ channel at FCC-hh with $30\,\text{ab}^{-1}$ integrated luminosity. The Monte Carlo errors on the fitted coefficients, when not explicitly specified, are at most of order *few* %.

3.D Universal Theories

In the SMEFT framework, Universal Theories are defined as those for which the leading BSM effects at order $1/\Lambda^2$ can be captured exclusively by operators that only involve SM bosons after an appropriate field redefinition [216]. This definition is clearly base-dependent, but before discussing it in a particular basis, let us give some UV perspective. Typical Universal Theories are those where new heavy states couple only to the SM bosons and models where the SM fermions are weakly coupled to the BSM sector via the vector and/or scalar SM currents [216].

Regardless of the chosen dimension-6 basis, Universal Theories are always described by 16 independent parameters [216]. In terms of the Warsaw basis, they are described by the following subset of operators:

$$\begin{aligned} &\mathcal{O}_{\varphi W},\, \mathcal{O}_{\varphi WB},\, \mathcal{O}_{\varphi B},\, \mathcal{O}_{\varphi G},\, \mathcal{O}_{3W},\, \mathcal{O}_{3G},\, \mathcal{O}_{\varphi D},\, \mathcal{O}_{\varphi\Box}, \\ &\mathcal{O}_{\varphi},\, \mathcal{O}_{\varphi JW},\, \mathcal{O}_{\varphi JB},\, \mathcal{O}_{2JW},\, \mathcal{O}_{2JB},\, \mathcal{O}_{2JG},\, \mathcal{O}_{y},\, \mathcal{O}_{2y}, \end{aligned} \tag{3.56}$$

where the last 7 correspond to the linear combinations defined in Table 3.D.1 [216]. For the operators that enter in the Vh production process, the Universal Theory scenario implies correlations among their WCs [162, 166, 216],

$$\begin{aligned} c_{\varphi q}^{(3)} &= c_{\varphi \ell}^{(3)}, \\ c_{\varphi q}^{(1)} &= \frac{Y_q}{Y_\ell} c_{\varphi \ell}^{(1)}, \\ c_{\varphi q}^{(1)} &= \frac{Y_q}{Y_j} c_{\varphi j}, \end{aligned} \tag{3.57}$$

for $j = u,\, d,\, e$, with Y_ψ being the hypercharge of the field ψ, and where for completeness we have included the leptonic counterpart to the operators of our interest.

The vertex corrections $\delta g_{L,R}^{Zq}$ for Universal Theories can be expressed in terms of the oblique Peskin-Takeuchi parameters as [117, 166, 216]

$$\delta g_{L,R}^{Zq} = \frac{1}{2} T_q^3 \left(\hat{T} - W - t_W^2 Y\right) + \frac{Q_q}{2} \frac{s_W^2}{1 - 2s_W^2} \left(W + \hat{T} - 2\hat{S} + Y\left(2 - t_W^2\right)\right), \tag{3.58}$$

which is valid for any SM fermion. This leads to the relations

$$\delta g_R^{Zu} = 2\left(\delta g_L^{Zu} + \delta g_L^{Zd}\right), \qquad \delta g_R^{Zd} = -\left(\delta g_L^{Zu} + \delta g_L^{Zd}\right). \tag{3.59}$$

It is trivial to check the third line in Eq. (3.57) by combining Eq. (3.26) and (3.59) [162, 166]. Hence, the 2 independent WCs relevant for diboson processes, $c_{\varphi q}^{(1)}$ and $c_{\varphi q}^{(3)}$ according to our choice, can be expressed as

$$\begin{aligned} c_{\varphi q}^{(3)} &= +\frac{\Lambda^2}{4m_W^2} g^2 \left(\frac{s_W^2}{1 - 2s_W^2}\left(\frac{Y}{2} - \hat{S}\right) + \frac{c_W^2}{1 - 2s_W^2}\frac{\hat{T}}{2} + \left(\frac{s_W^2}{1 - 2s_W^2} - 1\right) W - c_W^2\, \delta g_{1z}\right), \\ c_{\varphi q}^{(1)} &= -\frac{\Lambda^2}{4m_W^2} g^2 \left(\frac{s_W^2}{3c_{2W}}\left(\frac{\hat{T} + W}{2} - \hat{S}\right) + \left(\frac{s_W^2}{c_{2W}} + t_W^2\right)\frac{Y}{6} + \frac{1}{3}\left(t_W^2 \delta\kappa_\gamma - s_W^2 \delta g_{1z}\right)\right). \end{aligned} \tag{3.60}$$

If $W, Y, \hat{T} \ll 1$, then these two WCs define two specific directions in the $\hat{S}$, δg_{1z}, $\delta\kappa_\gamma$ space. Sometimes, like in Ref. [162, 164], the directions $\delta g_{1z} c_W^2 + \frac{s_W^2}{c_{2W}}\hat{S}$ and $\delta\kappa_\gamma - \hat{S}$ for convenience. Notice that, in the main text, we made a different assumption: $\delta g_L^{Zq} \ll 1$, which nullifies two

Universal Theories	Warsaw basis
$\mathcal{O}_{\varphi JW}$	$\frac{g^2}{4}\left(\mathcal{O}^{(3)}_{\varphi q,ii}+\mathcal{O}^{(3)}_{\varphi \ell,ii}\right)$
$\mathcal{O}_{\varphi JB}$	$\frac{g_Y^2}{2}\left(\sum_{k=q,\ell} Y_k \mathcal{O}^{(1)}_{\varphi k,ii}+\sum_{j=u,d,e} Y_j \mathcal{O}_{\varphi j,ii}\right)$
$\mathcal{O}_{2JW}$	$\frac{g^2}{2}\left(\frac{1}{2}\mathcal{O}^{(3)}_{qq,iijj}-\frac{1}{2}\mathcal{O}_{\ell\ell,iijj}+\mathcal{O}_{\ell\ell,ijji}+\mathcal{O}^{(3)}_{\ell q,ijji}\right)$
$\mathcal{O}_{2JB}$	$g_Y^2\left(Y_q^2\mathcal{O}^{(1)}_{qq,iijj}+\sum_{k=\ell,u,d,e} Y_k^2\mathcal{O}_{kk,iijj}+2Y_qY_\ell\mathcal{O}^{(1)}_{\ell q,iijj}\right.$ $+2Y_qY_e\mathcal{O}_{qe,iijj}+2\sum_{k=u,d} Y_k(Y_e\mathcal{O}_{ek,iijj}+Y_q\,\mathcal{O}^{(1)}_{qk,iijj})$ $\left.+\sum_{k=u,d,e} 2Y_\ell Y_k\mathcal{O}_{\ell k,iijj}+2Y_uY_d\mathcal{O}^{(1)}_{ud,iijj}\right)$
$\mathcal{O}_{2JG}$	$g_s^2\left(-\frac{1}{6}\mathcal{O}^{(1)}_{qq,iijj}+\frac{1}{4}\mathcal{O}^{(1)}_{qq,ijji}+\frac{1}{4}\mathcal{O}^{(3)}_{qq,ijji}+2\mathcal{O}^{(8)}_{ud,iijj}\right.$ $\left.+\sum_{k=u,d} 2\mathcal{O}^{(8)}_{qk,iijj}-\frac{1}{6}\mathcal{O}_{kk,iijj}+\frac{1}{2}\mathcal{O}_{kk,ijji}\right)$
$\mathcal{O}_y$	$y_{u,ij}\mathcal{O}_{u\varphi,ij}+[V_{CKM}y_d]_{ij}\,\mathcal{O}_{d\varphi,ij}+y_{e,ij}\mathcal{O}_{e\varphi,ij}$+h.c.
$\mathcal{O}_{2y}$	$-y_{u,il}\;y^\dagger_{u,kj}\left(\frac{1}{6}\mathcal{O}^{(1)}_{qu,ijkl}+\mathcal{O}^{(8)}_{qu,ijkl}\right)$ $-[V_{CKM}y_d]_{il}\left[y_d^\dagger V_{CKM}^\dagger\right]_{kj}\left(\frac{1}{6}\mathcal{O}^{(1)}_{qd,ijkl}+\mathcal{O}^{(8)}_{qd,ijkl}\right)$ $-\frac{1}{2}y_{e,il}y^\dagger_{e,kj}\mathcal{O}_{\ell e,ijkl}+y_{u,ij}\,[V_{CKM}y_d]_{kl}\,\mathcal{O}^{(1)}_{quqd,ijkl}$ $-y_{e,ij}\,[y_u]_{kl}\,\mathcal{O}^{(1)}_{lequ,ijkl}+y_{e,ij}\left[y_d^\dagger V_{CKM}^\dagger\right]_{kl}\mathcal{O}_{ledq,ijkl}$ + h.c.

Table 3.D.1: Universal Theories basis operators in terms of the Warsaw basis. There are other 9 operators that map one-to-one with the Warsaw basis, see Eq. (3.56). The indices in the operators, CKM and Yukawa matrices are generation indices and there is an implicit sum over those that are repeated. Y_ψ is the hypercharge of the field ψ.

directions in the $\hat{S}$, $\hat{T}$, W, Y space and maps $c^{(1)}_{\varphi q}$, $c^{(3)}_{\varphi q}$ onto the δg_{1z}, $\delta\kappa_\gamma$ plane.

This page is intentionally left blank.

Chapter 4

Gauge anomalies in the SMEFT

“This is just as it must be. ”

— Niels Bohr, as quoted by C. P. Snow in The Physicists - A generation that changed the world (1981), p.96

4.1 Introduction

In Chapter 3, we showed a concrete example of how to use the theoretical tools to assess the potential of the future experiments. Now, we will change the focus and start looking more deeply at the theoretical tool itself. This is relevant because gaining a deeper knowledge of the inner structure and properties of a tool is the only certain way to unlock and exploit its full potential.

In that spirit, the community has devoted bigger efforts to the formal study of EFTs over the last years. An EFT is a Quantum Field Theory and as such it must fulfil some minimal consistency requirements. One of the most basic is generating an unitary scattering matrix, which arises from the elementary principle of probability conservation [47,228]. If unitarity were not respected, the theory would not make sensible predictions for the probability of transitioning between states. The loss of unitarity is, then, one of the biggest threats for the sanity of any quantum theory.

A possible cause of unitarity loss is a remarkable effect intrinsic to the quantum nature of QFTs: (chiral) anomalies. Anomalies can not be defined without previously stressing the fundamental importance of symmetries. The usefulness of symmetries in Physics is beyond doubt, however, in QFT they take an essential constructive role. More precisely, the requirement of local gauge symmetries in a theory constrains greatly the interactions allowed and has become our preferred and very successful way to model fundamental interactions. Our modern understanding of fundamental forces of nature is fully based on symmetries. Even more, as stressed in Chapter 2, gauge and global symmetries are basic constructive principles for EFTs.

Since the earliest days of quantum mechanics, we have known that the classical properties of a system might not preserved at quantum level and this is not less true for symmetries. A Lagrangian that possesses a certain symmetry at classical level can yield a quantum theory that breaks such a symmetry due to quantum corrections. The symmetry is said to be broken by anomalies. The existence of anomalies for a classically-conserved symmetry can be determined by computing the 1-loop correction to the divergence of the classically-conserved Noether current. Details about the computations of anomalies can be found in Section 4.2 and in any modern QFT textbook or in reviews like Ref. [229]. Here, we will only review the essential results before

returning to discuss their importance for the consistency of EFTs.

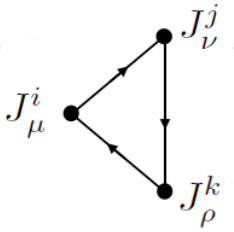

Figure 4.1.1: One-loop triangle diagram that generates anomalies. $J^{A,B,C}_\mu$ are the classically conserved currents of the (global or local) symmetries A, B, and C. All the fermions charged under those symmetries run in the loop.

The presence of anomalies can be traced back to a non-vanishing divergence of a 1-loop 3-point Green function involving 3 classically-conserved Noether currents:

$$\partial^\mu \langle 0|J^A_\mu(x)\, J^B_\nu(y)\, J^C_\rho(z)\,|0\rangle \neq 0, \tag{4.1}$$

where $J^i_\mu = \overline{\psi}\gamma_\mu T^i \psi$ is the classically-conserved Noether current of the (global or local) symmetry $i = A, B, C$, with T^i the symmetry generator in the irrep under which the fermion transforms[1], and the product of currents is understood to be time ordered [230]. The inequality is generated by 1-loop triangle diagrams like the one showed in Fig. 4.1.1, where the external legs are the Noether currents, and all the fermions in the theory charged under such currents run in the loop. The computation boils down to

$$\partial^\mu \langle 0|J^A_\mu(x)\, J^B_\nu(y)\, J^C_\rho(z)\,|0\rangle \propto D^{ABC} = \sum_{LH\psi} \mathrm{tr}\left(T_A\{T_B, T_C\}\right) - \sum_{RH\psi} \mathrm{tr}\left(T_A\{T_B, T_C\}\right), \tag{4.2}$$

where D^{ABC} is the so-called anomaly polynomial. There is an anomaly if and only if that polynomial is non-vanishing. And that happens when there are are right-handed (RH) fermions with different charges than the left-handed (LH) ones, hence the usual name of chiral anomalies. Notice that for the case of all abelian symmetries, the trace simplifies to $q^\psi_A q^\psi_B q^\psi_C$. From Eq. (4.2), one can obtain, e.g. via background field methods, the usual expression for an anomalous current J^A_μ [229, 231, 232]:

$$\langle \partial^\mu J^A_\mu \rangle = g_B\, g_C \frac{D^{ABC}}{32\pi^2} \epsilon^{\mu\nu\rho\sigma} F^B_{\mu\nu} F^C_{\rho\sigma}, \tag{4.3}$$

where the expectation value of the divergence of the current is taken in presence of a fixed background field and g_B (g_C) is the gauge coupling associated to the field strength $F^B_{\mu\nu}$ ($F^C_{\rho\sigma}$). If any of the symmetries B or C is non-abelian, the corresponding group indices will appear contracted between the generator included in D^{ABC} and the corresponding field strength. If the symmetry A is non-abelian, A can be interpreted as the group index.

The computation of an anomaly is essentially the same for global and local gauge symmetries, but its consequences differ. Here, we will cover the latter case and we leave the case of global symmetries for Chapter 5. A gauge anomaly poses two threats to a QFT. One is the lack of renormalisability up to infinite energy. This happens because gauge symmetry, particularly for non-abelian groups, softens the divergences while the anomaly breaks the symmetry, hence reviving the divergences. However, this is not a concern for EFTs which, by definition, are equipped with a finite cutoff Λ.

[1]The generator does not need to be the same for each fermion chirality, i.e. the symmetry might be chiral.

The second threat posed by gauge anomalies is the loss of unitarity or Lorentz invariance, since gauge symmetry is needed to establish the equivalence between the covariant and the physical gauges of a theory, which allows it to respect both unitarity and Lorentz invariance at the same time. In fact, their possible loss is usually the main reason behind the requirement of no gauge anomalies in an EFT. Notice that in an EFT one can ask for unitarity only for energies up to the cutoff. Gauge anomalies could generate a loss of unitarity below such scale. However, the problem can be avoided by lifting one crucial assumption: that the gauge boson must be massless. If the gauge boson is allowed to have a mass, an anomalous gauge EFT can be quantized consistently with unitarity and Lorentz invariance up to the cutoff scale [233]. In that case, the gauge anomaly just signals the existence of a cutoff and an anomalous spectrum above it.

The procedure to quantize this anomalous EFT with a massive gauge boson works for abelian, non-abelian and mixed gauge anomalies. The trick is to introduce a non-dynamical fictitious pure-gauge pseudo-scalar field θ that couples derivatively to the anomalous fermions and cancels the anomaly. This gives an anomaly-free gauge-invariant EFT that is just a different description of the physical anomalous EFT. The latter is recovered for the gauge choice $\theta = 0$. The gauge boson has a mass generated at loop level by the anomaly and the gauge-artefact θ can be understood as the would-be NGB "eaten" by the massive gauge boson, although it is not necessary to suppose a Higgs-mechanism in the UV. Additionally, one can derive an upper bound on the cutoff of this anomalous EFT given by the gauge boson mass and the gauge couplings and charges[2]. For more details, see Ref. [233].

At this stage, it is useful to notice that the assignment of the anomaly to one of the currents in Eq. (4.2) is ambiguous. In an UV complete theory, one has always the freedom to choose which symmetry current carries an anomaly (see e.g. the sections on anomalies of classic textbooks such as [231, 234, 235], or [236]). This can be understood precisely as the freedom to add local counterterms (such as Eq. (4.6), which we will properly introduce later) related to momentum shift ambiguities in loop diagrams, as we will explicitly show in subsection 4.2.3. In particular, in a theory free of gauge anomalies, one can (and should) always choose the regulator and the counterterms such that the effective action does not shift under a gauge transformation. It is for instance done when computing the axial anomaly that determines the pion decay rate to two photons at leading order, and it is a consistency requirement, namely that our theory must be such that massless vectors couple to exactly conserved currents.

So far, we have established the reasons for our interest in anomalies and, more specifically gauge anomalies as well as stating their consequences for EFTs. The SM was built as a fully renormalisable QFT, which excludes the possibility of allowing any gauge anomaly in it. In fact, the hypercharge assignment of the SM fermion fields ensures the absence of said anomalies as we show in Appendix 4.A.

The SMEFT, on the other hand, could accommodate some gauge anomalies since it is an EFT with some massive gauge fields. Nevertheless, it was understood that sharing the field content of the anomaly-free SM was enough to avoid the presence of gauge anomalies. This belief was not doubted nor checked thoroughly until very recently. Some of the first efforts to check it brought to the spotlight the following dimension-6 operators [237]:

$$\begin{aligned}
&\mathcal{O}_{\varphi\psi_R} = i\frac{c_{\varphi\psi,ij}}{\Lambda^2}\left(H^\dagger \overleftrightarrow{D}_\mu H\right)\overline{\psi}^i_R\gamma^\mu\psi^j_R\ , \\
&\mathcal{O}^{(1)}_{\varphi\psi_L} = i\frac{c^{(1)}_{\varphi\psi,ij}}{\Lambda^2}\left(H^\dagger \overleftrightarrow{D}_\mu H\right)\overline{\psi}^i_L\gamma^\mu\psi^j_L\ , \quad \mathcal{O}^{(3)}_{\varphi\psi_L} = i\frac{c^{(3)}_{\varphi\psi,ij}}{\Lambda^2}\left(H^\dagger \overleftrightarrow{D}^a_\mu H\right)\overline{\psi}^i_L\tau^a\gamma^\mu\psi^j_L\ ,
\end{aligned} \tag{4.4}$$

[2]Interestingly, the strength of the anomaly enters into this upper bound for abelian and mixed anomalies, but not for the non-abelian case [233].

where we use the conventions of Ref. [116] and $\psi_{L,R}$ spans over the SM chiral fermion fields. These operators, in the broken phase, modify the gauge interactions of the fermions at order $1/\Lambda^2$ in a chiral fashion. Hence, they generate additional triangle diagrams whose contribution to the anomaly is not naively ensured to cancel, despite respecting the hypercharge choice that wipes out the dimension-4 gauge anomalies (for a detailed discussion of the results in Ref. [237], see Appendix 4.B). Coincidentally, the subset of these operators with quarks fields were studied in Chapter 3.

If there were new gauge anomalies at dimension 6, what would this mean for SMEFT? Would this impose constraints on its parameter space? How could this affect its matching with UV models? Would there be a simple way to tell whether the UV completion of the SM is an anomalous sector or not by measuring a few observables? And if there are no new gauge anomalies, what can we conclude about the UV models that can match onto SMEFT? Would this be expected to hold at any order in $1/\Lambda$? All those questions drive our exploration of this topic, but before even trying to wonder about them we must test the existence of anomalies at dimension 6.

Throughout the rest of this chapter, we will answer the question of whether the operators in Eq. (4.4) can generate new gauge anomalies in SMEFT at dimension 6 via triangle diagrams. We will do it using a known but unconventional technique that simplifies the computations and is introduced in Section 4.2. Then, in Section 4.3, we analyse the problem with a simple toy model. This toy model allows us to use conventional and textbook-like techniques first, and then our technique introduced before, which validates the results offered by the latter and, most importantly, offer insights into the ultimate origin of the result. Finally, we apply the technique shown in Section 4.2 to the SMEFT in Section 4.4. We summarize and reflect on our findings in Section 4.5.

4.2 Bosonic EFT techniques

4.2.1 Anomalous fermions in the IR from the UV

How anomalies are transported across energy scales is an old and fruitful question that leads inevitably to analyse the relation between anomalies and EFTs. This relation is profoundly influenced by one remarkable fact: anomalies do not renormalise and must be consistently matched across all the energies [229, 231, 234]. Although the best known application of this is in the context of QCD and with global symmetries, in what is known as 't Hooft's anomaly matching [238], its relevance for gauge symmetries should not be minimised. More precisely, the line of reasoning in 't Hooft's argument is highly general and can be easily applied to gauge anomalies as we will show in the following. It is important to remark that this procedure has been in the literature for decades [231, 233, 239, 240]. Here, we will review it but with our focus aimed at its application to the SMEFT.

Consider an anomaly-free renormalisable gauge theory which possesses a chiral fermion spectrum. Its scalar sector comprises a charged scalar with a non-vanishing VEV v which interacts with the fermions via Yukawa terms. Hence, the fermions are in general massive and there is at least one massive gauge boson. By adjusting properly the Yukawa couplings, we can make some fermions much heavier than the rest of them. In particular, we can generate a group of heavy fermions that are anomalous among themselves. The group of light fermions, given our assumption of an anomaly-free theory, must contribute to the gauge anomalies exactly in the opposite way [233, 238].

Since there is a gap in the fermion mass spectrum, we can integrate out the heavy fermions. If the mass of the physical scalar is similar to the one of the fermions, we can integrate it out

too. Instead, we assume that the massive gauge boson has a smaller mass than the previously mentioned particles thanks to a small gauge coupling. Hence, we can derive from our original renormalisable theory an EFT which contains all the gauge bosons, massive or not, and a set of anomalous chiral light fermions. This EFT should be free of gauge anomalies because it was derived from an UV model with such a feature, but if we compute triangle diagrams with its light fermions, we would obtain non-vanishing anomaly polynomials. Therefore, the EFT should reflect in some way the heavy fermions contribution to the anomalies so it cancels the anomalous triangle diagrams with light fermions [231, 233]. The argument does not break down with the inclusion of non-renormalisable couplings involving the fermions that could generate additional anomalies, as long as they can be added to both the light and heavy fermions.

It is clear that the light fermions in our argument play the same role than the spectator fermions found in 't Hooft's anomaly matching and that the fake gauge bosons in the latter, here become real. Moreover, this analogy allows us to go one step further: we could take a theory and integrate out all of its fermions. If the original theory had gauge anomalies, they could be cancelled with the addition of light spectator fermions, then run the argument explained in the previous paragraph and finally decouple the spectator fermions to obtain a purely bosonic EFT, which should show the gauge anomalies of the original theory [229, 233, 239]. Thus, how does the EFT acknowledge the existence of UV fermions that cancel the anomaly? We will answer this question in subsection 4.2.2

4.2.2 Gauge variant terms in the EFT

An EFT acknowledges the existence of heavy anomalous fermions via the so-called Wess-Zumino (WZ) terms. They are gauge-variant terms, since they are anomalous, and can be derived in all generality as a solution to a Slavnov-Taylor identity by assuming the Wess-Zumino consistency conditions for anomalies [231, 240]. Nevertheless, here we will skip their formal derivation and limit ourselves to work with gauge variations at linear order. Moreover, we will treat in detail only the case of several independent abelian gauge fields because this is enough to analyse the anomalies generated by triangle diagrams. The non-abelian generalisation can be done straightforwardly although the formulae become more cumbersome.

For the rest of this section, we will assume an EFT whose gauge group is a product of abelian groups, $G = \otimes_i \mathrm{U}(1)_i$, and contains several charged scalars $\phi_i = \frac{f_i + h_i}{\sqrt{2}} e^{i\theta_i/f_i}$ such that some of those gauge symmetries are spontaneously broken. The Wess-Zumino terms can be classified in two classes [241]. First, we have the axionic (or Peccei-Quinn) terms

$$\mathcal{L}_{EFT,\,ax} = \frac{\mathcal{C}_{ijk}}{16\pi^2} \frac{\theta_i}{f_i} F_{j,\mu\nu} \tilde{F}_k^{\mu\nu}\,, \tag{4.5}$$

where $F_{j,\mu\nu}$ is the field strength of the abelian gauge field $A_{j,\mu}$, and $\tilde{F}_j^{\mu\nu}$ is its dual defined as $\tilde{F}_j^{\mu\nu} = \frac{1}{2}\epsilon^{\mu\nu\rho\sigma} F_{j,\rho\sigma}$. We assume that all the repeated indices are summed over. Notice that the gauge variation of these terms comes exclusively from the NGB. Moreover, the name of this class of operators emphasizes the fact that they can be written also for NGBs of global symmetries and, in that case, includes the famous $aF\tilde{F}$ operator that is ubiquitous in axion physics. Nevertheless, here we will restrict ourselves to NGBs of gauge symmetries.

The second class of Wess-Zumino terms is the Generalized Chern-Simons terms (GCS), which can be written as

$$\mathcal{L}_{EFT,\,GCS} = \frac{E_{ijk}}{8\pi^2} A_{i,\mu} A_{j,\nu} \tilde{F}_k^{\mu\nu}\,. \tag{4.6}$$

It is clear that the term vanishes for $i = j$. Moreover, not all the GCS terms are independent

since

$$A_{i,\mu}A_{j,\nu}\tilde{F}_k^{\mu\nu} + A_{k,\mu}A_{i,\nu}\tilde{F}_j^{\mu\nu} + A_{j,\mu}A_{k,\nu}\tilde{F}_i^{\mu\nu} = \epsilon^{\mu\nu\rho\sigma}\partial_\mu\left(A_{i,\nu}A_{j,\rho}A_{k,\sigma}\right). \tag{4.7}$$

This indicates that if all the indices are different, there are two independent terms. If any pair of the indices i, j, k is equal, the RHS vanishes and the term with the different index in the dual field strength tensor vanishes. Then, the equation relates the two remaining term and there is only one independent GCS term for the case of 2 equal indices.

The WCs $\mathcal{C}_{ijk}$ and E_{ijk} have to be computed at 1-loop level from triangle diagrams like the ones showed in Fig. 4.2.1, where the diagrams (a) and (b) correspond to axionic and GCS terms respectively. We show explicitly how to do this for a toy model in subsection 4.2.3. Nevertheless, we wish to do some important remarks before diving into the loop computation. First, from the normalisation of the operators and their energy dimensions, one can notice that the WCs are expected to not be suppressed by the masses of the heavy fermions that originate them. More precisely, those WCs will represent a non-decoupling effect. In fact, this is a reflection of the non-renormalisation property of anomalies and will be confirmed by the explicit computation of the WCs.

Second, it is useful to notice that in the UV model which generates the EFT one expects three kinds of operators that can generate the vertices in the triangle diagrams:

$$\theta_i\overline{\psi}_L\psi_R + h.c., \quad A_\mu\overline{\psi}_{L/R}\gamma^\mu\psi_{L/R}, \quad \text{and} \quad \partial_\mu\left(\theta_i\right)\overline{\psi}_{L/R}\gamma^\mu\psi_{L/R}, \tag{4.8}$$

where ψ represents generically the fermions in the UV that are integrated out. The first two operators are the usual ones that can be derived from dimension-4 Yukawa and minimal gauge coupling terms, respectively. There could also be operators at higher order in $1/\Lambda$ that generate them in the broken phase. The third kind of operator can be generated with dimension-4 terms via a chiral rotation and will appear generically from higher-dimensional operators.

When computing the WC values from the UV, it becomes useful to consider the derivative of the NGB as an independent bosonic source, i.e. $\partial_\mu\theta_i \equiv \hat{A}_{\mu,i}$, which will generate additional GCS terms[3]. The couplings of $\partial_\mu\theta_i$ with fermions will be generically suppressed by f_i and this will be reflected in the corresponding $E_{ij,k}$ coefficients, but that is the only difference in the computation with respect to the real gauge fields since the fermion loop is the same. Additionally, notice that the GCS terms computed with $\partial_\mu\theta_i$ can be combined with the axionic terms after integration by parts.

The third and final remark is that when there are no gauge anomalies, we do not expect the GCS terms to be zero on their own in a general case, since they depend on the regularisation scheme. This could generate apparent gauge anomalies, which in reality are irrelevant, i.e. can be eliminated with the addition of a local counterterm [231, 241]. The most reliable way of checking the presence of gauge anomalies is computing the gauge variation of the effective action, including the Wess-Zumino terms.

4.2.3 Triangle diagram computations

In this subsection, we show how to compute the WCs of the Wess-Zumino terms in Eq. (4.5) and Eq. (4.6) from one-loop diagrams. We will do it with a fully abelian toy model, although the generalization to more complete cases is straightforward[4]. We consider a heavy (chiral) fermion, ψ, coupled to several Abelian gauge fields, $A_{i,\mu}$. It will acquire its mass via a Yukawa interaction to a scalar field, ϕ, whose imaginary component gives rise to an axion, θ. First, we will use a

[3]Formally, one could compute axionic terms with it too, but its field strength tensor vanishes trivially.

[4]This toy model has the only purpose of illustrating the computation of the WZ terms in a general case and should not be taken as a fully consistent theory on its own.

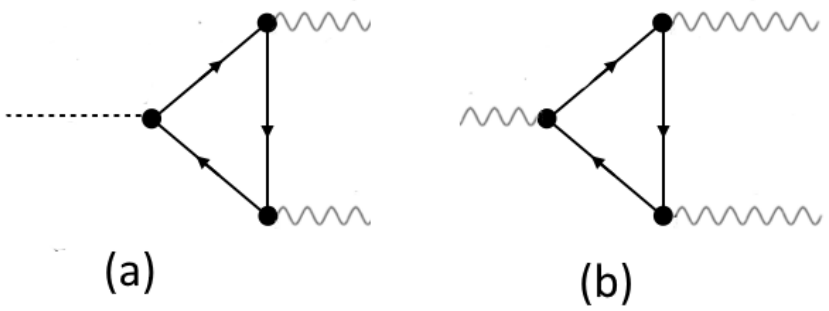

Figure 4.2.1: General one-loop contributions to WZ terms.

fully renormalisable model. The fermionic Lagrangian of the model is as follows:

$$\mathcal{L}_\psi = i\overline{\psi}\gamma^\mu \left(\partial_\mu - i[\alpha_i - \beta_i\gamma_5]A_{i,\mu}\right)\psi - y(\overline{\psi_L}\psi_R\phi + h.c.)\ , \tag{4.9}$$

where $\psi_{R/L} = \frac{1\pm\gamma_5}{2}\psi$ have gauge charges $q^i_{R/L} = \alpha_i \mp \beta_i$. The scalar field ϕ has gauge charges $q^i_\phi = q^i_L - q^i_R = 2\beta_i$, which are fixed by the gauge invariance of the Yukawa term.

The bosonic Lagrangian is the usual

$$\mathcal{L}_{A,\phi} = -\frac{1}{4g_i^2}F_{i,\mu\nu}F_i^{\mu\nu} + |D_\mu\phi|^2 - V\left(|\phi|\right). \tag{4.10}$$

We assume that the scalar has a non-vanishing VEV f and parametrise it as $\phi = \frac{f+h}{\sqrt{2}}e^{i\frac{\theta}{f}}$, where h is the physical scalar and θ is the NGB to be absorbed by a massive gauge boson. With this parametrisation, we can expand the Yukawa terms of the Lagrangian as

$$\mathcal{L}_\psi \supset -y\frac{f+h}{\sqrt{2}}\overline{\psi}_L\psi_R - y\frac{f+h}{\sqrt{2}}q^\psi_\theta i\frac{\theta}{f}\overline{\psi}_L\psi_R + \mathcal{O}\left(\theta^2\right). \tag{4.11}$$

Hence, the mass of the heavy fermion is $m_\psi = \frac{yf}{\sqrt{2}}$. It is easy to see by comparison with Eq. (4.9) that $q^\psi_\theta = 1$. Nevertheless, we will leave this parameter general to facilitate the application of these techniques to the SMEFT[5].

As we show explicitly below, at energies below the mass of the heavy fermion, the model presented above can be matched to the following EFT Lagrangian,

$$\mathcal{L}_{\text{EFT}} \supset \frac{\mathcal{C}_{ij}}{16\pi^2}\frac{\theta}{f}F_i\tilde{F}_j + \frac{E_{ij,k}}{8\pi^2}A_{i,\mu}A_{j,\nu}\tilde{F}_k^{\ \mu\nu}\ , \tag{4.12}$$

where the sum over $i, j(, k)$ is implicit. Now, we will compute the values of those WCs, starting with the axionic terms and then moving onto the GCS terms. We will include dimension-6 operators in our toy model and show how the computation changes just afterwards.

Axionic terms

The axionic terms in the EFT arise via the (off-shell) diagrams of Fig. 4.2.2 (note that, when computing the one-loop EFT below the fermion masses, we should not compute diagrams with

[5]In fact, in the SM Yukawa sector, the operators $\pi^3\overline{u}_L u_R$ and $\pi^3\overline{d}_L d_R$, where π^3 is the NGB to be absorbed by the Z boson, appear with opposite signs (see Eq. (4.49)).

axions or gauge bosons propagators, since this would be a double counting with respect to amplitudes computed in the EFT).

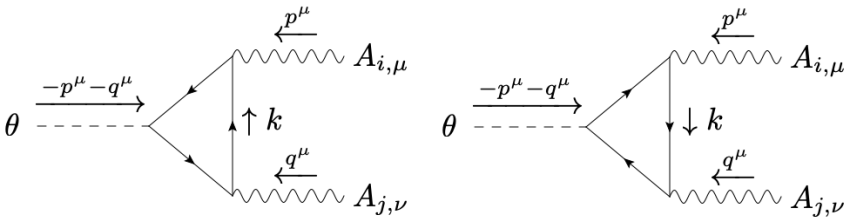

Figure 4.2.2: One-loop contributions to the axion-gauge field coupling

Cutting off the external legs and matching with the Lagrangian coefficient $-c_{ij,\mu\nu}\frac{\theta}{v}A_{i,\mu}A_{j,\nu}$, we get

$$c_{ij,\mu\nu} = \frac{q_\theta^\psi m_\psi}{f}\int\frac{d^4k}{(2\pi)^4}\,\mathrm{Tr}\left(\gamma_5\frac{\not{k}+\not{p}+m_\psi}{(k+p)^2-m_\psi^2+i\epsilon}\Gamma_i^\mu\frac{\not{k}+m_\psi}{k^2-m_\psi^2+i\epsilon}\Gamma_j^\nu\frac{\not{k}-\not{q}+m_\psi}{(k-q)^2-m_\psi^2+i\epsilon}\right) + (i,\mu,q\leftrightarrow j,\nu,q)\ , \tag{4.13}$$

where we defined $\Gamma_i^\mu \equiv \gamma^\mu(\alpha_i - \beta_i\gamma_5)$. To extract from this expression the piece proportional to the Levi–Civita tensor $\epsilon^{\mu\nu\rho\sigma}$, it is enough to focus on terms with one or three γ_5 in the trace. The corresponding expression is finite, and when evaluated in the $m_\psi \to \infty$ limit, we obtain

$$\mathcal{C}_{ij} = -\frac{q_\theta^\psi}{3}\left(3\alpha_i\alpha_j + \beta_i\beta_j\right). \tag{4.14}$$

Note also that, if we kept the chiral fermion mass finite, the form factors in (4.13) (and below in (4.15)) would map to a tower of higher-dimensional operators in the EFT, see, e.g., Appendix D of Ref. [242] for an explicit example.

Generalised Chern–Simons terms

To compute the GCS couplings, the relevant diagrams are those in Fig. 4.2.3. They read

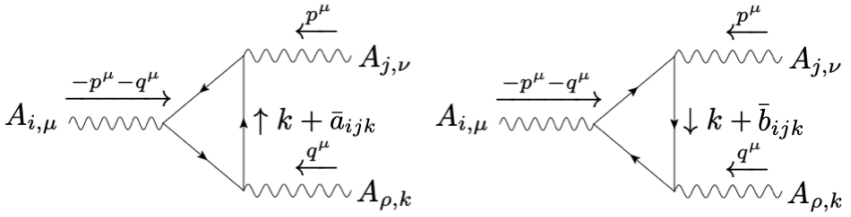

Figure 4.2.3: One-loop contributions to the triple gauge field coupling

$$\int\frac{d^4k}{(2\pi)^4}\,\mathrm{Tr}\left(\frac{\not{k}+\not{\bar{a}}_{ijk}+m_\psi}{(k+\bar{a}_{ijk})^2-m_\psi^2+i\epsilon}\Gamma_k^\rho\frac{\not{k}+\not{\bar{a}}_{ijk}-\not{q}+m_\psi}{(k+\bar{a}_{ijk}-q)^2-m_\psi^2+i\epsilon}\Gamma_i^\mu\frac{\not{k}+\not{\bar{a}}_{ijk}+\not{p}+m_\psi}{(k+\bar{a}_{ijk}+p)^2-m_\psi^2+i\epsilon}\Gamma_j^\nu\right) + (j,\nu,p,\bar{a}_{ijk}\leftrightarrow k,\rho,q,\bar{b}_{ijk})\ . \tag{4.15}$$

We introduce the two shift vectors $\bar{a}_{ijk}, \bar{b}_{ijk}$ in the computation to keep track of the arbitrary momentum shift we are allowed to do in each loop. The full computation is convergent, but

each diagram in Fig. 4.2.3 contributes via a linearly divergent expression and therefore a shift of k in one diagram impacts the final result. In a very simplistic and non-rigorous way, Eq. (4.15) is like the computation of

$$\lim_{k\to\infty} f(k+a) - f(k) = \lim_{k\to\infty} a f'(k) + ..., \tag{4.16}$$

where $f(x)$ diverges for $x \to \infty$ but $f'(x)$ and omitted higher derivatives converge in the same limit. For a more rigorous derivation, see section 22.3 of Ref. [231]. The different behaviour with respect to Eq. (4.13), where the integral diverges at most logarithmically, is due to the presence of one additional gamma matrix that prevents the cancellation of the Dirac trace in the k^3 term.

Before proceeding, let us review briefly the role of the shift vectors. They are a reflection of the triangle diagrams scheme dependence and the possibility of choosing which current exhibits the anomaly [231, 241]. When there is a genuine anomaly, a smart choice of the shift vectors can remove it from two of the currents but not from all of them at the same time. No choice is fully satisfactory for all the possible cases, so here we mention just some of them [231]. If two of the currents belong to gauge symmetries and the remaining to a global symmetry, the shift vector must be such that the anomaly is only on the global current. If none of the currents is gauged, the choice of the shift vector is a matter of convenience and the usual choice is to place the anomalies in the currents that are spontaneously broken or treat them all symmetrically [231].

Returning to the computation of the GCS terms, we focus again on the terms with odd numbers of γ_5 in the trace in order to extract it. Furthermore, we only care about non-decoupling EFT terms in the $m_\psi \to \infty$ limit, which must be of the form A^3 or $\partial A A^2$ since any higher dimensional operator has to be suppressed by m_ψ, the only large scale which enters in the computation. Thus, it is enough to look at the zeroth and first order of (4.15) in p, q, a, b. The end result is

$$-\frac{\epsilon^{\mu\nu\rho\sigma}}{4\pi^2}\Bigg(p_\sigma\left[\alpha_j\alpha_k\beta_i + \alpha_i\alpha_k\beta_j - \alpha_i\alpha_j\beta_k + \frac{\beta_i\beta_j\beta_k}{3}\right] - q_\sigma\left[\alpha_j\alpha_k\beta_i - \alpha_i\alpha_k\beta_j + \alpha_i\alpha_j\beta_k + \frac{\beta_i\beta_j\beta_k}{3}\right] + \frac{(\bar{b}_{ijk} - \bar{a}_{ijk})_\sigma}{2}\left[\alpha_j\alpha_k\beta_i + \alpha_i\alpha_k\beta_j + \alpha_i\alpha_j\beta_k + \beta_i\beta_j\beta_k\right]\Bigg) . \tag{4.17}$$

To preserve the vector current (see e.g. Appendix A of Ref. [241] or Ref. [231] for a careful derivation), we must relate the two shift vectors as

$$-\bar{b}_{ijk} = \bar{a}_{ijk} = a^{(p)}_{ijk} p + a^{(q)}_{ijk} q \ . \tag{4.18}$$

This allows us to match Eq. (4.17) to the amplitude obtained from the GCS term $E_{ij,k} A_i A_j \tilde{F}_k$, of the effective Lagrangian Eq. (4.12), which in momentum space reads

$$-\frac{\epsilon^{\mu\nu\rho\sigma}}{4\pi^2}((E_{jk,i} - E_{kj,i})(-p-q)_\sigma + (E_{ki,j} - E_{ik,j})p_\sigma + (E_{ij,k} - E_{ji,k})p_\sigma) \ . \tag{4.19}$$

The GCS couplings $E_{ij,k}$ are then uniquely determined in terms of the charges α_i, β_i and the shift vectors $a_{ijk^{(p)}}$ by requiring that they obey the following two conditions:

$$\text{(i)} \quad E_{ij,k} = -E_{ji,k} \ , \quad \text{(ii)} \quad E_{ij,k} + E_{jk,i} + E_{ki,j} = 0 \ . \tag{4.20}$$

The first relation follows from the antisymmetry of $A_i A_j \tilde{F}_k$ under the exchange of i and j, while the second relation is a consequence of the fact that $A_i A_j \tilde{F}_k + A_j A_k \tilde{F}_i + A_k A_i \tilde{F}_j$ is a total derivative. The two expressions Eq. (4.17) and Eq. (4.19) will then be equivalent for arbitrary

momenta p and q and arbitrary charges α_i and β_i provided that the shift vectors satisfy:

$$a_{ijk} \equiv a_{ijk}^{(p)} = -a_{kij}^{(q)} \ , \quad a_{ijk} = a_{jik} \ , \quad a_{ijk} + a_{kij} + a_{jki} = 1 \ . \tag{4.21}$$

It then follows that

$$E_{ij,k} = (a_{ikj} - a_{jki}) \left(\alpha_i \alpha_j + \frac{1}{3} \beta_i \beta_j \right) \beta_k + (1 - a_{ijk})(\alpha_i \beta_j - \beta_i \alpha_j) \alpha_k \ . \tag{4.22}$$

The shift vectors are chosen in order to enforce that the physical gauge symmetries are conserved, namely that the EFT is invariant under them. For the case we are treating now, where all the vertices arise from dimension-4 gauge invariant operators, we choose symmetric shift vectors, i.e. $a_{ijk} = 1/3$. This choice and Eq. (4.22) determine the GCS terms in Eq. (4.12).

Finally, we stress again that the value of the GCS terms is dependent of the regularisation scheme or, more explicitly, of the shift-vectors choice. A different value of the shift vectors could generate the appearance of seemingly gauge anomalies, which in turn are irrelevant and can be eliminated with a suitable local counterterm. The proof of this fact can be found in Appendix A of Ref. [241] and we skip it to avoid deviating from the main topic.

Addition of dimension-6 couplings

Let us consider now how the computation changes in presence of chiral dimension-6 operators. We add

$$i \frac{c_L}{\Lambda^2} \left(\phi^\dagger \overleftrightarrow{D}_\mu \phi \right) \overline{\psi}_L \gamma^\mu \psi_L + i \frac{c_R}{\Lambda^2} \left(\phi^\dagger \overleftrightarrow{D}_\mu \phi \right) \overline{\psi}_R \gamma^\mu \psi_R \ , \tag{4.23}$$

to the model defined in Eq. (4.9) and Eq. (4.10). Due to the non-vanishing VEV of the scalar field, these operators induce a shift of the fermion gauge charges at order $1/\Lambda^2$,

$$q_{R/L}^i = \alpha_i \mp \beta_i + q_\phi^i \frac{c_{R/L} f^2}{\Lambda^2}, \tag{4.24}$$

which can be absorbed with the redefinition

$$\begin{aligned} \alpha_i \to \tilde{\alpha}_i &= \alpha_i + \frac{q_\phi^i}{2} \frac{f^2}{\Lambda^2} (c_L + c_R) \, , \\ \beta_i \to \tilde{\beta}_i &= \beta_i + \frac{q_\phi^i}{2} \frac{f^2}{\Lambda^2} (c_L - c_R) \, . \end{aligned} \tag{4.25}$$

By replacing $\alpha_i, \quad \beta_i \to \tilde{\alpha}_i, \tilde{\beta}_i$ in Eq. (4.14), one can use it to compute straightforwardly the axionic terms at order $1/\Lambda^2$. Notice that keeping only the pieces at order $1/\Lambda^2$ is equivalent to insert the dimension-6 operator in the triangle diagram at only one of the vertices at the time.

More care is required for the GCS terms. In particular, we need to revisit the choice of the shift vectors. This is because we want to force the cancellation of gauge anomalies generated by the renormalisable interactions but not the possible anomalies generated by dimension-6 operators. In fact, our goal in Section 4.3 and 4.4 will be to see if the former ensures the latter.

Thus, let us consider the following transformation of the fields,

$$\psi_{L/R} \to e^{i \epsilon_i q_{L/R}^i} \psi_{L/R} \ , \quad \theta \to \theta + \epsilon_i (q_L^i - q_R^i) f \ , \quad A_{i,\mu} \to A_{i,\mu} + \delta_{ij} \partial_\mu \epsilon_j \ . \tag{4.26}$$

Using the expression in Eq. (4.22) of the coefficients $E_{ij,k}$ in terms of the shift vectors, the

variation of the EFT Lagrangian (4.12) reads[6]

$$\delta_i \mathcal{L}_{\rm EFT} = -\frac{(1-a_{jki})D^{ijk}}{32\pi^2}\epsilon_i F_j \tilde{F}_k \ , \tag{4.27}$$

where $D^{ijk} \equiv q_L^i q_L^j q_L^k - q_R^i q_R^j q_R^k = 2\tilde{\beta}_i\tilde{\beta}_j\tilde{\beta}_k + 2(\tilde{\alpha}_i\tilde{\alpha}_j\tilde{\beta}_k + \tilde{\alpha}_j\tilde{\alpha}_k\tilde{\beta}_i + \tilde{\alpha}_k\tilde{\alpha}_i\tilde{\beta}_j)$ is nothing else but the $U(1)_i \times U(1)_j \times U(1)_k$ anomaly polynomial.

We will mark with a hatted index, like $\hat{\imath}$, the vertices generated by dimension-4 couplings and leave without a hat the index corresponding to the vertex at order $1/\Lambda^2$. Hence, picking k as the one at order $1/\Lambda^2$, which possibly generates non-vanishing gauge anomalies, the consistency of the EFT Lagrangian at the quantum level, namely $\delta_i \mathcal{L}_{\rm EFT} = 0$, forces to choose

$$a_{k\hat{\imath}\hat{\jmath}} = 1 \ , \quad a_{i\hat{\jmath}k} = -1 \ , \tag{4.28}$$

where the last equality follows from Eq. (4.21). After this choice, the computation of $E_{\hat{\imath}\hat{\jmath},k}$ at order $1/\Lambda^2$ is completed.

One last comment is in order concerning the computation of GCS terms with the bosonic source $\partial_\mu\theta$. As we said before, the computation does not differ from the one explained above because the couplings α and β can be defined for $\partial_\mu\theta$, with the only difference that they are expected to be suppressed at least by $1/f$ with respect to the analogous couplings for an actual gauge field. The shift vectors choice does not change either.

4.3 Gauge anomalies from dimension-6 operators: a toy model

In this section, we will discuss in detail whether dimension-6 operators can generate gauge anomalies with a simple toy model. Its simplicity will allow us to carry out the discussion via two different methods. First, we will follow a text-book like approach, computing the conserved Noether current of a chiral global symmetry and asking when can we gauge it. Second, we will integrate out the fermions of the toy model to obtain a bosonic EFT and we will analyse its Wess-Zumino terms, using the techniques described in Section 4.2. Performing the analysis via both different techniques will allow us to not only validate the results obtained with the bosonic EFT but also to gain an insight on the origin of the result.

The toy model that we will consider consists of two LH and two RH Weyl fermions[7], arranged in two Dirac fermions $\psi_{k=1,2}$, a complex scalar φ and a gauge field A_μ of field strength F_A. Its Lagrangian density is:

$$\begin{aligned}\mathcal{L} = &-\frac{1}{4g_A^2}F_{A,\mu\nu}^2 - |\partial\varphi|^2 - V(|\varphi|) + i\overline{\psi}_k \not{D}\psi_k \\ &+ i\frac{c_{L,k}}{\Lambda^2}\left(\varphi^\dagger \overleftrightarrow{\partial}_\mu \varphi\right)\overline{\psi}_{k,L}\gamma^\mu\psi_{k,L} + i\frac{c_{R,k}}{\Lambda^2}\left(\varphi^\dagger \overleftrightarrow{\partial}_\mu \varphi\right)\overline{\psi}_{k,R}\gamma^\mu\psi_{k,R} \ ,\end{aligned} \tag{4.29}$$

where $D_\mu\psi_k = (\partial_\mu + iq_k^A A_\mu)\psi_k$ contains a vector-like coupling to A_μ. Summation over repeated indices is implicit. Notice that φ is uncharged under the gauge symmetry $U(1)_A$ and the fermions are massless. We do not include bare mass terms for the fermions, although they are allowed by the gauge symmetry, since we want to study which chiral global symmetries of

[6] Our results are a factor of 2 off with respect to the ones in [241], so that anomaly cancellation holds in the low-energy EFT in our case. It can be verified by an explicit computation in the UV model that the RHS of (4.27) corresponds to the variation of the quantum effective action associated to the heavy fermion, see for instance Ref. [231].

[7] The minimalistic option of only one Weyl fermion of each chirality leads to trivial solutions.

Eq. (4.29) can be consistently gauged. For simplicity, we postpone the inclusion of Yukawa couplings to subsection 4.3.2.

4.3.1 Current (non-)conservation in triangle diagrams

Let us start by identifying the Noether currents that are classically conserved. The Noether current for $U(1)_A$ is

$$J_\mu^A = q_k^A \overline{\psi}_k \gamma_\mu \psi_k \ . \tag{4.30}$$

In addition, the theory has global (chiral) symmetries. Let us study the one under which $\varphi \to e^{i q_\varphi^B \epsilon_B} \varphi$, $\psi_k \to e^{i q_k^B \gamma_5 \epsilon_B} \psi_k$, while the other ones can be found in Appendix 4.C. The Noether current of the symmetry of our interest is

$$J_\mu^B = -i q_\varphi^B \left(\varphi^\dagger \overleftrightarrow{\partial}_\mu \varphi + 2i \frac{c_{L,k}}{\Lambda^2} |\varphi|^2 \overline{\psi}_{k,L} \gamma_\mu \psi_{k,L} + 2i \frac{c_{R,k}}{\Lambda^2} |\varphi|^2 \overline{\psi}_{k,R} \gamma_\mu \psi_{k,R} \right) + q_k^B \overline{\psi}_k \gamma_\mu \gamma_5 \psi_k \ . \tag{4.31}$$

Using the equations of motion (eoms),

$$\begin{aligned} &\Box \varphi + V'(|\varphi|) + i \frac{c_{L,k}}{\Lambda^2} \partial_\mu \varphi \overline{\psi}_{k,L} \gamma^\mu \psi_{k,L} + i \frac{c_{L,k}}{\Lambda^2} \partial_\mu \left(\varphi \overline{\psi}_{k,L} \gamma^\mu \psi_{k,L} \right) + (L \leftrightarrow R) = 0 \ , \\ &\not{D} \psi_{k,L/R} + \frac{c_{L/R,k}}{\Lambda^2} \left(\varphi^\dagger \overleftrightarrow{\partial}_\mu \varphi \right) \gamma^\mu \psi_{k,L/R} = 0 \ , \end{aligned} \tag{4.32}$$

it is easy to see that the current is conserved, i.e. $\partial^\mu J_\mu^B = 0$ (actually, the parts proportional to q_φ^B and q_k^B vanish independently, since they correspond to independent symmetries of the action). This result holds both in the broken and unbroken phase, since the eoms do not change, neither do the expressions of the currents.

Now, when can we gauge the symmetry $U(1)_B$ of current J_μ^B, i.e., when is it anomaly free? The usual anomaly cancellation at dimension 4 would enforce:

$$U(1)_A^2 \times U(1)_B : \ \left(q_k^A \right)^2 q_k^B = 0 \ , \quad U(1)_B^3 : \ \left(q_k^B \right)^3 = 0 \ , \tag{4.33}$$

where we sum over repeated indices. This implies $q_1^B = -q_2^B$ and, if $q_k^B \neq 0$, $q_1^A = \pm q_2^A$. The other possible anomalies vanish trivially since $U(1)_A$ is vector-like and $U(1)_B$ axial.

Had we now gauged $U(1)_B$, the Lagrangian would be

$$\begin{aligned} \mathcal{L} = &- \frac{1}{4 g_A^2} F_{A,\mu\nu}^2 - \frac{1}{4 g_B^2} F_{B,\mu\nu}^2 - |D_\mu \varphi|^2 - V(|\varphi|) + i \overline{\psi}_k \not{D} \psi_k \\ &+ i \frac{c_{L,k}}{\Lambda^2} \left(\varphi^\dagger \overleftrightarrow{D}_\mu \varphi \right) \overline{\psi}_{k,L} \gamma^\mu \psi_{k,L} + i \frac{c_{R,k}}{\Lambda^2} \left(\varphi^\dagger \overleftrightarrow{D}_\mu \varphi \right) \overline{\psi}_{k,R} \gamma^\mu \psi_{k,R} \end{aligned} \tag{4.34}$$

where now $D_\mu \psi_k = (\partial_\mu + i q_k^A A_\mu + i q_k^B \gamma_5 B_\mu) \psi_k$, $D_\mu \varphi = (\partial_\mu + i q_\varphi^B B_\mu) \varphi$.

We proceed to compute the three-point correlation functions of symmetry currents at one-loop level in the usual way. More precisely, we compute:

$$\partial^\mu \langle 0 | J_\mu^B(x) J_\nu^A(y) J_\rho^A(z) | 0 \rangle \ , \tag{4.35}$$

the discussion being straightforwardly generalized to other current combinations. In the unbroken phase, the dimension-6 pieces of J_μ^B cannot be combined with the fermionic legs from the two J_μ^A to form a one-loop diagram. Indeed, that would demand closing the two Higgs legs from J_μ^B in a second loop. Consequently, at one loop the computation is the same as if the

dimension-6 terms were absent and we find

$$\underline{\text{unbroken phase}}\text{: } \partial^\mu \langle 0|J^B_\mu(x)J^A_\nu(y)J^A_\rho(z)|0\rangle = 0 \iff \left(q^A_k\right)^2 q^B_k = 0\ . \tag{4.36}$$

Diagrammatically, defining Γ_L as in Fig. 4.3.1, this arises from the fact that[8] $-(p+q)_\mu \Gamma_L^{\mu\nu\rho}(p,q) = \frac{1}{4\pi^2}\epsilon^{\nu\rho\alpha\beta}p_\alpha q_\beta$, and oppositely for Γ_R [243, 244].

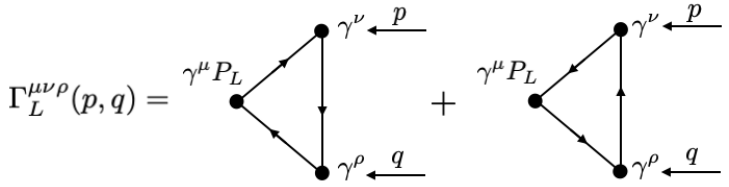

Figure 4.3.1: Triangle diagrams leading to anomalies in the unbroken phase. Solid lines are fermion propagators and we indicate which combination of Dirac matrices enters each vertex.

We study now the broken phase. There, we parametrize $\varphi = \frac{v+h}{\sqrt{2}}e^{i\frac{\theta}{v}}$, with real v. The Goldstone boson θ transforms under $U(1)_B$ as $\delta\theta = v q^B_\varphi \epsilon_B$, and the radial mode h is neutral under all symmetry groups. This parametrization allows us to write

$$J^B_\mu = q^B_\varphi \left(v\partial_\mu\theta + \frac{c_{L,k}v^2}{\Lambda^2}\overline{\psi}_{k,L}\gamma_\mu\psi_{k,L} + \frac{c_{R,k}v^2}{\Lambda^2}\overline{\psi}_{k,R}\gamma_\mu\psi_{k,R}\right) + q^B_k\overline{\psi}_k\gamma_\mu\gamma_5\psi_k + \text{ terms involving } h\ . \tag{4.37}$$

The terms that depend on h cannot contribute to anomalies at one-loop for the same reason than in the unbroken case, so we focus on the pieces that are independent of bosonic fields or depend on the NGB θ only.

Let us study the diagrams that enter the computation of $\partial^\mu\langle 0|J^B_\mu(x)J^A_\nu(y)J^A_\rho(z)|0\rangle$. There are diagrams proportional to $\left(q^A_k\right)^2 q^B_k$, of the form $\left(q^A_k\right)^2 q^B_k(\Gamma_L - \Gamma_R)$, that lead to the same contribution to the anomaly as in the unbroken phase. In addition, there are two other kinds of diagrams, proportional to q^B_φ. These are the purely fermionic diagrams sensitive to the pieces of the current proportional to $c_{L/R}$, and the ones where the current connects to a Goldstone boson propagator (see Fig. 4.3.2). In the latter, there appears the three-point coupling between the NGB and the fermions obtained from Eq. (4.29):

$$\mathcal{L} \supset -\frac{v c_{L,k}}{\Lambda^2}\partial_\mu\theta\overline{\psi}_{k,L}\gamma^\mu\psi_{k,L} - \frac{v c_{R,k}}{\Lambda^2}\partial_\mu\theta\overline{\psi}_{k,R}\gamma^\mu\psi_{k,R}\ . \tag{4.38}$$

The two diagrams in Fig. 4.3.2 cancel each other exactly when contracting them with $-(p+q)_\mu$ and, consequently

$$\underline{\text{broken phase}}\text{: } \partial^\mu \langle 0|J^B_\mu(x)J^A_\nu(y)J^A_\rho(z)|0\rangle = 0 \iff \left(q^A_k\right)^2 q^B_k = 0\ . \tag{4.39}$$

In particular, we do not find any condition on $c_{L/R}$, just as in the unbroken phase. As could have been expected, the IR dynamics, namely the choice of the broken or unbroken phase, does not change the conclusions regarding anomalies. Cancellations similar to that illustrated in Fig. 4.3.2 can also be found in the unbroken phase, as presented in Appendix 4.D.

It is important to notice that if we had focused only on the diagram on the right of Fig. 4.3.2,

[8] To conserve the vector-like current J^A_μ, we impose $p_\nu\Gamma_L^{\mu\nu\rho}(p,q) = q_\rho\Gamma_L^{\mu\nu\rho}(p,q) = 0$.

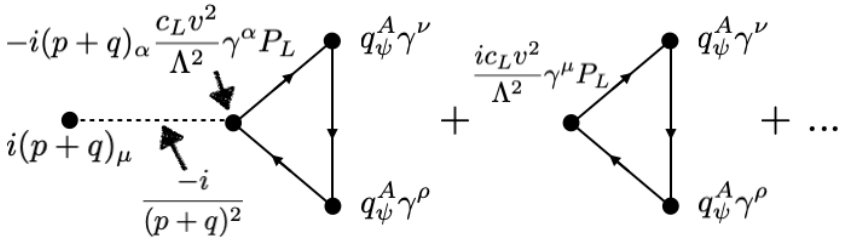

Figure 4.3.2: Triangle diagrams proportional to q_φ^B (the +... refers to the same diagrams with the orientation of the fermionic arrows reversed). Solid lines are fermion propagators, the dashed one is a NGB propagator and we indicate which combination of Dirac matrices and momenta enters each vertex.

we would have arrived at a constraint on the dimension-6 WCs of the form

$$\left(q_k^A\right)^2 q_\varphi^B (c_{L,k} - c_{R,k}) = 0, \tag{4.40}$$

but this does not correspond to the full contribution of the Noether current. This is the kind of spurious constraint found in Ref. [237]. A detailed discussion of their results can be found in Appendix 4.B.

The discussion in this subsection can be summarized as follows: classically, a coupling $K^\mu(\partial_\mu\theta + vq_\varphi^B B_\mu)$ is gauge-invariant even if K^μ is not conserved, and that remains true at the quantum level. To finalize this section, let us remark once more the key role played of the diagram with a NGB propagator, which cancels the contribution from the gauge coupling modification at dimension 6.

4.3.2 Bosonic EFT and Wess-Zumino terms

We can reach the same conclusions of subsection 4.3.1 through a different path. In the broken phase, the chiral fermions can acquire a mass in the presence of a Yukawa term. Gauge anomalies do not depend on the precise values of Yukawa and gauge couplings, as long as they remain perturbative, and therefore we are free to assume that the mass of the fermions is much bigger than the one of the bosons. In this situation, it is sensible to integrate out the fermions and define a bosonic EFT.

As explained in Section 4.2, in a bosonic EFT, the anomalies of the heavy fields are encoded in WZ terms [233, 240, 245]. This reasoning is not modified by the presence of dimension-6 operators. If the latter generated genuine anomalies, they could be cancelled by adding light fermions with appropriate dimension-6 couplings to the theory, and similar WZ terms should be present to carry those new anomalies when the heavy fermions are integrated. As we will show in the following, no such WZ term is generated.

In order to compute the WZ terms for the toy model in Eq. (4.29), we must modify it in two ways. First, we gauge the chiral symmetry associated to the current J_μ^B ignoring for the moment its anomalies. Second, we give a mass to the Weyl fermions by adding to the Lagrangian the Yukawa term

$$\delta\mathcal{L} = -y_k \varphi \overline{\psi}_{k,L}\psi_{k,R} + h.c.\ , \tag{4.41}$$

where we chose y_k real. Gauge invariance of the Lagrangian imposes $2q_k^B = q_\varphi^B$, and the Noether current in Eq. (4.31) respects the same anomalous Ward identities as in the case with massless fermions [246, 247].

In the broken phase, the fermions acquire a mass $m_k = \frac{y_k v}{\sqrt{2}}$ that allows us to integrate them

out. In the EFT below m_k, the anomalous WZ terms for our toy model read

$$\mathcal{L}_{\rm EFT} = -\frac{C_{AA}}{16\pi^2}\frac{\theta}{v}F_A\tilde{F}_A - \frac{C_{AB}}{16\pi^2}\frac{\theta}{v}F_A\tilde{F}_B - \frac{C_{BB}}{16\pi^2}\frac{\theta}{v}F_B\tilde{F}_B - \frac{E_{ABA}}{8\pi^2}A_\mu B_\nu \tilde{F}_A^{\mu\nu} - \frac{E_{ABB}}{8\pi^2}A_\mu B_\nu \tilde{F}_B^{\mu\nu} \ . \quad (4.42)$$

The coefficients can be computed as explained in Section 4.2 and the result is

$$C_{AA} = \left(q_k^A\right)^2 \ , \quad C_{AB} = 0 \ , \quad C_{BB} = \frac{2\left(q_k^B\right)^2}{3} \ , \quad E_{ABA} = \frac{4\left(q_k^A\right)^2 q_k^B}{3} \ , \quad E_{ABB} = 0 \ . \quad (4.43)$$

It is straightforward to notice from Eq. (4.43) that the usual anomalies are reproduced in the EFT. Indeed,

$$\delta\mathcal{L}_{\rm eff} = -\frac{\epsilon_A}{24\pi^2}2\left(q_k^A\right)^2 q_k^B F_A\tilde{F}_B - \frac{\epsilon_B}{24\pi^2}\left[\left(q_k^A\right)^2 q_k^B F_A\tilde{F}_A + 2\left(q_k^B\right)^3 F_B\tilde{F}_B\right] \ , \quad (4.44)$$

where $\epsilon_{A/B}$ are the parameters of the gauge transformations under which $\delta A_\mu = -\partial_\mu\epsilon_A$, $\delta B_\mu = -\partial_\mu\epsilon_B$ and $\delta\theta = v q_\varphi^B \epsilon_B$. We see there that the gauge transformations of the bosonic EFT are zero if and only if the UV anomalies in Eq. (4.33) cancel. Moreover, there is no anomalous shift proportional to $c_{L/R}$, confirming that their values have no impact on the gauge invariance of the theory.

4.4 Bosonic EFT for the SMEFT

For the case of the SMEFT, it is clear that the bosonic-EFT technique explained in Section 4.2 and applied to a toy model in subsection 4.3.2 is easier to apply than the traditional current based computations. We focus on triangle diagrams and therefore we are sensitive only to the linear parts of non-abelian field strengths and gauge transformations of NGBs and gauge fields. All formulae below should be read accordingly, for instance $W^a_{\mu\nu} = \partial_\mu W^a_\nu - \partial_\nu W^a_\mu$ for the $\mathrm{SU}(2)_L$ electroweak gauge fields. This also means that we do not check explicitly if anomalies are cancelled in square and pentagon diagrams, that contribute to the non-linear part of the non-abelian field strength. However, it is known that those diagrams are related to the triangle diagrams by (classical) gauge invariance and therefore we expect the same behaviour.

The bosonic EFT technique requires us to integrate out all the fermions of the theory, which is impossible to do in SMEFT if one respects the measured masses of the fermions. However, let us remind once again that anomalies are independent of the numerical value of Yukawa and gauge couplings as long as perturbative unitarity and the confining properties of the gauge interactions remain unchanged. This allow us to study a deformed version of SMEFT and claim that the results are valid for the phenomenologically relevant case as well. In our version of SMEFT, the electroweak gauge couplings g and g' are reduced, for instance to g, $g' \lesssim 0.01$, and all the Yukawa couplings are raised to $y_\psi \sim 1$. Additionally, we must add singlet RH neutrinos ν_R in order to give neutrinos a mass via a standard Yukawa term. We assign a general hypercharge Y_ν to the RH neutrinos, but it can be checked that fixing $Y_\nu = 0$ at any moment in our computations does not affect the final results. Additionally, we do not include any dimension-6 operator involving these RH neutrino fields. In this way, we are allowed to integrate out all the fermions and keep only the bosons in our EFT.

Before checking the WZ terms, we briefly review the interactions with electroweak gauge fields and NGBs that will be relevant for the analysis. We parametrize the NGBs in the Higgs doublet as

$$H = e^{i\frac{\pi^a}{v}\sigma^a}\begin{pmatrix} 0 \\ \frac{h+v}{\sqrt{2}} \end{pmatrix} \ . \quad (4.45)$$

Under an electroweak gauge transformation $U = e^{i\frac{\sigma^a}{2}\epsilon^a + iY_H\epsilon_Y}$, they transform at linear order as

$$\delta\pi^a = \frac{v}{2}\epsilon^a - v\delta^{a3}Y_H\epsilon_Y \ . \tag{4.46}$$

The bosonic piece of the dimension-6 operators in Eq. (4.4) contains, at linear order again,

$$iH^\dagger \overleftrightarrow{D}_\mu H = -v^2\left(Y_H B_\mu - \frac{W^3_\mu}{2}\right) + v\partial_\mu\pi^3 \ , \quad iH^\dagger \overleftrightarrow{D}^a_\mu H = -\left(\frac{v^2}{2}W^a_\mu - v^2\delta^{a3}Y_H B_\mu + v\partial_\mu\pi^a\right) \ , \tag{4.47}$$

and one can check that these expressions are gauge-invariant at leading order. We find the following modifications to LH gauge couplings,

$$\begin{aligned}-\overline{\psi}_{L,i}\Bigg(\delta_{ij}\left[Y_H \not{B} + T^a \not{W}^a\right] + \left[v^2\left(Y_H \not{B} - \frac{\not{W}^3}{2}\right) - v\not{\partial}\pi^3\right]\left[\frac{c^{(1)}_{\varphi\psi,ij}}{\Lambda^2} - 2T^3\frac{c^{(3)}_{\varphi\psi,ij}}{\Lambda^2}\right] \\ + 2T^{a=1,2}\frac{c^{(3)}_{\varphi\psi,ij}}{\Lambda^2}\left[\frac{v^2}{2}\not{W}^a + v\not{\partial}\pi^a\right]\Bigg)\psi_{L,j} \ ,\end{aligned} \tag{4.48}$$

where $T^a = \frac{\tau^a}{2}$, and for RH fields the equivalent expression is obtained by replacing $T^{a=1..3} \to 0$, $c^{(1)}_{\varphi\psi} \to c_{\varphi\psi}$ and $c^{(3)}_{\varphi\psi} \to 0$. In the Yukawa couplings, we have

$$\begin{aligned}\mathcal{L} \supset & - y_u\overline{Q}_L\tilde{H}u_R - y_d\overline{Q}_L H d_R - y_e\overline{L}_L H e_R - y_\nu\overline{L}_L\tilde{H}\nu_R + h.c. \\ = & -\frac{y_u}{\sqrt{2}}\left((v+i\pi^3)\overline{u}_L + i(\pi^1+i\pi^2)\overline{d}_L\right)u_R - \frac{y_d}{\sqrt{2}}\left((v-i\pi^3)\overline{d}_L + i(\pi^1-i\pi^2)\overline{u}_L\right)d_R \\ & - \frac{y_e}{\sqrt{2}}\left((v-i\pi^3)\overline{e}_L + i(\pi^1-i\pi^2)\overline{\nu}_L\right)e_R - \frac{y_\nu}{\sqrt{2}}\left((v+i\pi^3)\overline{\nu}_L + i(\pi^1+i\pi^2)\overline{e}_L\right)\nu_R + h.c. \ ,\end{aligned} \tag{4.49}$$

where we omitted writing explicitly the generation indices.

4.4.1 Wess-Zumino terms

Let us first review what our technique yields for the SM at dimension 4. In the effective theory obtained from the SM below the mass of all the fermions, focusing on neutral bosons and NGBs (the charged ones are treated identically), one finds the following couplings:

$$\begin{aligned}\mathcal{L}_{\rm EFT} \supset & -\frac{1}{16\pi^2}\frac{\pi^3}{v}B_{\mu\nu}\tilde{B}^{\mu\nu}\left(3\left[Y_u^2 + Y_Q Y_u - Y_d^2 - Y_Q Y_d\right] + Y_\nu^2 + Y_L Y_\nu - Y_e^2 - Y_e Y_L\right) \\ & -\frac{1}{16\pi^2}\frac{\pi^3}{v}B_{\mu\nu}\tilde{W}^{3,\mu\nu}\left(\frac{3(Y_d + 4Y_Q + Y_u)}{2} + \frac{Y_e + 4Y_L + Y_\nu}{2}\right) \\ & -\frac{1}{8\pi^2}B_\mu W^3_\nu\tilde{B}^{\mu\nu}\frac{(Y_\nu + Y_e)(Y_e + Y_L + Y_\nu) + 3(Y_u - Y_d)(Y_d + Y_Q + Y_u)}{2} \\ & -\frac{1}{8\pi^2}B_\mu W^3_\nu\tilde{W}^{3,\mu\nu}\frac{3(Y_u + Y_d) + Y_e + Y_\nu}{4} \ ,\end{aligned} \tag{4.50}$$

where as we said we restrict to the linear pieces in the non-abelian field strengths. The variation of the action reads,

$$\begin{aligned}\delta\mathcal{L}_{\rm EFT} = &-\frac{\epsilon_Y}{16\pi^2}\left[\left(6Y_Q^3+2Y_L^3-3Y_u^3-3Y_d^3-Y_e^3-Y_\nu^3\right)B_{\mu\nu}\tilde{B}^{\mu\nu}+\frac{3Y_Q+Y_L}{2}W^3_{\mu\nu}\tilde{W}^{3,\mu\nu}\right]\\ &-\frac{\epsilon_3}{16\pi^2}\left(3Y_Q+Y_L\right)B_{\mu\nu}\tilde{W}^{3,\mu\nu},\end{aligned} \tag{4.51}$$

where we have used relations imposed by the classical gauge invariance of the Yukawa terms, such as $Y_u = Y_Q + Y_H$. Demanding that those variations vanish, we recover the known $\mathrm{U}(1)_Y^3$ and $\mathrm{U}(1)_Y\times\mathrm{SU}(2)_L^2$ anomaly cancellation conditions (see Appendix 4.A and e.g. [248]).

Now, we can study the WZ terms which arise from inserting one dimension-6 vertex in the triangle diagrams. For convenience, we define the following gauge-invariant (at linear order) combinations of gauge fields and NGBs:

$$A_{0,\mu}\equiv v^2\left(Y_H B_\mu-\frac{W^3_\mu}{2}\right)-v\partial_\mu\pi^3\ ,\quad A_{\pm,\mu}\equiv\frac{v^2}{2}W^\pm_\mu+v\partial_\mu\pi^\pm\ , \tag{4.52}$$

and their field strengths

$$F_{0,\mu\nu}=v^2\left(Y_H B_{\mu\nu}-\frac{W^3_{\mu\nu}}{2}\right)\ ,\quad F_{\pm,\mu\nu}=\frac{v^2}{2}W^\pm_{\mu\nu} \tag{4.53}$$

(we remind that we work at linear order in non-abelian gauge fields). Anomalous EFT couplings at dimension-6 arise from the diagrams in Fig. 4.4.1.

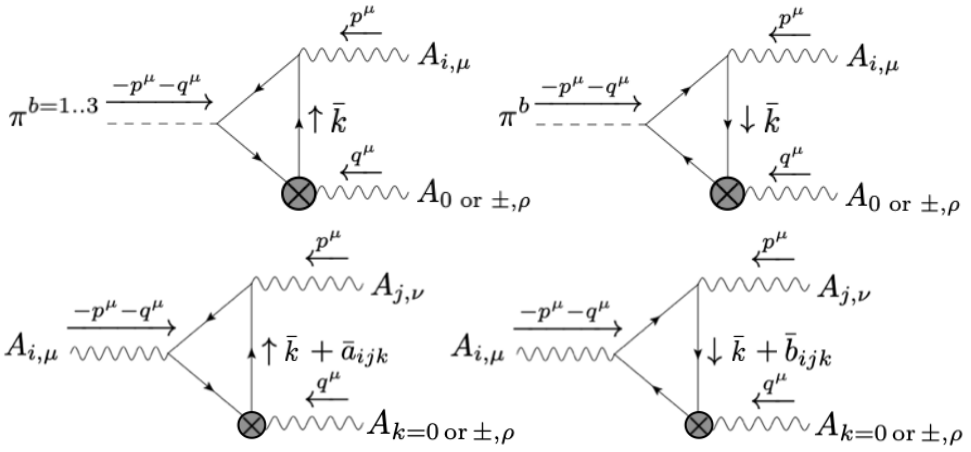

Figure 4.4.1: Triangle diagrams leading to anomalous EFT terms. A black crossed circle indicates a dimension-six EFT coupling. The vectors $\bar{a}$ and $\bar{b}$ correspond to shift ambiguities of the loop momentum $\bar{k}$ inherent to the second kind of diagrams.

Let us start with the diagrams in the upper half of Fig. 4.4.1, those with one dimension-4 insertion of a Goldstone coupling. They lead to the following EFT couplings,

$$\mathcal{L}_{\rm EFT}\supset-\frac{1}{16\pi^2}\mathcal{C}_{F_0B}\frac{\pi^3}{v}F_0\tilde{B}-\frac{1}{16\pi^2}\mathcal{C}_{F_0W^3}\frac{\pi^3}{v}F_0\tilde{W}^3, \tag{4.54}$$

with

$$\begin{aligned}\mathcal{C}_{F_0B} =& -\frac{1}{3\Lambda^2}\Big[3\left(c^{(1)}_{\varphi d}(2Y_d+Y_Q)-c^{(1)}_{\varphi u}(Y_Q+2Y_u)+c^{(1)}_{\varphi Q}(Y_d-Y_u)+c^{(3)}_{\varphi Q}(Y_d+4Y_Q+Y_u)\right)\\ &+c^{(1)}_{\varphi e}(2Y_e+Y_L)+c^{(1)}_{\varphi L}(Y_e-Y_\nu)+c^{(3)}_{\varphi L}(Y_e+4Y_L+Y_\nu)\Big],\\ \mathcal{C}_{F_0W^3} =& \frac{1}{6\Lambda^2}\Big[3c^{(1)}_{\varphi d}+3c^{(1)}_{\varphi u}+12c^{(1)}_{\varphi Q}+c^{(1)}_{\varphi e}+4c^{(1)}_{\varphi L}\Big],\end{aligned} \tag{4.55}$$

where we have traced over the generation indices. To this, we should add the triangle diagrams with two insertions of dimension-4 gauge currents, those in the lower part of Fig. 4.2.2. This leads to the following EFT terms,

$$\begin{aligned}\mathcal{L}_{\rm EFT} \supset& -\frac{E_{A_0BB}}{8\pi^2\Lambda^2}A_{0,\mu}B_\nu\tilde{B}^{\mu\nu}-\frac{E_{A_0W^3B}}{8\pi^2\Lambda^2}A_{0,\mu}W^3_\nu\tilde{B}^{\mu\nu}-\frac{E_{A_0BW^3}}{8\pi^2\Lambda^2}A_{0,\mu}B_\nu\tilde{W}^{3,\mu\nu},\\ &-\frac{E_{BW^3F_0}}{8\pi^2\Lambda^2}B_\mu W^3_\nu\tilde{F}_0^{\mu\nu}-\frac{E_{A_0W^3W^3}}{8\pi^2\Lambda^2}A_{0,\mu}W^3_\nu\tilde{W}^{3,\mu\nu},\end{aligned} \tag{4.56}$$

with

$$\begin{aligned}E_{A_0BB} =& c^{(1)}_{\varphi u}(Y_Q-Y_u)(Y_Q+2Y_u)-c^{(1)}_{\varphi d}(Y_d-Y_Q)(2Y_d+Y_Q)-c^{(1)}_{\varphi Q}\left(Y_d^2+Y_dY_Q-4Y_Q^2+Y_QY_u+Y_u^2\right),\\ &-c^{(3)}_{\varphi Q}(Y_d-Y_u)(Y_d+Y_Q+Y_u)-\frac{1}{3}c^{(1)}_{\varphi e}(Y_e-Y_L)(2Y_e+Y_L),\\ &-\frac{1}{3}c^{(1)}_{\varphi L}\left(Y_e^2+Y_eY_L-4Y_L^2+Y_LY_\nu+Y_\nu^2\right)-\frac{1}{3}c^{(3)}_{\varphi L}(Y_e^2+Y_LY_e+Y_\nu^2+Y_\nu Y_e)\\ E_{A_0W^3B} =& \frac{1}{2}c^{(1)}_{\varphi u}(Y_Q-Y_u)+\frac{1}{2}c^{(1)}_{\varphi d}(Y_d-Y_Q)+c^{(1)}_{\varphi Q}(Y_d-Y_u)+c^{(3)}_{\varphi Q}(Y_d-2Y_Q+Y_u),\\ &+\frac{1}{6}c^{(1)}_{\varphi e}(Y_e-Y_L)+\frac{1}{3}c^{(1)}_{\varphi L}(Y_e-Y_\nu)-\frac{1}{3}c^{(3)}_{\varphi L}(Y_e-2Y_LY_e+Y_\nu)\\ E_{A_0BW^3} =& \frac{1}{2}c^{(1)}_{\varphi u}(Y_Q+2Y_u)-\frac{1}{2}c^{(1)}_{\varphi d}(2Y_d+Y_Q)-\frac{1}{2}c^{(1)}_{\varphi Q}(Y_d-Y_u)-\frac{1}{2}c^{(3)}_{\varphi Q}(Y_d+4Y_Q+Y_u),\\ &-\frac{1}{6}c^{(1)}_{\varphi e}(2Y_e+Y_L)-\frac{1}{6}c^{(1)}_{\varphi L}(Y_e-Y_\nu)-\frac{1}{6}c^{(3)}_{\varphi L}(Y_e+4Y_LY_e+Y_\nu)\\ E_{BW^3F_0} =& \frac{3}{2}c^{(1)}_{\varphi u}Y_u-\frac{3}{2}c^{(1)}_{\varphi d}Y_d-\frac{3}{2}c^{(1)}_{\varphi Q}(Y_d-Y_u)-\frac{3}{2}c^{(3)}_{\varphi Q}(Y_d+Y_u),\\ &-\frac{1}{2}c^{(1)}_{\varphi e}Y_e-\frac{1}{2}c^{(1)}_{\varphi L}(Y_e-Y_\nu)-\frac{1}{2}c^{(3)}_{\varphi L}(Y_e+Y_\nu),\\ E_{A_0W^3W^3} =& \frac{1}{12}\left(3c^{(1)}_{\varphi u}+3c^{(1)}_{\varphi d}+12c^{(1)}_{\varphi Q}+c^{(1)}_{\varphi e}+4c^{(1)}_{\varphi L}\right).\end{aligned} \tag{4.57}$$

Notice that, because of the definition of A_0 in Eq. (4.52), we have gathered together the GCS terms with an actual gauge field and those with the derivative of the NGB.

At this level, it is not clear that the dimension-6 operators do not generate gauge anomalies. We will now show it explicitly for the $\mathrm{U}(1)_Y^3$ anomaly, which is represented in the variation of the Lagrangian for the terms proportional to $\epsilon_Y B_{\mu\nu}\tilde{B}^{\mu\nu}$, as it can be seen from Eq. (4.51). Hence, let us collect all the operators from Eq. (4.54) and Eq. (4.56) which could generate such a term under an hypercharge gauge variation. They are:

$$\begin{aligned}\mathcal{L}_{\rm EFT} \supset& -\frac{1}{16\pi^2}\mathcal{C}_{F_0B}\frac{\pi^3}{v}F_0\tilde{B}-\frac{E_{A_0BB}}{8\pi^2\Lambda^2}A_{0,\mu}B_\nu\tilde{B}^{\mu\nu}\\ \supset& -vY_H\frac{1}{16\pi^2}\mathcal{C}_{F_0B}\pi^3B\tilde{B}+v\frac{E_{A_0BB}}{8\pi^2\Lambda^2}\partial_\mu\left(\pi^3\right)B_\nu\tilde{B}^{\mu\nu},\end{aligned} \tag{4.58}$$

where in the second line we decomposed A_0 and its field strength using their definitions, Eq. (4.52) and Eq. (4.53), and kept the relevant pieces. We can integrate by parts the second term to transform this part of the Lagrangian into

$$\begin{aligned} &- v Y_H \frac{1}{16\pi^2} \mathcal{C}_{F_0 B} \pi^3 B \tilde{B} - v \frac{E_{A_0 BB}}{16\pi^2 \Lambda^2} \pi^3 B_{\mu\nu} \tilde{B}^{\mu\nu} + ... \\ &= - v \left(Y_H \mathcal{C}_{F_0 B} + \frac{E_{A_0 BB}}{\Lambda^2} \right) \frac{\pi^3}{16\pi^2} B_{\mu\nu} \tilde{B}^{\mu\nu} + ..., \end{aligned} \tag{4.59}$$

where ... stands for the total derivative terms that will vanish upon integration. Using the formulae in Eq. (4.57) and Eq. (4.55) and relations required by the classical gauge invariance of the theory such as $Y_u = Y_Q + Y_H$, it is possible to show that

$$Y_H \mathcal{C}_{F_0 B} + \frac{E_{A_0 BB}}{\Lambda^2} = 0. \tag{4.60}$$

Therefore, these terms cancel exactly and there is no $\mathrm{U}(1)_Y^3$ gauge anomaly in SMEFT generated by chiral dimension-6 operators.

It is worth noting that the GCS terms cancel among themselves. As an example, let us consider the operator $W_\mu^3 B_\nu \tilde{B}^{\mu\nu}$ that was neglected in Eq. (4.58) and can be obtained from different terms of the EFT Lagrangian,

$$\begin{aligned} &- \frac{E_{A_0 BB}}{8\pi^2 \Lambda^2} A_{0,\mu} B_\nu \tilde{B}^{\mu\nu} - \frac{E_{A_0 W^3 B}}{8\pi^2 \Lambda^2} A_{0,\mu} W_\nu^3 \tilde{B}^{\mu\nu} - \frac{E_{B W^3 F_0}}{8\pi^2 \Lambda^2} B_\mu W_\nu^3 \tilde{F}_0^{\mu\nu}, \\ \supset &- \frac{v^2}{8\pi^2 \Lambda^2} \left(\frac{1}{2} E_{A_0 BB} + Y_H E_{A_0 WB} + Y_H E_{BWF_0} \right) W_\mu^3 B_\nu \tilde{B}^{\mu\nu}, \end{aligned} \tag{4.61}$$

and it can be checked directly by using Eq. (4.57) and the relations given by the gauge invariance of the Yukawa terms that the combination of WC between parenthesis vanishes. The same procedure can be applied to all the other terms in Eq. (4.54) and Eq. (4.56) to reach the conclusion that chiral dimension-6 operators in SMEFT do not generate gauge anomalies.

This result could have been anticipated: the only objects which can be formed using axionic and GCS terms, and which do not spoil the gauge-invariance of the bosonic EFT, have the following schematic form [241, 249]:

$$(\partial_\mu \theta_i - A_{i,\mu})(\partial_\nu \theta_j - A_{j,\mu}) \tilde{F}_k^{\mu\nu} \ , \tag{4.62}$$

where the gauge transformations of θ_i are such that $\partial_\mu \theta_i - A_{i,\mu}$ is gauge-invariant (in other words, θ_i corresponds to the longitudinal component of A_i). For the expression in Eq. (4.62) not to vanish, one needs at least two different massive gauge fields due to the antisymmetric structure of $\tilde{F}_k^{\mu\nu}$. However, there is only one massive gauge field, the Z boson, in the neutral sector of the SMEFT. Therefore, any non-vanishing WZ term in the bosonic EFT must break gauge invariance, but we do not find any such term at dimension-6.

Our results agree with the ones in Ref. [250], which uses different techniques and a toy model. As a final comment, notice that our explicit computations are limited to the neutral gauge sector and triangle diagrams. But the same reasoning applies to the charged gauge bosons and the computations can be extended to square and pentagon diagrams to include the non-linear pieces of the strength tensors.

4.5 Conclusions

In this chapter, we have studied if non-renormalisable interactions, more precisely dimension-6 operators, generate gauge anomalies in an EFT whose field content does not generate anomalies with operators of dimension up to 4. In particular, we have applied our techniques to show that gauge anomaly cancellation does not impose any constraint on dimension-6 WCs in the SMEFT. We have proved that a non-anomalous BSM sector can lead to fully independent dimension-6 WCs in the SMEFT.

On the other hand, if the BSM sector were found to be anomalous, we would conclude that is incomplete and require the existence of additional particles of interactions to cancel the anomalies. This argument relies heavily in our hypothesis that nature is fully described by gauge quantum field theories. Keeping such hypothesis is sensible since all our explorations of nature have proved it right, with the exception of processes where gravity is relevant. Additionally, we have already used EFTs with an anomalous field content, expecting to discover additional fermions at higher energies to cancel the anomalies. In particular, that is the nature of the top EFTs used in the 1980s and early 1990s before the discovery of the top quark.

The assertions made above are possible only with a solid knowledge of the theoretical tools at hand, and shows exactly what we look for in this and the following chapters. More precisely, in the next chapter we will revisit the relation between EFTs and anomalies, but focusing on global symmetries. This will allows us to explore topics related to a question that we implicitly left open in a previous paragraph: could we distinguish between anomalous and non-anomalous BSM sectors by measuring a few WCs? Given the relation between anomalies and chirality, we could also ask: could we say whether the UV spectrum is chiral or not from the value of WCs? The study of those questions will lead us to connect several not-trivially related topics.

Appendix to Chapter 4

4.A Gauge anomalies in the Standard Model

In the Standard Model, gauge anomaly cancellation is not ensured for arbitrary hypercharge assignment. The theory is free from $\mathrm{SU}(3)_c^3$ anomalies (this means taking 3 $\mathrm{SU}(3)_c$ currents) thanks to it being a vector-like gauge symmetry. On the other hand, there are no $\mathrm{SU}(2)_L^3$ anomalies thanks to group-theory properties of SU(2), despite the chiral nature of this gauge symmetry. There are no gauge anomalies involving only one $\mathrm{SU}(2)_L$ or $\mathrm{SU}(3)_c$ current since they are proportional to the vanishing trace of the generators [232, 248].

Hence, the only possible gauge anomalies in the SM involve the hypercharge group $\mathrm{U}(1)_Y$. We will show how asking these anomalies to cancel selects the hypercharge of each SM fermion. This can be done for each fermion generation independently, so we will consider just one of them. First, we start considering the mixed anomaly $\mathrm{U}(1)_Y\times\mathrm{SU}(2)_L^2$, i.e. we take one hypercharge and two weak currents. The anomaly polynomial is

$$D^{BWW} = \frac{3}{2}Y_Q + \frac{1}{2}Y_L, \tag{4.63}$$

where Y_Q and Y_L are the hypercharges of the quark and lepton doublets respectively. There is no contribution from RH fermion fields since they are singlets under $\mathrm{SU}(2)_L$. The factor $\frac{1}{2}$ in both terms comes from the conventional normalization of the generators of $\mathrm{SU}(N)$ in the fundamental representation, $\mathrm{Tr}(T^aT^b) = \frac{\delta^{ab}}{2}$. And the factor 3 in the quark term signals the 3 colours of quarks contributing equally.

In similar fashion, we can compute the anomaly polynomial for $\mathrm{U}(1)_Y\times\mathrm{SU}(3)_c^2$:

$$D^{BGG} = 2\frac{1}{2}Y_Q - \frac{1}{2}Y_d - \frac{1}{2}Y_u, \tag{4.64}$$

where we observe that only the quarks contribute, since the leptons are colourless. Also, the RH fields contribute with opposite sign and the factor 2 in front of Y_Q is due to the 2 fields inside the $\mathrm{SU}(2)_L$ doublet. The $\frac{1}{2}$ factors have the same origin than before. The last mixed anomaly to compute is $\mathrm{U}(1)_Y\times\mathrm{Grav}^2$, where we take two gravity currents. It reads simply

$$D^{BRR} = 6Y_Q + 2Y_L - 3Y_d - 3Y_u - Y_e, \tag{4.65}$$

where each quark has a factor 3 due to its colours and there is a factor 2 for each weak doublet. Finally, the anomaly polynomial for $\mathrm{U}(1)_Y^3$ is

$$D^{BBB} = 6Y_Q^3 + 2Y_L^3 - 3Y_d^3 - 3Y_u^3 - Y_e^3. \tag{4.66}$$

An overall normalization in the hypercharge is irrelevant and therefore we are free to choose $Y_e = 1$. After asking for

$$D^{BBB} = D^{BRR} = D^{BGG} = D^{BWW} = 0, \tag{4.67}$$

we obtain an unique solution:

$$Y_Q = \frac{1}{6}, \quad Y_L = -\frac{1}{2}, \quad Y_u = \frac{2}{3}, \quad Y_d = -\frac{1}{3}, \quad Y_e = 1. \tag{4.68}$$

4.B On spurious gauge anomalies caused by dimension-6 operators

The authors of Ref. [237] claimed that the SMEFT at dimension six and for arbitrary values of its WCs has gauge anomalies that have to be cancelled order by order in the $1/\Lambda$ expansion. Such anomaly cancellation condition takes the form of sum rules for the WCs. In particular, the anomalies found in Ref. [237] are traced back to the operators in Eq. (4.4). In order to satisfy the sum rules, the WCs of those operators should fulfil

$$c_{\varphi q}^{(3)} = c_{\varphi \ell}^{(3)} \ , \tag{4.69}$$

$$\frac{c_{\varphi q}^{(1)}}{Y_q} = \frac{c_{\varphi \ell}^{(1)}}{Y_L} = \frac{c_{\varphi u}}{Y_u} = \frac{c_{\varphi d}}{Y_d} = \frac{c_{\varphi e}}{Y_e} \ , \tag{4.70}$$

where Y_ψ is the hypercharge of the SM fields and the WCs are traced over generations, $c_{\varphi q}^{(3)} = \sum_i c_{\varphi q,ii}^{(3)}$ for instance. Furthermore, it is asserted that any anomaly-free UV extension of the SM that can be matched onto the SMEFT will respect such constraints on the Wilson coefficients.

The results obtained in Section 4.4 contradict the findings of Ref. [237]. More precisely, they show that the conditions (4.69)-(4.70) are not needed to ensure that the SMEFT is gauge-anomaly free. In this appendix, we discuss in more detail the reasons of the disagreement and our arguments against their result. First, in subsection 4.B.1, we rederive the results of Ref. [237] from simple anomaly-polynomial computations and discuss why this is a flawed method. Second, in subsection 4.B.2, we show two anomaly free extensions of the SM and match them to the SMEFT at tree-level. The first model violates the conditions on Eq. (4.69) and Eq. (4.70), constituting a counterexample of their results, while the second model satisfies the constraints. We discuss why several models would satisfy such constraints.

4.B.1 Spurious gauge anomalies in the SMEFT from explicit anomaly polynomials

The argument given in Ref. [237] goes as follows: in the broken phase of the theory, fixing the Higgs field to its VEV, we obtain from the SMEFT operators in Eq. (4.4) a modification to the three-points couplings between gauge fields and fermions. Demanding the conservation of the new fermionic current to which the gauge field couples yields relations between the dimension-6 SMEFT coefficients.

More precisely, we have, when $H = \left(0, \ \frac{v}{\sqrt{2}}\right)^T$,

$$iH^\dagger \overleftrightarrow{D}_\mu H = -v^2 \left(Y_H B_\mu - \frac{W_\mu^3}{2} \right) \ , \quad iH^\dagger \overleftrightarrow{D}_\mu^a H = \delta^{a3} Y_H B_\mu - \frac{v^2}{2} W_\mu^a \ , \tag{4.71}$$

and the operators in Eq. (4.4) induce the following modifications to gauge vertices,

$$
\begin{aligned}
&-\overline{\psi}_i \delta_{ij} \left(Y_\psi \not{B} + T^a \not{W}^a \right) \psi_j \\
&\to -\overline{\psi}_i \Bigg(\underbrace{\left[Y_\psi \delta_{ij} + v^2 Y_H \left\{ \frac{c^{(1)}_{\varphi\psi,ij}}{\Lambda^2} - 2T^3 \frac{c^{(3)}_{\varphi\psi,ij}}{\Lambda^2} \right\} \right]}_{\equiv T^B_{ij}} \not{B} + \underbrace{T^a \left[\delta_{ij} + v^2 \frac{c^{(3)}_{\varphi\psi,ij}}{\Lambda^2} \right]}_{\equiv T^{W,a}_{ij}} \not{W}^a \underbrace{-v^2 \frac{c^{(1)}_{\varphi\psi,ij}}{2\Lambda^2}}_{\equiv T^{W_3}_{ij}} \not{W}^3 \Bigg) \psi_j \ ,
\end{aligned}
\tag{4.72}
$$

where $T^a = \frac{\tau^a}{2}$ or 0 for left- and right-handed fermions respectively, and for RH fermions $c^{(1)}_{\varphi\psi} \equiv c_{\varphi\psi}$ and $c^{(3)}_{\varphi\psi} = 0$. We also defined new flavoured "generators" from the gauge field-fermions couplings. Then, one can compute the anomaly polynomials D^{ijk} associated to those new generators. Organising the result as an expansion in Λ^{-2}, they vanish at leading order since they correspond to the ones of the SM. At dimension-6, they read

$$
\begin{aligned}
D^{BBB} &= 3Y_\varphi \frac{v^2}{\Lambda^2} \left(6Y_Q^2 c^{(1)}_{\varphi Q,ii} + 2Y_L^2 c^{(1)}_{\varphi L,ii} - 3Y_u^2 c_{\varphi u,ii} - 3Y_d^2 c_{\varphi d,ii} - Y_e^2 c_{\varphi e,ii} \right) \equiv 3Y_\varphi \frac{v^2}{\Lambda^2} \mathcal{A} \\
D^{BG^AG^B} &= Y_\varphi \delta^{AB} \frac{v^2}{2\Lambda^2} \left(2c^{(1)}_{\varphi Q,ii} - c_{\varphi u,ii} - c_{\varphi d,ii} \right) \\
D^{BW^{a=1,2}W^{b=1,2}} &= \delta^{ab} \frac{v^2}{2\Lambda^2} \left(3 \left[2Y_Q c^{(3)}_{\varphi Q,ii} + Y_\varphi c^{(1)}_{\varphi Q,ii} \right] + 2Y_L c^{(3)}_{\varphi L,ii} + Y_\varphi c^{(1)}_{\varphi L,ii} \right) \\
D^{BBW^3} &= -\frac{v^2}{2\Lambda^2} \left(\mathcal{A} + 4Y_\varphi \left[3Y_Q c^{(3)}_{\varphi Q,ii} + Y_L c^{(3)}_{\varphi L,ii} \right] \right) \\
D^{BRR} &= Y_\varphi \frac{v^2}{\Lambda^2} \left(6c^{(1)}_{\varphi Q,ii} + 2c^{(1)}_{\varphi L,ii} - 3c_{\varphi u,ii} - 3c_{\varphi d,ii} - c_{\varphi e,ii} \right)
\end{aligned}
\tag{4.73}
$$

Demanding that all those expressions vanish yields the results of Ref. [237].

4.B.2 Tree-level (counter)examples

In this subsection, we review the explicit tree-level matching between two UV models and the SMEFT in order to, first, give a counterexample to the results in Ref. [237] and, second, show how certain models could misleadingly support those results. We will use the conventions and results contained in Ref. [184] that gives the complete tree-level matching of general BSM models onto dimension-6 SMEFT.

Heavy right-handed singlet Majorana fermion

We start by considering a model that extends the SM with a heavy neutral lepton, i.e., a SM singlet Majorana fermion N with a Majorana mass M_N. This is a simplified version of the see-saw type-I mechanism used to give a mass to the neutrinos and can be generalized without modifying our conclusions. The full UV Lagrangian of this model is the SM Lagrangian plus the usual kinetic and mass terms for N and the following interaction terms:

$$
\mathcal{L}^{\text{Int}}_{BSM} = -\left(\lambda_N\right)_i \bar{N} \tilde{H}^\dagger \ell_{L,i}, \tag{4.74}
$$

where $i = 1, 2, 3$, and we neglect higher-dimensional interaction terms which would not change our results and might obscure the discussion [184].

The heavy singlet fermion can be integrated out to match onto the SMEFT. This generates three classes of higher-dimensional operators with dimension not bigger than 6: the Weinberg

operator $\mathcal{O}_5$ and the dimension-6 operators $\mathcal{O}_{\varphi\ell}^{(1)}$ and $\mathcal{O}_{\varphi\ell}^{(3)}$ [184]. More specifically, the WCs of these three operators read [184]:

$$\frac{1}{\Lambda^2}\,(c_5)_{ij} = \frac{(\lambda_N)_j\,(\lambda_N)_i}{2M_N}, \tag{4.75}$$

$$\frac{1}{\Lambda^2}\left(c_{\varphi\ell}^{(1)}\right)_{ij} = \frac{(\lambda_N)_i^*\,(\lambda_N)_j}{4M_N^2}, \tag{4.76}$$

$$\frac{1}{\Lambda^2}\left(c_{\varphi\ell}^{(3)}\right)_{ij} = -\frac{(\lambda_N)_i^*\,(\lambda_N)_j}{4M_N^2}. \tag{4.77}$$

On the other hand, it is clear that no operator involving quarks can be generated and hence $c_{\varphi q}^{(3)} = c_{\varphi q}^{(1)} = c_{\varphi u} = c_{\varphi d} = 0$. Notice that the contribution to the Weinberg operator WC can be cancelled easily by the addition of a second copy of N with suitable couplings.

Therefore, this model violates both constraints in Eqs. (4.69)-(4.70). At the same time, the UV renormalisable model that this EFT comes from is anomaly free because it is just the SM plus a singlet Majorana fermion, which has no anomaly. Furthermore, this is a vector-like extension of the SM and hence there cannot be non-decoupling BSM effects. Indeed, the additional fermion can be explicitly decoupled by sending $M_N \to \infty$.

In conclusion, the model here presented constitutes a clear counterexample to the claims made in Ref. [237]. Furthermore, there is plenty of similar simple models which would lead to the same conclusion, e.g. the addition of a heavy hypercharged fermion or a heavy vector-like quark.

Heavy U(1) gauge field

Now, we briefly review a model that has been used as a cross-check in Ref. [237]. Let us add to the SM a massive gauge boson $\mathcal{B}_\mu$ that comes from a $U(1)$ gauge group that commutes with the rest of the SM gauge group. We denote its mass $M_\mathcal{B}$ and are agnostic about its ultimate origin. We suppose that this new gauge field couples to all the fermion and scalar fields of the SM in a flavour-universal manner and then its interaction terms are [184]:

$$\mathcal{L}_{BSM}^{\text{Int}} = -\,g_\mathcal{B}\,q_\ell^\mathcal{B}\,\mathcal{B}_\mu\,\bar{\ell}_L^i\gamma^\mu\ell_L^i - g_\mathcal{B}\,q_q^\mathcal{B}\,\mathcal{B}_\mu\,\bar{q}_L^i\gamma^\mu q_L^i \tag{4.78}$$

$$-\,g_\mathcal{B}\,q_e^\mathcal{B}\,\mathcal{B}_\mu\,\bar{e}_R^i\gamma^\mu e_R^i - g_\mathcal{B}\,q_u^\mathcal{B}\,\mathcal{B}_\mu\bar{u}_R^i\gamma^\mu u_R^i - g_\mathcal{B}\,q_d^\mathcal{B}\,\mathcal{B}_\mu\,\bar{d}_R^i\gamma^\mu d_R^i \tag{4.79}$$

$$-\,(g_\mathcal{B}\,q_\varphi^\mathcal{B}\,\mathcal{B}^\mu\,\varphi^\dagger iD_\mu\varphi + \text{h.c.}). \tag{4.80}$$

The conclusions of this analysis are independent of the flavour-universality assumption, which we make for simplicity.

This model is not automatically anomaly-free and, in particular there can be mixed anomalies between the new gauge group and the SM one. The equations that must be satisfied by the charges under $\mathcal{B}$ are:

$$\langle\mathcal{B}BB\rangle:\ 0 = 6q_q^\mathcal{B}y_q^2 + 2q_\ell^\mathcal{B}y_\ell^2 - q_e^\mathcal{B}y_e^2 - 3q_u^\mathcal{B}y_u^2 - 3q_d^\mathcal{B}y_d^2, \tag{4.81}$$

$$\langle\mathcal{B}WW\rangle:\ 0 = 6q_q^\mathcal{B} + 2q_\ell^\mathcal{B}, \tag{4.82}$$

$$\langle\mathcal{B}GG\rangle:\ 0 = 2q_q^\mathcal{B} - q_u^\mathcal{B} - q_d^\mathcal{B}, \tag{4.83}$$

$$\langle\mathcal{B}RR\rangle:\ 0 = 6q_q^\mathcal{B} + 2q_\ell^\mathcal{B} - q_e^\mathcal{B} - 3q_u^\mathcal{B} - 3q_d^\mathcal{B}, \tag{4.84}$$

where R refers to the Ricci tensor which appears in the gravitational anomaly.

After integrating out the massive gauge boson $\mathcal{B}_\mu$, we obtain an EFT Lagrangian with several

dimension-6 operators [184], but not $\mathcal{O}_{\varphi l}^{(3)}$ nor $\mathcal{O}_{\varphi q}^{(3)}$. Then, Eq. (4.69) will be satisfied trivially. On the other hand, the operators involved in Eq. (4.70) are generated with the following non-zero WCs:

$$\frac{1}{\Lambda^2}\left(c_{\varphi l}^{(1)}\right)_{ij} = -\, g_{\mathcal{B}}^2 \frac{q_\varphi^{\mathcal{B}}\, q_\ell^{\mathcal{B}}}{M_{\mathcal{B}}^2}\delta_{ij} \tag{4.85}$$

$$\frac{1}{\Lambda^2}\left(c_{\varphi q}^{(1)}\right)_{ij} = -\, g_{\mathcal{B}}^2 \frac{q_\varphi^{\mathcal{B}}\, q_q^{\mathcal{B}}}{M_{\mathcal{B}}^2}\delta_{ij} \tag{4.86}$$

$$\frac{1}{\Lambda^2}\left(c_{\varphi e}\right)_{ij} = -\, g_{\mathcal{B}}^2 \frac{q_\varphi^{\mathcal{B}}\, q_e^{\mathcal{B}}}{M_{\mathcal{B}}^2}\delta_{ij} \tag{4.87}$$

$$\frac{1}{\Lambda^2}\left(c_{\varphi d}\right)_{ij} = -\, g_{\mathcal{B}}^2 \frac{q_\varphi^{\mathcal{B}}\, q_d^{\mathcal{B}}}{M_{\mathcal{B}}^2}\delta_{ij} \tag{4.88}$$

$$\frac{1}{\Lambda^2}\left(c_{\varphi u}\right)_{ij} = -\, g_{\mathcal{B}}^2 \frac{q_\varphi^{\mathcal{B}}\, q_u^{\mathcal{B}}}{M_{\mathcal{B}}^2}\delta_{ij}, \tag{4.89}$$

and then, up to an overall common factor, there is a one-to-one correspondence between the fermion charges and the 5 non-vanishing WCs. In consequence, we can rewrite the UV anomaly conditions in Eqs. (4.81)-(4.84) in terms of the WCs as follows:

$$0 = 6c_{\varphi q}^{(1)} y_q^2 + 2c_{\varphi l}^{(1)} y_\ell^2 - c_{\varphi e} y_e^2 - 3c_{\varphi u} y_u^2 - 3c_{\varphi d} y_d^2, \tag{4.90}$$

$$0 = 6c_{\varphi q}^{(1)} + 2c_{\varphi l}^{(1)}, \tag{4.91}$$

$$0 = 2c_{\varphi q}^{(1)} - c_{\varphi u} - c_{\varphi d}, \tag{4.92}$$

$$0 = 6c_{\varphi q}^{(1)} + 2c_{\varphi l}^{(1)} - c_{\varphi e} - 3c_{\varphi u} - 3c_{\varphi d}. \tag{4.93}$$

These are the equations found in Table 1 of Ref. [237] for the special case $c_{\varphi q}^{(3)} = c_{\varphi l}^{(3)} = 0$ and their only solution is Eq. (4.70). Hence, the UV anomaly cancellation condition of the model is the reason behind the fulfilment of these conditions on the WCs. Notice that this model belongs to the Universal Theories class because the BSM sector couples to the SM only through the scalar and fermion vector currents already present in the SM [216]. It is known that those theories, when matched onto the SMEFT, always obey accidentally Eqs. (4.69)-(4.70) [166, 216].

4.C Global symmetries in the toy model

The toy model considered in subsection 4.3.1 has several global symmetries. Focusing only on the scalar and fermionic sector, each of the fields, ϕ, $\psi_{1,L}$, $\psi_{2,L}$, $\psi_{1,R}$ and $\psi_{2,R}$, can be phase-shifted independently. Hence, there are 5 independent U(1) symmetries. One linear combination of them corresponds to the global part of the gauge symmetry of the model and another one is the global symmetry studied in the text.

There remain 3 global symmetries and we denote their transformation parameters as ϵ_i with

$i = 1, 2, 3$. The scalar and fermion fields transform under them as

$$\begin{aligned}
\phi \to & e^{i(\epsilon_1+\epsilon_2)}\phi \\
\psi_1 \to & e^{i\gamma_5\left(-\epsilon_1 \frac{2\left(q_2^B\right)^2+\left(q_\phi^B\right)^2}{2q_1^B q_\phi^B}+\epsilon_2 \frac{q_1^B}{q_\phi^B}\right)+i\epsilon_3}\psi_1 \\
\psi_2 \to & e^{i\gamma_5\left(\epsilon_1 \frac{q_2^B}{q_\phi^B}-\epsilon_2 \frac{2\left(q_1^B\right)^2+\left(q_\phi^B\right)^2}{2q_2^B q_\phi^B}\right)-i\epsilon_3 \frac{q_1}{q_2}}\psi_2,
\end{aligned} \tag{4.94}$$

where we arbitrarily chose that the scalar field transforms equally under two of them.

4.D Ward-Takahashi identity in the unbroken phase

In order to confirm that there are no anomalies coming from the kind of dimension-6 terms studied in this note, it is useful to display cancellations similar to those in Fig. 4.3.2, but in the unbroken phase of our toy model of Section 4.3. This means that we need to study a correlator which is sensitive (at one-loop) to an insertion of the dimension-6 part of the current in Eq. (4.31) (as we said in Section 4.3, this is not the case for the usual correlator in Eq. (4.35)). The simplest such correlator is

$$\langle 0|J_\mu^B(x)J_\nu^A(y)J_\rho^A(z)\varphi(x_1)\varphi^\dagger(x_2)|0\rangle \ , \tag{4.95}$$

and the Ward-Takahashi (WT) identity which follows from the classical symmetry in the absence of anomalies is

$$\begin{aligned}
&\partial^\mu\langle 0|J_\mu^B(x)J_\nu^A(y)J_\rho^A(z)\varphi(x_1)\varphi^\dagger(x_2)|0\rangle \\
&\qquad + q_\varphi^B\left[\delta^{(4)}(x-x_1)-\delta^{(4)}(x-x_2)\right]\langle 0|J_\nu^A(y)J_\rho^A(z)\varphi(x_1)\varphi^\dagger(x_2)|0\rangle = 0 \ ,
\end{aligned} \tag{4.96}$$

where contact terms are present since $\varphi^{(\dagger)}$ is charged under $U(1)_B$, unlike $J^A_{\nu(\rho)}$.

Let us compute the correlator in Eq. (4.95) at one-loop, focusing on the diagrams proportional to q_φ^B. They are displayed in Fig. 4.D.1.

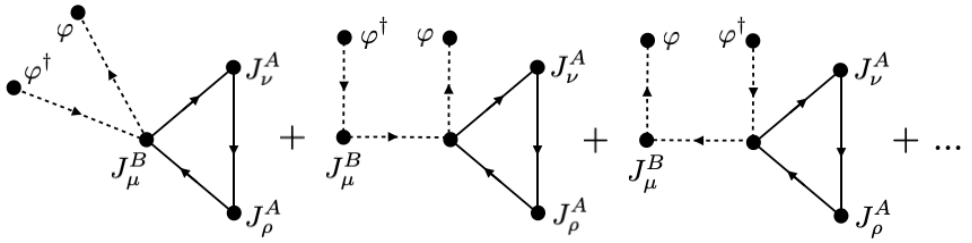

Figure 4.D.1: Triangle diagrams proportional to q_φ^B entering the correlator in Eq. (4.95) in the unbroken phase (the +... refers to the same diagrams with the orientation of the fermionic arrows reversed). Solid lines are fermion propagators and dashed lines are scalar propagators.

We obtain

$$\begin{aligned}
&\langle 0|J_\mu^B(x)J_\nu^A(y)J_\rho^A(z)\varphi(x_1)\varphi^\dagger(x_2)|0\rangle \\
&\qquad = iq_\varphi^B\frac{c_L}{\Lambda^2}\int\frac{d^4p\,d^4q}{(2\pi)^8}\frac{e^{i[p\cdot(x-x_1)+q\cdot(x-x_2)]}}{(p^2-m_\varphi^2)(q^2-m_\varphi^2)}(D_{L,1}+D_{L,2}+D_{L,3})^{\mu\nu\rho}+(L\leftrightarrow R) \ ,
\end{aligned} \tag{4.97}$$

where the $D_{L,i}$s correspond to the individual diagrams in Fig. 4.D.1. They respectively read

$$\begin{aligned} D^{\mu\nu\rho}_{L,1} &\equiv -2\Gamma^{\mu\nu\rho}_{L}(x,y,z) \ , \\ D^{\mu\nu\rho}_{L,2} &\equiv \int \frac{d^4\tilde{x}\, d^4l}{(2\pi)^4} e^{i(l+p)\cdot(\tilde{x}-x)} \frac{l^\mu + q^\mu}{l^2 - m_\varphi^2} (l-p)_\alpha \Gamma^{\alpha\nu\rho}_{L}(\tilde{x},y,z) \ , \\ D^{\mu\nu\rho}_{L,3} &\equiv D^{\mu\nu\rho}_{L,2}\big|_{p\leftrightarrow q, x_1\leftrightarrow x_2} \ , \end{aligned} \tag{4.98}$$

where

$$\Gamma^{\mu\nu\rho}_{L}(x,y,z) \equiv \langle 0|\overline{\psi}_L \gamma^\mu \psi_L(x) J^A_\nu(y) J^A_\rho(z)|0\rangle \tag{4.99}$$

refers to the fermion loop, about which we just need to know its dependence on the spacetime points and momenta. The other correlator which enters the WT identity in Eq. (4.96) receives contributions from the diagrams in Fig. 4.D.2, and reads

$$\begin{aligned} &\langle 0|J^A_\nu(y) J^A_\rho(z) \varphi(x_1) \varphi^\dagger(x_2)|0\rangle \\ &\qquad = \frac{c_L}{\Lambda^2} \int \frac{d^4p\, d^4q\, d^4\tilde{x}}{(2\pi)^8} \frac{e^{i[(p\cdot(\tilde{x}-x_1)+q\cdot(\tilde{x}-x_2)]}}{(p^2-m_\varphi^2)(q^2-m_\varphi^2)} (p-q)_\alpha \Gamma^{\alpha\nu\rho}_{L}(\tilde{x},y,z) + (L\leftrightarrow R) \ . \end{aligned} \tag{4.100}$$

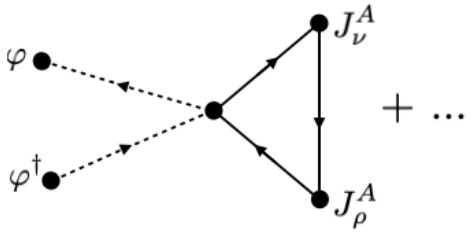

Figure 4.D.2: Triangle diagrams entering the second correlator in Eq. (4.96) in the unbroken phase (the +... refers to the same diagrams with the orientation of the fermionic arrows reversed). Solid lines are fermion propagators and dashed lines are scalar propagators.

From these expressions, it is straightforward to check that the WT identity is verified, irrespective of the value (and the regularization) of the fermion loop[9] $\Gamma^{\mu\nu\rho}_{L(R)}$.

[9] As can be inferred from our computation, the WT identity would hold for any function $\Gamma_{L(R)}$ - or equivalently, for any gauge-invariant current coupled to $\varphi^\dagger \overleftrightarrow{\partial} \varphi$ in the Lagrangian.

This page is intentionally left blank.

Chapter 5

On non-anomalous axion couplings and chiral extensions of the SM

"The task is, not so much to see what no one has yet seen; but to think what nobody has yet thought, about that which everybody sees."

— Erwin Schrödinger, as quoted by
L. von Bertalanffy in Problems of Life (1952)

5.1 Introduction

Our quest for BSM physics has become a broad search, where several target particles or models have secured a sizeable amount of attention. The axion is, perhaps, the class of particle that has gained more traction over the last few years[1]. Although axions are hard to find at colliders, the variety of experiments that can search for them is remarkable and still growing. The experimental program of axion searches for the next decade is vast, exciting and promising [251, 252]. Thus, any effort from the theoretical community to understand better this hypothetical particle should be of great value.

To be more precise, an axion is a pseudo-scalar particle that arises as the pseudo-Nambu-Goldstone boson (pNGB) of some approximate spontaneously broken global symmetry[2]. Its inception goes back to 45 years ago, originally just as a solution to the strong CP problem of QCD [253–256], what we call the QCD axion. Since then, axions have become one of the main DM candidates and they appear naturally in many NP models, for example in those connected with string theory (see e.g. Ref. [257] and references therein) and CHMs [258–260]. Its pNGB nature, with the spontaneous symmetry breaking occurring at some scale f well above the EW scale, makes natural to study axion phenomenology with an EFT, in particular what concerns its interaction with SM particles. Furthermore, an axion EFT provides a more model-independent framework to interpret the results from many different experimental searches, which is very relevant given the variety of UV models that can give generate axions.

The need for an axion EFT was soon recognized and the pioneering work of Georgi, Kaplan and Randall [261] laid out the foundations for most of what has been done until this day. Within

[1] A simple search in INSPIRE-HEP shows that the number of papers per year containing the word axion in the title grew from 19 in 2001 to 66 in 2012, and 285 in 2020.

[2] Notice that we call axion to what is usually called axion-like-particle (ALP). We reserve the name QCD axion for those axions aimed at solving the strong QCD problem via the PQ mechanism.

the EFT, the set of couplings between an axion and two gauge bosons is of special interest from a phenomenological point of view. Among them, the couplings of an axion to photons and gluons have been extensively studied since they are the most phenomenologically relevant couplings of the QCD axion. It is also well-known that those couplings render clear information about the UV model that generates the axion, since they are proportional to mixed global-gauge anomalies, which are not affected by the RG running [240, 245, 262]. This kind of relation between EFT couplings of a pNGB and anomalies have been known since the 1960s because they also play a key role in pion physics. Nevertheless, it was pointed out recently [263] that when matching some UV models to an axion EFT, anomalies are not enough to determine the axion couplings to massive gauge bosons, such as the W and Z bosons.

The groundbreaking paper by Georgi, Kaplan, and Randall included the assumption of a linearly realised EWSB, which in turn implies that the axion coupling to EW bosons is exclusively given by structures consistent with an UV SU(2)×U(1) anomaly [261]. Assuming a linearly realised EWSB is not only a reasonable assumption but is, in fact, favoured by experimental results. However, the current lack of clear signs of BSM physics and the broad exploration of axion physics lead us to review and question each assumption on our models. And, as we will see throughout this chapter, the aforementioned assumption in Ref. [261] has profound consequences for axion physics.

The correct axion EFT when the assumption of linearly realised EWSB is lifted has been identified previously in the literature [264]. In particular, it was found that when EWSB is realized non-linearly, there are additional operators leading to (derivative) couplings between an axion and the EW gauge bosons. This effectively increases the dimension of the axion EFT parameter space. However, the relation between these operators and anomaly matching with an UV model was not analysed in detail. Could there be any relation between those operators and the mismatch with anomalies found in Ref. [263]? That is one of the questions we will answer throughout this chapter.

From a separate point of view, an EFT with non-linearly realised EWSB is one of the smoking guns of heavy chiral matter that has been integrated out, as pointed out in Ref. [146] and reviewed in subsection 2.4.3. Extensions of the SM with heavy chiral fermions are some of the most difficult to build consistently, being stringently constrained by gauge-anomaly cancellation conditions (see Ref. [265] for a systematic analysis of fermion extensions of the SM, including chiral and vector-like models). However, the anomaly-free condition only restricts the UV charges of the particles but leaves open the possibility that particles belonging to a vector-like representation of $\mathrm{SU}(2)_L\times\mathrm{U}(1)_Y$ acquire a *chiral* mass spectrum in the IR.

Given all these pieces, it seems possible that there is a clear connection among axion couplings to gauge bosons, anomalies, non-linear EWSB and chiral extensions of the SM. Uncovering this relation is the main goal of this chapter. First, in Section 5.2, we will review when the axion couplings to gauge bosons in an EFT are determined by anomalies. In particular, we will clarify when the couplings and the anomalies are unrelated, which will show clearly the impact of having chiral matter in the UV[3]. Then, in Section 5.3 we will discuss how to build a chiral extension of the SM and its relation with non-linearly realised EWSB. We build an explicit minimal chiral extension of the SM in subsection 5.3.2. Section 5.4 connects axions to chiral extensions of the SM. First, in subsection 5.4.1, we modify the model presented in subsection 5.3.2 to include an axion. Then, in subsection 5.4.2, we take that model and match it to an axion EFT in order to discuss its axion couplings to EW gauge bosons. Finally, in Section 5.4.3, we show that the minimal models presented before, though heavily constrained, are still allowed by experimental results and hence, they are phenomenologically relevant.

[3]We will not delve into a detailed derivation of these results, which can be found in Ref. [249].

5.2 Anomalies in axion EFTs

In this section, we will review the relation between axion couplings to gauge bosons and anomalies. First, we will focus on couplings to abelian gauge bosons. This case is of great importance since the axion coupling to photons is the one involved in its stellar production and in its detection at experiments, in both cases via a Primakoff process [266].

5.2.1 Abelian gauge bosons

It is common lore that the axion coupling to gauge bosons in an EFT is given at leading order by the following dimension-5 operator:

$$\mathcal{L}_{\rm EFT} \supset -g^2 \frac{\mathcal{C}}{16\pi^2 f} a\, F_{\mu\nu}\tilde{F}^{\mu\nu} \ , \tag{5.1}$$

where g is the gauge coupling constant of the gauge field A with field strength $F_{\mu\nu}$, $\tilde{F}^{\mu\nu} \equiv \frac{\epsilon^{\mu\nu\rho\sigma}}{2} F_{\rho\sigma}$, f is a dimensionful scale and $\mathcal{C}$ a number. The axion a is understood as the Nambu-Goldstone boson (GB) of a spontaneously broken PQ symmetry $\mathrm{U}(1)_{\rm PQ}$, under which the gauge boson is uncharged. Similarly, the axion is neutral under the gauge symmetry $U(1)_A$. The action of the PQ symmetry is normalized such that the axion shifts as $\delta_{\rm PQ} a = \epsilon_{\rm PQ} f$.

This operator is generated by a loop of heavy fermions that are charged under both PQ and $U(1)_A$ symmetries and that have been integrated out of the EFT. We define the mixed anomaly polynomial $D^{\mathrm{PQ},AA}$ as follows:

$$D^{\mathrm{PQ},AA} = \sum_{\mathrm{LH}\ \psi} q_\psi^{PQ} \left(q_\psi^A\right)^2 - \sum_{\mathrm{RH}\ \psi} q_\psi^{PQ} \left(q_\psi^A\right)^2 , \tag{5.2}$$

where LH (RH) ψ are all the left(right)-handed heavy fermions that enter in the loop, q_ψ^{PQ} is their PQ charge and q_ψ^A is their gauge charge. The usual statement is that $\mathcal{C}$ is the anomaly coefficient $D^{\mathrm{PQ},AA}$ corresponding to those fermions, i.e. $\mathcal{C} = D^{\mathrm{PQ},AA}$. Hence, the amplitude involving one axion and two gauge fields is determined by anomalies.

Such statement about $\mathcal{C}$ and anomalies is true when the gauge field is massless, but not entirely when A has non-zero mass. In the latter case, one additional gauge invariant operator becomes available [249]. Then, we like to think of the EFT of an axion and a massive abelian gauge field as being split as

$$\mathcal{L} \supset -g^2 \frac{D^{\mathrm{PQ}AA}}{16\pi^2 f} a F_{\mu\nu}\, \tilde{F}^{\mu\nu} - g \frac{\mathcal{C} - D^{\mathrm{PQ}AA}}{8\pi^2 f} \partial_\mu a \left(\frac{\partial_\nu \theta_A}{m_A} - g A_\nu\right) \tilde{F}^{\mu\nu} \ , \tag{5.3}$$

where θ_A is the NGB that provides the longitudinal degree of freedom for the massive A field and m_A is the mass of the latter. This way of writing the EFT shows explicitly that for a massive gauge field, $\mathcal{C}$ is not necessarily equal to $D^{\mathrm{PQ},AA}$ but anomaly matching still holds, because only the first term shifts under the PQ symmetry. Additionally, the presence of the would-be NGB absorbed by the gauge field reminds that such possibility does not exist for a massless gauge field. Finally, it generalizes to the non-abelian case more straightforwardly.

Although the non-vanishing mass of A_μ is a necessary condition for the mismatch $\mathcal{C} \neq D^{\mathrm{PQ},AA}$, it is not sufficient. Instead, what is sufficient for a generic PQ is that the fermions that have been integrated out are chiral with respect to the gauge field A. As mentioned in Section 5.1, chirality of the UV charges and of the mass eigenstates are not equivalent conditions. What matters here

is the notion of IR chirality[4], i.e. that the RH and LH components of the integrated-out massive eigenstates have different couplings to the gauge boson A. Notice that the chiral couplings ensure that A is massive.

We remark that Eq. (5.1) and Eq. (5.3) are completely equivalent at the level of scattering amplitudes. In other words, in both cases the phenomenology of the axion, namely the matrix elements between physical states, is captured by the only coefficient $\mathcal{C}$. There is no difference in the phenomenology predicted by anomalous and non-anomalous terms, the only way to see the mismatch is to measure $\mathcal{C}$ and compare it with $D^{\mathrm{PQ},AA}$, which has to be computed from the UV model. This feature of the abelian case remains true even in the presence of several abelian gauge fields. As we will see later, in the non-abelian case, the presence of only anomalous or both anomalous and non-anomalous terms leads to a different phenomenology.

There is one further subtlety in the abelian case. From an UV point of view, where one has control over the UV model, one can choose the PQ symmetry due to an irreducible ambiguity in the assignation of PQ charges to the fermions (see Ref. [263,267] for the case of lepton and baryon numbers). This freedom can be used to enforce $\mathcal{C} = D^{\mathrm{PQ},AA}$, although with some limitations. The ambiguity in the fermion charges determination is caused by vector-like global symmetries. If those symmetries are gauged, new terms like Eq. (5.1) can be written in the EFT. If the number of such operators, whose coefficients are sensitive to PQ anomalies, is bigger than the number of unfixed global vector-like symmetries overlapped with PQ, one can choose the PQ symmetry to enforce $\mathcal{C} = D^{\mathrm{PQ},AA}$ in some but not all of them (see Appendix 5.A for details). Notice that the PQ-choice freedom does not exist from a purely IR point of view and therefore the second term in Eq. (5.3) should always be included in the EFT. Equivalently, in a bottom-up approach, one should always consider the possibility of the mismatch between anomalies and axion couplings.

5.2.2 Non-abelian gauge bosons

The generalization of Eq. (5.3) to the non-abelian case can not be done in detail without specifying the symmetry breaking pattern. Hence, we will focus on the case relevant for the SM and use the electroweak gauge bosons. In this subsection, we will be very general about the fermionic spectrum that could generate the axion-gauge bosons interactions and we delay comments regarding the specific case of the SM spectrum to subsection 5.2.3.

Let us start by generalizing the operator in Eq. (5.1) to the case of an axion coupling to the SM EW gauge fields

$$\mathcal{L} \supset -\frac{g^2 C_{WW}}{16\pi^2}\frac{a}{f}W^a\tilde{W}^a - \frac{g'^2 C_{BB}}{16\pi^2}\frac{a}{f}B\tilde{B}\,. \tag{5.4}$$

We only included two coefficients to respect the $\mathrm{SU}(2)_L\times\mathrm{U}(1)_Y$ gauge symmetry. This is consistent with the constraining form of the mixed PQ anomalies with the $\mathrm{SU}(2)$ non-abelian factor of the SM gauge group.

Nevertheless, Eq. (5.4) does not capture all the possible terms, because there exist non-abelian analogues of the second term in Eq. (5.3). For the SM, there are 3 of those PQ- and gauge-invariant operators [264]:

$$\partial_\mu a\,\mathrm{Tr}(TV_\nu)\,\tilde{B}^{\mu\nu}\ , \quad \partial_\mu a\,\mathrm{Tr}(V_\nu\,\tilde{W}^{\mu\nu})\ , \quad \partial_\mu a\,\mathrm{Tr}(TV_\nu)\mathrm{Tr}(T\tilde{W}^{\mu\nu})\ , \tag{5.5}$$

where we have used the Goldstone matrix U and its Maurer-Cartan form, defined as [264, 268]

$$U = e^{i\frac{\pi^a}{v}\sigma^a}\ , \quad D_\mu U = \partial_\mu U - igW_\mu U + ig'B_\mu U\frac{\sigma_3}{2}\ , \tag{5.6}$$

[4]During the rest of this chapter, we will mean "IR chiral" by "chiral" unless stated otherwise.

where π^a are the longitudinal components of the Z and W bosons, to define the operators

$$V_\mu = D_\mu U U^\dagger \ , \quad T = U\sigma_3 U^\dagger \ . \tag{5.7}$$

The σ^a are the Pauli matrices and $v \approx 246$ GeV is the electroweak VEV.

Let us stress that the terms in Eq. 5.13 will appear with a non-vanishing WC only when fermions that are chiral with respect to the Z and W bosons have been integrated out and their WC are not related to mixed PQ-gauge anomalies [249]. This establishes a clear connection between chiral matter and non-anomalous axion couplings. Although the use of the Goldstone matrix U in Eq. (5.5) could misleadingly indicate that a non-linear EWSB is enough for those terms to appear, we stress the need of massive chiral fermions. Even more, notice that when EWSB is linearly realized, one can also choose to parametrise the Higgs doublet as $H = \frac{v+h}{\sqrt{2}}U$ without modifying the described physics [146] and, therefore, the terms in Eq. (5.5) should not appear even if they can be written. The connection between non-linear EWSB and non-anomalous axion couplings is via the required presence of chiral matter, as we will discuss in the next section. For the rest of this subsection, we will discuss the phenomenological differences caused by these new terms.

If the operators in Eq. (5.4) were the whole story, they would induce correlations between the different EFT operators when written in terms of the vector massive eigenstates. In fact, using the latter, Eq. (5.4) becomes

$$-\frac{16\pi^2}{e^2}\mathcal{L} \supset C_{\gamma\gamma}\frac{a}{f}F\tilde{F} + 2\frac{C_{Z\gamma}}{c_W s_W}\frac{a}{f}F\tilde{Z} + \frac{C_{ZZ}}{c_W^2 s_W^2}\frac{a}{f}Z\tilde{Z} + \frac{2C_{WW}}{s_W^2}W^+\tilde{W}^- \ , \tag{5.8}$$

where the coefficients read

$$C_{\gamma\gamma} = C_{WW} + C_{BB}, \quad C_{Z\gamma} = c_W^2 C_{WW} - s_W^2 C_{BB}, \quad C_{ZZ} = c_W^4 C_{WW} + s_W^4 C_{BB}, \tag{5.9}$$

and where $c_W = \cos(\theta_W)$, $s_W = \sin(\theta_W)$, and $t_W = \tan(\theta_W)$ with θ_W the Weinberg angle, and we denoted the photon and Z-boson field strengths by F and Z, respectively. The four coefficients in Eq. (5.8) are determined by C_{BB} and C_{WW} only. Thus, there must be correlations among the processes involving one axion and two electroweak gauge fields. This is different from the abelian case, that would allow independent coefficients for each gauge field pair. Such correlations can take the form of sum rules between EFT coefficients[5], for instance:

$$C_{\gamma\gamma} + s_W^{-2}(1 - t_W^2)C_{Z\gamma} - \frac{1}{s_W^2 c_W^2}C_{ZZ} = 0, \quad C_{\gamma\gamma} + s_W^{-2}C_{Z\gamma} - (1 + t_W^{-2})C_{WW} = 0. \tag{5.10}$$

Sum rules can also be written at the level of observable quantities such as partial decay rates of the axion, as we will see explicitly in subsection 5.4.1.

However, the terms in Eq. (5.5) also generate amplitudes involving one axion and two gauge bosons in addition to that of Eq. (5.4), since

$$\begin{aligned}
\partial_\mu a \,\mathrm{Tr}\,(TV_\nu)\, \tilde{B}^{\mu\nu} &\supset -i\partial_\mu a \left(gW_\nu^3 - g'B_\nu\right)\tilde{B}^{\mu\nu}\big|_{\text{lin.}} \ , \\
\partial_\mu a \,\mathrm{Tr}\left(V_\nu \tilde{W}^{\mu\nu}\right) &\supset -\frac{i}{2}\partial_\mu a \left(gW_\nu^a \tilde{W}^{a,\mu\nu} - g'B_\nu \tilde{W}^{3,\mu\nu}\right)\big|_{\text{lin.}} \ , \\
\partial_\mu a \,\mathrm{Tr}\,(TV_\nu)\,\mathrm{Tr}\left(T\tilde{W}^{\mu\nu}\right) &\supset -\frac{i}{2}\partial_\mu a \left(gW_\nu^3 - g'B_\nu\right)\tilde{W}^{3,\mu\nu})\big|_{\text{lin.}} \ ,
\end{aligned} \tag{5.11}$$

[5]The sum-rules are understood to hold at energy scales where the W and Z bosons are dynamical degrees of freedom.

where we used the same letter to refer to the gauge fields and to their field strengths, and where we ignore the non-linear piece of the field strength, i.e. $W^a_{\mu\nu}|_{\rm lin} = \partial_\mu W^a_\nu - \partial_\nu W^a_\mu$, because the axion couplings to two gauge fields are only sensitive to the linear part[6]. Up to numerical coefficients, the terms presented before can be integrated by parts to obtain

$$-\frac{c_1 g'}{16\pi^2 f} a\left(gW^3 - g'B\right)\tilde{B}\,, \quad -\frac{c_2 g}{16\pi^2 f} a(gW^a\tilde{W}^a - g'B\tilde{W}^3)\,, \quad -\frac{c_3 g}{16\pi^2 f} a\left(gW^3 - g'B\right)\tilde{W}^3\,, \tag{5.12}$$

respectively. Added up and rewritten using the vector massive eigenstates, they lead to

$$-\frac{e^2}{16\pi^2}\frac{a}{f}\left(\frac{c_1+c_2+c_3}{c_W s_W}\frac{a}{f}F\tilde{Z} + \frac{(c_2+c_3)c_W^2 - c_1 s_W^2}{c_W^2 s_W^2}\frac{a}{f}Z\tilde{Z} + \frac{2c_2}{s_W^2}W^+\tilde{W}^-\right). \tag{5.13}$$

It should be noted that the expression above does not contain any $aF\tilde{F}$ term, consistently with our previous analysis: anomalous terms capture all the processes involving one axion and two photons because the latter have always vector-like couplings to matter.

In addition, the new terms increase the parameter space of axion EFTs, which can be seen explicitly by noticing that they generically violate sum rules such as Eq. (5.10). Using the conventions in Eq. (5.13), we find that the modification to those sum rules is:

$$C_{\gamma\gamma} + s_W^{-2}(1-t_W^2)C_{Z\gamma} - \frac{1}{s_W^2 c_W^2}C_{ZZ} = \frac{c_1 - c_2 - c_3}{2c_W^2 s_W^2}\,, \tag{5.14}$$

$$C_{\gamma\gamma} + s_W^{-2}C_{Z\gamma} - (1+t_W^{-2})C_{WW} = \frac{c_1 - c_2 + c_3}{2s_W^2}\,. \tag{5.15}$$

Notice that the combination c_1+c_2 does not violate the sum rules, as expected since it corresponds to the operator $a\left(g^2W^a\tilde{W}^a - g'^2B\tilde{B}\right)$, which is just a linear combinations of those in Eq. (5.4).

What we found in Eq. (5.15) shows that, unlike what happens in the abelian case, there are genuine differences between the phenomenological predictions using only Eq. (5.4) or adding those in (5.5). For instance, the use of the non-linear realization of the SM gauge group allowed for the axion couplings to go beyond the $SU(2)$ trace structure in Eq. (5.4), so that the non-anomalous terms cannot simply be integrated by parts to recover the usual phenomenology of the anomalous terms. We will give a precise example of how these differences are generated from the UV in subsection 5.4.1.

5.2.3 On the SM-axion EFT

The axion EFT discussed in subsection 5.2.2 could be straightforwardly used as a part of the most general SM-axion EFT. However, it is imperative to reflect on which fermions can be integrated out and, therefore, contribute to the WCs. Let us start supposing that the only fermions in nature are the ones in the SM. Hence, in the UV theory at tree level, there are axion interactions with the SM particles. All of the latter are captured by the following SM-axion effective Lagrangian, keeping up to $d = 5$ operators:

$$\begin{aligned}\mathcal{L}_a^{d\leq 5} = {} & \frac{1}{2}(\partial_\mu a)^2 - \frac{1}{2}m_a^2 a^2 + \frac{\partial^\mu a}{f}\sum_\psi \bar{\psi}\,\mathbf{C}^{(\psi)}\gamma_\mu\psi \\ & - \frac{g_s^2 C_{GG}}{16\pi^2}\frac{a}{f}G\tilde{G} - \frac{g^2 C_{WW}}{16\pi^2}\frac{a}{f}W\tilde{W} - \frac{g'^2 C_{BB}}{16\pi^2}\frac{a}{f}B\tilde{B}\,,\end{aligned} \tag{5.16}$$

[6]For the rest of this chapter, we will consider the fields strengths always restricted to their linear pieces unless stated otherwise.

where the sum over ψ is taken over chiral fermions of the SM and $\mathbf{C}^{(\psi)}$ is a hermitian matrix in generation space. Here, the C_{XX} coefficients are the anomaly coefficients of the PQ symmetry with the gauge group of gauge field X, when it is restricted to the SM fields only. Note that we work in the basis where the $d = 5$ axion-Higgs operator $\partial^\mu a H^\dagger i \overleftrightarrow{D}_\mu H$ has been shifted away via an axion field redefinition [261].

Since we are interested in axion couplings to gauge bosons, we could consider integrating out all SM fermions to end up with a bosonic EFT. However, in the SM, not even the top can safely be integrated out when considering the axion couplings to W/Z bosons. Hence, if the axion couples to SM fields, one cannot rely on an EFT analysis when inspecting the axion couplings to massive gauge bosons and one should compute loop contributions in the full theory (see e.g. [269]). On the other hand, an interesting EFT limit exists if we consider the possibility that axion couplings to W/Z bosons are generated by extra fermions that are chiral under $SU(2)_L \times U(1)_Y$. The mass of those fermions is forced by experimental results to be at least several hundreds of GeV. Consequently, they can safely be integrated out when discussing the axion couplings to W/Z bosons.

In order to form the full SM-axion EFT below the mass scale of the aforementioned new chiral fermions, one should add to the couplings in Eq. (5.16) the contributions of the heavy fermions which are integrated out. This brings additional terms, in particular couplings between the axion and the electroweak gauge fields which do not simply add up to the C_{XX}, as discussed in subsection 5.2.2. Henceforth, during the rest of this chapter we focus on the contribution of the heavy chiral fields. In particular, we devote Section 5.3 to chiral extensions of the SM and how to relate them with axion EFTs. Then, in subsection 5.4.2, we identify the contribution of heavy chiral fermions to axion couplings for a specific model, and we keep in mind when discussing phenomenology that the full amplitudes may include a loop contribution from the SM fermions in Eq. (5.16).

5.3 Chiral extensions of the SM

5.3.1 The case for heavy chiral fermions

Our current knowledge of the Universe indicates that the observable matter is composed mostly by fermions, with bosons playing a key role in their interactions. Therefore, and given the strongly suspected existence of unknown additional matter, it should not be surprising that the BSM sector contains more fermions. The minimalistic idea of an additional fourth generation of quarks and leptons has been considered for more than 30 years (see e.g. Ref. [270, 271]) but it was excluded by experimental results also long time ago [272]. This is basically due to the chiral nature of the fermions in a SM generation, which generates non-decoupling effects.

On the other hand, BSM models with vector-like fermions allow them to have a mass before EWSB and hence, their effects decouple. Experimental searches keep pushing up the lower bound on the masses of vector-like fermions, particularly for the coloured ones, and they represent one of the main constraints on some BSM models [273, 274]. However, this apparent success in the exploration of fermionic extensions of the SM can not be extrapolated straightforwardly to chiral fermions because of their different and less explored phenomenology.

As it was explored systematically in Ref. [265] and we will revisit here, the exclusion of a fourth generation of quarks and leptons does not mean that the existence of new chiral fermions should be excluded. In fact, given the non-observation of vector-like fermions, it is a possibility that deserves more of our attention. The challenge is, therefore, to establish which sets of new chiral fermions are still allowed and build minimal models that allow us to explore easily their phenomenology. Additionally, as we will show in subsection 5.4.2, they can serve as UV

completions that showcase interesting phenomenological signatures of axions.

When trying to build a BSM model with new heavy chiral fermions, there are two important consequences of their chirality that should be kept in mind at all times. First, they will contribute non-trivially to the gauge anomalies of the theory. Since the SM set of fermions is free of anomalies on its own, the new chiral fermions should also cancel the gauge anomalies among them. Before passing to the second consequence, let us discuss in more detail the constrains imposed by gauge anomaly cancellation on the irreducible representations that we can use for the chiral fermions, following Ref. [265].

Let us suppose a set of N fermions transforming under the SM gauge irreps (R_i^C, R_i^W, Y_i). These new fermions must form a real representation of $\mathrm{SU}(3)_C$ to avoid the appearance of massless coloured states. An automatic consequence of this constraint is the vanishing of the $\mathrm{SU}(3)_C^3$ gauge anomaly. The remaining anomaly polynomials to be cancelled are:

$$\mathrm{SU}(3)_C^2 \times \mathrm{U}(1)_Y \,:\, \textstyle\sum_{i=1}^N N_i^W\, C\left(R_i^C\right) Y_i, \tag{5.17}$$

$$\mathrm{SU}(2)_W^2 \times \mathrm{U}(1)_Y \,:\, \textstyle\sum_{i=1}^N N_i^C\, C\left(R_i^W\right) Y_i, \tag{5.18}$$

$$\mathrm{U}(1)_Y^3 \,:\, \textstyle\sum_{i=1}^N N_i^C\, N_i^W\, Y_i^3, \tag{5.19}$$

$$\mathrm{Grav.}^2 \times \mathrm{U}(1)_Y \,:\, \textstyle\sum_{i=1}^N N_i^C\, N_i^W\, Y_i, \tag{5.20}$$

where $N_i^W \equiv \dim(R_i^W)$, $N_i^C \equiv \dim(R_i^C)$ and the index $C(R)$ of a certain representation is defined as $C(R)\delta_{ab} = \mathrm{Tr}(T_R^a T_R^b)$, with the index of the fundamental normalised to $C(N) = 1/2$ for $\mathrm{SU}(N)$[7]. There is one additional anomaly, the global anomaly of the $\mathrm{SU}(2)_W$ known as Witten anomaly [276]. This anomaly disappears when $\sum_{i=1}^N N_i^C\, C\left(R_i^W\right)$ is an integer number[8].

The second important consequence of being chiral is that those fermions must acquire its mass through a Higgs mechanism (see Ref. [56] for a derivation of this classic result with new techniques that we will revisit in Chapter 6) and therefore they might impact on Higgs precision observables. The latter can be largely avoided if the added fermions are colourless, although they might be soon heavily constrained by other Higgs measurements, as we will see in subsection 5.4.3. Furthermore, the origin of the fermion mass must be considered when integrating it out. In fact, if one integrates out a heavy particle that acquires all its mass through EWSB, the model must be matched onto the HEFT instead of the SMEFT, as discussed in subsection 2.4.3 [277]. This leads naturally to the presence of a non-linearly realized EWSB and to its connection with non-anomalous axion couplings.

In the following, we will first build a minimal extension of the SM with chiral fermions in subsection 5.3.2. Then, we will extend its scalar sector in order to allow for an axion in subsection 5.4.1 and will discuss its matching to an axion EFT and the axion couplings to gauge bosons in subsection 5.4.2, making a clear connection with Section 5.2. A discussion about experimental constraints on this extension is left for Section 5.4.3.

5.3.2 A minimal model

We wish to identify a phenomenologically viable and minimal chiral extension of the SM. Although for our axion-related studies we will need a second Higgs doublet later, here we stick to a single Higgs doublet. We introduce a set of chiral fermions transforming irreducibly under

[7] For $\mathrm{SU}(2)_W$, we have $C(R_i^W) = N^W\left((N^W)^2 - 1\right)/12$. On the other hand, an irreducible representation of $\mathrm{SU}(3)_C$ is not uniquely defined by its dimension, but by its Dynkin labels (a_1, a_2), where $a_i > 0$. These labels are related to the dimension as by $N^C = (1 + a_1)(1 + a_2)(1 + a_1/2 + a_2/2)$ and the index is given by $C\left(R^C\right) = N^C\left(a_1^2 + 3a_1 + a_1 a_2 + 3a_2 + a_2^2\right)/24$ [232, 275].

[8] With the chosen normalisation, $C\left(R_i^W\right)$ is half-integer for $N^W = 2 + 4n$, with $n \in \mathbb{N}_0$, and an integer in any other case.

$SU(3)_c \times SU(2)_L \times U(1)_Y$ as (R_c, R_L, Y) and, following Ref. [265], we require the criteria:

1. No massless fermion after EW symmetry breaking, apart from SM gauge singlets;
2. No gauge and Witten [276] anomalies;
3. Compatibility with Higgs coupling modifications;
4. No allowed bare mass terms.

If a bare mass term were to be allowed by the SM gauge symmetry, the mass of the fermions would be naturally heavier than the EW scale, thus enforcing an automatic decoupling in all observables. This case is phenomenologically allowed, but it is not of our interest as we will discuss in subsection 5.4.2. So, we will focus on the case where the bare mass terms are either accidentally suppressed compared to the EW scale or forbidden by extra discrete gauge symmetries.

Condition 3 restricts the choice of colour representations to the trivial one, $R_c = 1$, so that SM Higgs production via gluon fusion is not affected by the new chiral sector. On the other hand, condition 1 restricts the allowed SU(2) representations, at least for renormalisable extensions. This is because, to become massive after EW symmetry breaking, the new chiral fermions need to couple to $H \sim \left(1, 2, \frac{1}{2}\right)$ via a Dirac-like Yukawa:

$$\bar{f}_L f_R H \quad \text{or} \quad \bar{f}_L f_R \tilde{H}\,, \tag{5.21}$$

with $\tilde{H} = i\sigma_2 H^*$. The quantum numbers of f_L and f_R can only be

$$f_L \sim (1, 2j_L + 1, Y)\,, \quad f_R \sim (1, 2j_R + 1, Y - \tfrac{1}{2}) \quad \text{or} \quad f_R \sim (1, 2j_R + 1, Y + \tfrac{1}{2})\,, \tag{5.22}$$

with j_L, j_R non-negative semi-integers and $|j_L - j_R| = 1/2$. Thus, the minimal possibility is $j_L = 1/2$ and $j_R = 0$.

Since the latter quantum numbers are reminiscent of the SM doublet and singlet leptons (for $Y = -\frac{1}{2}$), we denote them as[9]

$$L_1 \sim (1, 2, Y)\,, \quad \left(E_1 \sim (1, 1, Y - \tfrac{1}{2}) \quad \text{or} \quad N_1 \sim (1, 1, Y + \tfrac{1}{2})\right). \tag{5.23}$$

Witten anomaly [276] requires an even number of $SU(2)_L$ doublets (see details in subsection 5.3.1 and Ref. [265]), so we minimally introduce a second doublet in the LH sector:

$$L_2 \sim (1, 2, -Y)\,, \tag{5.24}$$

where the hypercharge is fixed by the cancellation of the $SU(2)_L^2 \times U(1)_Y$ anomaly. At this point we need to consider $U(1)_Y$-gravitational and $U(1)_Y^3$ anomalies. The latter are already cancelled in the LH sector since $L_1 + L_2$ forms a vector-like pair whose bare mass has to be forbidden or suppressed to fulfil criteria 4. On the other hand, we need an additional RH singlet with opposite-sign hypercharge, such that the RH sector becomes

$$\left\{\begin{array}{l} E_1 \sim (1, 1, +Y - \frac{1}{2}) \\ E_2 \sim (1, 1, -Y + \frac{1}{2}) \end{array}\right\} \quad \text{or} \quad \left\{\begin{array}{l} N_1 \sim (1, 1, +Y + \frac{1}{2}) \\ N_2 \sim (1, 1, -Y - \frac{1}{2}) \end{array}\right\} \tag{5.25}$$

If we choose only one of those pairs, e.g. $E_{1,2}$, we can write two Yukawa terms:

$$-\mathcal{L}_Y = y_{E_1} \bar{L}_1 E_1 H + y_{E_2} \bar{L}_2 E_2 \tilde{H} + \text{h.c.}\,. \tag{5.26}$$

After EWSB, only the $T_L^3 = -\frac{1}{2}\left(+\frac{1}{2}\right)$ component of the $L_1\,(L_2)$ doublet with electric charge $Q = -\frac{1}{2} + Y\left(+\frac{1}{2} - Y\right)$ picks up a mass, while the remaining component of each doublet is unpaired

[9] From here onwards, it is understood that doublets are LH and singlets are RH Lorentz spinors.

and stays massless. This can be seen also from counting degrees of freedom: while there are 4 LH Weyl fermions, there are only 2 RH Weyl fermions and since we forbid any Majorana mass, two of the LH fermions will be massless. We would have reached the same conclusion if we had picked the $N_{1,2}$ pair. For the particular case $Y = -\frac{1}{2}$, these massless fermions would be electrically neutral but they would still interact with the Z boson, which is enough to rule them out.

Thus, we need to include both pairs of RH fermions, $E_{1,2}$ and $N_{1,2}$, to avoid massless fermions after EWSB. In conclusion, the minimal setup that fulfils criteria 1-4 is

$$L_1 \sim (1,2,+Y)\,, \quad E_1 \sim (1,1,+Y-\tfrac{1}{2})\,, \quad N_1 \sim (1,1,+Y+\tfrac{1}{2})\,, \tag{5.27}$$

$$L_2 \sim (1,2,-Y)\,, \quad E_2 \sim (1,1,-Y+\tfrac{1}{2})\,, \quad N_2 \sim (1,1,-Y-\tfrac{1}{2})\,. \tag{5.28}$$

Their Yukawa interactions are

$$-\mathcal{L}_Y = y_{E_1}\bar{L}_1 E_1 H + y_{E_2}\bar{L}_2 E_2 \tilde{H} + y_{N_1}\bar{L}_1 N_1 \tilde{H} + y_{N_2}\bar{L}_2 N_2 H + \text{h.c.}\,, \tag{5.29}$$

and all chiral fermions pick up a mass after EW symmetry breaking. One could think that the particular case of $Y = 0$ leads to a more minimal setup, but this turns out to be false because one fermion would remain massless[10], in contradiction with criterion 1.

In the minimal setup of Eq. (5.27)-(5.28), gauge anomaly cancellation is immediate since its field content is vector-like with respect to the SM gauge group. Nonetheless, we still consider it a chiral field content because we do not include bare mass terms and only use EWSB to generate their masses. This leads to a spectrum where the massive states couple asymmetrically when projected onto their LH or RH components, which is what we consider as "chiral", as discussed in Section 5.2. We remain agnostic about the reason that suppresses the bare masses with respect to the Yukawa couplings with the Higgs boson. However, notice that bare mass terms can be forbidden by using discrete gauge symmetries, for instance a $\mathbb{Z}_2$ symmetry under which L_1, E_1, N_1 and all SM leptons are odd, and the other fields even, is anomaly-free and sufficient to forbid bare mass terms, while allowing for all the Yukawa couplings.

5.4 Minimal chiral axion model

5.4.1 An axion for the minimal viable chiral extension of the SM

The minimal model presented in the subsection 5.3.2 is not capable of hosting an axion field as the NGB of a spontaneously broken $\mathrm{U}(1)_{PQ}$ symmetry. In order to incorporate the axion into it, we need to extend its scalar sector. Here, we provide a renormalisable UV completion of the SM-axion Lagrangian which is inspired by the standard DFSZ [278, 279] axion. However, we do not require the axion to solve the strong CP problem; we improperly keep the PQ label, even though the axion does not necessarily has a QCD anomaly, and we do not forbid additional sources of $\mathrm{U}(1)_{PQ}$ breaking giving an axion mass that is unrelated to the axion decay constant. Nevertheless, we do not discuss any explicit source of PQ breaking in what follows and we derive all our results from a PQ-preserving Lagrangian. Even more, the axion mass is irrelevant for our one-loop computations with fermion lines.

The main modification of this minimal axion-chiral extension of the SM with respect to the minimal model presented in subsection 5.3.2 is in its scalar sector, which now contains a complex

[10] In fact, the anomaly-free field content $L_1 \sim (1,2,0)$, $E_1 \sim (1,1,-\frac{1}{2})$, $N_1 \sim (1,1,+\frac{1}{2})$, $L_2 \sim (1,2,0)$, whose Yukawa sector is $-\mathcal{L}_Y = y^{\alpha}_{E_1}\bar{L}_\alpha E_1 H + y^{\alpha}_{N_1}\bar{L}_\alpha N_1 \tilde{H} + \text{h.c.}$, with $\alpha = 1,2$ a flavour index. Without loss of generality, one can do a $U(2)$ flavour rotation such that $y_{E_1} \propto (0,1)$. Hence, the $Q = T^3_L = 1/2$ component of L_1 remains massless.

SM singlet Φ and two Higgs doublets $H_{1,2} \sim \left(1, 2, \frac{1}{2}\right)$. The scalar potential is

$$V(H_1, H_2, \Phi) = V_{\text{r.i.}}(|H_1|, |H_2|, |\Phi|, |H_1^\dagger H_2|) + \lambda H_1^\dagger H_2 \Phi^2 + \text{h.c.}\,, \tag{5.30}$$

which contains all the re-phasing invariant terms allowed by gauge invariance plus a non-hermitian operator. The latter breaks the three re-phasing symmetries $\mathrm{U}(1)_\Phi \times \mathrm{U}(1)_{H_1} \times \mathrm{U}(1)_{H_2}$ into two linearly independent U(1)'s that we identify with $\mathrm{U}(1)_Y \times \mathrm{U}(1)_{PQ}$. The PQ charges of H_1 and H_2, X_1 and X_2 respectively, are constrained to fulfil

$$X_1 - X_2 = 2\,, \tag{5.31}$$

where we have normalized the PQ charge of Φ as $X_\Phi = 1$.

If only one of the Higgs doublets interacts with the 2 families of new chiral leptons, there would be no dimension-5 axion-gauge boson couplings in the EFT below the mass of the exotic leptons (see proof in Appendix 5.B). Hence, the Yukawa Lagrangian in Eq. 5.29 must be modified to include explicitly both doublets. The possible modification we use is[11]

$$-\mathcal{L}_Y = y_{E_1} \bar{L}_1 E_1 H_1 + y_{E_2} \bar{L}_2 E_2 \tilde{H}_2 + y_{N_1} \bar{L}_1 N_1 \tilde{H}_2 + y_{N_2} \bar{L}_2 N_2 H_1 + \text{h.c.}\,, \tag{5.32}$$

which implies the following constraints on the $\mathrm{U}(1)_{PQ}$ charges:

$$\begin{aligned} -X_{L_1} + X_{E_1} + X_1 &= 0\,, \qquad -X_{L_1} + X_{N_1} - X_2 = 0\,, \\ -X_{L_2} + X_{E_2} - X_2 &= 0\,, \qquad -X_{L_2} + X_{N_2} + X_1 = 0\,. \end{aligned} \tag{5.33}$$

We recall that, although gauge symmetry allows the bare mass terms $L_1 L_2$, $E_1 E_2$ and $N_1 N_2$, they can be forbidden, e.g. via a discrete gauge symmetry, in order to avoid decoupling effects. We could also have chosen different assignments of $H_{1,2}$ in Eq. (5.32), which amounts to different choices of PQ symmetry, and induce different axion and/or Higgs boson phenomenology. Henceforth, we stick to this choice and briefly discuss other cases in Appendix 5.B. We do not specify the Higgs fields assignment in the SM Yukawa couplings, we simply assume that it only involves $H_{1,2}$, and that it does not generate tree-level flavour-changing neutral currents. One possibility is to couple them as in the original DFSZ model [278, 279], in which case Eq. (5.16) is simply the usual DFSZ axion-SM EFT. However, we focus here on the contributions from the extra heavy fermions.

The next step is to identify the axion field in terms of the phases of the different scalars:

$$H_1 \supset \frac{v_1}{\sqrt{2}} e^{i\frac{a_1}{v_1}} \begin{pmatrix} 0 \\ 1 \end{pmatrix}, \quad H_2 \supset \frac{v_2}{\sqrt{2}} e^{i\frac{a_2}{v_2}} \begin{pmatrix} 0 \\ 1 \end{pmatrix}, \quad \Phi \supset \frac{v_\Phi}{\sqrt{2}} e^{i\frac{a_\Phi}{V_\Phi}}\,, \tag{5.34}$$

where we have neglected EM-charged and radial modes that have no projection on the axion field a. In order to identify the latter in terms of $a_{1,2,\Phi}$, let us write down the classically conserved PQ current, restricted to the scalar sector

$$\begin{aligned} J_\mu^{\text{PQ}} &= -\Phi^\dagger i \overleftrightarrow{\partial_\mu} \Phi - X_1 H_1^\dagger i \overleftrightarrow{\partial_\mu} H_1 - X_2 H_2^\dagger i \overleftrightarrow{\partial_\mu} H_2 + \dots \\ &= V_\Phi \partial_\mu a_\Phi + X_1 v_1 \partial_\mu a_1 + X_2 v_2 \partial_\mu a_2 + \dots\,, \end{aligned} \tag{5.35}$$

where we only included the terms relevant for the identification of the axion. Following the

[11] Given the charges of the heavy leptons, this is analogous to a type-2 2HDM [280].

Goldstone theorem $\langle 0|J_\mu^{PQ}|a\rangle \sim ifp_\mu$, the axion field must be defined as

$$a = \frac{1}{f}\left(V_\Phi a_\Phi + X_1 v_1 a_1 + X_2 v_2 a_2\right), \quad f^2 = V_\Phi^2 + X_1^2 v_1^2 + X_2^2 v_2^2, \tag{5.36}$$

so that $J_\mu^{\rm PQ} \supset f\partial_\mu a$. Under a PQ transformation, we have that $a_{1,2} \to a_{1,2} + \kappa X_{1,2} v_{1,2}$ and $a_\Phi \to a_\Phi + \kappa v_\Phi$. Hence, the axion field transforms as $a \to a + \kappa f$.

We require the axion field to be neutral under the hypercharge gauge group to avoid kinetic mixing with the Z boson [252], which translates into the condition $X_1 Y_1 v_1^2 + X_2 Y_2 v_2^2 = 0$, where $Y_{1,2} = \frac{1}{2}$ is the hypercharge of the Higgs doublets. From this condition and Eq. (5.31), we can fix all the PQ charges in the scalar sector in terms of v_1/v_2 as follows:

$$X_\Phi = 1, \qquad X_1 = 2\sin^2\beta, \qquad X_2 = -2\cos^2\beta, \tag{5.37}$$

where we use the customary definitions $v_1/v = \cos\beta$, and $v_2/v = \sin\beta$, with $v = \sqrt{v_1^2 + v_2^2} \simeq 246$ GeV [280]. Substituting these expressions into Eq. (5.36) we obtain

$$f^2 = V_\Phi^2 + v^2(\sin 2\beta)^2. \tag{5.38}$$

In the limit $V_\Phi \gg v$, we can approximate $f \simeq V_\Phi$.

Once the axion field has been identified, we can proceed to compute its couplings to the new chiral leptons. They can be derived by inverting the first relation in Eq. (5.36) to express $a_{1,2}$ in terms of a. This leads to replace $a_{1(2)}/v_{1(2)} \to X_{1(2)}\, a/f$ in Eq. (5.34) and inserting it into Eq. (5.32) yields

$$\begin{aligned} -\mathcal{L}_Y \supset\ & m_{E_1}\left(e^{iX_1\frac{a}{f}}\right)\bar{E}_{L_1}E_1 + m_{E_2}\left(e^{-iX_2\frac{a}{f}}\right)\bar{E}_{L_2}E_2 \\ & + m_{N_1}\left(e^{-iX_2\frac{a}{f}}\right)\bar{N}_{L_1}N_1 + m_{N_2}\left(e^{iX_1\frac{a}{f}}\right)\bar{N}_{L_2}N_2 + \text{h.c.}, \end{aligned} \tag{5.39}$$

where we have decomposed the doublets as $L_i = (N_{L_i}, E_{L_i})^T$, and defined the Dirac masses $m_{E_i} = y_{E_i}\frac{v_1}{\sqrt{2}}$ and $m_{N_i} = y_{N_i}\frac{v_2}{\sqrt{2}}$, where $i = 1, 2$. We could remove the axion field from the mass terms by redefining the fermion fields via a field-dependent chiral transformation. The non-invariance of the fermion kinetic terms plus possible anomalous transformations lead in turn to an axion effective Lagrangian similar to the one in Eq. (5.16). Nevertheless, it is easier to obtain the axion-gauge bosons couplings in the basis of Eq. (5.39). The EFT terms that arise due to anomalous transformations can be found in Appendix 5.B.

5.4.2 Axion EFT of the minimal chiral axion model

Now, we derive the axion EFT below the mass of the new chiral fermions in the model presented in subsection 5.4.1. First, we define the massive eigenstates $N_i = N_i + N_{L_i}$, $E_i = E_i + E_{L_i}$ and extract their gauge couplings from

$$\begin{aligned} \mathcal{L} \supset\ & \overline{L_i}\gamma^\mu\left(g\frac{\sigma^a}{2}W_\mu^a + g'(-1)^{i+1}YB_\mu\right)L_i + g'\overline{N_i}\gamma^\mu(-1)^{i+1}\left(Y+\frac{1}{2}\right)B_\mu N_i \\ & + g'\overline{E_i}\gamma^\mu(-1)^{i+1}\left(Y-\frac{1}{2}\right)B_\mu E_i\,. \end{aligned} \tag{5.40}$$

For simplicity, we assume equal masses within a SU(2) doublet, i.e. $m_{N_i} = m_{E_i}$. Using the formulae in Appendix 5.A and Chapter 4, the axion couplings in the EFT read

$$\mathcal{L} \supset -g'^2 \frac{(1+12Y^2)(X_1-X_2)}{96\pi^2}\frac{a}{f}B\tilde{B} - g^2\frac{X_1-X_2}{96\pi^2}\frac{a}{f}W^a\tilde{W}^a - gg'\frac{X_1-X_2}{96\pi^2}\frac{a}{f}B\tilde{W}^3 \ , \tag{5.41}$$

where we used the same letter to refer to the gauge fields and to their field strengths . Although we normalized $X_1 - X_2 = 2$ previously, we kept it in Eq. (5.41) to make the charge dependence explicit.

It is important to notice that the last term in Eq. (5.41) can not be reproduced by an UV PQ anomaly because there is no non-vanishing $\mathrm{U}(1)_{PQ}\times\mathrm{U}(1)_Y\times\mathrm{SU}(2)_L$ anomaly coefficient. More precisely, it does not match the usual ansatz in Eq. (5.4), but it can be obtained from a combination of the EFT terms in Eq. (5.5)[12]. Therefore, the model considered here is an example of a statement we made previously: the terms in Eq. (5.5) appear at dimension 5 in the Lagrangian when chiral fermions are integrated out, and are not suppressed by the mass of the heavy fermions. If we had allowed for bare mass term for the fermions, these non-decoupling effect would have been absent, justifying the criterion 4 in subsection 5.3.2.

It is useful to express Eq. (5.41) in terms of mass eigenstates. Focusing on the neutral gauge bosons, we obtain

$$\begin{aligned}-\frac{16\pi^2}{e^2}\mathcal{L} \supset\ & (X_1-X_2)\left(2Y^2+\frac{1}{2}\right)\frac{a}{f}F\tilde{F} + (X_1-X_2)\left(-t_W\left(4Y^2+\frac{1}{2}\right)+\frac{t_W^{-1}}{2}\right)\frac{a}{f}F\tilde{Z} \\ & + (X_1-X_2)\left(t_W^2\left(2Y^2+\frac{1}{6}\right)-\frac{1}{6}+\frac{t_W^{-2}}{6}\right)\frac{a}{f}Z\tilde{Z} \ ,\end{aligned} \tag{5.42}$$

The fact that these couplings do not derive solely from UV anomalies becomes evident when one finds out that the sum rules in Eq. (5.10) are violated as follows:

$$C_{\gamma\gamma} + s_W^{-2}(1-t_W^2)C_{Z\gamma} - \frac{1}{s_W^2c_W^2}C_{ZZ} = \frac{X_1-X_2}{12c_W^2s_W^2} \ , \tag{5.43}$$

$$C_{\gamma\gamma} + s_W^{-2}C_{Z\gamma} - (1+t_W^{-2})C_{WW} = \frac{X_2-X_1}{12s_W^2} \ . \tag{5.44}$$

This means that one cannot define any PQ symmetry whose UV anomalies reproduce Eq. (5.42) (see Appendix 5.B for more details). This breakdown of the sum rules, that can be directly tested given an observation of the axion-gauge boson couplings, is a smoking gun of the presence of a chiral heavy sector charged under the PQ symmetry.

Although some additional assumptions are needed, it is useful to reformulate the sum rules in Eq. (5.10) in terms of observables, for instance partial axion decay rates. If $m_a > 2m_Z$, all the decays of an axion to gauge bosons are allowed and therefore we can consider all the following decay rates (see [281]):

$$\Gamma(a\to\gamma\gamma) = C_{\gamma\gamma}^2\frac{\alpha^2m_a^3}{64\pi^3f^2} \ , \quad \Gamma(a\to WW) = C_{WW}^2\frac{\alpha^2m_a^3}{32\pi^3s_W^4f^2} \ , \tag{5.45}$$

$$\Gamma(a\to ZZ) = C_{ZZ}^2\frac{\alpha^2m_a^3}{64\pi^3s_W^4c_W^4f^2} \ , \quad \Gamma(a\to Z\gamma) = C_{Z\gamma}^2\frac{\alpha^2m_a^3}{32\pi^3s_W^2c_W^2f^2} \ , \tag{5.46}$$

[12]It can be checked that one finds $c_3 = 0$ when matching Eq. (5.41) onto Eq. (5.4) and (5.5). This is due to the fact that c_3 violates custodial symmetry, while we used the simplifying custodial limit $m_{N_i} = m_{E_i}$ in our computation, which is also motivated by electroweak precision tests, as discussed later.

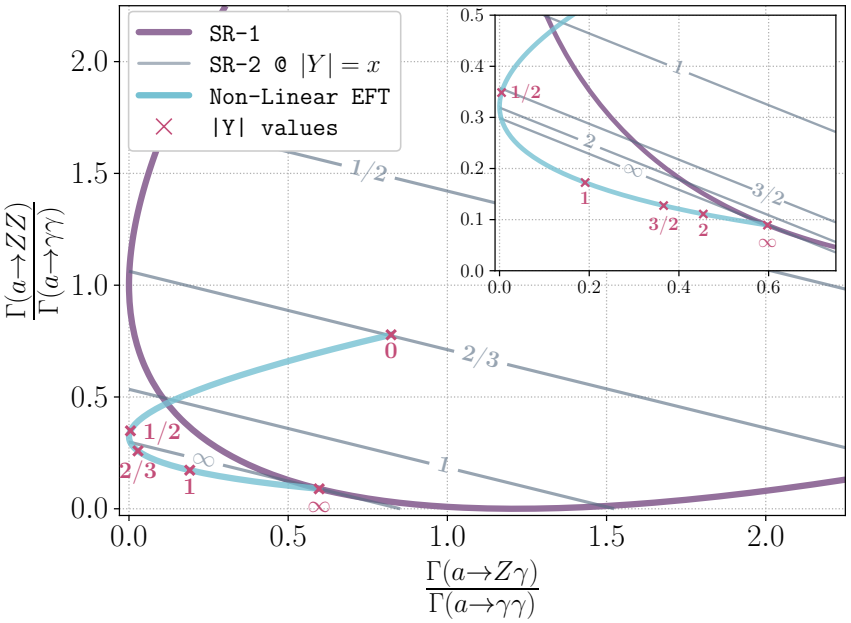

Figure 5.4.1: Plot of the ratio of decay rates $\frac{\Gamma(a\to ZZ)}{\Gamma(a\to\gamma\gamma)}$ as a function of the ratio of decay rates $\frac{\Gamma(a\to Z\gamma)}{\Gamma(a\to\gamma\gamma)}$, assuming that the decays are kinematically allowed. The anomaly-based sum rule SR-1, given in Eq. (5.47), corresponds to the purple curve. The sum rule SR-2, given in Eq. (5.48), can only be traced on a plane if a ratio of partial rates is fixed. We therefore fix $\frac{\Gamma(a\to WW)}{\Gamma(a\to\gamma\gamma)}$ to its value derived from Eq. (5.42) as a function of Y. Each grey line then corresponds to the linear relation in Eq. (5.48) when we scan values of Y. Finally, the blue curve uses the explicit couplings in Eq. (5.42).

where we neglect the SM contributions and the coefficients C_{XY} are defined in Eq. (5.8). Using the first identity in Eq. (5.10), one sees that the following holds:

$$\text{SR-1:}\quad \left[\frac{\Gamma(a\to ZZ)}{\Gamma(a\to\gamma\gamma)} - 1 - \frac{\left(t_W^2-1\right)^2}{2t_W^2}\frac{\Gamma(a\to Z\gamma)}{\Gamma(a\to\gamma\gamma)}\right]^2 - \frac{2\left(t_W^2-1\right)^2}{t_W^2}\frac{\Gamma(a\to Z\gamma)}{\Gamma(a\to\gamma\gamma)} = 0\,, \tag{5.47}$$

which is a relation between two quantities that can be traced on a plane. Another sum rule that follows from both identities in Eq. (5.10) is

$$\text{SR-2:}\quad \Gamma(a\to\gamma\gamma) + \frac{1}{2}\left(t_W^{-2}-1\right)\Gamma(a\to WW) - t_W^{-2}\Gamma(a\to ZZ) + \frac{1}{2}\left(1-t_W^{-2}\right)\Gamma(a\to Z\gamma) = 0\,. \tag{5.48}$$

These sum rules can be tested with low-energy measurement. If at least one of them is violated, we can conclude that the fermionic UV completion is chiral, whereas a vector-like one (e.g. a KSVZ-like model) always satisfies them. The violation of the sum rules in our specific model is displayed in Fig. 5.4.1, where one can see that the model only satisfies both sum rules when $|Y|\to\infty$.

We should stress the caveat that SM loop contributions also violate the naive sum rules, so they should be taken into account. In particular, the axion-fermion couplings in Eq. (5.16), which are responsible for the SM loop corrections to the sum rule, should be reconstructed from low-energy data in order to extract the bosonic EFT terms on which the sum rule can be tested.

The phenomenological analysis of how to test experimentally these sum rules would follow similar lines to what is found in Ref. [269, 282], although considering more decay channels. The computation of the SM loop contributions is non-trivial and hence we leave this analysis for future work.

5.4.3 Experimental constraints

In this section, we will explore several experimental constraints on the heavy chiral fermions contained in the minimal model introduced in subsection 5.3.2. Most of the constraints discussed here apply for that minimal model or its version with an extended scalar sector presented in subsection 5.4.1. We will discuss specifically how the bounds differ for each one of them when required.

Electroweak precision tests

The contribution of the new exotic fermions in Eqs. (5.27)-(5.28) to the oblique S and T parameters is [265]

$$S = \frac{1}{6\pi}\left[\left(1 - 2Y\log\frac{m_{N_1}^2}{m_{E_1}^2}\right) + \left(1 + 2Y\log\frac{m_{N_2}^2}{m_{E_2}^2}\right) + \mathcal{O}\left(\frac{m_Z^2}{m_{N,E}^2}\right)\right] \approx \frac{1}{3\pi}\,, \tag{5.49}$$

$$\begin{aligned} T = {} & \frac{1}{16\pi c_W^2 s_W^2 m_Z^2}\left(m_{N_1}^2 + m_{E_1}^2 - 2\frac{m_{N_1}^2 m_{E_1}^2}{m_{N_1}^2 - m_{E_1}^2}\log\frac{m_{N_1}^2}{m_{E_1}^2}\right) \\ & + \frac{1}{16\pi c_W^2 s_W^2 m_Z^2}\left(m_{N_2}^2 + m_{E_2}^2 - 2\frac{m_{N_2}^2 m_{E_2}^2}{m_{N_2}^2 - m_{E_2}^2}\log\frac{m_{N_2}^2}{m_{E_2}^2}\right) \approx 0\,, \end{aligned} \tag{5.50}$$

where the approximation in the last steps holds in the custodial limits $m_{N_1} = m_{E_1}$ and $m_{N_2} = m_{E_2}$. Recent fits for oblique parameters, e.g. from Gfitter [283], yield

$$S = 0.05 \pm 0.11\,, \qquad T = 0.09 \pm 0.13\,, \tag{5.51}$$

which are easily satisfied in the custodial limit.

Higgs couplings

The new heavy fermions can modify significantly loop-induced Higgs decay rates, in particular for $h \to \gamma\gamma$ and $h \to Z\gamma$. In this subsection, we analyse the constraints derived from such processes. To fix our conventions, consider a fermion ψ of mass m_ψ with couplings given by the following Lagrangian:

$$\mathcal{L}_\psi = \overline{\psi}(i\partial\!\!\!/ - m_\psi)\psi - \frac{x_\psi m_\psi}{v}h\overline{\psi}\psi + eQ_\psi\overline{\psi}\gamma^\mu\psi A_\mu + \frac{e}{c_W s_W}\overline{\psi}\gamma^\mu\left(\frac{T_\psi^3}{2} - Q_\psi s_W^2 - \frac{T_\psi^3}{2}\gamma_5\right)\psi Z_\mu\,, \tag{5.52}$$

where h is the 125 GeV Higgs, A_μ and Z_μ the photon and Z boson fields, T_ψ^3 is the eigenvalue of the third generator of $SU(2)_L$ when it acts on the left-handed component of ψ ($\psi_L = \frac{1-\gamma^5}{2}\psi$), so that $T_\psi^3 = \pm\frac{1}{2}$ when ψ_L arises from a doublet in the fundamental of $SU(2)_L$, and x_ψ is a number. Its one-loop contributions to the amplitudes $h \to \gamma\gamma$ and $h \to \gamma Z$ are [284]

$$\mathcal{A}_{\gamma\gamma}^\psi \approx \frac{4}{3}x_\psi Q_\psi^2\,, \quad \mathcal{A}_{Z\gamma}^\psi \approx -\frac{1}{3}x_\psi Q_\psi\frac{T_\psi^3 - 2Q_\psi s_W^2}{c_W}\,, \tag{5.53}$$

where we assumed $m_\psi \gg m_h \gtrsim m_Z$, which holds for the heavy fermions we consider here. In the SM, these amplitudes are dominated by the loop of the W gauge boson interfering negatively with the loop of the top quark and they amount to $A_{\gamma\gamma}^{\rm SM} \approx -6.5$ and $\mathcal{A}_{\gamma Z}^{\rm SM} \approx 5.7$ at LO. The dominant QCD NLO effects give a correction of order 5% [284].

These formulae can be applied to the model in Eq. (5.32). However, the parameter x_ψ in (5.52) depends on the entries of the two Higgs doublets potential. Indeed, the generic vacuum of a 2HDM is parametrized by two angles α, β. The former is the angle of the rotation that diagonalizes the mass-squared matrix of the scalars and the latter is defined as

$$\beta = \tan\left(\frac{v_2}{v_1}\right), \tag{5.54}$$

where v_i is the VEV of H_i [280]. For a $SU(2)_L$ doublet $Q_L = (u_L, d_L)$ and a singlet d_R, the Yukawa couplings to the light Higgs, which we choose to be the known 125 GeV particle for definiteness, read,

$$\overline{Q_L} d_R H_1 + h.c. \supset m_d \left(1 - \frac{\sin\alpha}{\cos\beta}\frac{h}{v}\right)\bar{d}d \ , \quad \overline{Q_L} d_R H_2 + h.c. \supset m_d \left(1 + \frac{\cos\alpha}{\sin\beta}\frac{h}{v}\right)\bar{d}d \ , \tag{5.55}$$

and the couplings of u_L to a singlet u_R are similarly obtained. Couplings of the light Higgs to the vector bosons are given by their SM values times $\sin(\beta-\alpha)$.

One possible way to obtain a SM-like light Higgs is going to the alignment limit $\beta - \alpha = \pi/2$, in which case the Higgs couplings to vector bosons and to fermions are SM-like, since $-\sin\alpha/\cos\beta = \cos\alpha/\sin\beta = 1$. Hence, the Higgs signals are modified as if there was only one Higgs doublet, namely as if the model was given by the Yukawa couplings in Eq. (5.29). One must then use $x_\psi = 1$ in Eq. (5.52) for all the heavy fermions, and this yields $\mathcal{A}_{\gamma\gamma}^{\rm new} \approx \frac{4}{3}(1+4Y^2)$. Writing the modified Higgs width to photons as

$$R_{\gamma\gamma} = \frac{\left|\mathcal{A}_{\gamma\gamma}^{\rm SM} + \mathcal{A}_{\gamma\gamma}^{\rm new}\right|^2}{\left|\mathcal{A}_{\gamma\gamma}^{\rm SM}\right|^2} \, , \tag{5.56}$$

a recent ATLAS analysis finds $R_{\gamma\gamma} = 1.00 \pm 0.12$ [285]. The only available possibility is that the new contribution interferes negatively with the SM amplitude, namely $\mathcal{A}_{\gamma\gamma}^{\rm new} \approx -2\mathcal{A}_{\gamma\gamma}^{\rm SM} \approx 13.0$. In such a case the allowed 2σ range is $1.43 \lesssim |Y| \lesssim 1.53$, as can be seen in Fig. 5.4.2.

A correlated signal in the γZ channel is $\mathcal{A}_{\gamma Z}^{\rm new} \approx -\frac{2}{3} c_W [1 - (1+8Y^2) t_W^2]$, leading to a large deviation in the region compatible with the diphoton channel bound, i.e. where $|Y| \approx 1.5$, as seen in Fig. 5.4.2. The γZ decay channel of the Higgs has not been observed yet and HL-LHC is expected to measure $\kappa_{\gamma Z}$ within a 10% precision [286]. Future lepton colliders would not offer any improvement on that bound and only FCC-hh could reach a precision below 1% [185].

The alignment limit of the model in Eq. (5.32) predicts, therefore, a strong departure of $R_{Z\gamma}$ from its SM-value. However, this conclusion can be evaded in other limits of the 2HDM. In particular, the modifications to the Higgs signals can be strongly suppressed in the so-called wrong-sign limit [287–289]. This seizes on the fact that only the sign of the top Yukawa has been measured. Thus, defining the labelling such that the top quark couples to $\tilde{H}_2$, we must enforce $\cos\alpha = \sin\beta \implies \alpha = \pm\left(\frac{\pi}{2} - \beta\right)$. The minus sign gives the alignment limit, but there is another viable option: the plus sign gives the wrong-sign limit, $\alpha + \beta = \frac{\pi}{2}$, so called because in this limit, the bottom-Higgs coupling is $-m_b/v$, i.e. -1 times its SM value. The gauge bosons couplings of the Higgs are not SM-like either, and are suppressed by

$$\sin(\beta-\alpha) = \sin\left(2\beta - \frac{\pi}{2}\right) = -\cos(2\beta) = -\frac{\cos^2\beta - \sin^2\beta}{\cos^2\beta + \sin^2\beta} = \frac{\tan^2\beta - 1}{\tan^2\beta + 1}, \tag{5.57}$$

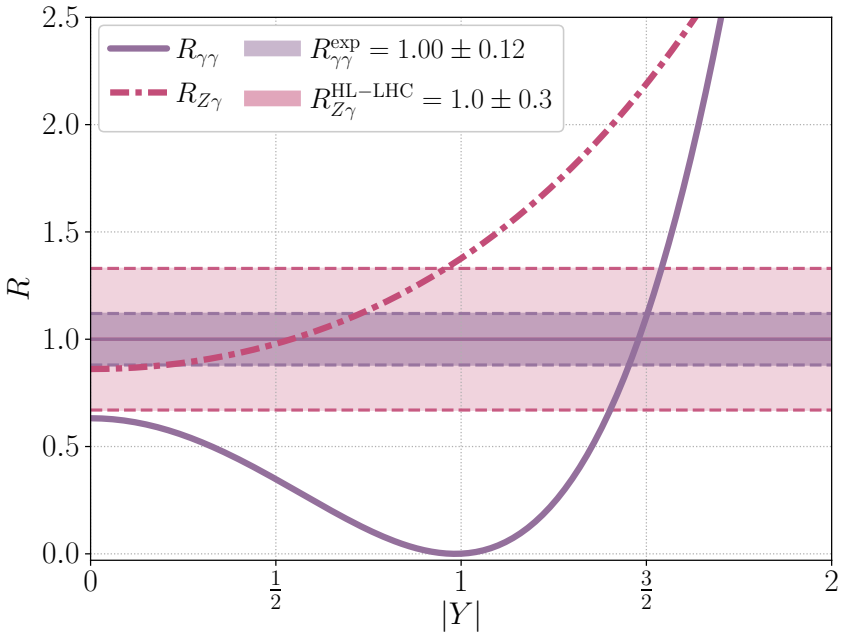

Figure 5.4.2: $R_{\gamma\gamma}$ and $R_{Z\gamma}$ as a function of $|Y|$ for the model in (5.32) in the alignment limit. The horizontal solid and dashed purple lines show the experimental value of $R_{\gamma\gamma}$ and the 1σ boundaries, respectively. The pink ones correspond to projections of $R_{Z\gamma}$ at HL-LHC.

which tends to 1 monotonically from below as $\beta \to \infty$. Current measurements of the Higgs couplings then impose $\tan\beta \gtrsim 4$ at 68% C.L. [290], while the limit is expected to reach $\tan\beta \gtrsim 12$ at HL-LHC [286]. In this limit, heavy fermions coupled to H_1 have $x_\psi = -1$ in Eq. (5.52), whereas those coupled to H_2 have $x_\psi = 1$, making possible cancellations in Eq. (5.53). In the case of our model in Eq. (5.32), the partial amplitudes in Eq. (5.53) simply vanish, and the modifications to the Higgs signals are those of a 2HDM in the wrong-sign limit without extra chiral matter.

Stable charged particles and direct searches

Except for $|Y| = 3/2$, the exotic leptons do not mix with the SM ones and the lightest state of the spectrum is electrically charged ($Q = Y \pm 1/2$) and stable because of an accidental exotic lepton number (due to Y). Charged relics are cosmologically dangerous and largely excluded (see e.g. Ref. [291–294]). These cosmological constraints can be avoided by invoking low-scale inflation with $\max\{H_I, T_{\rm RH}\} \lesssim$ TeV, which leads to either these particles being diluted by inflation or never being thermally produced.

On the other hand, the exotic leptons in our model can be produced at hadron colliders through the Drell-Yann process. Since they are generally charged and stable particles, they would yield striking signatures at colliders, e.g. in the forms of charged tracks, anomalous energy loss in calorimeters and/or longer time of flights. We show in Figure 5.4.3 the production cross sections and experimental limits [297] on the cross section at LHC for exotic leptons with $|Q| = 1, 2$, which corresponds to $Y = 3/2$. Although that precise hypercharge value allows the mixing between SM and exotic leptons, we neglect it to simplify the analysis. Notice that the mixing can be avoided by imposing the conservation of an exotic lepton number.

For the case of fully degenerate exotic leptons, one must consider the production of 2 indistinguishable leptons with the same $|Q|$ and, therefore the bound on their mass is $M \gtrsim 840$

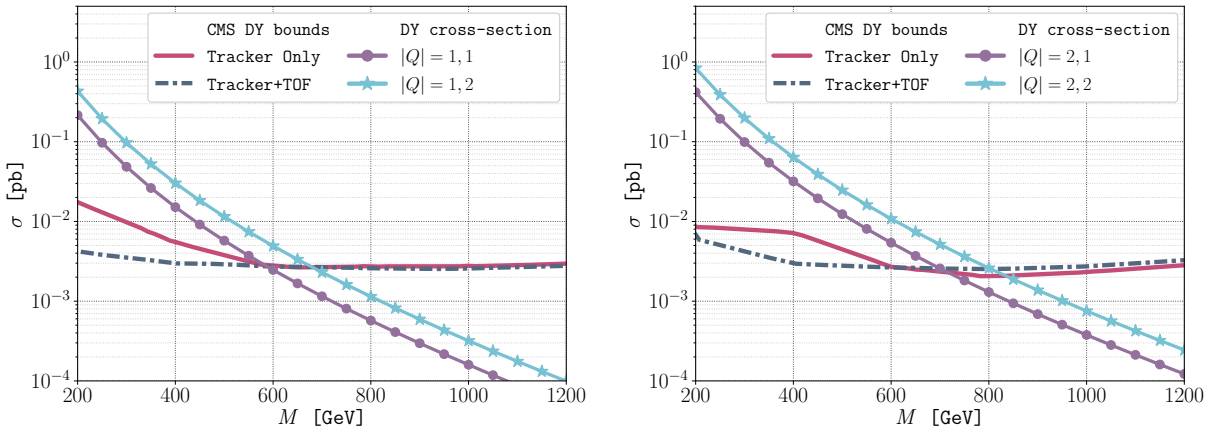

Figure 5.4.3: Drell-Yann cross-section and experimental bounds for the exotic leptons at LHC (13 TeV) as a function of their mass M for $|Q| = 1$ (left panel) and $|Q| = 2$ (right panel). The purple lines with circle shaped markers are the cross section for 1 exotic lepton with mass M and the cyan lines with star-shaped markers are for 2 degenerate exotic leptons with the same $|Q|$. The cross-sections were computed at LO (see e.g. [292, 295]) with MSTW2008 PDFs [296]. The curves without markers show the experimental results obtained by CMS [297] using only the tracker (continuous dark red line) and the tracker+TOF technique (dot dashed dark blue line).

GeV, which comes from the states with $|Q| = 2$ as can be seen from the right panel of Fig. 5.4.3. If one of the exotic families is heavier than the other but each doublet is still degenerate, the bound relaxes to $M \gtrsim 720$ GeV. The situation of different masses in the doublet, unfavoured by EW precision data as explained before, would relax the bound for the $|Q| = 1$ lepton in 80 GeV. Although the experimental results allow to further relax the bound for $|Q| = 1$ in ~ 40 GeV, this would make the decay of the $|Q| = 2$ lepton possible via a W boson. We leave the phenomenological analysis of such case, together with the case of mixing among exotic lepton families, for future work.

If one lifts the prohibition of mixing between SM and exotic leptons, the phenomenology of the $Y = 3/2$ case changes substantially. $Q = 2$ can decay into a W boson and a $Q = 1$ exotic fermion, which in turn can mix with the SM leptons and decay into $Z\ell$ or $h\ell$. The lower bounds for these scenarios at LHC are $M \gtrsim 500$ GeV [298] and a more detailed analysis is also left for future work. Finally, for $Y \neq 3/2$ but $Q \lesssim 2$, one can assume an approximate bound of $M \gtrsim 700$ GeV [297]. These mass values correspond to an electroweak-generated mass with Yukawas that nearly saturate the perturbative unitarity limit.

5.5 Conclusions

In this chapter, we aimed at uncovering an interesting connection between several topics. We started from pointing out that the widely-known relation between axion couplings to gauge bosons and PQ global anomalies is not always respected. The clarification that the aforementioned relation is violated when chiral fermions have been integrated out led our interest towards those extensions of the SM which would provide a realistic example of that phenomenon, i.e. extensions with chiral fermions. The chiral nature of those fermions leads to match onto HEFT, which has a non-linearly realised EWSB, when they are integrated out.

Let us frame our findings in the context of the Vafa-Witten theorem [299], which states

that in vector-like CP-conserving theories, there can not be a spontaneous breaking of the CP symmetry. Notably, this theorem fixes the QCD axion VEV to a value such that the pure QCD vacuum always respects CP, guaranteeing the PQ-mechanism. On the other hand, this theorem does not apply in chiral theories, like the SM, where additional irreducible contributions to the QCD axion VEV are expected [252]. Then, our results indicate that the decorrelation between axion couplings in the EFT and anomalies can be seen as a warning of the invalidity of the Vafa-Witten theorem, since indicates the presence of chiral fermions in the UV.

We also found a phenomenological way to test the relation between anomalies and axion couplings in the form of sum-rules. We showed explicitly how, under certain assumptions, they can be written as simple relations among partial axion decay rates. In sight of the connections mentioned before, the violation of these sum rules can also be seen as an indication of the presence of heavy chiral fermions. The obtention of experimental prospects for testing these sum rules is a very interesting line of work that we wish to explore in the near future. This could enhance the interest in axion searches at colliders.

Finally, we explored the experimental constraints on the minimal model of axion and chiral matter we built. This showed that the model is heavily constrained but still allowed. It could be either discovered or almost completely excluded in near future experiments like HL-LHC.

Considering that both non-anomalous axion couplings to EW gauge bosons and chiral extensions of the SM are topics which have enjoyed little attention from the community, this highlights the need for a broader approach towards model building in order to assess correctly our knowledge of nature. There might be surprises in the corners that we have not yet enlightened.

Appendix to Chapter 5

5.A EFT matching with a product of abelian gauge groups

In this appendix, we provide explicit loop computations to match a model with a collection of heavy chiral fermions coupled to a product of abelian gauge bosons to an EFT Lagrangian of the type showed in Eq. (5.3), involving axion terms as well as GCS operators.[13] Here, gauge couplings will be absorbed in the gauge fields, and they can be reinstated by making the replacement $A_{i,\mu} \to g_i A_{i,\mu}$ for each gauge field in all the formulae.

Computations like this have already been performed in the literature, for instance in Ref. [241] whose approach we follow closely (see also Ref. [300] for a recent and similar computation relevant for radiative decays of the Z boson). However, those discussions usually concern models of additional gauge symmetries, and to our knowledge rarely axion models. Therefore, as in Section 5.2, we repeat the necessary details and insist on the treatment proper to axion models.

5.A.1 Explicit loop computation

In this section, we repeat the computations performed in subsection 4.2.3 but for the relevant case of mixed PQ-gauge anomalies. We will highlight only the differences w.r.t. that computation. A self-contained computation can be found in Appendix A of Ref. [249]. We consider a heavy (chiral) fermion, ψ, coupled to several Abelian gauge fields, $A_{i,\mu}$. It will acquire its mass via a Yukawa interaction to a scalar field, ϕ, whose imaginary component gives rise to an axion, θ. The Lagrangian of the model is the same than in Eq. (4.9), with the difference that the gauge field A_i can be the "fake" PQ gauge field (henceforth, hatted indices $\hat{\imath}, \hat{\jmath}, \hat{k}$ will denote physical gauge symmetries, in particular not the PQ symmetry).

As we explicitly show below, at energies below the mass of the heavy fermion, the interactions between the axions and the gauge fields can be matched to the following EFT Lagrangian,

$$\mathcal{L}_{\rm EFT} \supset -\frac{3\alpha_i\alpha_j + \beta_i\beta_j}{48\pi^2}\frac{\theta}{f}F_i\tilde{F}_j + \frac{E_{ij,k}}{8\pi^2}A_{i,\mu}A_{j,\nu}\tilde{F}_k^{\mu\nu} \ , \tag{5.58}$$

where the sum over $i, j(, k)$ is implicit and we wrote $\phi = \frac{f}{\sqrt{2}}e^{i\frac{\theta}{f}}$. The GCS coefficients that are needed for our discussion are given by

$$E_{{\rm PQ}\hat{\imath},\hat{\jmath}} = 2\left(\alpha_{\rm PQ}\alpha_{\hat{\imath}} + \frac{1}{3}\beta_{\rm PQ}\beta_{\hat{\imath}}\right)\beta_{\hat{\jmath}} \ , \quad E_{\hat{\imath}\hat{\jmath},{\rm PQ}} = 2(\alpha_{\hat{\imath}}\beta_{\hat{\jmath}} - \beta_{\hat{\imath}}\alpha_{\hat{\jmath}})\alpha_{\rm PQ} \ . \tag{5.59}$$

Actually, only $E_{{\rm PQ}\hat{\imath},\hat{\jmath}}$ is relevant for PQ anomaly matching since $E_{\hat{\imath}\hat{\jmath},{\rm PQ}}$ does not contribute to the mixed PQ-gauge anomaly, but the value of the latter will be needed to check the invariance

[13] We followed a traditional approach with an explicit calculation of one-loop Feynman diagrams to match the UV-model onto the EFT Lagrangian. It would be interesting to re-derive the results more directly from the universal one-loop effective action, see Ref. [277] and references therein for a recent review.

of the EFT Lagrangian under a physical gauge transformation.

Axion terms

The axion terms in the EFT are computed just as in subsection 4.2.3, with the only difference of taking $q_\theta^\psi = 1$. After considering that, the $m_\psi \to \infty$ limit of Eq. (4.13) corresponds to the first term written in (5.58).

Note also that, if we kept the chiral fermion mass finite, the form factors in (4.13) (and below in (4.15)) map to a tower of higher-dimensional operators in the EFT, see, e.g., Appendix D of Ref. [242] for an explicit example.

Generalised Chern–Simons terms

The computation of these terms is also fully analogous to the one in subsection 4.2.3 up to Eq. (4.22). Once the terms dealing purely with actual gauge symmetries are computed, we must compute the ones with the PQ symmetry. For that, let us consider the following transformation of the fields,

$$\psi_{L/R} \to e^{i\epsilon_i q^i_{L/R}}\psi_{L/R} \ , \quad \theta \to \theta + \epsilon_i(q^i_L - q^i_R)f \ , \quad A_{i,\mu} \to A_{i,\mu} + \delta_{ij}\partial_\mu\epsilon_j \ . \tag{5.60}$$

Using the expression in Eq. (4.22) of the GCS coefficients $E_{ij,k}$ in terms of the shift vectors, the variation of the EFT Lagrangian (5.58) reads[14]

$$\delta_i\mathcal{L}_{\rm EFT} = -\frac{(1-a_{jki})D^{ijk}}{32\pi^2}\epsilon_i F_j\tilde{F}_k \ , \tag{5.61}$$

where $D^{ijk} \equiv q^i_L q^j_L q^k_L - q^i_R q^j_R q^k_R = 2\beta_i\beta_j\beta_k + 2(\alpha_i\alpha_j\beta_k + \alpha_j\alpha_k\beta_i + \alpha_k\alpha_i\beta_j)$ is nothing else but the $U(1)_i \times U(1)_j \times U(1)_k$ anomaly polynomial. By considering i and j to be gauge symmetries and k the PQ symmetry, which has possible non-vanishing mixed gauge anomalies, the consistency of the EFT Lagrangian at the quantum level, namely $\delta_i\mathcal{L}_{\rm EFT} = 0$, forces to choose

$$a_{{\rm PQ}\hat{\imath}\hat{\jmath}} = 1 \ , \quad a_{\hat{\imath}\hat{\jmath}{\rm PQ}} = -1 \ , \tag{5.62}$$

where the last equality follows from Eq. (4.21). Plugging back these values of the shift vectors, we arrive at the expression of the GCS coefficients announced in (5.59).

It can be checked in particular that these results guarantee that the whole EFT Lagrangian remains invariant under the action of an unbroken symmetry, i.e., a symmetry under which the scalar field ϕ is neutral, $q^{\hat{\imath}}_\phi = \beta_{\hat{\imath}} = 0$. In that case the axion θ itself does not shift under the action of $A_{\hat{\imath}}$. The individual GCS terms do, but in a correlated way. Indeed, when $\beta_{\hat{\imath}} = 0$, from (5.59), we obtain

$$\mathcal{L}_{\rm EFT} \supset \frac{\alpha_{\rm PQ}\alpha_{\hat{\imath}}\beta_{\hat{\jmath}}}{2\pi^2}\left(A_{{\rm PQ},\mu}A_{\hat{\imath},\nu}\tilde{F}^{\mu\nu}_{\hat{\jmath}} + A_{\hat{\imath},\mu}A_{\hat{\jmath},\nu}\tilde{F}^{\mu\nu}_{\rm PQ}\right) = -\frac{\alpha_{\rm PQ}\alpha_{\hat{\imath}}\beta_{\hat{\jmath}}}{2\pi^2}A_{{\rm PQ},\mu}A_{\hat{\jmath},\nu}\tilde{F}^{\mu\nu}_{\hat{\imath}} + \text{tot. derivative} \ ,$$

that is gauge invariant with respect to $A_{\hat{\imath}}$, as it should.

[14] Our results are a factor of 2 off with respect to the ones in [241], so that anomaly cancellation holds in the low-energy EFT in our case. It can be verified by an explicit computation in the UV model that the RHS of Eq. (5.61) corresponds to the variation of the quantum effective action associated to the heavy fermion, see for instance Ref. [231]. This holds irrespective of the fact that i corresponds to a genuine gauge symmetry or the PQ one.

5.A.2 Anomaly matching with axion terms only

In the main text, we argued that, contrary to the simple case of the axion decay into two photons, in general the phenomenology of an axion coupled to gauge fields is not uniquely specified by the knowledge of mixed gauge-PQ UV anomalies as, indeed, the latter are only reproduced when combining the axion and the GCS terms. Still, it is interesting to ask under which conditions will the axion terms alone reproduce the UV anomalies[15].

When the heavy fermion is coupled to massless gauge bosons only, like the photons, the scalar field ϕ has to be gauge neutral, $\beta_{\hat{\imath}} = \beta_{\hat{\jmath}} = 0$ and, according to Eq. (5.59), the GCS terms are absent. So the axion term is the only one that can reproduce the anomalous shift under a PQ transformation. However, when the heavy fermion has also an axial coupling to at least one (massive) gauge field, $\beta_{\hat{\imath}} \neq 0$, then a GCS term is needed in the EFT to add up to the shift of the axion term in order to reproduce the full UV anomaly.

But even in the case of an axial gauge symmetry, it might still be possible that the mixed PQ anomaly is borne by the axion term only provided that the PQ symmetry is conveniently chosen. In these models, there need to be unbroken vector-like symmetries that can be used to redefine what one calls the PQ symmetry. For instance, the minimal model in Eq. (4.9) has a "ψ-number" symmetry under which $\psi \to e^{i\epsilon_\psi}\psi$. Similarly, the model in Section 5.4.1 has two unbroken lepton number symmetries. The PQ charges are defined up to these vector-like transformations. They do not affect the axion couplings [263, 267], but they modify the GCS terms and the UV anomalies, in a way consistent with anomaly matching as discussed above. For the axion term to capture the full PQ anomaly, we need to impose that

$$\delta_{\rm PQ}\left(\frac{E_{{\rm PQ}\hat{\imath},\hat{\jmath}}}{8\pi^2}A_{{\rm PQ},\mu}A_{\hat{\imath},\nu}\tilde{F}^{\mu\nu}_{\hat{\jmath}}\right) = -\frac{E_{{\rm PQ}\hat{\imath},\hat{\jmath}}}{16\pi^2}\epsilon_{\rm PQ}F_{\hat{\imath}}\tilde{F}_{\hat{\jmath}} = 0\ . \tag{5.63}$$

It is therefore necessary and sufficient that $E_{{\rm PQ}\hat{\imath},\hat{\jmath}} + E_{{\rm PQ}\hat{\jmath},\hat{\imath}} = 0$, i.e., given the explicit expression (5.59) of the GCS coefficients,

$$3(\alpha_i\beta_{\hat{\jmath}} + \beta_i\alpha_{\hat{\jmath}})\alpha_{\rm PQ} + 2\beta_i\beta_{\hat{\jmath}}\beta_{\rm PQ} = 0\ . \tag{5.64}$$

When that condition is fulfilled, the mixed PQ gauge anomaly coefficient simply becomes

$$D^{{\rm PQ}\hat{\imath}\hat{\jmath}} = \frac{(3\alpha_i\alpha_{\hat{\jmath}} + \beta_i\beta_{\hat{\jmath}})}{3}q_\phi^{\rm PQ}\ , \tag{5.65}$$

where $q_\phi^{\rm PQ} = q_L - q_R = 2\beta_{\rm PQ}$ is the PQ charge of the scalar field ϕ. We recognize here the coefficient of the axion term (times the axion charge).

Note that in the presence of several chiral gauge fields and for generic values of the fermion gauge charges, the axion couplings are not expected to match all mixed anomalies of the PQ symmetry at once, whatever the choice of the PQ charges of the UV fermions. In subsection 5.4.2, we showed that this fact has observational consequences for non-abelian theories, which take the form of the violation of sum rules. For abelian theories, the statement is mostly formal, but it still applies. An illustration of this is obtained when restricting the gauge theory of the model in subsection 5.4.1 to the photon and the Z boson only (or equivalently, to the hypercharge and T_3 generators in the UV). It is then shown in Appendix 5.B.2 that the PQ charge assignment in the UV cannot match the anomaly coefficients and the couplings $a\gamma\gamma, a\gamma Z, aZZ$ in the EFT.

[15] A connected case is the one of a single physical massive gauge field, the axion θ becoming the longitudinal component. The contribution of a heavy fermion of the $U(1)^3$ gauge anomaly is then fully captured, in generic gauge, by the axion term – it is not possible to write a GCS term involving a single gauge field [301]. This is consistent with the well-known result of Ref. [233] that spontaneously broken gauge symmetry with anomalous fermion content can be consistently quantized.

However, for each individual axion coupling, there exists one convenient PQ charge obtained from (5.64). Note that if the heavy fermion has a vector-like charge under one of the gauge symmetries and a chiral one under the other (e.g. $\beta_{\hat{i}} = 0, \beta_{\hat{\jmath}} \neq 0$), then the suitable PQ charge is purely chiral ($\alpha_{\rm PQ} = 0$).

5.A.3 CCWZ approach to the EFT

Consider a model like the one in Eq. (4.9) coupled weakly to a "fake" gauge field for the PQ global symmetry. This "fake" gauge field should be understood as a classical current that we use to keep track of anomalies. At the end, we can always set it to zero to recover the physical theory. We would like to point out that it is always possible to rearrange the EFT Lagrangian in Eq. (5.58), and more generally any EFT of axions a_n and gauged Goldstone bosons $\theta_{\hat{\imath}}$, as a combination of the following terms,

$$-\frac{\mathcal{C}_{n\hat{\imath}\hat{\jmath}}}{16\pi^2 f_n} a_n F_{\hat{\imath},\mu\nu} \tilde{F}^{\mu\nu}_{\hat{\jmath}} \quad , \quad -\mathcal{E}_{n\hat{\imath}\hat{\jmath}} \left(\frac{\partial_\mu a_n}{f_n} - A^{\rm PQ}_{n,\mu} \right) \left(\frac{\partial_\nu \theta_{\hat{\imath}}}{m_{A_{\hat{\imath}}}} - A_{\hat{\imath},\nu} \right) \tilde{F}^{\mu\nu}_{\hat{\jmath}} \ . \tag{5.66}$$

(plus other possible PQ- and gauge-invariant terms which do not involve the axions), where $A_{\hat{\jmath}}$ can be massless but $A_{\hat{\imath}}$ has to be massive. The two kinds of terms are respectively anomalous and gauge-invariant, generalizing both operators in Eq. (5.3). The several axions a_n and gauge NGBs $\theta_{\hat{\imath}}$ find their UV origin in the phases of Higgs fields, and both operators are obtained by integrating out fermions. In order to fulfil PQ anomaly matching, we must therefore have $\mathcal{C}_{n\hat{\imath}\hat{\jmath}} = D^{{\rm PQ}_n \hat{\imath}\hat{\jmath}}$, the UV mixed anomaly coefficients of the n-th PQ symmetry. This rearrangement is straightforwardly done from our explicit formulae, but it can also be simply understood from a field redefinition of the UV theory. For that, we generalize further the UV model in Eq. (4.9) and consider the case of a renormalisable UV theory involving several charged chiral fermions ψ_u getting their masses via Yukawa couplings to several Higgs fields ϕ_X:

$$\mathcal{L}_{\rm UV} = i\overline{\psi}_u \gamma^\mu \left(\partial_\mu - i[\alpha_{i,u} - \beta_{i,u}\gamma_5] A_{i,\mu} \right) \psi_u - \left(y^X_{uv}\, \overline{\psi}_{u,L} \psi_{v,R}\, \phi_X + h.c. \right) \ . \tag{5.67}$$

The gauge fields are split in two categories: the ones with respect to which the fermions are vector-like and which can be massless (if they get a mass from some other source, it is irrelevant for our argument), and the necessarily massive ones under which the fermions are chiral. For those massive vectors A_i (among which the PQ gauge field), it is possible to define fields θ_i out of the phases θ_X of the Higgs fields, that shift as $\theta_i \to m_{A_i} \delta^j_i \epsilon_j$ under the j-th gauge symmetry[16]. Thus, we can make the fermions uncharged under the massive gauge fields by redefining them

[16] Precisely, the mass term for the gauge fields,

$$\mathcal{L} \supset \frac{1}{2} M^2_{ij} A_{i,\mu} A^\mu_j \ , \tag{5.68}$$

arises from the axion kinetic terms (themselves obtained from the Higgs fields kinetic terms)

$$\mathcal{L} \supset \frac{1}{2} (\partial_\mu \theta_I - q^i_I v_I A_{i,\mu})^2 \tag{5.69}$$

so that $M^2_{ij} = q^i_I q^j_I v^2_I$. Diagonalizing $M^2 = O^T M'^2 O$, for an orthogonal matrix O and $M'^2 = {\rm diag}(m^2_{A_i})$, $A'_i = (OA)_i$ define the massive vector fields of masses m_{A_i} and the associated gauge parameters are $\epsilon'_i = (O\epsilon)_i$. Thus, defining $X_{iI} = \frac{O_{ij} q^j_I v_I}{m_{A_i}}$ which is orthogonal (recall that we introduce fake gauge fields for each PQ symmetry, so in particular there is one massive field for each phase of a Higgs scalar), $\theta'_i = (X\theta)_i$ shifts as $m_{A_i} \delta^j_i \epsilon'_j$ under the gauge symmetries defined by the vectors A'_i. We can also define $q'^{\,i}_I = (O^T q_I)^i$ and check that we consistently have $\frac{\theta_I}{v_I} = q'^{\,i}_I \frac{\theta'_i}{m_{A_i}}$. We work with the primed fields and drop the primes.

as follows [134, 135],

$$\psi_{u,L/R} \to e^{i\frac{\theta_i}{m_{A_i}} q^i_{u,L/R}} \psi_{u,L/R} \ . \tag{5.70}$$

Since the fermions are now uncharged (except under the vector-like gauge symmetries), there cannot remain any axion in the Yukawa couplings. Also, the field redefinitions modify the minimal coupling to gauge fields in the covariant derivative as follows:

$$\overline{\psi_u}\gamma^\mu \left(\partial_\mu - i[\alpha_{i,u} - \beta_{i,u}\gamma_5]A_{i,\mu}\right)\psi_u \to \overline{\psi_u}\gamma^\mu \left(\partial_\mu + i[\alpha_{i,u} - \beta_{i,u}\gamma_5]\left[\frac{\partial_\mu \theta_i}{m_{A_i}} - A_{i,\mu}\right]\right)\psi_u \ , \tag{5.71}$$

which is correctly gauge invariant when the fermions are neutral. Thus, integrating the latter out (in perturbation theory or beyond) cannot generate anything else than terms which are made out of $\frac{\partial_\mu \theta_i}{m_{A_i}} - A_{i,\mu}$ [233, 302, 303], among which terms such as the second ones in (5.66). To such terms, one needs to add the Jacobian contribution due to the anomalous transformation of the path integral measure [304], which are nothing but the first terms in (5.66) for the physical axions $\theta_i \equiv a_n$, see the previous section for details. Anomaly matching between the UV and the IR is obvious in this approach, although we stress that the physical amplitude between one axion and 2 gauge bosons might not agree with the anomaly.

5.B Axion couplings and PQ anomalies in SM chiral extensions

In this appendix, we discuss the axion couplings in the SM chiral extension of subsection 5.4.1, and we compare them to the UV PQ anomalies. In particular, we match them one by one using the prescription of (5.65), which determines how to fix the fermion PQ charges so that the axion coupling under study is reproduced by the corresponding PQ anomaly. We show how this prescription should be properly used when the PQ symmetry is restricted by the fact that it should commute with gauge symmetries.

5.B.1 General 2HDM assignment and axion couplings

For generality, we first present what the axion couplings would be if we assigned the two Higgses differently than in Eq. (5.32). Let us denote H_ψ the Higgs that appears in ψ's Yukawa term (only one can appear if the PQ is to be exact and the axion classically massless). Our Yukawa sector thus looks as follows,

$$-\mathcal{L}_Y = y_{E_1}\bar{L}_1 E_1 H_{E_1} + y_{E_2}\bar{L}_2 E_2 H_{E_2} + y_{N_1}\bar{L}_1 N_1 H_{N_1} + y_{N_2}\bar{L}_2 N_2 H_{N_2} + \text{h.c.}\,, \tag{5.72}$$

and the axion content of each Higgs field, which can be H_i or $\tilde{H}_i$, is written $H_\psi = e^{iX_{H_\psi}\frac{a}{f}}\begin{pmatrix}0 & \frac{v_{H_\psi}}{\sqrt{2}}\end{pmatrix}^T$, so that the (Yukawa) axion fermion coupling is $\frac{y_\psi v_{H_\psi}}{\sqrt{2}}\bar{\psi}_L\psi_R e^{iX_{H_\psi}\frac{a}{f}}$+h.c. In terms of the PQ charges of the fermions, one has

$$X_{H_{E_i}} = X_{L_i} - X_{E_i} \ , \quad X_{H_{N_i}} = X_{L_i} - X_{N_i} \ . \tag{5.73}$$

We derive the axion EFT below the mass of the new fermions, using the formulae in Appendix 5.A. For that, we define the massive eigenstates $N_i = N_i + N_{L_i}$, $E_i = E_i + E_{L_i}$, where

$$L_1 = \begin{pmatrix} N_{L_1} \\ E_{L_1} \end{pmatrix} \ , \quad L_2 = \begin{pmatrix} E_{L_2} \\ N_{L_2} \end{pmatrix} \ , \tag{5.74}$$

and extract their gauge couplings from

$$\mathcal{L} \supset \quad \overline{L_i}\gamma^\mu \left(g\frac{\sigma^a}{2}W_\mu^a + g'(-1)^{i+1} Y B_\mu \right) L_i + g'\overline{N_i}\gamma^\mu (-1)^{i+1}\left(Y+\frac{1}{2}\right) B_\mu N_i$$
$$+ g'\overline{E_i}\gamma^\mu (-1)^{i+1}\left(Y-\frac{1}{2}\right) B_\mu E_i \ . \tag{5.75}$$

Assuming equal masses within a $SU(2)$ doublet for simplicity ($m_{N_i} = m_{E_i}$), the axion couplings in the EFT read[17]

$$\mathcal{L} \supset -g'^2 \frac{(1+12Y^2)X^+ + 6YX^-}{192\pi^2}\frac{a}{f}B\tilde{B} - g^2\frac{X^+}{192\pi^2}\frac{a}{f}W^a\tilde{W}^a\big|_{\text{lin.}} - gg'\frac{X^+ + 6YX^-}{192\pi^2}\frac{a}{f}B\tilde{W}^3\big|_{\text{lin.}} \tag{5.76}$$

where

$$X^+ = \sum_i \left(X_{H_{N_i}} + X_{H_{E_i}} \right) \ , \quad X^- = \sum_i \left(X_{H_{N_i}} - X_{H_{E_i}} \right) \ . \tag{5.77}$$

From this formula, we can immediately check that there are no dimension-5 axion-gauge bosons couplings if all the Higgses in (5.72) are expressed in terms of a single one, as given in Eq. (5.29). Indeed, one then has $X_{H_{N_1}} + X_{H_{N_2}} = X_{H_{E_1}} + X_{H_{E_2}} = 0$, such that $X^+ = X^- = 0$. Actually, this has a nice interpretation in terms of our discussion of Section 5.2. Let us focus on the $aB\tilde{B}$ coupling for simplicity. The mass terms and the axion couplings in (5.72) have a $U(1)^5$ symmetry - broken to $U(1)^3$ by weak interactions -, spanned by the hypercharge $U(1)_Y$ and four fermion numbers $U(1)_{\psi=E_i,N_i}$. Thus the PQ symmetry must be a linear combination of those. We can choose it to be fully aligned with $U(1)_Y$ without affecting the discussion of anomaly matching in the axion EFT, since the axion does not shift under the vector-like fermion symmetries. Then, gauging again the PQ symmetry, one finds that the fields cannot differentiate between the PQ or the B gauge field, since each fermion ψ couples to a single combination of them, $Y_\psi(A_{\text{PQ},\mu} + A_\mu)$, hence there cannot be any GCS term in the EFT, simply because one cannot write a non-vanishing GCS term with a single gauge field. Also, each fermion couples to a single axion, the phase of the single Higgs, so that there is a single axion term. Consequently, the axion term is given by the $U(1)_Y^3$ anomaly coefficient, or by the $U(1)_{\text{PQ}}U(1)_Y^2$ anomaly coefficient, which are identical by assumption. Eventually, since the full set of heavy fermions has no $U(1)_Y^3$ anomaly, there is no possible axion coupling in the EFT.

5.B.2 Matching with the UV PQ anomaly coefficients

We now verify that the prescription in (5.65) reproduces the axion couplings of (5.76). Let us recall why such a prescription is needed. The interactions in (5.72) have two unbroken lepton number symmetries $U(1)_{L_1}$ and $U(1)_{L_2}$, which are anomalous with respect to the chiral gauge symmetries $SU(2)_L \times U(1)_Y$. Therefore, the PQ UV anomalies can be modified by adding to the fermion PQ charges a component along those fermion numbers, namely by redefining $U(1)_{\text{PQ}} \to U(1)_{\text{PQ}} + \alpha\,(U(1)_{L_1} + U(1)_{L_2})$, with α an arbitrary number (the antisymmetric combination $U(1)_{L_1} - U(1)_{L_2}$ is anomaly free). This number can be used to modify each mixed PQ anomaly so that it matches the corresponding axion coupling in (5.76). We show how this is achieved in what follows.

[17] With our assumption of equal masses within a doublet, the diagrams for the $aW^a\tilde{W}^b$ process can be obtained using our abelian formulae with $\alpha = \beta = \frac{1}{4}$, and supplemented by a factor

$$\sum_{i=1,2(\text{flavours})} \sum_{j=1,2(\psi^j=\text{N,E})} (\sigma^{\{a}\sigma^{b\}})_{[1+i+j],[1+i+j]} X_{\psi_i^j} \ ,$$

where we defined $x_2 = x \mod 2$, $[x] = x_2 + 2(1 - x_2)$.

For that, we compute the anomalous terms arising after a PQ rotation that removes the axion from the mass terms,

$$L_i \to e^{iX_{L_i}\frac{a}{f}} L_i\,, \quad N_i \to e^{iX_{N_i}\frac{a}{f}} N_i\,, \quad E_i \to e^{iX_{E_i}\frac{a}{f}} E_i\,, \tag{5.78}$$

where $i = 1, 2$. The anomalous terms read

$$\delta\mathcal{L} = -g^2 \frac{\mathcal{A}_W^{ab}}{16\pi^2}\frac{a}{f} W^a \tilde{W}^b - g'^2 \frac{\mathcal{A}_B}{16\pi^2}\frac{a}{f} B\tilde{B}\ , \tag{5.79}$$

where the anomaly polynomials are

$$\mathcal{A}_W^{ab} = \frac{(X_{L_1} + X_{L_2})\delta^{ab}}{2}\ , \quad \mathcal{A}_B = \frac{X^+ - 2(X_{L_1} + X_{L_2})}{4} + YX^- + Y^2X^+\ , \tag{5.80}$$

where $X^\pm$ have been defined in appendix 5.B.1, and we recognize in particular the contribution of the unbroken anomalous fermion number $U(1)_{L_1} + U(1)_{L_2}$.

We now specialize to the Higgs assignment in Eq. (5.32), for which we have the relations Eq. (5.33), which imply $X^+ = 2(X_1 - X_2), X^- = 0$ so that we get

$$\mathcal{A}_W^{ab} = \frac{(X_{L_1} + X_{L_2})\delta^{ab}}{2} \quad \mathcal{A}_B = -\frac{X_{L_1} + X_{L_2} + (X_2 - X_1)(1 + 4Y^2)}{2}\ . \tag{5.81}$$

Restricting (5.79) to the neutral mass eigenstates, one finds

$$\begin{aligned} -\frac{16\pi^2}{e^2}\delta\mathcal{L} = {} & (X_1 - X_2)\left(2Y^2 + \frac{1}{2}\right) F\tilde{F} \\ & + \left(-t_W\left[(X_1 - X_2)\left(4Y^2 + 1\right) - (X_{L_1} + X_{L_2})\right] + t_W^{-1}[X_{L_1} + X_{L_2}]\right) F\tilde{Z} \\ & + \left(t_W^2\left[(X_1 - X_2)\left(2Y^2 + \frac{1}{2}\right) - \frac{X_{L_1} + X_{L_2}}{2}\right] + t_W^{-2}\frac{X_{L_1} + X_{L_2}}{2}\right) Z\tilde{Z}\ . \end{aligned} \tag{5.82}$$

Note that (5.82) verifies the constraints in Eq. (5.9), as it should. As expected the photon terms match with the ones in Eq. (5.42). To match the photon-Z terms, one needs an axial PQ, as discussed around Eq. (5.65). However, given the relations in Eq. (5.33), it is impossible to define the PQ symmetry such that it is chiral on each heavy fermion, namely one cannot enforce

$$X_{L_1} + X_{E_1} = 0\,, \qquad X_{L_1} + X_{N_1} = 0\ , \quad X_{L_2} + X_{E_2} = 0\,, \qquad X_{L_2} + X_{N_2} = 0\,, \tag{5.83}$$

unless the PQ charges of the Higgses are non generic, namely if they verify $X_1 = -X_2$. This clash comes from the fact that we defined the PQ symmetry on the UV fields so that it commutes with all gauge symmetries. In particular, both components of the $SU(2)$ doublets L_i have the same PQ charge. Starting from a generic $U(1)_{\rm PQ}$ charge assignment, $X_1 = -X_2$ can be reached by considering a suitable linear combination of the hypercharge and the original PQ symmetry. If we want to keep a generic PQ charge assignment, another option is to impose a slightly weaker, but equally efficient constraint, which is that the PQ symmetry is axial "on average"[18],

$$X_{L_1} + X_{L_2} + X_{E_1} + X_{E_2} = 0\,, \qquad X_{L_1} + X_{L_2} + X_{N_1} + X_{N_2} = 0\,. \tag{5.84}$$

[18] One does not need to demand that the PQ anomalous contribution of the GCS vanishes for each integrated massive fermion, but only that it does at the level of a subset or all of the heavy fermions.

This yields in particular

$$\text{Axial PQ}: X_{L_1} + X_{L_2} = \frac{X_1 - X_2}{2} \ , \tag{5.85}$$

thanks to which the photon-Z terms in Eq. (5.82) and (5.42) match. Finally, to understand the $Z\tilde{Z}$ coupling, let us first write down the kinetic terms in terms of photons and Zs:

$$\begin{aligned} &e\overline{N_i}\gamma^\mu(-1)^{i+1}\left[\left(Y+\frac{1}{2}\right)A_\mu + \left(-t_W\left(Y+\frac{1}{4}+\frac{1}{4}\gamma_5\right) + t_W^{-1}\frac{1-\gamma_5}{4}\right)Z_\mu\right]N_i \\ &+ e\overline{E_i}\gamma^\mu(-1)^{i+1}\left[\left(Y-\frac{1}{2}\right)A_\mu - \left(t_W\left(Y-\frac{1}{4}-\frac{1}{4}\gamma_5\right) + t_W^{-1}\frac{1-\gamma_5}{4}\right)Z_\mu\right]E_i \end{aligned} \tag{5.86}$$

The photon coupling is of course vector-like. We know from (5.65) that a systematic way to get the right $Z\tilde{Z}$ coupling from the anomaly is to choose the PQ symmetry such that $3\alpha_{\text{PQ}}\alpha_Z + \beta_{\text{PQ}}\beta_Z = 0$ for each integrated field. That means demanding

$$\begin{aligned} 6X_{L_i}\left(-t_W\left(Y+\frac{1}{4}\right)+\frac{t_W^{-1}}{4}\right) + (-1)^i X_{i+1 \bmod 2}\left(t_W\left(3Y+1\right) - \frac{t_W^{-1}}{2}\right) = 0 \\ 6X_{L_i}\left(-t_W\left(-Y+\frac{1}{4}\right)+\frac{t_W^{-1}}{4}\right) + (-1)^{i+1} X_i\left(t_W\left(-3Y+1\right) - \frac{t_W^{-1}}{2}\right) = 0 \ . \end{aligned} \tag{5.87}$$

Those conditions are again too restrictive, namely they impose conditions on $X_{1,2}$, but choosing $\sum(3\alpha_{\text{PQ}}\alpha_Z + \beta_{\text{PQ}}\beta_Z) = 0$ for a whole (N_i, E_i) pair is allowed for generic Higgs charges, and sufficient. The condition to enforce is the sum of the two contributions in (5.87),

$$3X_{L_i}(t_W^{-1} - t_W) + (-1)^i X_{i+1 \bmod 2}\left(t_W\left(3Y+1\right) - \frac{t_W^{-1}}{2}\right) + (-1)^{i+1} X_i\left(t_W\left(-3Y+1\right) - \frac{t_W^{-1}}{2}\right) = 0 \ , \tag{5.88}$$

hence

$$X_{L_1} + X_{L_2} = \frac{t_W^{-1} - 2t_W}{3(t_W^{-1} - t_W)}(X_1 - X_2) \tag{5.89}$$

With this choice, the $aZ\tilde{Z}$ in Eq. (5.82) and (5.42) match.

The couplings to the charged bosons $W^\pm$ can also be understood along those lines. Comparing Eq. (5.82) and (5.42), we see that we would like that

$$X_{L_1} + X_{L_2} = \frac{X_1 - X_2}{3} \tag{5.90}$$

for them to match. This relation is again achieved when we enforce that $3\alpha_{\text{PQ}}\alpha_W + \beta_{\text{PQ}}\beta_W = 0$, where $\alpha_W = \beta_W$ since the coupling to Ws is purely left-handed. We cannot enforce it at the level of each fermion without constraining $X_{1,2}$, as we are now quite used to, but we can impose a similar constraint on a full doublet (N_i, E_i). It means that $4X_{L_i} + X_{N_i} + X_{E_i} = 0$. With Eq. (5.33), we see that this gives (5.90).

As a final remark, notice that we did not need to worry about the PQ variation of other hypothetical axion terms, such as the (pure gauge) ones that feature the longitudinal component of the Z boson a_Z, of the form $a_Z F\tilde{F}$, etc. This is due to the fact that we chose the PQ symmetry so that a_Z is PQ neutral, as can be seen from Eq. (5.37).

This page is intentionally left blank.

Chapter 6

Scattering Amplitudes for BSM

“If you are receptive and humble, mathematics will lead you by the hand.”

— Paul Dirac, as quoted by G. Farmelo in The Strangest Man: The Hidden Life of Paul Dirac, Mystic of the Atom (2009), p. 435

6.1 Stepping back to leap forward

Throughout this thesis, we have used extensively Effective Field Theories and stressed how they allow us to parametrize the unknown UV physics in a largely model-independent way. However, we must remain wary of the intrinsic assumptions that they come with. Additionally, the inclusion of higher orders in the series expansion is systematic but far from trivial, thanks to the rapidly growing number of higher-dimensional operators and the redundancies that one must take care of (see e.g. Ref. [44, 45] and Chapter 2).

Thus, a very appropriate question is whether a better method to parametrize NP effects at low energies can be found. Ideally, it should be fully independent of assumptions on the UV physics. Additionally, the computation of higher order corrections should be as easy as the leading order pieces. This question has started to be addressed by the community in the last few years and some recent developments have shown promising results.

The common approach to answer the question is going back to the essentials. The huge success of Quantum Field Theory to describe elementary particles and their interactions over the last half century has made us believe that all the answers, at least below the Planck scale, must be found by using it. Nevertheless, we can not forget that QFT has inherent difficulties and is loaded with hypothesis. Then, we could ignore QFT for a moment and reconsider those objects that are closer to what we can measure: physical states in the Hilbert space and the scattering amplitude matrix. Most observables can be traced back to those two theoretical objects.

It is well known that on-shell scattering amplitudes for massless particles can be built and described much more easily with the use of the helicity spinor formalism, which seizes on powerful constraints arising from Lorentz invariance [54,305]. In fact, both on-shell scattering amplitudes and helicity spinors seem to be living a second youth. They have been in use for decades to compute amplitudes and cross-sections in some phenomenologically relevant limits [187], and, mostly, to compute scattering amplitudes in massless theories (see Ref. [305] for a review). Some of those theories are of phenomenological relevance, such as QCD and gravity, where they

simplify enormously the computation of gluon or graviton scattering. Moreover, the formalism has been implemented in computer programs (see e.g. Ref. [306–308]). And recently, it has been shown that on-shell massless scattering amplitudes ease the computation of anomalous dimensions and Renormalisation-Group evolution equations [309–314].

However, it is not enough for our ultimate purposes of replacing EFTs since, in a bottom-up approach, it is not sensible to assume all particles to be massless. Several attempts of extending the formalism to the massive case were made, but the breakthrough of a systematic extension to arbitrary spins and masses was done just a few years ago [54]. Hence, the thorough study of (on-shell) Scattering Amplitudes for BSM begun.

In this chapter, we will explore how the helicity spinor formalism and scattering amplitudes built with it can be used to improve our understanding of BSM Physics. As a first step, in Section 6.2 we will focus on the massless case. The massless helicity spinor formalism will be presented in subsection 6.2.1, then in subsection 6.2.2, we show how it simplifies the computation of amplitudes, even when Feynman diagrams are still used, for Vh production processes like the ones studied in Chapter 3. In subsection 6.2.3, we review how, for a given spectrum of massless particles, helicity spinors can be used to build systematically all the scattering amplitudes in a theory with minimal assumptions. In Section 6.3 we review briefly the Scattering Amplitudes for BSM program built upon the idea of repeating such construction for SMEFT.

The aforementioned program can not be carried out without the general extension of the helicity spinor formalism to the massive case, which we present in Section 6.4. As with the massless case, we first present the general formalism in subsection 6.4.1, then we explain how to use it to build massive scattering amplitudes in subsection 6.4.2. The high-energy limit of the massive case, which connects it to the massless case and is an important tool to extract interesting results, is presented in subsection 6.4.3. Finally, we apply this formalism to the amplitudes of VVh and $VVhh$ processes in Section 6.5, where we rederive some results already present in the literature and show original results that include a larger set of BSM-generated structures.

6.2 Massless helicity amplitudes

6.2.1 Massless helicity spinor formalism

This formalism originates from the key fact that the Lorentz algebra $\mathrm{SL}(2,\mathbb{C})$ can be decomposed into $\mathrm{SU}(2)\times\mathrm{SU}(2)$ for the massless case. Hence, the 4-momentum p^μ of a massless particle can be written as a bi-spinor upon contraction with a four-vector of Pauli matrices , i.e.

$$p_\mu \sigma^\mu_{\alpha\dot\beta} = p_{\alpha\dot\beta} = \lambda_\alpha \tilde\lambda_{\dot\beta} \equiv |p\rangle_\alpha [p|_{\dot\beta}, \tag{6.1}$$

where

$$\sigma^\mu_{\alpha\dot\beta} = (\mathbf{1}_{2x2}, \vec\sigma)\,, \quad \overline\sigma^{\mu,\alpha\dot\beta} = (\mathbf{1}_{2x2}, -\vec\sigma)\,, \tag{6.2}$$

and σ^i are the Pauli matrices (see Appendix 6.A for our conventions). The angle and square spinors are 2-component commuting spinors that represent independent solutions to the massless Dirac equation (Weyl equation). Their Lorentz indices are raised and lowered with Levi-Civita tensors. The power of the spinor helicity formalism relies partially in the possibility of working abstractly with these spinors and only later relate them with momentum vectors [54, 56, 305].

If the momentum p^μ is complex-valued, the angle and square spinors are independent. Although such a situation is unphysical, considering complex momenta is an useful trick. When the momentum is restricted to the physical case of real values, the angle and square spinors are

related by conjugation [56, 305],

$$(|p\rangle_\alpha)^\dagger = [p|_{\dot\alpha}, \quad \left(|p]^{\dot\alpha}\right)^\dagger = -\langle p|^\alpha. \tag{6.3}$$

Throughout this chapter, we will work with all incoming particles unless stated otherwise. It is useful to clarify the relation between the properties of incoming particles and the helicity spinors. They are related as follows:

1. Incoming fermion with $h = +1/2 \to |p]^{\dot\alpha}$
2. Incoming fermion with $h = -1/2 \to |p\rangle_\alpha$
3. Incoming anti-fermion with $h = +1/2 \to [p|_{\dot\alpha}$
4. Incoming anti-fermion with $h = -1/2 \to \langle p|^\alpha$

It is easy to notice that square and angle spinors are defined up to an overall scaling that leaves the four-momentum invariant. This is a consequence of the existence of the Little Group, i.e. the subgroup of the Lorentz group that leaves invariant the momentum of an on-shell particle. For the massless case, the Little Group is SO(2) ≃U(1). Under this group, the square and angle spinors transform precisely as

$$|p\rangle \to t|p\rangle, \quad |p] \to t^{-1}|p], \tag{6.4}$$

where $t \in \mathbb{C}$. For real momentum, t is an unitary complex number, i.e. a phase, while for general complex momentum, it can be any non-zero complex number. Although for now this invariance might seem incidental, it plays a key role in the construction of on-shell amplitudes, as we will see in subsection 6.2.3.

A key ingredient to express on-shell amplitudes in term of helicity spinors are the angle and square spinor brackets. For two light-like vectors p^μ and q^μ, we define

$$[p|q] \equiv [p|_{\dot\alpha}|q]^{\dot\alpha}, \quad \langle p|q\rangle \equiv \langle p|^\alpha|q\rangle_\alpha \tag{6.5}$$

as the square and angle spinor brackets respectively. Notice they are antisymmetric under commutation of their arguments, i.e. $[p|q] = -[q|p]$ and similarly for the angle-shaped one, since the Lorentz indices are contracted with a Levi-Civita tensor. All other possible combinations of bra and kets vanish, and for real momenta the angle and square brackets are related by complex conjugation,

$$[p|q]^* = \langle q|p\rangle, \qquad \text{for } p^\mu, \quad q^\mu \in \mathbb{R}. \tag{6.6}$$

Additionally, the angle and square brackets are linked to the product of 4 momenta by the identity

$$\langle p|q\rangle[p|q] = -(p+q)^2 = -2p\cdot q, \tag{6.7}$$

which also establishes a direct connection with the Mandelstam variables. To fix notation, we define the general Mandelstam variables as

$$s_{ij} = (p_i + p_j)^2, \quad s_{ijk} = (p_i + p_j + p_k)^2. \tag{6.8}$$

In particular, we have $s = s_{12}$, $t = s_{13}$ and $u = s_{14}$ for 4-particle scattering.

Another useful contraction of helicity spinors is the following:

$$[p|\gamma^\mu|k\rangle = \langle k|\gamma^\mu|p], \tag{6.9}$$

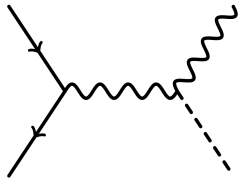

Figure 6.2.1: Feynman diagram for the process $qq' \to Vh$ at tree-level in the SM for massless quarks.

where it should be understood that the 2-component spinors project out the matching sigma-matrix contained in γ^μ. This can be easily contracted with a third momentum, q_μ,

$$q_\mu[p|\gamma^\mu|k\rangle \equiv [p|\overline{q}|k\rangle = \langle k|q|p], \tag{6.10}$$

where we use the line over the middle momentum to mark which sigma from γ^μ is selected.

6.2.2 Application to diboson processes

In this subsection, we will show how the use of massless helicity spinors can facilitate the computation of amplitudes for definite helicity states (helicity amplitudes), even when they are still fundamentally computed via Feynman diagrams. The two main advantages are the compactness of the final expressions and the quick selection of only the helicity states that will contribute to the final cross-section. As example, we will compute at leading order the amplitude of the process $q\overline{q} \to Vh$, where $V = W, Z$. These amplitudes correspond to the signal of the diboson production process studied in detail in Chapter 3, where the reader can find a detailed explanation of why this process is interesting to search for BSM Physics. Here, we will only repeat that offers a unique window to Higgs dynamics and the EWSB mechanism at high energies.

The amplitude of interest can be written as [187]

$$\mathcal{M}\left(1_q, 2_{\overline{q}}, 3_V, 4_h\right) = \sum D \cdot C \cdot \mathcal{T}\left(h_q, h_{\overline{q}}, h_V\right), \tag{6.11}$$

where D contains the couplings involved, C encodes the colour structure of the amplitude, $\mathcal{T}$ represents the kinematics dependence, and we sum over the contributing Feynman diagrams. $\mathcal{T}$ is the only factor that depends on the momentum and helicity of the involved particles[1] and we will focus on it first.

We start computing the SM amplitude in Fig. 6.2.1, which involves a V boson propagating in the s-channel. Exchange of quarks in the t- and u-channels are absent for massless quarks, which is the most relevant case for collider phenomenology. The helicity spinor that represents the incoming quark and anti-quark are determined by their helicity according to the rules 1-4. Additionally, we must include the polarization vector of the V boson $\epsilon^{\nu,-h_V}$, where we use the opposite polarization because of having assumed all incoming particles. The Feynman rules tell us that we also must take into account for the kinematics piece a Dirac matrix and the virtual boson propagator,

$$\gamma^\mu \left(\frac{\eta_{\mu\nu} - \frac{q_\mu q_\nu}{m_V^2}}{\hat{s} - m_V^2 + m_V \Gamma_V} \right), \tag{6.12}$$

where q^μ is the momentum of the virtual particle and we have imposed momentum conservation, $q^2 = \hat{s}$. It must be understood that the fermion helicity spinors will select the sub-matrix σ^μ

[1] In chiral theories, D will generically depend on the fermion helicity, but not on its momentum.

inside γ^μ with the appropriate indices. This already allows to exclude the cases where quark and anti-quark have the same helicity.

The amplitude that we are computing is phenomenologically relevant only in the case of a massive vector boson V, then we need a generalization of the helicity spinors for massive momentum. In this section, we will use the one showed in Ref. [307]. This generalisation arises from the observation that any non-light-like massive four-vector k_μ can be decomposed into two lightlike four-vectors with respect to an arbitrary lightlike four-vector q_μ that must satisfy $k \cdot q \neq 0$. Then, we can write

$$k_\mu = k_\mu^q + \frac{k^2}{2k \cdot q} q, \tag{6.13}$$

where k_μ^q is called associated vector and is also light-like. Then, each term on the r.h.s of the last equation can be written in terms of massless spinors [307]. In subsection 6.4, we will present a different way of generalizing helicity spinors to the massive case.

By making use of Eq. 6.13, we can define the polarisation vectors for the external massive gauge boson as[2]

$$\begin{aligned} \epsilon_\mu^+(k,q) &= \frac{[q|\gamma_\mu|k^q\rangle}{\sqrt{2}[q|k^q]}, \quad \epsilon_\mu^-(k,q) = \frac{\langle q|\gamma_\mu|k^q]}{\sqrt{2}\langle q|k^q\rangle}, \\ \epsilon_\mu^0(k,q) &= -\frac{\langle k^q|\gamma_\mu|k^q]}{2m_k} - \frac{m_k}{2}\frac{\langle q|\gamma_\mu|q]}{[k^q|q]\langle q|k^q\rangle}, \end{aligned} \tag{6.14}$$

where $m_k = \sqrt{|k^2|}$ is the mass of the vector boson. Notice that these vectors can be expressed with dotted and undotted indices by contraction with Pauli matrices and using Eq. (6.73). For example,

$$\epsilon^{0,\dot{\alpha}\alpha}(k,q) = \overline{\sigma}^{\mu,\dot{\alpha}\alpha}\epsilon_\mu^0(k,q) = -\frac{|k^q]^{\dot{\alpha}}\langle k^q|^\alpha}{m_k} - m_k\frac{|q]^{\dot{\alpha}}\langle q|^\alpha}{[k^q|q]\langle q|k^q\rangle}. \tag{6.15}$$

After all these definitions, we are ready to compute the kinematic part of the amplitude for any given helicity of the final states. As an example, we consider the case of $h_q = -1/2$ and general h_V, in which $\mathcal{T}$ has the form[3]

$$\mathcal{T}\left(-\frac{1}{2},\frac{1}{2},h_V\right) = \frac{[2|\gamma^\mu|1\rangle\epsilon_\mu^{-h_V}}{\hat{s} - m_V^2 + im_V\Gamma_V} \tag{6.16}$$

Thus, for instance if $h_V = 1$, we simply obtain

$$\mathcal{T}\left(-\frac{1}{2},\frac{1}{2},1\right) = \frac{1}{\hat{s} - m_V^2 + im_V\Gamma_V}\langle 2|\gamma^\mu|1]\epsilon_\mu^{-1}(-p_3)\,. \tag{6.17}$$

where p_3^μ is the momentum of the outgoing vector boson V and, since we are working with all ingoing particles, then the polarisation vector takes the opposite momentum. With the same procedure than in Eq. 6.15, the last equation can be simplified to

$$\mathcal{T}\left(-\frac{1}{2},\frac{1}{2},1\right) = \frac{1}{\hat{s} - m_V^2 + im_V\Gamma_V}\frac{[2|\,(-3)^q]\langle q_{-3}|1\rangle}{\sqrt{2}\langle q_{-3}|\,(-3)^q\rangle}, \tag{6.18}$$

where we write (-3) to remind that we are taking the opposite momentum for the vector boson.

[2]Notice that we use the definition of massive spinors and polarization vectors from Ref. [307], but the definition of massless spinors from Ref. [56] which differ in what is denoted with angle and square brackets.

[3]In the massless fermion limit, the subleading piece of the unitary propagator cancels out after imposing momentum conservation.

For a generic non-light-like four-vector $k^\mu = (k^0, \boldsymbol{k})$, we define the reference vector q_k as

$$q_k^\mu = \left(\text{sign}\left(k^0\right)|\boldsymbol{k}|, -\boldsymbol{k}\right). \tag{6.19}$$

This implies that the reference vector in the polarization of our V boson is $\left(-|p_3|, \overrightarrow{p_3}\right)$.

Following Ref. [333], one can show that for two light-like four vectors A_μ and B_μ, we have

$$\begin{aligned} [A|B] &= \frac{A_T^- B^+ - B_T^- A^+}{\sqrt{A^+ B^+}}, \\ \langle A|B\rangle &= [A|B]^*, \end{aligned} \tag{6.20}$$

where we used the definitions

$$\begin{aligned} p^- &= p^0 - p^2, \quad p^+ = p^0 + p^2, \\ p_T^- &= p^0 - ip^3, \quad p_T^+ = p^1 + ip^3, \end{aligned} \tag{6.21}$$

valid for an arbitrary four-vector p^μ. This is done after deciding to quantize the spin along the y axis, which implies using the following basis of Pauli matrices:

$$\sigma^0 = \mathbf{1}_{2\times 2}, \quad \sigma^1 = \begin{pmatrix} 0 & 1 \\ 1 & 0 \end{pmatrix}, \quad \sigma^2 = \begin{pmatrix} 1 & 0 \\ 0 & -1 \end{pmatrix}, \quad \sigma^3 = \begin{pmatrix} 0 & i \\ -i & 0 \end{pmatrix}. \tag{6.22}$$

Finally, because of how the scattering-angle θ was defined in Section 3.3.3, it is easier to compute the amplitude in the centre-of-mass frame of the incoming quarks and then express as much as possible of it in terms of Lorentz invariants such as the Mandelstam variables. Hence, we use the following expressions for the 4-momentum of the different particles of our interest

$$\begin{aligned} p_q^\mu &= \left(\sqrt{\hat{s}}, 0, 0, -\sqrt{\hat{s}}\right), \\ p_{\overline{q}}^\mu &= \left(\sqrt{\hat{s}}, 0, 0, \sqrt{\hat{s}}\right), \\ p_V^\mu &= \left(\sqrt{m_V^2 + \overrightarrow{p}_V^{\,2}}, |\overrightarrow{p}_V|\sin(\theta), 0, |\overrightarrow{p}_V|\cos(\theta)\right), \\ p_h^\mu &= p_q^\mu + p_{\overline{q}}^\mu - p_V^\mu, \end{aligned} \tag{6.23}$$

where energy conservation and on-shell conditions imply $|\overrightarrow{p}_V| = \sqrt{\frac{\left(\hat{s} - m_h^2 + m_V^2\right)^2}{4\hat{s}} - m_V^2}$. Notice that we have written the momenta for the physical outgoing V and h bosons.

Applying all the formulae shown in the previous paragraphs to Eq. (6.18), we obtain

$$\mathcal{T}\left(-\frac{1}{2}, \frac{1}{2}, 1\right) = \frac{ie^{i\theta}}{2\sqrt{2}} \frac{\sqrt{\hat{s}}\left(1 - \cos(\theta)\right)}{\hat{s} - m_V^2 + im_V\Gamma_V}, \tag{6.24}$$

where θ is the scattering angle defined as in Section 3.3.3 (see Fig. 3.3). The same steps can be repeated for all the other possible polarisations.

Now, let us briefly review the computation of the coupling and coloured pieces, D and C. The latter is just $\delta_{a,b}$, where a and b are the colour indices of the quark and anti-quark. D, on the other hand, is the product of the quark gauge coupling to the vector boson, $g_{\overline{q}qV}$, and the coupling between 2 vector bosons and the Higgs boson, g_{VVh}. The former depends on the

helicity of the quark in chiral theories like the SM. Altogether, we obtain

$$D_{h_q}C = g_{\bar{q}qV}g_{VVh}\delta_{a,b} = \left.\begin{cases} -(g_2^2+g_Y^2)m_Z\left(\frac{1-h_q}{2}T_q^3 - Q_q s_W^2\right) \text{ for } V=Z \\ -\frac{g_2^2}{\sqrt{2}}m_W\left(\frac{1-h_q}{2}\right) \text{ for } V=W \end{cases}\right\}\delta_{a,b}, \tag{6.25}$$

where we show the specific results for the W and Z bosons, g_2 (g_Y) is the gauge couplings of the gauge group $\mathrm{SU}(2)_L$ ($\mathrm{U}(1)_Y$), and s_W is the sine of Weinberg's angle. Gathering together Eq. (6.24) and (6.25), we reproduce the SM amplitudes in Appendices 3.A.1 and 3.A.3 up to an arbitrary and unphysical phase[4].

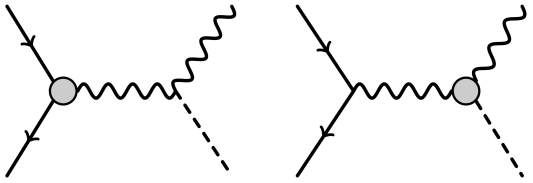

Figure 6.2.2: Feynman diagrams for the process $qq' \to Vh$ at tree-level including one higher-dimensional operator, represented by the grey circle, that modifies either the quark or Higgs gauge vertex.

The next step is to repeat the computation for the case where we include a dimension-6 operator from SMEFT. There are contributions like the ones in Fig. 6.2.2, where the higher-dimensional operator modifies the gauge vertices of the SM. The operators $\mathcal{O}_{\varphi q}^{(1),(3)}$ and $\mathcal{O}_{\varphi(u,d)}$, defined in Eq. (3.1)-(3.4), can generate the diagram on the left in Fig. 6.2.2; while the operators $\mathcal{O}_{\varphi \mathrm{W}}$ or $\mathcal{O}_{\varphi\widetilde{\mathrm{W}}}$, defined in Eq. (3.5) and (3.6), generate the diagram on the right. The kinematic structure of these diagrams is exactly the same than in the SM diagram, with only the coupling piece D receiving modifications at order $1/\Lambda^2$. Hence, the computation of $\mathcal{T}$ in the previous paragraphs can be reused.

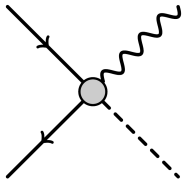

Figure 6.2.3: Feynman diagram for the process $qq' \to Vh$ at tree-level including one higher-dimensional operator, represented by the grey circle, that generates a contact term.

The remaining contribution comes from diagrams like the one in Fig. 6.2.3, where a higher-dimensional operator generates a contact term among all the involved particles. At dimension 6 in SMEFT, this can only be caused by the operators $\mathcal{O}_{\varphi q}^{(1),(3)}$ and $\mathcal{O}_{\varphi(u,d)}$. The part of those operators that generates the contact term follows the general structure

$$\mathcal{O} \supset hV_\mu \bar{q}'\gamma^\mu q, \tag{6.26}$$

and therefore the Lorentz structure is equal to the SM gauge coupling. Thus, the kinematic piece of the amplitude $\mathcal{T}$ will be like the corresponding one for the SM but without the propagator of

[4]This common phase, which might depend on the helicity, can be safely removed from the SM and BSM amplitudes as long as it appears in both for same helicity configuration.

the intermediate particle. More concretely, for the same helicity configuration considered before, we have

$$\mathcal{T}_{\text{Contact, }\frac{1}{\Lambda^2}}\left(-\frac{1}{2},\frac{1}{2},1\right)=\langle 2|\gamma^{\mu}|1]\epsilon^{-h_V}\left(-p_3\right). \tag{6.27}$$

The computation proceeds just like we showed before and the rest of differences with respect to the SM case will be contained in D. It can be easily checked that the results agree with the formulae in Appendices 3.A.1 and 3.A.3

6.2.3 Bootstrapping massless helicity amplitudes

What we call "bootstrap" consists basically of constraining or building physical observables (or objects very close to them) from essential physical and mathematical consistency requirements, instead of computing them from a microscopic model [315]. That is the spirit that we will follow during the rest of this chapter. In fact, massless 3-point amplitudes are completely fixed by the massless little group, locality and the special 3-particle kinematics [54, 55, 305]. There are only 2 non-trivial solutions if we allow for complex momenta: holomorphic, where we only use triangle brackets, and anti-holomorphic, using only square brackets. The general formula is given by [55, 305]:

$$\mathcal{M}\left(1^{h_1},2^{h_2},3^{h_3}\right)=g\begin{cases}\langle 1|2\rangle^{-h_1-h_2+h_3}\,\langle 2|3\rangle^{h_1-h_2-h_3}\,\langle 3|1\rangle^{-h_1+h_2-h_3}, & \text{for } h<0 \quad \text{(H)},\\ [1|2]^{h_1+h_2-h_3}\,\;[2|3]^{-h_1+h_2+h_3}\,[3|1]^{h_1-h_2+h_3}, & \text{for } h>0 \quad \text{(AH)},\end{cases} \tag{6.28}$$

where $h=\sum_{i=1}^{3}h_i$. The key property that allows such a strict constrain on the massless amplitudes is its transformation under the Little-Group. In general, a massless amplitude is a Lorentz-invariant function of the helicity spinors that transforms under a Little-Group rescaling as

$$\mathcal{M}\to t^{-2h}\mathcal{M}, \tag{6.29}$$

where h is defined as before, but with the sum running over all the particles in the amplitude. The rescaling factor of the amplitude is usually called "helicity weight" [54, 305]. Finally, let us remind that a n-point amplitude has mass dimension [55]

$$[\mathcal{M}_n]=4-n, \tag{6.30}$$

hence the coupling constant g in Eq. (6.28) has a mass dimension [54, 55]

$$[g]=1-|h|. \tag{6.31}$$

This already hints that renormalisable interactions might only generate amplitudes with certain helicity configurations.

We move now onto the 4-point amplitudes, which can be split into 2 contributions,

$$\mathcal{M}\left(1,2,3,4\right)=\mathcal{M}\left(1,2,3,4\right)_{NF}+\mathcal{M}\left(1,2,3,4\right)_{F}, \tag{6.32}$$

where the first piece is known as the non-factorisable amplitude and is generated by 4-point contact interactions. This piece is constrained by the helicity of the external states in a similar way to the 3-point amplitude, but it is not enough to determine it uniquely. In general, it will be a linear combination of independent spinor structures that correspond to the same helicity state. In some cases, this non-factorisable term vanishes on-shell or is determined by additional symmetries [305, 316].

The second piece in Eq. (6.32), $\mathcal{M}(1,2,3,4)_F$, is called the factorizable part of the amplitude.

It can be obtained sticking together 3-point amplitudes and using on-shell recursion relations that enforce the correct factorization. We focus on the case where the factorisable amplitude is at tree-level. This confers to the amplitude a very simple analytic structure that is captured entirely by its poles, which can only be simple. To respect locality, the only possible origin of those simple poles are the propagators of exchanged particles that go on-shell in the pole. This means that the residue of the 4-point amplitude is determined by two on-shell 3-point subamplitudes.

Then, we can express the factorizable part of the 4-point amplitude as[5]

$$\mathcal{M}(1,2,3,4)_F = \sum_I \mathcal{M}_L(1,2,I)\frac{1}{p_I^2}\mathcal{M}_R(I,3,4) = \sum_I$$

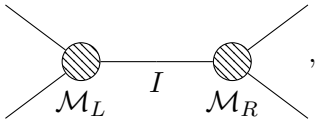

, (6.33)

where the sum runs over all possible tree-level Feynman diagrams and all possible intermediate on-shell particles. This "on-shell recursion relation" can be easily generalised to construct n-point amplitudes from $(n-1)$-point amplitudes. Additionally, this expression is manifestly gauge invariant [305].

The construction of higher-point amplitudes with recursion relations imposed by locality is a very powerful method. It can be used to exclude the existence of a theory with a single self-interacting massless spin-1 particle, and if there are several copies of such a particle, the coupling constant must satisfy the Jacobi identity [54]. The same analysis can be extended to higher spins, including gravity. It also shows that consistent theories with three-particle amplitudes satisfying $h_1 + h_2 + h_3 = 0$ are only allowed for scalars, i.e. with $h_1 = h_2 = h_3 = 0$ [54]. The last example we want to mention is that the Britto-Cachazo-Feng-Witten (BCFW) recursion relations [317, 318] can be used to obtain all higher-point gluon (graviton) tree-level on-shell amplitudes from the input of just the 3-point gluon (graviton) on-shell amplitudes [305].

6.3 Towards a replacement for EFTs with Scattering Amplitudes

The attempt to parametrize BSM Physics by assuming the SM spectrum and building all the possible on-shell scattering amplitudes allowed by unitarity, Lorentz invariance and global symmetries has become what we call the Scattering Amplitudes for BSM program. A similar and related program is the positivity program, which looks for constraints on higher-dimensional operators from mathematical properties of the amplitudes, although usually making a heavier use of QFT and Lagrangians. The positivity program will not be covered in this work and more about it can be found for example in Ref. [47, 48, 319]

The strategy of avoiding QFT and just working with scattering matrix elements is not completely new. In fact, it was a very popular theoretical tool during the 1950-1960s, when QFT seemed plagued of infinities that could only be erased for the simple case of QED. Once UV models for the strong and weak interaction were found in QCD and QFD, allowing for precise predictions of observables, the scattering matrix moved out of the spotlight. Interestingly, there were very early derivations of some SM features using scattering amplitudes and imposing perturbative tree-level unitarity [320–323].

The situation in which scattering amplitudes reached their peak of popularity highlights one of the cornerstones of the program: its bottom-up essence. This makes it ideal for when there is no good candidate (or no candidate at all) for an UV theory and ones desires to include all the possibilities. Moreover, the number of assumptions needed is minimal and they are

[5] There are certain conditions that must be fulfilled for this to be valid. These are related to the convergence in the infinity of the on-shell amplitude after a complex momentum shift. See Chapter 3 of Ref. [305] for details.

rooted in basic features of the theory and our observations [56]. Additionally, using on-shell amplitudes brings the advantage of dealing only with physical objects. This means avoiding gauge redundancies or operators related by EOMs and/or integration by parts [56]. Hence, the bottom-up parametrization of BSM Physics might become simpler without losing generality.

A goal of the program is to obtain a fully on-shell description of the SMEFT or, more generally, HEFT [55]. One starts with three-point amplitudes among all the SM particles and then, via recursion relations and adding the non-factorisable pieces, one could build systematically all the higher-point amplitudes. This is the same that has been done for some simpler theories [305].

Even before reaching the ultimate goal of constructing all the n-point amplitudes, there are several interesting questions that one can ask along the way [55]. Which features of the SMEFT and/or the SM are already encoded there without the need of quantum fields? How do different BSM models express themselves in the language of scattering amplitudes? Can this new perspective give us new insights on how to distinguish different possible completions of the SM? Could this new description lead us to find new and better observables?

However, for this program to work, we need one key element that we have not presented yet: a general extension of massive helicity spinors to the massive case that allows us to build massive scattering amplitudes by bootstrapping them and not relying on Feynman diagrams derived from Lagrangians. The condition of describing massive on-shell momenta is unavoidable if one wants to describe SMEFT (or the just the SM) in a bottom-up approach, since the broken phase is the only natural option to consider and most of the particles are massive there [56]. The proposal for massive helicity spinors presented in subsection 6.2.2 does not offer a clear path towards higher spins nor insight on how to bootstrap massive amplitudes. We will use the next section to present a suitable generalisation that was found a few years ago [54].

Before delving into the formalism, we would like to quickly review the results already available in the literature. Ref. [324] built all the 3-point massive amplitudes of the SM, including gravitational vertices, and studied their high-energy limit. A tree-level EFT including gluons coupled to an scalar or a vector boson was studied comprehensively in Ref. [325]. A similar task, but only using the bosons in the EW sector of SMEFT was completed shortly after in Ref. [55], which also mapped their amplitudes to the corresponding sector of SMEFT at dimension-6 and studied the 4-point amplitude $VVhh$ in the SM to find relations among the couplings that are a landmark of gauge symmetry and the SM Higgs. This study was enlarged by Ref. [56], which included fermions to replicate more accurately the particle content of the EW sector of SMEFT. They computed all the 3-point amplitudes including higher-dimensional corrections and studied their high-energy behaviour, which is enough to, for example, uncover the need of a antisymmetric coupling among different massive spin-1 bosons [56]. Additionally, they computed the 4-point amplitude $\psi^c\psi Zh$ and its high-energy limit, from where the need of a Higgs mechanism for the fermion masses in chiral theories was rederived [56]. In a similar spirit, Ref. [326] studies neutrino oscillations and derives the PMNS matrix from on-shell massive amplitudes. A first attempt to use on-shell amplitudes to build an EFT for dark-matter was done in Ref. [327], focusing on higher-spin dark-matter.

A different work direction has been the development of systematic procedures to obtain basis of amplitudes and operators. Ref. [328] presents a general method to build non-factorisable on-shell amplitudes and establish their bijective correspondence to an independent and complete operator basis of an EFT. They apply it to SMEFT at dimension 6, where their basis correspond to the Weinberg's operator and the Warsaw basis up to linear combinations. Ref. [329] establishes a formula to obtain the minimal dimension of the operator leading to any given helicity amplitude and present a systematic procedure to eliminate redundancies. A general method to obtain 4-point contact terms involving massive particles of spin up to 1 is presented in Ref. [330]. Then, Ref. [331] aims at the same problem and presents an even more general procedure and results.

Let us stress that obtaining 4-point contact terms in the massive case is highly non-trivial due to redundancies and dependencies among spinor structures.

6.4 Massive helicity amplitudes

6.4.1 Massive helicity spinors

The extension of the helicity spinor formalism to the massive case has been attacked by different authors. From here on, we follow Ref. [54] and the conventions in Ref. [56]. Our starting point will be noticing that for a general on-shell momentum we have

$$\det\left(p_\mu \sigma^\mu_{\alpha\dot{\alpha}}\right) = \det\left(p_{\alpha\dot{\alpha}}\right) = \frac{1}{2}\epsilon^{\alpha\beta}\epsilon^{\dot{\alpha}\dot{\beta}} p_{\alpha\dot{\alpha}} p_{\beta\dot{\beta}} = m^2. \tag{6.34}$$

Hence, in the massless case, $p_{\alpha\dot{\alpha}}$ is a rank-1 2×2 matrix which therefore can be written as the direct product of two 2-component vectors, just as it was done in Eq. (6.1). This does not work for the massive case because $p_{\alpha\dot{\alpha}}$ has rank 2.

However, a rank-2 matrix can be written as the sum of two independent rank-1 matrices. This leads to decompose a massive on-shell momentum in two sets of helicity spinors as

$$\mathbf{p}_{\alpha\dot{\alpha}} = \lambda^I_\alpha \tilde{\lambda}_{I,\dot{\alpha}} = |\mathbf{p}\rangle^I_\alpha [\mathbf{p}|_{I,\dot{\alpha}}, \tag{6.35}$$

where $I = 1, 2$ and boldface is used to denote a massive momentum and its corresponding spinors. The index I is contracted via a Levi-Civita tensor as usual. In fact, the index I is the Little Group index in the massive case. For massive momentum, the Little Group is SU(2) and hence the spinors transform under it as

$$|\mathbf{p}\rangle^I_\alpha \to W^I_J |\mathbf{p}\rangle^J_\alpha, \quad [\mathbf{p}|_{I,\dot{\alpha}} \to \left(W^{-1}\right)^J_I [\mathbf{p}|_{J,\dot{\alpha}}, \tag{6.36}$$

where W^I_J is, for real momentum, a matrix in the SU(2) subgroup of $\mathrm{SL}(2,\mathbb{C})$[6]. Angle and square helicity spinors can be exchanged easily by using the Dirac equation of motion (EOM):

$$\mathbf{p}_{\alpha\dot{\alpha}}|\mathbf{p}]^{I,\dot{\alpha}} = m|\mathbf{p}\rangle^I_\alpha, \quad \overline{\mathbf{p}}^{\dot{\alpha}\alpha}|\mathbf{p}\rangle^I_\alpha = m|\mathbf{p}]^{I,\dot{\alpha}}, \quad [\mathbf{p}|^I_{\dot{\alpha}}\overline{\mathbf{p}}^{\dot{\alpha}\alpha} = -m\langle\mathbf{p}|^{I,\alpha}, \quad \langle\mathbf{p}|^{I,\alpha}\mathbf{p}_{\alpha\dot{\alpha}} = -m[\mathbf{p}|^I_{\dot{\alpha}}. \tag{6.37}$$

These massive helicity spinors are easily extendable to particles of any spin S. In fact, all the equations presented up to here are independent of the particle spin. The situation changes when one wants to use them to write down an amplitude, which should reflect the possible helicity (polarisation) states of the external particles. However, the generalisation is straightforward since any spin representation can be obtained by combining spin-1/2 representations, and the massive helicity spinors are precisely doublets of SU(2) [54].

More precisely, the polarization of a massive particle of spin S can be represented by a completely symmetric SU(2) tensor of rank $2S$. An amplitude that includes such particle will carry Little Group indices $I_1, ..., I_{2S}$ and must be fully symmetric in them. Thus, in an amplitude containing a fermion with momentum p and a vector boson of momentum q, we should find one spinor $|\mathbf{p}]^I$ and two spinors $|\mathbf{q}]^{\{J_1}|\mathbf{q}]^{J_2\}}$, the latter with their indices properly symmetrized as indicated [54, 56]. This fact will be widely used in Section 6.4.2 to bootstrap massive scattering amplitudes.

Notice that Eq. (6.35) is equivalent to writing $\mathbf{p}_\mu$ as the sum of two light-like momenta p^I_μ and then rewriting those two with massless helicity spinors. The choice of p^I_μ is arbitrary,

[6] For general complex momentum, $W^I_J \in \mathrm{GL}(2)$. GL(2) is reduced to SL(2) after choosing $\det\left(|\mathbf{p}\rangle^I_\alpha\right) = \det\left(|\mathbf{p}]_{I,\dot{\alpha}}\right) = m$

which amounts to the arbitrary choice of a spin quantization axis. Different values for $I_1, ..., I_{2s}$ yield the different possible polarizations of a particle along the chosen axis. For instance, the transverse polarizations of a spin-1 massive particle are obtained for $I_1 = I_2 = 1, 2$, while the case $I_1 \neq I_2$ corresponds to the longitudinal polarization. However, there is a particularly convenient choice of p_μ^I that we will cover in the subsection 6.4.3.

Concluding this subsection, with the formalism here explained we can write the polarisation vector of a massive spin-1 boson as

$$\varepsilon_\mu^{\{IJ\}} = \frac{\langle \mathbf{p}^{\{I}|\sigma_\mu|\mathbf{p}^{J\}}]}{\sqrt{2}m}, \tag{6.38}$$

or with dotted and undotted indices,

$$\varepsilon_{\alpha\dot{\alpha}}^{\{IJ\}} = \sqrt{2}\frac{|\mathbf{p}\rangle_\alpha^{\{I}[\mathbf{p}|_{\dot{\alpha}}^{J\}}}{m}. \tag{6.39}$$

The two transverse polarisations, + and −, and the longitudinal one are identified as

$$\begin{aligned}
\varepsilon_\mu^+ \equiv \varepsilon_\mu^{11} &= \frac{\langle \mathbf{p}^1|\sigma_\mu|\mathbf{p}^1]}{\sqrt{2}m}, \\
\varepsilon_\mu^- \equiv \varepsilon_\mu^{22} &= \frac{\langle \mathbf{p}^2|\sigma_\mu|\mathbf{p}^2]}{\sqrt{2}m}, \\
\varepsilon_\mu^0 \equiv \varepsilon_\mu^{\{12\}} &= \frac{\langle \mathbf{p}^1|\sigma_\mu|\mathbf{p}^2] + \langle \mathbf{p}^2|\sigma_\mu|\mathbf{p}^1]}{2m},
\end{aligned} \tag{6.40}$$

where we have used the symmetrisation convention that can be found in App. 6.A. The similarity with the convention used in subsection 6.2.2 is clear, and indeed they can be matched by the choosing an appropriate reference vector. Also, the convention in this subsection yields expressions that are simpler and easier to generalise.

6.4.2 Bootstrapping massive amplitudes

In the massive case, the scattering amplitudes are covariant under the SU(2) Little-Group, with the representation under such group fixed by the spin of each particle. Hence, there is no concept of "helicity weight". Still, Little-Group covariance constrains powerfully the allowed structure of massive amplitudes. More precisely, an amplitude involving 3 particles of spin S_1, S_2, and S_3 will carry the Little-Group indices of the 3 particles and will be completely symmetric over them, i.e.

$$\mathcal{M}(\mathbf{1},\mathbf{2},\mathbf{3}) = \mathcal{M}_3^{\{I_1^{(1)},...,I_{2S_1}^{(1)}\},\{I_1^{(2)},...,I_{2S_2}^{(2)}\},\{I_1^{(3)},...,I_{2S_3}^{(3)}\}}, \tag{6.41}$$

where $I_i^{(n)}$ is the i-th Little-Group index of the n-th particle. It is interesting to notice that one can expand the amplitude in powers of $|\mathbf{p_i}\rangle_\alpha^I$ since any $[\mathbf{p_i}|^{I,\dot{\alpha}}$ can be exchanged via the EOM, Eq. (6.37). Thus,

$$\mathcal{M}_3^{\{I_i^{(1)}\},\{I_i^{(2)}\},\{I_i^{(3)}\}} = \prod_{i=1}^{3}\left(|\mathbf{p_i}\rangle_{\alpha_1^{(i)}}^{I_1^{(i)}}...|\mathbf{p_i}\rangle_{\alpha_{2S_i}^{(i)}}^{I_{2S_i}^{(i)}}\right)\mathcal{M}_3^{\{\alpha_1^{(1)},...,\alpha_{2S_1}^{(1)}\},\{\alpha_1^{(2)},...,\alpha_{2S_2}^{(2)}\},\{\alpha_1^{(3)},...,\alpha_{2S_3}^{(3)}\}}, \tag{6.42}$$

where $\alpha_i^{(j)}$ is the i-th Lorentz index of the j-th particle.

Now, the task of building the 3-point amplitude is reduced to find a basis for the symmetric tensor $\mathcal{M}_3^{\{\alpha_1^{(1)},...,\alpha_{2S_1}^{(1)}\},\{\alpha_1^{(2)},...,\alpha_{2S_2}^{(2)}\},\{\alpha_1^{(3)},...,\alpha_{2S_3}^{(3)}\}}$ in the $\mathrm{SL}(2,\mathbb{C})$ space. Here we will only cover the

fully massive case, while a general discussion can be found in Section 4 of Ref. [54]. A possible choice is [54],

$$\mathcal{O}_{\alpha\beta} = \mathbf{p}_{1,\{\alpha\dot{\beta}}\mathbf{p}_{2,\beta\}}^{\dot{\beta}}, \quad \epsilon_{\alpha\beta}. \tag{6.43}$$

Although this choice allows for a systematic and well justified construction, it is not the most practical. It is possible to prove that an equivalent way of building the amplitudes is taking the following basis [324]:

$$\epsilon_{\dot{\alpha}\dot{\beta}}, \quad \epsilon_{\alpha\beta}, \tag{6.44}$$

and using in the expansion of Eq. 6.41 both squared and triangle spinors. As we said before, for a particle of spin S, there should be $2S$ spinors, either square or triangle. Let us show how practical this procedure is with a very simple example.

Consider a massive fermion ψ, its conjugate (anti-fermion) ψ^c and a massive spin-1 vector boson V. Let us compute the 3-point amplitude involving them, i.e. the equivalent of a gauge coupling for a fermion with a massive gauge boson (but we have assumed nothing about gauge symmetries). If we number the anti-fermion and fermion as **1** and **2** respectively, we know that we will need one spinor $|\mathbf{1}\rangle_{\alpha}^{I^{(1)}}$ (or $|\mathbf{1}]_{\dot{\alpha}}^{I^{(1)}}$) and one spinor $|\mathbf{2}\rangle_{\alpha}^{I^{(2)}}$ (or $|\mathbf{2}]_{\dot{\alpha}}^{I^{(2)}}$). The presence of a spin-1 particle requires the presence of 2 spinors, which can be both triangle, both square or one of each type. The Little-Group indices of these 2 latter spinors must be symmetrised, e.g. $|\mathbf{3}\rangle_{\alpha}^{\{I_1^{(3)}}|\mathbf{3}]_{\dot{\alpha}}^{I_2^{(3)}\}} \equiv |\mathbf{3}\rangle|\mathbf{3}]$[7]. Then, it is clear that the most general amplitude that we can write for these particles is [56]

$$\mathcal{M}\left(\mathbf{1}_{\psi^c}, \mathbf{2}_{\psi}, \mathbf{3}_V\right) = \frac{c^R_{\psi^c\psi V}}{\overline{\Lambda}}[\mathbf{1}|\mathbf{3}][\mathbf{2}|\mathbf{3}] + \frac{c^{LR0}_{\psi^c\psi V}}{m_V}\langle\mathbf{1}|\mathbf{3}\rangle[\mathbf{2}|\mathbf{3}] + \frac{c^{RL0}_{\psi^c\psi V}}{m_V}[\mathbf{1}|\mathbf{3}]\langle\mathbf{2}|\mathbf{3}\rangle + \frac{c^L_{\psi^c\psi V}}{\overline{\Lambda}}\langle\mathbf{1}|\mathbf{3}\rangle\langle\mathbf{2}|\mathbf{3}\rangle, \tag{6.45}$$

where we can see that all the independent spinor structures must be summed with independent coefficients, and we omit writing the fully symmetrised Little-Group indices of the amplitude and the spinor structures. We also introduced the vector boson mass m_V and the cutoff $\overline{\Lambda}$ of the general EFT that would generate this amplitude. The coefficients and the cutoff are the next topics we will discuss in detail.

The coefficients of the spinor structures must be Lorentz invariants. Hence, in general, they are functions of the Mandelstam variables $s_{ij} = (p_i + p_j)^2$. However, for the special case of 3-point amplitudes, it is trivial to show that all the possible Mandelstam variables are just a combination of the squared masses of the external particles, and hence the coefficients are constant. In 4 and higher-point amplitudes, such simplification is not possible and the dependence on the Mandelstam variables must be considered [54]. Imposing perturbative tree-level unitarity yields, in general, correlations among coefficients.

Three-point amplitudes might depend on various scales, such as the particle masses and the EFT cutoff $\overline{\Lambda}$. In fact, these are the only dimensionful parameters that appear in the computation of scattering amplitudes. For instance, scalar vacuum expectation values do not appear explicitly. In a bottom-up approach, $\overline{\Lambda}$ shall be understood as the cutoff of the broken-phase theory. The power of this cutoff that appears in an amplitude might be different from the unbroken phase. More precisely, terms in an amplitude suppressed by $\overline{\Lambda}^n$ can be generated by unbroken-phase theory operators of order m^k/Λ^{n+k}, for $k \geqslant 0$, where m is a generic external particle mass and Λ is the unbroken-phase cutoff.

The assignment of powers of $\overline{\Lambda}$ to different terms of a three-point amplitudes can be justified via the high-energy limit to be discussed in subsection 6.4.3 and by looking at the growth of

[7] From now on, the Little-Group indices of external particles in amplitudes should be understood as being symmetrised. We will avoid writing them explicitly unless required for reasons of clarity.

4-point amplitudes constructed by gluing 3-point amplitudes [56]. A simple justification is that, since 3-point amplitudes have mass dimension 1 according to Eq. 6.30, hence a linear growth with energy is allowed by perturbative unitarity, but growths with a power $n \geqslant 2$ must be suppressed by $\overline{\Lambda}^n$. We will show how to compute the growth with energy in subsection 6.4.3. The rule explained above has the implicit assumption that the NP above $\overline{\Lambda}$ is decoupling. If it were not decoupling, $\overline{\Lambda}$ can not be taken much higher than m and a correct assignment should be performed by looking systematically at higher-point amplitudes, which has not been performed yet for SMEFT or HEFT [56].

If we considered only renormalisable interactions, i.e. not suppressed by the cutoff, the emergence of gauge symmetries would be expected. By relaxing this requirement at the non-renormalisable level, the bottom-up approach also allows to consider general extensions of the SM [56].

Before moving onto 4-point amplitudes, we want to use the simple example shown before to discuss CP properties. Parity sends $|\mathbf{p}\rangle^I \leftrightarrow |\mathbf{p}]_I$ and $|\mathbf{p}]^I \leftrightarrow -|\mathbf{p}\rangle_I$. Then, under the assumption that $\mathbf{1}_{\psi^c}$ and $\mathbf{2}_{\psi}$ are conjugate of each other, CP transformations would interchange their labels and flip all the helicities. This allows us to classify the spinor structures in two classes according to their CP transformation properties. On one hand, $[\mathbf{1}|\mathbf{3}]\langle\mathbf{2}|\mathbf{3}\rangle$ and $\langle\mathbf{1}|\mathbf{3}\rangle[\mathbf{2}|\mathbf{3}]$ are self-conjugate, while on the other hand $[\mathbf{1}|\mathbf{3}][\mathbf{2}|\mathbf{3}]$ and $\langle\mathbf{1}|\mathbf{3}\rangle\langle\mathbf{2}|\mathbf{3}\rangle$ map one onto each other, revealing their nature of dipole operators [56]. However, we must tread carefully and make statements on CP based only on squared amplitudes, since the overall phase of an amplitude is unphysical.

Now, we focus on the construction of massive on-shell 4-point amplitudes. Just as in the massless case, these have a factorisable part and a non-factorisable part. The former contains single-particle poles and can be built by gluing two massive on-shell 3-point amplitudes with the appropriate propagator, which in this case will feature the mass of the exchanged particle.

For instance, let us consider the exchange of a massive vector boson, with mass m. The gluing prescription is [56]

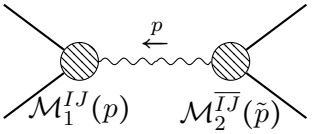

$$= -\frac{1}{p^2 - m^2}\left[\frac{\mathcal{M}_1^{IJ}(p) + \mathcal{M}_1^{JI}(p)}{2}\epsilon_{I\overline{I}}\epsilon_{J\overline{J}}\frac{\mathcal{M}_2^{\overline{IJ}}(\tilde{p}) + \mathcal{M}_2^{\overline{JI}}(\tilde{p})}{2}\right]_{p^2=m^2}, \tag{6.46}$$

where $\tilde{p}$ indicates that the momentum must be taken as outgoing w.r.t. that diagram, while we usually consider all incoming momenta. We have symmetrised explicitly the 3-point amplitudes and the quantity between square brackets must be computed with the intermediate particle on-shell. A general prescription for gluing amplitudes with intermediate particles with non-zero spin can be found in Appendix A.5 of Ref. [56], from where we take the conventions.

Also in full analogy to the massless case, there are amplitudes where the residue in one channel is non-local and has a pole in a different channel. In general, this occurs when the 3-point amplitudes include a minimal coupling, i.e. a coupling between a vector boson and 2 particles of spin S where the high-energy limit is dominated by the configuration with the 2 latter particles having opposite helicity [54]. In this situation, the requirement of consistent factorisation leads to the emergence of gauge-symmetry relations. This can also be used to justify that some high-spin particles can not be elementary (see Sect. 5 of Ref. [54] for details).

The non-factorisable part of the 4-point amplitude, which represents the contact interactions, is computed in the same way than the 3-point amplitude: the external particles determine the allowed spinors and then one must build all the independent kinematic structures with positive powers of those spinors and consistent with the Little Group. Although the construction of different Lorentz-invariant spinor structures is trivial, the selection of an independent set of them is rather cumbersome due to several relations rooted in Schouten identities and EOMs.

The development of some of this basis for several relevant cases and of a systematic procedure to find them has been tackled in some recent publications [330, 331].

The structures in a basis for a given amplitude must be combined with arbitrary coefficients. The positive-power condition ensures the consistent factorisation on single particle poles of the full amplitude, avoiding contributions from both factorisable and non-factorisable pieces to the residues. As it was discussed before, the general coefficients appearing in the non-factorisable piece must be considered as general functions of the Mandelstam variables s_{ij}. They can be suppressed by powers of the cutoff $\overline{\Lambda}$ accordingly to their energy growth and considering that perturbative unitarity forbids any energy growth in a 4-point amplitude.

6.4.3 The high-energy limit: connecting massive with massless

As we said before, there is a choice of p_μ^I that facilitates the connection between massive and massless helicity spinors. That choice is aligning the spatial part of p_μ^I with the direction of motion of the particle. For a particle moving along the z axis, we can denote

$$\mathbf{p}_\mu = p_{H,\mu} + p_{L,\mu}, \tag{6.47}$$

where

$$p_{H,\mu} = \frac{E+p}{2}\,(1,0,0,1)\,, \quad p_{L,\mu} = \frac{E-p}{2}\,(1,0,0,-1)\,. \tag{6.48}$$

In the high-energy limit, i.e. for $E >> m$, $p_{H,\mu}$ scales with E while $p_{L,\mu}$ does it with m^2/E. Hence, the former will dominate at high energies and the latter will do so at low energies. Given that both $p_{H,\mu}$ and $p_{L,\mu}$ are light-like, we can write

$$\mathbf{p}_{\alpha\dot\alpha} = |p_H\rangle_\alpha [p_H|_{\dot\alpha} + |p_L\rangle_\alpha [p_L|_{\dot\alpha}, \tag{6.49}$$

where on the right-hand side we have used massless helicity spinors, which obey all the usual relations (see Appendix 6.A for details). In particular, they fulfil [54, 56],

$$\langle p_H|p_L\rangle = [p_L|p_H] = m. \tag{6.50}$$

This decomposition implies that angle and square massive spinors will map onto massless spinors with definite (and opposite) helicity, as one expects from the behaviour of the massless spinors. An easy way of seeing this is the following. By comparison between Eq. (6.35) and (6.49), we notice that we have expanded the massive spinors as follows:

$$\begin{aligned} |\mathbf{p}\rangle_\alpha^I &= |p_H\rangle_\alpha\, \xi^{-,I} + |p_L\rangle_\alpha\, \xi^{+,I}, \\ |\mathbf{p}]^{I,\dot\alpha} &= |p_H]_\alpha\, \xi^{+,I} - |p_L]_\alpha\, \xi^{-,I}, \end{aligned} \tag{6.51}$$

where $\xi^\pm$ are 2-component vectors in the Little Group space that we choose as

$$\xi^+ = \begin{pmatrix} 1 \\ 0 \end{pmatrix}, \quad \xi^- = \begin{pmatrix} 0 \\ 1 \end{pmatrix}, \tag{6.52}$$

so that $I = 1$ ($I = 2$) picks the positive (negative) polarization. Thus, applying the high energy limit to massive helicity spinors boils down to do the replacements

$$|\mathbf{p}\rangle_\alpha^I \xrightarrow{E>>m} |p_H\rangle_\alpha\, \xi^{-,I}, \quad |\mathbf{p}]^{I,\dot\alpha} \xrightarrow{E>>m} |p_H]_\alpha\, \xi^{+,I}, \tag{6.53}$$

and similarly for their counterparts $\langle\mathbf{p}|$ and $[\mathbf{p}|$. As we said before, the square and angle massive

brackets map onto opposite helicities at high-energies.

The previous observation leads to a simple implementation of the high-energy limit, elegantly referred to as "unbolding" the spinors, that just entails sending $|p_L\rangle$, $|p_L]$ $\xrightarrow{E>>m}$ 0. The name of this implementation origins from that it implies [54, 56]

$$|\mathbf{p}\rangle \xrightarrow{E>>m} |p_H\rangle \equiv |p\rangle, \qquad |\mathbf{p}] \xrightarrow{E>>m} |p_H] \equiv |p]. \tag{6.54}$$

Despite its convenience, the unbolding procedure must be used carefully, particularly in the case of 3-point amplitudes, because it could lead to ill-defined results such as 0/0.

More formally, the high-energy limit can be defined via the redefinition $|p_L\rangle = m|\hat{p}_L\rangle$, $|p_L] = m|\hat{p}_L]$, and then taking $m \to 0$ for fixed E and $\overline{\Lambda}$ [54, 56]. This can be thought as equivalent to take $E \to \infty$ with the masses and $E/\overline{\Lambda}$ held constant. To avoid divergences and keep the particles on-shell, this limit should be understood in the complex plane.

How does the high-energy limit affect the amplitudes? Using the expansion in Eq. 6.51, it is easy to see that any amplitude decomposes into different spin states of the external particles as,

$$\mathcal{M}^{\{I_1 \dots I_{2S}\}} = \sum_h \left(\left(\xi^{+,I}\right)^{S+h} \left(\xi^{-,I}\right)^{S-h} \right)^{\{I_1 \dots I_{2S}\}} \mathcal{M}_h, \tag{6.55}$$

where we write it sketchily for the case of only one massive particle of spin S, with $h = -S, -S+1, ..., S$. The expansion is trivially generalisable. Therefore, the high-energy behaviour of each helicity configuration can be obtained by applying it individually to each $\mathcal{M}_h$. The latter are extracted directly from the above expansion because, with appropriate conventions [56], each symmetrised combination of ξ^+ and ξ^- of a particle can be identified with a different helicity state.

Now, we will use this high-energy limit to justify the suppression by the mass or the cut-off in 3-point amplitudes. We use the same amplitude that we computed in subsection 6.4.2, $\mathcal{M}\left(\mathbf{1}_{\psi^c}, \mathbf{2}_{\psi}, \mathbf{1}_V\right)$. The use of the unbolding procedure leads straightforwardly to

$$\begin{aligned} [\mathbf{1}|\mathbf{3}][\mathbf{2}|\mathbf{3}] &\to [1_H|3_H][2_H|3_H] = [1|3][2|3] \sim E^2, \\ \langle \mathbf{1}|\mathbf{3}\rangle\langle \mathbf{2}|\mathbf{3}\rangle &\to \langle 1_H|3_H\rangle\langle 2_H|3_H\rangle = \langle 1|3\rangle\langle 2|3\rangle \sim E^2. \end{aligned} \tag{6.56}$$

This quadratic growth with energy threatens perturbative unitarity unless $E < \overline{\Lambda}$. Hence, the coefficients $c^{L/R}_{\psi^c\psi V}$ should be suppressed by $\overline{\Lambda}$, where the power of $\overline{\Lambda}$ is determined by the fact that a linear growth with energy in a 3-point amplitude is acceptable [56].

Applying the same procedure to one of the other 2 spinor structures would render

$$\langle \mathbf{1}|\mathbf{3}\rangle[\mathbf{2}|\mathbf{3}] \to \langle 1|3\rangle[2|3] = -\langle 1|3|2] = \langle 1|\,(1+2)\,|2] = 0, \tag{6.57}$$

where we have used momentum conservation. The same result is obtained with $[\mathbf{1}|\mathbf{3}]\langle \mathbf{2}|\mathbf{3}\rangle$. This a direct consequence of the peculiar 3-particle kinematics [56, 305]. It also means that the leading piece in the high-energy limit must include at least one spinor of the type $|i_L]$ (or $|i_L\rangle$) and hence it will grow at most linearly with energy and one of the brackets will be $\sim m$. Since such growth is acceptable for 3-particle amplitudes, the coefficients $c^{RL0}_{\psi^c\psi V}$ can be suppressed just by a mass, which will cancel with one of the brackets at high-energy. This interaction, valid up to infinite energy, might be generated by renormalisable operators from a Lagrangian point of view.

6.5 A case of study: VVh and VVhh

In this last section, we will study the on-shell amplitudes VVh and $VVhh$, with $V = W, Z$. These amplitudes are interesting because their tree-level coupling in the SM obey a specific relation due to gauge symmetry:

$$\frac{\left(g^{SM}_{VVh}\right)^2}{2m_V^2} = g^{SM}_{VVhh}. \tag{6.58}$$

In several popular BSM scenarios, g_{VVh} and g_{VVhh} receive corrections that break the SM relation [332]. Moreover, this relation is also characteristic from the Higgs doublet structure. Hence, these amplitudes offer the opportunity to study deviations from the SM, possible ways to disentangle different BSM scenarios, a place where to look for differences between SMEFT and HEFT and a window into the nature of EWSB and the elementariness of the Higgs boson [332]. Also, if computed in enough generality, they could be easily extrapolated to models with additional scalars and vector bosons.

Ref. [55] already studied these amplitudes focusing on the SM case, here we extend such study to include more BSM contributions. With the inclusion of additional structures we pursue questions such as: Is there a high energy limit that prefers the SM or some other specific BSM scenario? Can these scattering amplitudes give us a new way to distinguish between different UV completions? What are the Lorentz structures that dominate the corrections to the SM at high energies and how are they generated? How much generality can we gain by computing with these techniques in comparison to the use of dimension-6 SMEFT operators?

We start by looking a the 3-point massive on-shell amplitude for 2 equal spin-1 bosons V and a scalar h, which can be written as [55, 56]

$$\mathcal{M}\left(\mathbf{1}_V, \mathbf{2}_V, \mathbf{3}_h\right) = \frac{c^R_{VVh}}{\overline{\Lambda}}[\mathbf{1}|\mathbf{2}]^2 + \frac{c^0_{VVh}}{m_V}[\mathbf{1}|\mathbf{2}]\langle\mathbf{1}|\mathbf{2}\rangle + \frac{c^L_{VVh}}{\overline{\Lambda}}\langle\mathbf{1}|\mathbf{2}\rangle^2. \tag{6.59}$$

Its high-energy behaviour was studied in detail in Ref. [56] and we will not repeat it here. The expression above includes all the possible spinor structures, independently of which UV completion of the SM is realised. Notice that this amplitude can be generalised to the case $VV'h$ with $V' \neq V$ by just renaming the coefficients.

The analysis of CP covariance of the VVh amplitude indicates that $[\mathbf{1}|\mathbf{2}]\langle\mathbf{1}|\mathbf{2}\rangle$ is invariant, while $[\mathbf{1}|\mathbf{2}]^2$ and $\langle\mathbf{1}|\mathbf{2}\rangle^2$ are exchanged one with each other. Making a connection with Lagrangians, the latter two structures must be generated by broken-phase operators like

$$\frac{c^{\pm}_{hVV}}{\overline{\Lambda}}\mathcal{O}^{\pm} = \frac{c^{\pm}_{hVV}}{\overline{\Lambda}}hV^{\pm}_{\mu\nu}V^{\pm,\mu\nu}, \tag{6.60}$$

where $V^{\pm}_{\mu\nu} = \left(V_{\mu\nu} \mp i\widetilde{V}_{\mu\nu}\right)/2$, with $V_{\mu\nu}$ and $\widetilde{V}_{\mu\nu}$ the gauge field strength and its dual, and the coefficients being defined as $c^{\pm}_{hVV} = c_{hVV} \pm i\widetilde{c}_{hVV}$. CP transformations will exchange $c^{+}_{hVV} \leftrightarrow c^{-}_{hVV}$ and then they will map directly onto the on-shell amplitude coefficients as $c^{\pm}_{hVV} \leftrightarrow c^{R/L}_{VVh}$ [55].

We move onto the 4-point amplitude $VVhh$ and start with its factorisable part, which we will compute at tree-level. The only possible intermediate particles are scalar and vector bosons. More precisely, a scalar boson can be exchanged via the s-channel and vector bosons are present

in the t and u-channels. Diagrammatically,

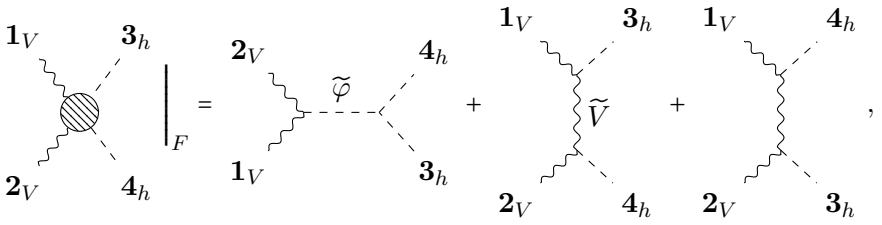

(6.61)

where we identify the intermediate particles as $\widetilde{\varphi}$ and $\widetilde{V}$ to indicate the possibility that they might be different from the external ones.

The s-channel is particularly easy to compute since the cubic scalar coupling lacks any spinor structure. The result is

$$\begin{aligned}&\mathcal{M}^{\tilde{\varphi}}\left(1_V,2_V,3_h,4_h\right)_s\times\left(s-m_{\tilde{\varphi}}^2\right)=\\&-m_h c_{hh\tilde{\varphi}}\left(\frac{c^R_{VV\widetilde{\varphi}}}{\Lambda^2}[\mathbf{1}|\mathbf{2}]^2+\frac{c^0_{VV\widetilde{\varphi}}}{m_V}[\mathbf{1}|\mathbf{2}]\langle\mathbf{1}|\mathbf{2}\rangle+\frac{c^L_{VV\widetilde{\varphi}}}{\Lambda^2}\langle\mathbf{1}|\mathbf{2}\rangle^2\right).\end{aligned}$$

Notice that the dimensionful part of the cubic scalar amplitude was arbitrarily chosen to be the Higgs mass [56]. Moreover, the coefficients of the $VV\widetilde{\varphi}$ vertex can be different from the ones in Eq. (6.59). If there were several scalars that can be exchanged in the s-channel, each of them will generate a contribution like the one in Eq. (6.62) and they have to be summed over.

The t-channel computation yields a rather more cumbersome result:

$$\begin{aligned}&\mathcal{M}^{\tilde{V}}\left(1_V,2_V,3_h,4_h\right)_t\times\left(t-m_{\tilde{V}}^2\right)=\\&-\frac{\left(c^0_{V\widetilde{V}h}\right)^2}{2}\left\{\frac{\left(m_V^2+m_{\tilde{V}}^2\right)\langle\mathbf{1}|\mathbf{2}\rangle[\mathbf{1}|\mathbf{2}]-m_V\left(\langle\mathbf{1}|\mathbf{2}\rangle\langle\mathbf{1}|p_3|\mathbf{2}]+[\mathbf{1}|\mathbf{2}][\mathbf{1}|\bar{p}_3|\mathbf{2}\rangle\right)+[\mathbf{1}|\bar{p}_3|\mathbf{2}\rangle\langle\mathbf{1}|p_3|\mathbf{2}]}{m_V^2}\right\}\\&-\frac{c^R_{V\widetilde{V}h}c^0_{V\widetilde{V}h}}{\Lambda}\frac{m_{\tilde{V}}}{m_V}\left(m_V\langle\mathbf{1}|\mathbf{2}\rangle[\mathbf{1}|\mathbf{2}]-[\mathbf{1}|\mathbf{2}][\mathbf{1}|\bar{p}_3|\mathbf{2}\rangle+m_V[\mathbf{1}|\mathbf{2}]^2-[\mathbf{1}|\mathbf{2}]\langle\mathbf{1}|p_3|\mathbf{2}]\right)-\frac{\left(c^R_{V\widetilde{V}h}\right)^2}{\Lambda^2}m_{\tilde{V}}^2[\mathbf{1}|\mathbf{2}]^2\\&-\frac{c^L_{V\widetilde{V}h}c^0_{V\widetilde{V}h}}{\Lambda}\frac{m_{\tilde{V}}}{m_V}\left(m_V\langle\mathbf{1}|\mathbf{2}\rangle[\mathbf{1}|\mathbf{2}]-\langle\mathbf{1}|\mathbf{2}\rangle\langle\mathbf{1}|p_3|\mathbf{2}]+m_V\langle\mathbf{1}|\mathbf{2}\rangle^2-\langle\mathbf{1}|\mathbf{2}\rangle[\mathbf{1}|\bar{p}_3|\mathbf{2}\rangle\right)-\frac{\left(c^L_{V\widetilde{V}h}\right)^2}{\Lambda^2}m_{\tilde{V}}^2\langle\mathbf{1}|\mathbf{2}\rangle^2\\&-\frac{c^R_{V\widetilde{V}h}c^L_{V\widetilde{V}h}}{\Lambda^2}\left(m_V^2\left(\langle\mathbf{1}|\mathbf{2}\rangle^2+[\mathbf{1}|\mathbf{2}]^2\right)+\left([\mathbf{1}|\bar{p}_3|\mathbf{2}\rangle\right)^2+\left(\langle\mathbf{1}|p_3|\mathbf{2}]\right)^2-2m_V\left(\langle\mathbf{1}|\mathbf{2}\rangle[\mathbf{1}|\bar{p}_3|\mathbf{2}\rangle+[\mathbf{1}|\mathbf{2}]\langle\mathbf{1}|p_3|\mathbf{2}]\right)\right).\end{aligned}$$

(6.62)

The u-channel can be obtained in a fully analogous computation and the result is

$$
\begin{aligned}
&\mathcal{M}^{\tilde{V}}\left(1_V,2_{V'},3_\varphi,4_{\varphi'}\right)_u\times\left(u-m_{\tilde{V}}^2\right)=\\
&-\frac{\left(c^0_{V\tilde{V}h}\right)^2}{2}\left\{\frac{\left(m_V^2+m_{\tilde{V}}^2\right)\langle\mathbf{1}|\mathbf{2}\rangle[\mathbf{1}|\mathbf{2}]+m_V\left(\langle\mathbf{1}|\mathbf{2}\rangle[\mathbf{1}|\bar{p}_3|\mathbf{2}\rangle+[\mathbf{1}|\mathbf{2}]\langle\mathbf{1}|p_3|\mathbf{2}\rangle\right)+[\mathbf{1}|\bar{p}_3|\mathbf{2}\rangle\langle\mathbf{1}|p_3|\mathbf{2}]}{m_Vm_V}\right\}\\
&-\frac{c^R_{V\tilde{V}h}c^0_{V\tilde{V}h}}{\Lambda}\frac{m_{\tilde{V}}}{m_V}\left(m_V[\mathbf{1}|\mathbf{2}]^2+[\mathbf{1}|\mathbf{2}][\mathbf{1}|\bar{p}_3|\mathbf{2}\rangle+m_V[\mathbf{1}|\mathbf{2}]\langle\mathbf{1}|\mathbf{2}\rangle+[\mathbf{1}|\mathbf{2}]\langle\mathbf{1}|p_3|\mathbf{2}]\right)-\frac{\left(c^R_{V\tilde{V}h}\right)^2}{\overline{\Lambda}^2}m_{\tilde{V}}^2[\mathbf{1}|\mathbf{2}]^2\\
&-\frac{c^L_{V\tilde{V}h}c^0_{V\tilde{V}h}}{\overline{\Lambda}}\frac{m_{\tilde{V}}}{m_V}\left(m_V\langle\mathbf{1}|\mathbf{2}\rangle^2+\langle\mathbf{1}|\mathbf{2}\rangle\langle\mathbf{1}|p_3|\mathbf{2}]+m_V\langle\mathbf{1}|\mathbf{2}\rangle[\mathbf{1}|\mathbf{2}]+\langle\mathbf{1}|\mathbf{2}\rangle[\mathbf{1}|\bar{p}_3|\mathbf{2}\rangle\right)-\frac{\left(c^L_{V\tilde{V}h}\right)^2}{\overline{\Lambda}^2}m_{\tilde{V}}^2\langle\mathbf{1}|\mathbf{2}\rangle^2\\
&-\frac{c^L_{V\tilde{V}h}c^R_{V\tilde{V}h}}{\overline{\Lambda}^2}\left(m_V^2\left(\langle\mathbf{1}|\mathbf{2}\rangle^2+[\mathbf{1}|\mathbf{2}]^2\right)+\left(\langle\mathbf{1}|p_3|\mathbf{2}]\right)^2+\left([\mathbf{1}|\bar{p}_3|\mathbf{2}\rangle\right)^2+2m_V\left(\langle\mathbf{1}|\mathbf{2}\rangle\langle\mathbf{1}|p_3|\mathbf{2}]+[\mathbf{1}|\mathbf{2}][\mathbf{1}|\bar{p}_3|\mathbf{2}\rangle\right)\right).
\end{aligned}
\tag{6.63}
$$

We have derived this amplitude including all the non-renormalisable contributions, extending the result in Ref. [55], which included only the renormalisable pieces.

The non-factorisable part of the 4-point amplitude can be written as

$$
\begin{aligned}
\mathcal{M}\left(\mathbf{1}_V,\mathbf{2}_V,\mathbf{3}_h,\mathbf{4}_h\right)_{NF}=\;& c^{(4,1)}_{VVhh}[\mathbf{1}|\mathbf{2}]\langle\mathbf{1}|\mathbf{2}\rangle+\frac{c^{(6,1)}_{VVhh}}{\overline{\Lambda}^2}[\mathbf{1}|\mathbf{p}_3|\mathbf{1}\rangle[\mathbf{2}|\mathbf{p}_3|\mathbf{2}\rangle+\frac{c^{(6,2)}_{VVhh}}{\overline{\Lambda}^2}[\mathbf{1}|\mathbf{2}][\mathbf{1}|\mathbf{p}_3|\mathbf{2}\rangle\\
&+\frac{c^{(6,3)}_{VVhh}}{\overline{\Lambda}^2}\langle\mathbf{1}|\mathbf{2}\rangle[\mathbf{1}|\mathbf{p}_3|\mathbf{2}\rangle+\frac{c^{(6,4)}_{VVhh}}{\overline{\Lambda}^2}[\mathbf{1}|\mathbf{2}]\langle\mathbf{1}|\mathbf{p}_3|\mathbf{2}]+\frac{c^{(6,5)}_{VVhh}}{\overline{\Lambda}^2}\langle\mathbf{1}|\mathbf{2}\rangle\langle\mathbf{1}|\mathbf{p}_3|\mathbf{2}\rangle\\
&+\frac{c^{(6,6)}_{VVhh}}{\overline{\Lambda}^2}\langle\mathbf{1}|\mathbf{2}\rangle^2+\frac{c^{(6,7)}_{VVhh}}{\overline{\Lambda}^2}[\mathbf{1}|\mathbf{2}]^2+\frac{c^{(8,1)}_{VVhh}}{\overline{\Lambda}^4}\left([\mathbf{1}|\bar{p}_3|\mathbf{2}\rangle^2-\langle\mathbf{1}|\bar{p}_3|\mathbf{2}]^2\right),
\end{aligned}
\tag{6.64}
$$

where the coefficient $c^{(n,i)}$ corresponds to a spinor structure that can be generated by broken-phase operators of dimension $d\geq n$ and i is just an order label within the basis for a given dimension n [330]. We have used the basis of spinor structures from Ref. [330] and the renormalisable part agrees with Ref. [55]. Notice that there is only one renormalisable spinor structure and thus corresponds to the SM coupling. There are seven structures that correspond to operators of dimension ≥ 6 and only one that requires an operator of dimension ≥ 8. The assignment of powers of the cutoff was performed according to the dimension n. Given that the main deviations from the SM are expected to come from operators of dimension 6, we will neglect the term with $c^{(8,1)}$ during the rest of our analysis.

It is interesting to notice that there is no dimension-6 operator in SMEFT that can generate these spinor structures labelled as $c^{(6,i)}$ [328]. Hence, they must be generated by operators that have a dimension higher than 6 in the unbroken phase and the broken-phase cutoff must be interpreted as $1/\overline{\Lambda}^2=m^n/\Lambda^{n+2}$, with $n>0$ and where $n+6$ is the dimension of the unbroken-phase operator. A further observation is that both the factorisable and non-factorisable pieces are easily generalisable to the case where the external vector bosons and/or the external scalars are not identical.

Our next step is studying the high-energy limit of this amplitude. First, we look for the relation between the VVh and $VVhh$ couplings found in the SM that ensures the unitarisation of vector boson scattering. In consequence, we will focus on the couplings that are present in the SM, and we will ignore all the spinor structures with coefficients suppressed by

$\overline{\Lambda}$. We are interested in the configuration with longitudinal polarisation for both vector bosons, $\mathcal{M}\left(\mathbf{1}_V^0, \mathbf{2}_V^0, \mathbf{3}_h, \mathbf{4}_h\right)$, where the superscript for the vector bosons indicate their polarisation, since this is the only configuration that might display a growth with energy in the SM [55, 332]. The analysis we will perform here was done previously in Ref. [332] and [55], here we will repeat it in a slightly more detailed way that in the latter and emphasize some interesting aspects.

In the high-energy limit, the factorisable part of the $VVhh$ amplitude shows a quadratic growth with the energy that comes from the t and u channels,

$$\begin{aligned}\mathcal{M}\left(\mathbf{1}_V^0, \mathbf{2}_V^0, \mathbf{3}_h, \mathbf{4}_h\right)_F &= \mathcal{M}\left(\mathbf{1}_V^0, \mathbf{2}_V^0, \mathbf{3}_h, \mathbf{4}_h\right)_{t+u} + \mathcal{O}\left(\frac{1}{m_V}\right) \\ &= -\frac{\left(c^0_{V\widetilde{V}h}\right)^2}{2m_V^2}\frac{t+u}{tu}\langle 1_H|3_H\rangle[3_H|2_H]\langle 2_H|3_H\rangle[3_H|1_H] + \mathcal{O}\left(\frac{1}{m_V}\right) \\ &= -\frac{\left(c^0_{V\widetilde{V}h}\right)^2}{2m_V^2}(t+u) + \mathcal{O}\left(\frac{1}{m_V}\right).\end{aligned} \tag{6.65}$$

The s-channel gives only sub-leading contributions since it behaves as a constant at high-energies. The non-factorisable part of the amplitude, restricted to renormalisable interactions, also shows a similar growth:

$$\begin{aligned}\mathcal{M}\left(\mathbf{1}_V^0, \mathbf{2}_V^0, \mathbf{3}_h, \mathbf{4}_h\right)_{NF} &= c^{(4,1)}_{VVhh}\langle 1_H|2_H\rangle[1_H|2_H] + \mathcal{O}(\frac{1}{m_V}) \\ &= -c^{(4,1)}_{VVhh}s + \mathcal{O}(\frac{1}{m_V}),\end{aligned} \tag{6.66}$$

where we neglect the terms of $c^{(4,1)}_{VVhh}$ that might depend on Mandelstam variables, since they are properly suppressed by powers of $\overline{\Lambda}$. Putting both pieces together, we have

$$\begin{aligned}\mathcal{M}\left(\mathbf{1}_V^0, \mathbf{2}_V^0, \mathbf{3}_h, \mathbf{4}_h\right) &= -c^{(4,1)}_{VVhh}\,s - \frac{\left(c^0_{V\widetilde{V}h}\right)^2}{2m_V^2}(t+u) + \mathcal{O}(\frac{1}{m_V}) \\ &= \left(\frac{\left(c^0_{V\widetilde{V}h}\right)^2}{2m_V^2} - c^{(4,1)}_{VVhh}\right)s + \mathcal{O}(\frac{1}{m_V}),\end{aligned} \tag{6.67}$$

since $s+t+u=0$ in the high-energy limit.

A growth with the square of the energy in a 4-point amplitude constitutes a violation of unitarity and hence must be forbidden in a renormalisable theory like the SM. To cancel such behaviour we must impose

$$\frac{\left(c^0_{V\widetilde{V}h}\right)^2}{2m_V^2} = c^{(4,1)}_{VVhh}. \tag{6.68}$$

It can be checked straightforwardly that this relation is satisfied by the SM after identifying

$$c^0_{V\widetilde{V}h}\Big|_{SM} = \begin{cases} g_2 m_W & \text{for } V=W \\ \frac{g_2}{2c_W}m_Z & \text{for } V=Z \end{cases}, \quad c^{(4,1)}_{VVhh}\Big|_{SM} = \begin{cases} \frac{g_2^2}{2} & \text{for } V=W \\ \frac{g_2^2}{8c_W^2} & \text{for } V=Z \end{cases}, \tag{6.69}$$

where g_2 is the $\mathrm{SU}(2)_L$ gauge coupling and $c_W = \cos(\theta_W)$ is the cosine of Weinberg's angle. Now, let us make some remarks about this result. First, we derived Eq. (6.68) without assum-

ing anything on which or how many scalars are exchanged in the s-channel, since the energy behaviour of such channel is blind to those details.

Second, Eq. (6.68) makes explicit that the condition exists even when the virtual vector boson is not identical to the external ones. If several species of spin-1 bosons can be exchanged in the t and u channels, the left-hand side of Eq. (6.68) should include a sum over them. Notice that in Ref. [56] the amplitude WZh was not considered because electric charge conservation is assumed. Here, we do not assume a priori such conservation and therefore $V\widetilde{V}h$ is allowed.

Third, it is interesting to analyse in which BSM scenarios this cancellation is spoiled. Under the assumption that no other spinor structure enters in the leading piece in Eq. (6.67), all the BSM effects will be encoded as corrections to $c^{(4,1)}_{VVhh}$ and $c^{0}_{V\widetilde{V}h}$ at higher orders in $1/\overline{\Lambda}$ (notice that we are again just keeping the constant piece of $c^{(4,1)}_{VVhh}$). Hence, from 6.68 one can derive cancellation conditions order by order in $1/\overline{\Lambda}$. A simple matching to dimension-6 SMEFT operators shows that these are violated for any modification of these couplings at order $1/\Lambda^2$ [332].

Now, we analyse the high-energy limit of the whole non-factorisable piece of the amplitude, which is absent from the literature so far. The objective of this is two-fold. On one hand, it allows us to identify what kind of growth with energy is generated by the different spinor structures. On the other hand, thanks to this procedure we can identify which final polarisation states might be more interesting to probe a certain type of spinor structure. For a full connection with similar studies using SMEFT, an identification of the higher-dimensional operators that generate the different spinor structures is required and is left for future work.

Polarisation	Coefficient	Spinor structure
+000	$\frac{c^{(6,1)}_{VVhh}}{\overline{\Lambda}^2}$	$-\langle 1_L\vert 3_H\rangle[1_H\vert 3_H]\,u$
	$\frac{c^{(6,2)}_{VVhh}}{\overline{\Lambda}^2}$	$[1_H\vert 2_H]\frac{[1_H\vert 3_H]}{[2_H\vert 3_H]}\,u$
−000	$\frac{c^{(6,1)}_{VVhh}}{\overline{\Lambda}^2}$	$[1_L\vert 3_H]\langle 1_H\vert 3_H\rangle u$
	$\frac{c^{(6,5)}_{VVhh}}{\overline{\Lambda}^2}$	$\langle 1_H\vert 2_H\rangle\frac{\langle 1_H\vert 3_H\rangle}{\langle 2_H\vert 3_H\rangle}u$
0 + 00	$\frac{c^{(6,1)}_{VVhh}}{\overline{\Lambda}^2}$	$-\langle 2_L\vert 3_H\rangle[2_H\vert 3_H]t$
	$\frac{c^{(6,4)}_{VVhh}}{\overline{\Lambda}^2}$	$[2_H\vert 1_H]\frac{[2_H\vert 3_H]}{[1_H\vert 3_H]}t$
0 − 00	$\frac{c^{(6,1)}_{VVhh}}{\overline{\Lambda}^2}$	$[2_L\vert 3_H]\langle 2_H\vert 3_H\rangle t$
	$\frac{c^{(6,3)}_{VVhh}}{\overline{\Lambda}^2}$	$\langle 1_H\vert 2_H\rangle\frac{\langle 2_H\vert 3_H\rangle}{\langle 1_H\vert 3_H\rangle}t$

Table 6.5.1: Pieces of the amplitude $\mathcal{M}\left(\mathbf{1}_V,\mathbf{2}_V,\mathbf{3}_h,\mathbf{4}_h\right)_{NF}$ that grow like E^3 in the high-energy limit. The polarisation in the first column is given in the order $\mathbf{1}_V\,\mathbf{2}_V\,\mathbf{3}_h\,\mathbf{4}_h$.

There are several polarization states where there is a growth with energy. The one that grows the fastest, as E^4, is the fully longitudinal, and for such state the expression of the amplitude reduces to

$$\mathcal{M}\left(\mathbf{1}^0_V,\mathbf{2}^0_V,\mathbf{3}_h,\mathbf{4}_h\right)_{NF}\xrightarrow[m/E\to 0]{}\frac{c^{(6,1)}_{VVhh}}{\overline{\Lambda}^2}[1_H|3_H]\langle 1_H|3_H\rangle[2_H|3_H]\langle 2_H|3_H\rangle=\frac{c^{(6,1)}_{VVhh}}{\overline{\Lambda}^2}\,t\,u, \tag{6.70}$$

where we notice that this growth is due only to the spinor structure $[\mathbf{1}|\mathbf{p}_3|\mathbf{1}\rangle[\mathbf{2}|\mathbf{p}_3|\mathbf{2}\rangle$. We have preferred to use spinor structures that depend only on independent variables, giving up explicit Bose symmetry. However, the latter can be restored by using momentum conservation and relations among different spinor structures. The explicitly Bose symmetric version of $[\mathbf{1}|\mathbf{p}_3|\mathbf{1}\rangle[\mathbf{2}|\mathbf{p}_3|\mathbf{2}\rangle$ is $([\mathbf{1}|\mathbf{p}_3|\mathbf{1}\rangle[\mathbf{2}|\mathbf{p}_4|\mathbf{2}\rangle + [\mathbf{1}|\mathbf{p}_4|\mathbf{1}\rangle[\mathbf{2}|\mathbf{p}_3|\mathbf{2}\rangle)$, which clearly indicates that it must be generated by an operator containing $\partial_\mu h \partial_\nu h V^\mu V^\nu$. Off-shell gauge-symmetric operators that contain such structure are dimension-8 operators such as $Q^{(1)}_{H^4} = \left(D_\mu H^\dagger D_\nu H\right)\left(D^\nu H^\dagger D^\mu H\right)$ and $Q^{(1)}_{W^2H^2D^2} = \left(D^\mu H^\dagger D^\nu H\right) W^I_{\mu\rho} W^{I,\rho}_\nu$ [44]. A precise matching to a basis of dimension-8 operators is left for future work.

Polarization	Coefficient	Spinor structure
$++00$	$\frac{c^{(6,1)}_{VVhh}}{\Lambda^2}$	$[1_H\|3_H][2_H\|3_H]\langle 1_L\|3_H\rangle\langle 2_L\|3_H\rangle$
	$\frac{c^{(6,2)}_{VVhh}}{\Lambda^2}$	$[1_H\|2_H][1_H\|3_H]\langle 3_H\|2_L\rangle$
	$\frac{c^{(6,4)}_{VVhh}}{\Lambda^2}$	$[2_H\|1_H][2_H\|3_H]\langle 3_H\|1_L\rangle$
	$\frac{c^{(6,6)}_{VVhh}}{\Lambda^2}$	$[1_H\|2_H]^2$
$--00$	$\frac{c^{(6,1)}_{VVhh}}{\Lambda^2}$	$[1_L\|3_H][2_L\|3_H]\langle 1_H\|3_H\rangle\langle 2_H\|3_H\rangle$
	$\frac{c^{(6,3)}_{VVhh}}{\Lambda^2}$	$-\langle 1_H\|2_H\rangle[1_L\|3_H]\langle 2_H\|3_H\rangle$
	$\frac{c^{(6,5)}_{VVhh}}{\Lambda^2}$	$-\langle 1_H\|2_H\rangle[3_H\|2_L]\langle 1_H\|3_H\rangle$
	$\frac{c^{(6,7)}_{VVhh}}{\Lambda^2}$	$\langle 1_H\|2_H\rangle^2$
$+-00$	$\frac{c^{(6,1)}_{VVhh}}{\Lambda^2}$	$[1_H\|3_H][2_L\|3_H]\langle 1_L\|3_H\rangle\langle 2_H\|3_H\rangle$
	$\frac{c^{(6,2)}_{VVhh}}{\Lambda^2}$	$-[1_H\|2_L][1_H\|3_H]\langle 3_H\|2_H\rangle$
	$\frac{c^{(6,3)}_{VVhh}}{\Lambda^2}$	$\langle 1_L\|2_H\rangle[3_H\|1_H]\langle 2_H\|3_H\rangle$
$-+00$	$\frac{c^{(6,1)}_{VVhh}}{\Lambda^2}$	$-[1_L\|3_H][2_H\|3_H]\langle 1_H\|3_H\rangle\langle 2_L\|3_H\rangle$
	$\frac{c^{(6,4)}_{VVhh}}{\Lambda^2}$	$-[2_H\|1_L][2_H\|3_H]\langle 3_H\|1_H\rangle$
	$\frac{c^{(6,5)}_{VVhh}}{\Lambda^2}$	$\langle 1_H\|2_L\rangle[3_H\|2_H]\langle 1_H\|3_H\rangle$

Table 6.5.2: Pieces of the amplitude $\mathcal{M}\left(\mathbf{1}_V, \mathbf{2}_V, \mathbf{3}_h, \mathbf{4}_h\right)_{NF}$ that grow like E^2 in the high-energy limit.

Then, there are 5 operators that generate a growth with the cube of the energy, $\sim E^3$. This happens in the final states where one of the vector bosons is longitudinally polarized and the other is transverse. The terms of the amplitude with such growth are displayed in Table 6.5.1. It is remarkable that $c^{(6,1)}_{VVhh}$ also generates this growth. The other terms correspond to the spinor structure $[\mathbf{1}|\mathbf{2}][\mathbf{1}|\mathbf{p}_3|\mathbf{2}\rangle$ and its conjugates and permutations. The amplitudes with purely

transversely polarized vector bosons grow at most like the square of the energy and we collect their expressions in Table 6.5.2.

6.6 Conclusions

In this chapter, we have explored one of the many trails towards new theoretical tools to describe what we know. Our hope is that by looking with a different lens we do not only uncover features that had been overlooked but, most importantly, discover a new path forward. Just as the rise of symmetries led us to a deeper understanding in the middle of the 20th century, this might be the time to find a new paradigm [22, 23].

In the first sections, we showed how a relatively old tool, massless helicity spinors, can help us to compute more efficiently the quantities we need to compare with experimental results. We remarked how this technique is rooted in properties of the Lorentz group and how they also give a constructive principle for certain theories. However, the biggest leap forward comes from the generalisation of this technique to the massive case for all masses and spins, that we explored from Section 6.3 onwards.

We reviewed the massive helicity spinor formalism and explained how to use it to build on-shell scattering amplitudes that give a description equivalent to EFTs, but with fewer assumptions and greater generality. Then, we took some particular amplitudes, VVh and $VVhh$ and showed how their detailed study can bring some insights into how BSM effects might appear in observables.

There is still much work left to do in this field and it constitutes one of the most promising avenues to explore in the near future. Some future directions are the systematic matching to UV models, which might bring further insight via the identification of classes of spinor structures that are typical of certain UV scenarios. Two more specific questions related to it are which are the imprints that partial compositeness leaves in scattering amplitudes and how could we distinguish the existence of additional compact, possibly warped, space-time dimensions. The application of this formalism to EFTs with CP-odd scalars, such as axion EFTs, is another interesting direction to explore.

Appendix to Chapter 6

6.A Spinor conventions

6.A.1 Generalities

We use the mostly minus metric,

$$\eta_{\mu\nu} = \eta^{\mu\nu} = \mathrm{diag}\,(+1,-1,-1,-1)\,, \tag{6.71}$$

which implies $p^2 = m^2 > 0$ for massive particles. We define the gamma matrices as

$$\gamma^\mu = \begin{pmatrix} 0 & (\sigma^\mu)_{\alpha\dot\beta} \\ (\overline{\sigma}^\mu)^{\dot\alpha\beta} & 0 \end{pmatrix}, \quad \gamma^5 = i\gamma^0\gamma^1\gamma^2\gamma^3 = \begin{pmatrix} -1 & 0 \\ 0 & 1 \end{pmatrix}. \tag{6.72}$$

The definition of $\sigma^\mu_{\alpha\dot\alpha}$ and $\overline{\sigma}^{\dot\beta\beta}_\mu$ was already given in the main text (see Eq. (6.2) and text above it). Here, we note the following relation between them:

$$\sigma^\mu_{\alpha\dot\alpha}\overline{\sigma}^{\dot\beta\beta}_\mu = 2\delta^\beta_\alpha\delta^{\dot\beta}_{\dot\alpha}. \tag{6.73}$$

We define the Levi-Civita 2-dimensional tensors as

$$\epsilon^{IJ} = \epsilon^{\alpha\beta} = \epsilon^{\dot\alpha\dot\beta} = -\epsilon_{IJ} = -\epsilon_{\alpha\beta} = -\epsilon_{\dot\alpha\dot\beta} = \begin{pmatrix} 0 & 1 \\ -1 & 0 \end{pmatrix}. \tag{6.74}$$

Finally, our symmetrisation conventions are as follows. Given two different tensors A^I and B^J, we define their symmetric combination as

$$A^{\{I}B^{J\}} = \begin{cases} A^IB^I & \text{if } I = J \\ \frac{1}{\sqrt{2}}\left(A^IB^J + A^JB^I\right) & \text{if } I \neq J \end{cases}. \tag{6.75}$$

If both tensors turn out to be equal, we have the much simpler

$$A^IA^J = A^{\{I}A^{J\}}. \tag{6.76}$$

These conventions agree with the ones in Ref. [56].

6.A.2 Massless and massive spinors

For completeness, the decomposition of a massive momentum into spinors with raised indices is

$$\overline{\mathbf{p}}^{\dot\alpha\alpha} = \epsilon^{IJ}\tilde\lambda^{\dot\alpha}_I\lambda^\alpha_J = -\tilde\lambda^{I,\dot\alpha}\lambda^\alpha_J = -|p]^{I,\dot\alpha}\langle p|^\alpha_I. \tag{6.77}$$

In the high-energy limit, the decomposition becomes

$$\overline{\mathbf{p}}^{\dot{\alpha}\alpha} = |p_H]^{\dot{\alpha}}\langle p_H|^{\alpha} + |p_L]^{\dot{\alpha}}\langle p_L|^{\alpha}. \tag{6.78}$$

And the identification between the helicity spinors and the usual 4D Dirac spinors is

$$u^I(p) = \begin{pmatrix} |p\rangle_{\alpha}^{I} \\ |p]^{I,\dot{\alpha}} \end{pmatrix}, \qquad v^I(p) = \begin{pmatrix} |p\rangle_{\alpha}^{I} \\ -|p]^{I,\dot{\alpha}} \end{pmatrix}, \tag{6.79}$$

$$\overline{u}_I(p) = \begin{pmatrix} -\langle p|_I^{\alpha} & [p|_{I,\dot{\alpha}} \end{pmatrix}, \qquad \overline{v}_I(p) = \begin{pmatrix} \langle p|_I^{\alpha} & [p|_{I,\dot{\alpha}} \end{pmatrix}, \tag{6.80}$$

where we follow the conventions in Ref. [56].

Chapter 7

Conclusion

> *"The effort to understand the Universe is one of the very few things which lifts human life a little above the level of farce and gives it some of the grace of tragedy."*
>
> — Steven Weinberg, The First Three Minutes (1982), Epilogue, p. 155

The era of the SM as the most successful model of nature in the history of mankind is known to have an end, but how soon it will come is unclear. Models that claimed to be natural successor the SM were created and promoted long before the latter was even fully confirmed. Yet, there is no warranty that the current generation of experiments will give us an undisputable and unambiguous proof of a change of era. A clear sign of what lies at the dawn of the BSM era seems unlikely. Probably, never before in the history of Physics we have seen more strongly this duality between the certainty of knowing that we need something else and not finding more evidence about what that is. This makes our times particularly perplexing, intriguing, and open to breakthroughs.

The absence of a clear preferred path forward can be seen as the perfect opportunity to reconsider and improve our tools as we keep exploring in all directions. Only this will ensure the continuous exploration and, very importantly, that we can extract all the possible information from of what we find. This reassessment process, in order to maximise the discovery potential of future explorations, is a yarn that runs all throughout this thesis.

Chapters 1 and 2 just laid out the current situation of particle physics in detail and presented in great generality some of the tools we expect to use in the future to uncover BSM Physics. In Chapter 3, we showed how two of those tools, EFTs and FCC-hh, could be used together in the future to look for BSM Physics. More precisely, we studied the Vh production process in the leptonic diphotonic channel, a process that could be studied for the first time at FCC-hh. This showcases the full potential of such proposed experiment. Furthermore, with the limited information that we have now, we optimised the observables to probe BSM Physics as deeply as possible. Additionally, we showed how the precision measurements we propose for FCC-hh could improve the results obtained with more precision-focused experiments like FCC-ee and CEPC, highlighting the complementarity between different kinds of colliders.

Studies like the one in Chapter 3 are relevant not only to strengthen the case for building a particular collider, but also to help in optimising the design parameter of its detectors. Their importance is rooted in our duty to allow our future selves and the upcoming generations of humans to explore nature with the best possible tools.

The importance of having a deep theoretical understanding of the models that we use was

showed in Chapters 4 and 5. There, we revisited the relations between EFTs and anomalies. First, in Chapter 4, we checked that SMEFT at dimension 6 is free of gauge anomalies from triangle diagrams for arbitrary values of its WCs.

Second, in Chapter 5, we revisited the relation between mixed global-gauge anomalies and axion couplings to gauge bosons in an axion EFT. We found that the anomalies do not always determine the axion coupling, despite doing it in the best known cases of photons and gluons. The relations is broken by the presence of heavy fermions that are chiral under the massive gauge boson in consideration. This does not lead to phenomenological consequences for the case of chiral abelian gauge bosons, and indeed the relation can be restored via a smart choice when building the UV model. However, the case of chiral non-abelian gauge bosons leads to the appearance of clear phenomenological consequences in the form of the violation of certain sum rules. Such phenomenon turns out to be an IR indicator of the presence of a chiral extension of the SM. In this way, we connected two topics that have not been on the main spotlight in recent times: axion couplings to non-abelian chiral gauge bosons, like the W and Z, and chiral extensions of the SM.

The sum rules found in Chapter 5 are a prime example of how a better theoretical understanding can sharpen our interpretation of the experimental results, making a measurement more meaningful. As we uncover this additional knowledge we delimit better our ignorance and leave a higher shoulder for others (or us) to stand on in the future.

Finally, Chapter 6 shows an effort to find new paradigms, in this case by revisiting old techniques. The development of the helicity spinors techniques have led to a second youth for the scattering amplitudes approach, which had been left in a secondary role since the 70s. Even though the computation of scattering amplitudes was never abandoned because they are an unavoidable intermediate step between QFT and the experiments, their properties had been seen as just an inheritance from QFT. Now, when the field is ripe enough to make further progress, we have explored how they can be used to parametrise BSM Physics and rediscover phenomena that were thought as hallmarks of QFT and gauge symmetries. Deeper insights about BSM Physics might be extracted from this approach in the near future.

This is a time when we have to reflect on how we are exploring nature, on which questions we are asking and will ask in the future. This thesis has showed just a very few ways of how to do it, yet it still covers short and long-term future. We hope that some of the techniques and results stay relevant in the next few decades. Meanwhile, there are many other directions to chart. We leave the exposition of precise future directions to the conclusions of each chapter due to the variety of topics covered in them and we give here just a brief general outlook.

On one hand, the profound (re)study of our theoretical tools is growing and starting to give more fruits. The positivity constraints and Scattering Amplitudes program are both attracting more and more attention and starting to render results of phenomenological relevance, so their connection to experimental results and to UV models should be a fertile field in the next decade. On the other hand, we can not forget that the transition of the community from a resonance-search mindset towards an EFT and precision measurements one is recent, given the high expectations of finding BSM particles at the LHC. Hence, we must keep thinking about observables, how to interpret measurements in terms of EFTs, and what they are telling us about the UV. This is vital to not miss the opportunities brought by LHC and its high-luminosity runs and extract as much information about nature as we can. What we might find during the exploration escapes the frontiers of our imagination and that is a strong reason to keep doing it.

Bibliography

[1] S. L. Glashow, *Partial Symmetries of Weak Interactions*, *Nucl. Phys.* **22** (1961) 579–588.

[2] S. Weinberg, *A Model of Leptons*, *Phys. Rev. Lett.* **19** (1967) 1264–1266.

[3] A. Salam, *Weak and Electromagnetic Interactions*, *Conf. Proc. C* **680519** (1968) 367–377.

[4] G. 't Hooft and M. J. G. Veltman, *Regularization and Renormalization of Gauge Fields*, *Nucl. Phys. B* **44** (1972) 189–213.

[5] D. J. Gross and F. Wilczek, *Ultraviolet Behavior of Nonabelian Gauge Theories*, *Phys. Rev. Lett.* **30** (1973) 1343–1346.

[6] P. W. Higgs, *Broken Symmetries and the Masses of Gauge Bosons*, *Phys. Rev. Lett.* **13** (1964) 508–509.

[7] P. W. Higgs, *Broken symmetries, massless particles and gauge fields*, *Phys. Lett.* **12** (1964) 132–133.

[8] F. Englert and R. Brout, *Broken Symmetry and the Mass of Gauge Vector Mesons*, *Phys. Rev. Lett.* **13** (1964) 321–323.

[9] G. S. Guralnik, C. R. Hagen, and T. W. B. Kibble, *Global Conservation Laws and Massless Particles*, *Phys. Rev. Lett.* **13** (1964) 585–587.

[10] P. W. Higgs, *Spontaneous Symmetry Breakdown without Massless Bosons*, *Phys. Rev.* **145** (1966) 1156–1163.

[11] T. W. B. Kibble, *Symmetry breaking in nonAbelian gauge theories*, *Phys. Rev.* **155** (1967) 1554–1561.

[12] **Particle Data Group** Collaboration, Particle Data Group, *Review of Particle Physics*, *Progress of Theoretical and Experimental Physics* **2020** (08, 2020) 083C01. 083C01.

[13] **Planck** Collaboration, N. Aghanim et al., *Planck 2018 results. I. Overview and the cosmological legacy of Planck*, *Astron. Astrophys.* **641** (2020) A1, [arXiv:1807.06205].

[14] **CMS** Collaboration, A. M. Sirunyan et al., *Constraints on anomalous Higgs boson couplings to vector bosons and fermions in its production and decay using the four-lepton final state*, arXiv:2104.12152.

[15] **Muon g-2** Collaboration, B. Abi et al., *Measurement of the Positive Muon Anomalous Magnetic Moment to 0.46 ppm*, *Phys. Rev. Lett.* **126** (2021), no. 14 141801, [arXiv:2104.03281].

[16] D. Guadagnoli, *Flavor anomalies on the eve of the Run-2 verdict*, *Mod. Phys. Lett. A* **32** (2017), no. 7 1730006, [arXiv:1703.02804].

[17] **LHCb** Collaboration, R. Aaij et al., *Test of lepton universality in beauty-quark decays*, arXiv:2103.11769.

[18] B. Capdevila, A. Crivellin, S. Descotes-Genon, J. Matias, and J. Virto, *Patterns of New Physics in $b \to s\ell^+\ell^-$ transitions in the light of recent data*, *JHEP* **01** (2018) 093, [arXiv:1704.05340].

[19] A. Pomarol, *Beyond the Standard Model*, in *2010 European School of High Energy Physics*, 2, 2012. arXiv:1202.1391.

[20] A. Wulzer, *Behind the Standard Model*, in *2015 European School of High-Energy Physics*, 1, 2019. arXiv:1901.01017.

[21] C. Csaki, C. Grojean, and J. Terning, *Alternatives to an Elementary Higgs*, *Rev. Mod. Phys.* **88** (2016), no. 4 045001, [arXiv:1512.00468].

[22] G. F. Giudice, *The Dawn of the Post-Naturalness Era*. 2019. arXiv:1710.07663.

[23] G. F. Giudice, M. McCullough, and T. You, *Self-Organised Localisation*, arXiv:2105.08617.

[24] **FCC** Collaboration, A. Abada et al., *FCC Physics Opportunities: Future Circular Collider Conceptual Design Report Volume 1*, *Eur. Phys. J. C* **79** (2019), no. 6 474.

[25] G. F. Giudice and M. McCullough, *A Clockwork Theory*, *JHEP* **02** (2017) 036, [arXiv:1610.07962].

[26] G. F. Giudice, Y. Kats, M. McCullough, R. Torre, and A. Urbano, *Clockwork/linear dilaton: structure and phenomenology*, *JHEP* **06** (2018) 009, [arXiv:1711.08437].

[27] P. W. Graham, D. E. Kaplan, and S. Rajendran, *Cosmological Relaxation of the Electroweak Scale*, *Phys. Rev. Lett.* **115** (2015), no. 22 221801, [arXiv:1504.07551].

[28] L. Tancredi, *Standard Model Review: Precision Calculations for LHC observables.*, in *DESY Virtual Theory Forum 2020*, 2020. Available at https://indico.desy.de/event/25488/contributions/57265/attachments/37024/46282/DESY_Tancredi.pdf. Last accesed on 21.06.2021.

[29] M. Farina, G. Panico, D. Pappadopulo, J. T. Ruderman, R. Torre, and A. Wulzer, *Energy helps accuracy: electroweak precision tests at hadron colliders*, *Phys. Lett. B* **772** (2017) 210–215, [arXiv:1609.08157].

[30] M. Abdughani, J. Ren, L. Wu, J. M. Yang, and J. Zhao, *Supervised deep learning in high energy phenomenology: a mini review*, *Commun. Theor. Phys.* **71** (2019), no. 8 955, [arXiv:1905.06047].

[31] G. Carleo, I. Cirac, K. Cranmer, L. Daudet, M. Schuld, N. Tishby, L. Vogt-Maranto, and L. Zdeborová, *Machine learning and the physical sciences*, *Rev. Mod. Phys.* **91** (2019), no. 4 045002, [arXiv:1903.10563].

[32] D. Guest, K. Cranmer, and D. Whiteson, *Deep Learning and its Application to LHC Physics*, *Ann. Rev. Nucl. Part. Sci.* **68** (2018) 161–181, [arXiv:1806.11484].

[33] G. Kasieczka et al., *The LHC Olympics 2020: A Community Challenge for Anomaly Detection in High Energy Physics*, arXiv:2101.08320.

[34] M. D. Klimek and M. Perelstein, *Neural Network-Based Approach to Phase Space Integration*, *SciPost Phys.* **9** (2020) 053, [arXiv:1810.11509].

[35] F. Bishara and M. Montull, *(Machine) Learning amplitudes for faster event generation*, arXiv:1912.11055.

[36] **HSF Physics Event Generator WG** Collaboration, S. Amoroso et al., *Challenges in Monte Carlo Event Generator Software for High-Luminosity LHC*, *Comput. Softw. Big Sci.* **5** (2021), no. 1 12, [arXiv:2004.13687].

[37] **Sherpa** Collaboration, E. Bothmann et al., *Event Generation with Sherpa 2.2*, *SciPost Phys.* **7** (2019), no. 3 034, [arXiv:1905.09127].

[38] C. W. Bauer, M. Freytsis, and B. Nachman, *Simulating collider physics on quantum computers using effective field theories*, arXiv:2102.05044.

[39] **NuQS** Collaboration, H. Lamm, S. Lawrence, and Y. Yamauchi, *Parton physics on a quantum computer*, *Phys. Rev. Res.* **2** (2020), no. 1 013272, [arXiv:1908.10439].

[40] C. W. Bauer, W. A. de Jong, B. Nachman, and D. Provasoli, *Quantum Algorithm for High Energy Physics Simulations*, *Phys. Rev. Lett.* **126** (2021), no. 6 062001, [arXiv:1904.03196].

[41] A. Y. Wei, P. Naik, A. W. Harrow, and J. Thaler, *Quantum Algorithms for Jet Clustering*, *Phys. Rev. D* **101** (2020), no. 9 094015, [arXiv:1908.08949].

[42] J. Ellis, M. Madigan, K. Mimasu, V. Sanz, and T. You, *Top, Higgs, Diboson and Electroweak Fit to the Standard Model Effective Field Theory*, arXiv:2012.02779.

[43] J. J. Ethier, F. Maltoni, L. Mantani, E. R. Nocera, J. Rojo, E. Slade, E. Vryonidou, and C. Zhang, *Combined SMEFT interpretation of Higgs, diboson, and top quark data from the LHC*, arXiv:2105.00006.

[44] C. W. Murphy, *Dimension-8 operators in the Standard Model Eective Field Theory*, *JHEP* **10** (2020) 174, [arXiv:2005.00059].

[45] H.-L. Li, Z. Ren, J. Shu, M.-L. Xiao, J.-H. Yu, and Y.-H. Zheng, *Complete Set of Dimension-8 Operators in the Standard Model Effective Field Theory*, arXiv:2005.00008.

[46] C. Degrande, G. Durieux, F. Maltoni, K. Mimasu, E. Vryonidou, and C. Zhang, *Automated one-loop computations in the SMEFT*, arXiv:2008.11743.

[47] T. Trott, *Causality, Unitarity and Symmetry in Effective Field Theory*, arXiv:2011.10058.

[48] X. Li, C. Yang, H. Xu, C. Zhang, and S.-Y. Zhou, *Positivity in Multi-Field EFTs*, arXiv:2101.01191.

[49] A. Adams, N. Arkani-Hamed, S. Dubovsky, A. Nicolis, and R. Rattazzi, *Causality, analyticity and an IR obstruction to UV completion*, *JHEP* **10** (2006) 014, [hep-th/0602178].

[50] B. Bellazzini, L. Martucci, and R. Torre, *Symmetries, Sum Rules and Constraints on Effective Field Theories*, *JHEP* **09** (2014) 100, [arXiv:1405.2960].

[51] B. Bellazzini, *Softness and amplitudes' positivity for spinning particles*, *JHEP* **02** (2017) 034, [arXiv:1605.06111].

[52] C. de Rham, S. Melville, A. J. Tolley, and S.-Y. Zhou, *UV complete me: Positivity Bounds for Particles with Spin*, *JHEP* **03** (2018) 011, [arXiv:1706.02712].

[53] C. de Rham, S. Melville, A. J. Tolley, and S.-Y. Zhou, *Positivity Bounds for Massive Spin-1 and Spin-2 Fields*, *JHEP* **03** (2019) 182, [arXiv:1804.10624].

[54] N. Arkani-Hamed, T.-C. Huang, and Y.-t. Huang, *Scattering Amplitudes For All Masses and Spins*, arXiv:1709.04891.

[55] R. Aoude and C. S. Machado, *The Rise of SMEFT On-shell Amplitudes*, *JHEP* **12** (2019) 058, [arXiv:1905.11433].

[56] G. Durieux, T. Kitahara, Y. Shadmi, and Y. Weiss, *The electroweak effective field theory from on-shell amplitudes*, *JHEP* **01** (2020) 119, [arXiv:1909.10551].

[57] **LHCb** Collaboration, T. Hadavizadeh, *Mixing and CP violation in charm decays at LHCb*, 5, 2021. arXiv:2105.08884.

[58] **Belle-II** Collaboration, R. Manfredi, *Measurements in charmless B decays at Belle II*, arXiv:2105.10259.

[59] **NA62** Collaboration, E. Cortina Gil et al., *Search for lepton number and flavour violation in K^+ and π^0 decays*, arXiv:2105.06759.

[60] **KOTO** Collaboration, J. K. Ahn et al., *Study of the $K_L \to \pi^0 \nu\bar{\nu}$ Decay at the J-PARC KOTO Experiment*, *Phys. Rev. Lett.* **126** (2021), no. 12 121801, [arXiv:2012.07571].

[61] **Muon g-2** Collaboration, T. Albahri et al., *Measurement of the anomalous precession frequency of the muon in the Fermilab Muon $g2$ Experiment*, *Phys. Rev. D* **103** (2021), no. 7 072002, [arXiv:2104.03247].

[62] **E34** Collaboration, M. Otani, *Status of the Muon g-2/EDM Experiment at J-PARC (E34)*, *JPS Conf. Proc.* **8** (2015) 025008.

[63] **ACME** Collaboration, V. Andreev et al., *Improved limit on the electric dipole moment of the electron*, *Nature* **562** (2018), no. 7727 355–360.

[64] H. Abramowicz et al., *Conceptual Design Report for the LUXE Experiment*, arXiv:2102.02032.

[65] Y. K. Semertzidis and S. Youn, *Axion Dark Matter: How to detect it?*, arXiv:2104.14831.

[66] **KATRIN** Collaboration, M. Aker et al., *The Design, Construction, and Commissioning of the KATRIN Experiment*, arXiv:2103.04755.

[67] **Hyper-Kamiokande** Collaboration, K. Abe et al., *The Hyper-Kamiokande Experiment - Snowmass LOI*, in *2022 Snowmass Summer Study*, 9, 2020. arXiv:2009.00794.

[68] R. K. Ellis et al., *Physics Briefing Book: Input for the European Strategy for Particle Physics Update 2020*, arXiv:1910.11775.

[69] **HESS** Collaboration, H. Abdalla et al., *Searches for gamma-ray lines and 'pure WIMP' spectra from Dark Matter annihilations in dwarf galaxies with H.E.S.S*, *JCAP* **11** (2018) 037, [arXiv:1810.00995].

[70] **ANTARES** Collaboration, A. Albert et al., *Search for neutrinos from the tidal disruption events AT2019dsg and AT2019fdr with the ANTARES telescope*, arXiv:2103.15526.

[71] **IceCube** Collaboration, T. Yuan, *High-energy particle physics with IceCube*, *J. Phys. Conf. Ser.* **1468** (2020), no. 1 012140, [arXiv:2001.08657].

[72] **CTA** Collaboration, H. Abdalla et al., *Sensitivity of the Cherenkov Telescope Array for probing cosmology and fundamental physics with gamma-ray propagation*, *JCAP* **02** (2021) 048, [arXiv:2010.01349].

[73] **LIGO Scientific, Virgo** Collaboration, B. P. Abbott et al., *Observation of Gravitational Waves from a Binary Black Hole Merger*, *Phys. Rev. Lett.* **116** (2016), no. 6 061102, [arXiv:1602.03837].

[74] **LIGO Scientific, Virgo, Fermi GBM, INTEGRAL, IceCube, AstroSat Cadmium Zinc Telluride Imager Team, IPN, Insight-Hxmt, ANTARES, Swift, AGILE Team, 1M2H Team, Dark Energy Camera GW-EM, DES, DLT40, GRAWITA, Fermi-LAT, ATCA, ASKAP, Las Cumbres Observatory Group, OzGrav, DWF (Deeper Wider Faster Program), AST3, CAASTRO, VINROUGE, MASTER, J-GEM, GROWTH, JAGWAR, CaltechNRAO, TTU-NRAO, NuSTAR, Pan-STARRS, MAXI Team, TZAC Consortium, KU, Nordic Optical Telescope, ePESSTO, GROND, Texas Tech University, SALT Group, TOROS, BOOTES, MWA, CALET, IKI-GW Follow-up, H.E.S.S., LOFAR, LWA, HAWC, Pierre Auger, ALMA, Euro VLBI Team, Pi of Sky, Chandra Team at McGill University, DFN, ATLAS Telescopes, High Time Resolution Universe Survey, RIMAS, RATIR, SKA South Africa/MeerKAT** Collaboration, B. P. Abbott et al., *Multi-messenger Observations of a Binary Neutron Star Merger*, *Astrophys. J. Lett.* **848** (2017), no. 2 L12, [arXiv:1710.05833].

[75] **LIGO Scientific** Collaboration, D. Shoemaker, *Gravitational wave astronomy with LIGO and similar detectors in the next decade*, arXiv:1904.03187.

[76] M. Maggiore et al., *Science Case for the Einstein Telescope*, *JCAP* **03** (2020) 050, [arXiv:1912.02622].

[77] European Space Agency (ESA), "Gravitational Wave mission selected, planet-hunting mission moves forward." ESA Website, June, 2017. Online, available at http://www.esa.int/Science_Exploration/Space_Science/Gravitational_wave_mission_selected_planet-hunting_mission_moves_forward. Last accesed on 28.05.2021.

[78] **LISA** Collaboration, P. Amaro-Seoane et al., *Laser Interferometer Space Antenna*, arXiv:1702.00786.

[79] E. Barausse et al., *Prospects for Fundamental Physics with LISA*, *Gen. Rel. Grav.* **52** (2020), no. 8 81, [arXiv:2001.09793].

[80] C. Caprini et al., *Detecting gravitational waves from cosmological phase transitions with LISA: an update*, *JCAP* **03** (2020) 024, [arXiv:1910.13125].

[81] R. Brito, V. Cardoso, and P. Pani, *Superradiance: New Frontiers in Black Hole Physics*, *Lect. Notes Phys.* **906** (2015) pp.1–237, [arXiv:1501.06570].

[82] R. Brito, S. Ghosh, E. Barausse, E. Berti, V. Cardoso, I. Dvorkin, A. Klein, and P. Pani, *Gravitational wave searches for ultralight bosons with LIGO and LISA*, *Phys. Rev. D* **96** (2017), no. 6 064050, [arXiv:1706.06311].

[83] D. Baumann, H. S. Chia, and R. A. Porto, *Probing Ultralight Bosons with Binary Black Holes*, *Phys. Rev. D* **99** (2019), no. 4 044001, [arXiv:1804.03208].

[84] C. Grojean and G. Servant, *Gravitational Waves from Phase Transitions at the Electroweak Scale and Beyond*, *Phys. Rev. D* **75** (2007) 043507, [hep-ph/0607107].

[85] M. Chala, V. V. Khoze, M. Spannowsky, and P. Waite, *Mapping the shape of the scalar potential with gravitational waves*, *Int. J. Mod. Phys. A* **34** (2019), no. 33 1950223, [arXiv:1905.00911].

[86] H. Al Ali et al., *The Muon Smasher's Guide*, arXiv:2103.14043.

[87] A. Dainese, M. Mangano, A. B. Meyer, A. Nisati, G. Salam, and M. A. Vesterinen, eds., *Report on the Physics at the HL-LHC,and Perspectives for the HE-LHC*, vol. 7/2019 of *CERN Yellow Reports: Monographs*. CERN, Geneva, Switzerland, 2019.

[88] **MATHUSLA** Collaboration, C. Alpigiani et al., *An Update to the Letter of Intent for MATHUSLA: Search for Long-Lived Particles at the HL-LHC*, arXiv:2009.01693.

[89] R. G. Suarez, *Long-Lived Particles at Future Colliders*, in *27th Cracow Epiphany Conference on Future of particle physics* , 2, 2021. arXiv:2102.07597.

[90] **European Strategy Group** Collaboration, *2020 Update of the European Strategy for Particle Physics*. CERN Council, Geneva, 2020.

[91] P. Bambade et al., *The International Linear Collider: A Global Project*, arXiv:1903.01629.

[92] R. Franceschini et al., *The CLIC Potential for New Physics*, arXiv:1812.02093.

[93] CERN, "LHC Long Term Schedule." LHC Commisioning Website, 2021. Online, available at https://lhc-commissioning.web.cern.ch/schedule/LHC-long-term.htm. Last accesed on 28.05.2021.

[94] **FCC** Collaboration, A. Abada et al., *FCC-hh: The Hadron Collider: Future Circular Collider Conceptual Design Report Volume 3*, *Eur. Phys. J. ST* **228** (2019), no. 4 755–1107.

[95] J. Gao, *CEPC Accelerator Status and TDR Progress*, in *HKIAS HEP Conference*, 2021. Available at https://indico.cern.ch/event/971970/contributions/4174479/attachments/2172831/3668586/CEPCStatusandTDRProgress-J.Gao-HKIAS-HEP-V4.pdf. Last accesed on 28.05.2021.

[96] C. Grojean, *Strategies in pursuing HEP once and the future*, in *Phenomenology Virtual Symposium 2020*, 2020. Available at `https://indico.cern.ch/event/858682/contributions/3840431/attachments/2033398/3403834/Grojean.pdf`. Last accesed on 28.05.2021.

[97] **CLICdp, CLIC** Collaboration, T. K. Charles et al., *The Compact Linear Collider (CLIC) - 2018 Summary Report*, `arXiv:1812.06018`.

[98] **FCC** Collaboration, A. Abada et al., *FCC-ee: The Lepton Collider: Future Circular Collider Conceptual Design Report Volume 2*, *Eur. Phys. J. ST* **228** (2019), no. 2 261–623.

[99] **CEPC Study Group** Collaboration, *CEPC Conceptual Design Report: Volume 1 - Accelerator*, `arXiv:1809.00285`.

[100] J. Osborne, A. Tudora, and B. Swatton, "Tunnelling for physics." CERN Courier Vol. 59 Num. 5 Page 27, Sept., 2019.

[101] R. Contino et al., *Physics at a 100 TeV pp collider: Higgs and EW symmetry breaking studies*, *CERN Yellow Rep.* (2017), no. 3 255–440, [`arXiv:1606.09408`].

[102] R. Contino, A. Podo, and F. Revello, *Composite Dark Matter from Strongly-Interacting Chiral Dynamics*, *JHEP* **02** (2021) 091, [`arXiv:2008.10607`].

[103] R. Contino, A. Mitridate, A. Podo, and M. Redi, *Gluequark Dark Matter*, *JHEP* **02** (2019) 187, [`arXiv:1811.06975`].

[104] C. Gross, A. Mitridate, M. Redi, J. Smirnov, and A. Strumia, *Cosmological Abundance of Colored Relics*, *Phys. Rev. D* **99** (2019), no. 1 016024, [`arXiv:1811.08418`].

[105] S. Weinberg, *Phenomenological Lagrangians*, *Physica A* **96** (1979), no. 1-2 327–340.

[106] T. Appelquist and J. Carazzone, *Infrared Singularities and Massive Fields*, *Phys. Rev. D* **11** (1975) 2856.

[107] S. Weinberg and M. Chalmers, "Still seeking solutions." CERN Courier Vol. 61 Num. 2, Mar., 2021.

[108] E. Fermi, *Tentativo di una teoria dell'emissione dei raggi beta*, *Ric. Sci.* **4** (1933) 491–495.

[109] M. McCullough, *Lectures at NExT Summer Workshop 2020 (2021).*, in *X NExT PhD Workshop*, 2020. Online, available at `https://indico.cern.ch/event/830792/sessions/389175/attachments/2218292/3755933/lecturenotes.pdf`. Last accesed on 12.06.2021.

[110] A. V. Manohar, *Introduction to Effective Field Theories*, `arXiv:1804.05863`.

[111] W. Buchmuller and D. Wyler, *Effective Lagrangian Analysis of New Interactions and Flavor Conservation*, *Nucl. Phys. B* **268** (1986) 621–653.

[112] I. Brivio, *SMEFTsim 3.0 — a practical guide*, *JHEP* **04** (2021) 073, [`arXiv:2012.11343`].

[113] G. Giudice, C. Grojean, A. Pomarol, and R. Rattazzi, *The Strongly-Interacting Light Higgs*, *JHEP* **06** (2007) 045, [`hep-ph/0703164`].

[114] G. D'Ambrosio, G. F. Giudice, G. Isidori, and A. Strumia, *Minimal flavor violation: An Effective field theory approach*, *Nucl. Phys. B* **645** (2002) 155–187, [hep-ph/0207036].

[115] S. Weinberg, *Baryon and Lepton Nonconserving Processes*, *Phys. Rev. Lett.* **43** (1979) 1566–1570.

[116] B. Grzadkowski, M. Iskrzynski, M. Misiak, and J. Rosiek, *Dimension-Six Terms in the Standard Model Lagrangian*, *JHEP* **10** (2010) 085, [arXiv:1008.4884].

[117] A. Falkowski and A. Falkowski, *Higgs Basis: Proposal for an EFT basis choice for LHC HXSWG*, .

[118] R. Alonso, E. E. Jenkins, A. V. Manohar, and M. Trott, *Renormalization Group Evolution of the Standard Model Dimension Six Operators III: Gauge Coupling Dependence and Phenomenology*, *JHEP* **04** (2014) 159, [arXiv:1312.2014].

[119] L. Lehman, *Extending the Standard Model Effective Field Theory with the Complete Set of Dimension-7 Operators*, *Phys. Rev. D* **90** (2014), no. 12 125023, [arXiv:1410.4193].

[120] B. Henning, X. Lu, T. Melia, and H. Murayama, *2, 84, 30, 993, 560, 15456, 11962, 261485, ...: Higher dimension operators in the SM EFT*, *JHEP* **08** (2017) 016, [arXiv:1512.03433]. [Erratum: JHEP 09, 019 (2019)].

[121] L. Lehman and A. Martin, *Low-derivative operators of the Standard Model effective field theory via Hilbert series methods*, *JHEP* **02** (2016) 081, [arXiv:1510.00372].

[122] H.-L. Li, Z. Ren, M.-L. Xiao, J.-H. Yu, and Y.-H. Zheng, *Complete Set of Dimension-9 Operators in the Standard Model Effective Field Theory*, arXiv:2007.07899.

[123] Y. Liao and X.-D. Ma, *An explicit construction of the dimension-9 operator basis in the standard model effective field theory*, *JHEP* **11** (2020) 152, [arXiv:2007.08125].

[124] C. Degrande, *A basis of dimension-eight operators for anomalous neutral triple gauge boson interactions*, *JHEP* **02** (2014) 101, [arXiv:1308.6323].

[125] C. Hays, A. Martin, V. Sanz, and J. Setford, *On the impact of dimension-eight SMEFT operators on Higgs measurements*, *JHEP* **02** (2019) 123, [arXiv:1808.00442].

[126] B. Bellazzini and F. Riva, *New phenomenological and theoretical perspective on anomalous ZZ and Zγ processes*, *Phys. Rev. D* **98** (2018), no. 9 095021, [arXiv:1806.09640].

[127] J. Ellis, H.-J. He, and R.-Q. Xiao, *Probing new physics in dimension-8 neutral gauge couplings at e^+e colliders*, *Sci. China Phys. Mech. Astron.* **64** (2021), no. 2 221062, [arXiv:2008.04298].

[128] S. Alioli, R. Boughezal, E. Mereghetti, and F. Petriello, *Novel angular dependence in Drell-Yan lepton production via dimension-8 operators*, *Phys. Lett. B* **809** (2020) 135703, [arXiv:2003.11615].

[129] R. Boughezal, F. Petriello, and D. Wiegand, *Disentangling SMEFT operators with future low-energy PVES experiments*, arXiv:2104.03979.

[130] A. Azatov, R. Contino, C. S. Machado, and F. Riva, *Helicity selection rules and noninterference for BSM amplitudes*, *Phys. Rev. D* **95** (2017), no. 6 065014, [arXiv:1607.05236].

[131] G. Panico, F. Riva, and A. Wulzer, *Diboson Interference Resurrection*, *Phys. Lett. B* **776** (2018) 473–480, [arXiv:1708.07823].

[132] A. Azatov, J. Elias-Miro, Y. Reyimuaji, and E. Venturini, *Novel measurements of anomalous triple gauge couplings for the LHC*, *JHEP* **10** (2017) 027, [arXiv:1707.08060].

[133] S. Willenbrock, *Symmetries of the standard model*, in *Theoretical Advanced Study Institute in Elementary Particle Physics: Physics in $D \geq 4$*, 10, 2004. hep-ph/0410370.

[134] S. R. Coleman, J. Wess, and B. Zumino, *Structure of phenomenological Lagrangians. 1.*, *Phys. Rev.* **177** (1969) 2239–2247.

[135] C. G. Callan, Jr., S. R. Coleman, J. Wess, and B. Zumino, *Structure of phenomenological Lagrangians. 2.*, *Phys. Rev.* **177** (1969) 2247–2250.

[136] R. Alonso, M. B. Gavela, L. Merlo, S. Rigolin, and J. Yepes, *The Effective Chiral Lagrangian for a Light Dynamical "Higgs Particle"*, *Phys. Lett. B* **722** (2013) 330–335, [arXiv:1212.3305]. [Erratum: Phys.Lett.B 726, 926 (2013)].

[137] G. Buchalla, O. Catà, and C. Krause, *Complete Electroweak Chiral Lagrangian with a Light Higgs at NLO*, *Nucl. Phys. B* **880** (2014) 552–573, [arXiv:1307.5017]. [Erratum: Nucl.Phys.B 913, 475–478 (2016)].

[138] I. Brivio, T. Corbett, O. J. P. Éboli, M. B. Gavela, J. Gonzalez-Fraile, M. C. Gonzalez-Garcia, L. Merlo, and S. Rigolin, *Disentangling a dynamical Higgs*, *JHEP* **03** (2014) 024, [arXiv:1311.1823].

[139] I. Brivio, J. Gonzalez-Fraile, M. C. Gonzalez-Garcia, and L. Merlo, *The complete HEFT Lagrangian after the LHC Run I*, *Eur. Phys. J. C* **76** (2016), no. 7 416, [arXiv:1604.06801].

[140] P. Kozów, *The W and Z scattering as a probe of physics beyond the Standard Model: Effective Field Theory approach*. PhD thesis, Warsaw U., 2019. arXiv:1908.07596.

[141] I. Brivio and M. Trott, *The Standard Model as an Effective Field Theory*, *Phys. Rept.* **793** (2019) 1–98, [arXiv:1706.08945].

[142] M. E. Peskin and T. Takeuchi, *Estimation of oblique electroweak corrections*, *Phys. Rev. D* **46** (1992) 381–409.

[143] G. D. Kribs, X. Lu, A. Martin, and T. Tong, *Custodial Symmetry (Violation) in SMEFT*, arXiv:2009.10725.

[144] A. Pich, I. Rosell, J. Santos, and J. J. Sanz-Cillero, *Fingerprints of heavy scales in electroweak effective Lagrangians*, *JHEP* **04** (2017) 012, [arXiv:1609.06659].

[145] B. Gavela, E. Jenkins, A. Manohar, and L. Merlo, *Analysis of General Power Counting Rules in Effective Field Theory*, *Eur. Phys. J. C* **76** (2016), no. 9 485, [arXiv:1601.07551].

[146] T. Cohen, N. Craig, X. Lu, and D. Sutherland, *Is SMEFT Enough?*, *JHEP* **03** (2021) 237, [arXiv:2008.08597].

[147] R. Alonso, E. E. Jenkins, and A. V. Manohar, *A Geometric Formulation of Higgs Effective Field Theory: Measuring the Curvature of Scalar Field Space*, *Phys. Lett. B* **754** (2016) 335–342, [arXiv:1511.00724].

[148] A. Falkowski and R. Rattazzi, *Which EFT*, *JHEP* **10** (2019) 255, [arXiv:1902.05936].

[149] R. E. Kallosh and I. V. Tyutin, *The Equivalence theorem and gauge invariance in renormalizable theories*, *Yad. Fiz.* **17** (1973) 190–209.

[150] J. de Blas, M. Chala, and J. Santiago, *Global Constraints on Lepton-Quark Contact Interactions*, *Phys. Rev. D* **88** (2013) 095011, [arXiv:1307.5068].

[151] S. Alioli, M. Farina, D. Pappadopulo, and J. T. Ruderman, *Catching a New Force by the Tail*, *Phys. Rev. Lett.* **120** (2018), no. 10 101801, [arXiv:1712.02347].

[152] J. Fuentes-Martin, A. Greljo, J. Martin Camalich, and J. D. Ruiz-Alvarez, *Charm physics confronts high-p_T lepton tails*, *JHEP* **11** (2020) 080, [arXiv:2003.12421].

[153] L. Ricci, R. Torre, and A. Wulzer, *On the W&Y interpretation of high-energy Drell-Yan measurements*, *JHEP* **02** (2021) 144, [arXiv:2008.12978].

[154] O. Domenech, A. Pomarol, and J. Serra, *Probing the SM with Dijets at the LHC*, *Phys. Rev. D* **85** (2012) 074030, [arXiv:1201.6510].

[155] S. Alioli, M. Farina, D. Pappadopulo, and J. T. Ruderman, *Precision Probes of QCD at High Energies*, *JHEP* **07** (2017) 097, [arXiv:1706.03068].

[156] M. Farina, C. Mondino, D. Pappadopulo, and J. T. Ruderman, *New Physics from High Energy Tops*, *JHEP* **01** (2019) 231, [arXiv:1811.04084].

[157] A. Biekötter, A. Knochel, M. Krämer, D. Liu, and F. Riva, *Vices and virtues of Higgs effective field theories at large energy*, *Phys. Rev. D* **91** (2015) 055029, [arXiv:1406.7320].

[158] A. Falkowski, M. Gonzalez-Alonso, A. Greljo, and D. Marzocca, *Global constraints on anomalous triple gauge couplings in effective field theory approach*, *Phys. Rev. Lett.* **116** (2016), no. 1 011801, [arXiv:1508.00581].

[159] A. Butter, O. J. P. Éboli, J. Gonzalez-Fraile, M. Gonzalez-Garcia, T. Plehn, and M. Rauch, *The Gauge-Higgs Legacy of the LHC Run I*, *JHEP* **07** (2016) 152, [arXiv:1604.03105].

[160] D. Liu and L.-T. Wang, *Prospects for precision measurement of diboson processes in the semileptonic decay channel in future LHC runs*, *Phys. Rev. D* **99** (2019), no. 5 055001, [arXiv:1804.08688].

[161] B. Henning, D. Lombardo, M. Riembau, and F. Riva, *Measuring Higgs Couplings without Higgs Bosons*, *Phys. Rev. Lett.* **123** (2019), no. 18 181801, [arXiv:1812.09299].

[162] R. Franceschini, G. Panico, A. Pomarol, F. Riva, and A. Wulzer, *Electroweak Precision Tests in High-Energy Diboson Processes*, *JHEP* **02** (2018) 111, [arXiv:1712.01310].

[163] A. Biekoetter, T. Corbett, and T. Plehn, *The Gauge-Higgs Legacy of the LHC Run II*, *SciPost Phys.* **6** (2019), no. 6 064, [arXiv:1812.07587].

[164] S. Banerjee, C. Englert, R. S. Gupta, and M. Spannowsky, *Probing Electroweak Precision Physics via boosted Higgs-strahlung at the LHC*, *Phys. Rev. D* **98** (2018), no. 9 095012, [arXiv:1807.01796].

[165] J. Baglio, S. Dawson, and I. M. Lewis, *An NLO QCD effective field theory analysis of W^+W^- production at the LHC including fermionic operators*, *Phys. Rev. D* **96** (2017), no. 7 073003, [arXiv:1708.03332].

[166] C. Grojean, M. Montull, and M. Riembau, *Diboson at the LHC vs LEP*, *JHEP* **03** (2019) 020, [arXiv:1810.05149].

[167] D. R. Green, P. Meade, and M.-A. Pleier, *Multiboson interactions at the LHC*, *Rev. Mod. Phys.* **89** (2017), no. 3 035008, [arXiv:1610.07572].

[168] J. Baglio, S. Dawson, and I. M. Lewis, *NLO effects in EFT fits to W^+W^- production at the LHC*, *Phys. Rev. D* **99** (2019), no. 3 035029, [arXiv:1812.00214].

[169] A. Azatov, D. Barducci, and E. Venturini, *Precision diboson measurements at hadron colliders*, *JHEP* **04** (2019) 075, [arXiv:1901.04821].

[170] J. Brehmer, S. Dawson, S. Homiller, F. Kling, and T. Plehn, *Benchmarking simplified template cross sections in WH production*, *JHEP* **11** (2019) 034, [arXiv:1908.06980].

[171] S. Banerjee, R. S. Gupta, J. Y. Reiness, and M. Spannowsky, *Resolving the tensor structure of the Higgs coupling to Z-bosons via Higgs-strahlung*, *Phys. Rev. D* **100** (2019), no. 11 115004, [arXiv:1905.02728].

[172] S. Banerjee, R. S. Gupta, J. Y. Reiness, S. Seth, and M. Spannowsky, *Towards the ultimate differential SMEFT analysis*, *JHEP* **09** (2020) 170, [arXiv:1912.07628].

[173] W. H. Chiu, Z. Liu, and L.-T. Wang, *Probing flavor nonuniversal theories through Higgs physics at the LHC and future colliders*, *Phys. Rev. D* **101** (2020), no. 3 035045, [arXiv:1909.04549].

[174] J. Baglio, S. Dawson, and S. Homiller, *QCD corrections in Standard Model EFT fits to WZ and WW production*, *Phys. Rev. D* **100** (2019), no. 11 113010, [arXiv:1909.11576].

[175] R. Boughezal, F. Petriello, and D. Wiegand, *Removing flat directions in standard model EFT fits: How polarized electron-ion collider data can complement the LHC*, *Phys. Rev. D* **101** (2020), no. 11 116002, [arXiv:2004.00748].

[176] F. Bishara, P. Englert, C. Grojean, M. Montull, G. Panico, and A. N. Rossia, *A New Precision Process at FCC-hh: the diphoton leptonic Wh channel*, *JHEP* **07** (2020) 075, [arXiv:2004.06122].

[177] S. Chen, A. Glioti, G. Panico, and A. Wulzer, *Parametrized classifiers for optimal EFT sensitivity*, arXiv:2007.10356.

[178] J. Baglio, S. Dawson, S. Homiller, S. D. Lane, and I. M. Lewis, *Validity of standard model EFT studies of VH and VV production at NLO*, *Phys. Rev. D* **101** (2020), no. 11 115004, [arXiv:2003.07862].

[179] J. J. Ethier, R. Gomez-Ambrosio, G. Magni, and J. Rojo, *SMEFT analysis of vector boson scattering and diboson data from the LHC Run II*, arXiv:2101.03180.

[180] F. Bishara, S. De Curtis, L. Delle Rose, P. Englert, C. Grojean, M. Montull, G. Panico, and A. N. Rossia, *Precision from the diphoton Zh channel at FCC-hh*, *JHEP* **04** (2021) 154, [arXiv:2011.13941].

[181] J. M. Butterworth, I. Ochoa, and T. Scanlon, *Boosted Higgs → $b\bar{b}$ in vector-boson associated production at 14 TeV*, *Eur. Phys. J. C* **75** (2015), no. 8 366, [arXiv:1506.04973].

[182] D. Liu and L.-T. Wang, *Probing new physics effects in the precision measurement of the di-boson at the LHC*, *Int. J. Mod. Phys. A* **34** (2019), no. 13n14 1940018.

[183] J. M. Butterworth, A. R. Davison, M. Rubin, and G. P. Salam, *Jet substructure as a new Higgs search channel at the LHC*, *Phys. Rev. Lett.* **100** (2008) 242001, [arXiv:0802.2470].

[184] J. de Blas, J. Criado, M. Perez-Victoria, and J. Santiago, *Effective description of general extensions of the Standard Model: the complete tree-level dictionary*, *JHEP* **03** (2018) 109, [arXiv:1711.10391].

[185] J. de Blas et al., *Higgs Boson Studies at Future Particle Colliders*, *JHEP* **01** (2020) 139, [arXiv:1905.03764].

[186] S. Dawson and P. P. Giardino, *Electroweak and QCD corrections to Z and W pole observables in the standard model EFT*, *Phys. Rev. D* **101** (2020), no. 1 013001, [arXiv:1909.02000].

[187] R. Kleiss and W. J. Stirling, *Spinor Techniques for Calculating p anti-p —> W+- / Z0 + Jets*, *Nucl. Phys. B* **262** (1985) 235–262.

[188] G. Panico, L. Vecchi, and A. Wulzer, *Resonant Diphoton Phenomenology Simplified*, *JHEP* **06** (2016) 184, [arXiv:1603.04248].

[189] E. Vryonidou and C. Zhang, *Dimension-six electroweak top-loop effects in Higgs production and decay*, *JHEP* **08** (2018) 036, [arXiv:1804.09766].

[190] C. Englert, M. McCullough, and M. Spannowsky, *Gluon-initiated associated production boosts Higgs physics*, *Phys. Rev. D* **89** (2014), no. 1 013013, [arXiv:1310.4828].

[191] J. Alwall, R. Frederix, S. Frixione, V. Hirschi, F. Maltoni, O. Mattelaer, H. S. Shao, T. Stelzer, P. Torrielli, and M. Zaro, *The automated computation of tree-level and next-to-leading order differential cross sections, and their matching to parton shower simulations*, *JHEP* **07** (2014) 079, [arXiv:1405.0301].

[192] **NNPDF** Collaboration, R. D. Ball, V. Bertone, S. Carrazza, L. Del Debbio, S. Forte, A. Guffanti, N. P. Hartland, and J. Rojo, *Parton distributions with QED corrections*, *Nucl. Phys. B* **877** (2013) 290–320, [arXiv:1308.0598].

[193] T. Sjöstrand, S. Ask, J. R. Christiansen, R. Corke, N. Desai, P. Ilten, S. Mrenna, S. Prestel, C. O. Rasmussen, and P. Z. Skands, *An introduction to PYTHIA 8.2*, *Comput. Phys. Commun.* **191** (2015) 159–177, [arXiv:1410.3012].

[194] **DELPHES 3** Collaboration, J. de Favereau, C. Delaere, P. Demin, A. Giammanco, V. Lemaître, A. Mertens, and M. Selvaggi, *DELPHES 3, A modular framework for fast simulation of a generic collider experiment*, *JHEP* **02** (2014) 057, [arXiv:1307.6346].

[195] M. Selvaggi, *DELPHES 3: A modular framework for fast-simulation of generic collider experiments*, *J. Phys. Conf. Ser.* **523** (2014) 012033.

[196] A. Mertens, *New features in Delphes 3*, *J. Phys. Conf. Ser.* **608** (2015), no. 1 012045.

[197] M. Cacciari, G. P. Salam, and G. Soyez, *FastJet User Manual*, *Eur. Phys. J. C* **72** (2012) 1896, [arXiv:1111.6097].

[198] M. Cacciari and G. P. Salam, *Dispelling the N^3 myth for the k_t jet-finder*, *Phys. Lett. B* **641** (2006) 57–61, [hep-ph/0512210].

[199] M. Cacciari, G. P. Salam, and G. Soyez, *The anti-k_t jet clustering algorithm*, *JHEP* **04** (2008) 063, [arXiv:0802.1189].

[200] C. Degrande, C. Duhr, B. Fuks, D. Grellscheid, O. Mattelaer, and T. Reiter, *UFO - The Universal FeynRules Output*, *Comput. Phys. Commun.* **183** (2012) 1201–1214, [arXiv:1108.2040].

[201] G. Ferrera, M. Grazzini, and F. Tramontano, *Associated WH production at hadron colliders: a fully exclusive QCD calculation at NNLO*, *Phys. Rev. Lett.* **107** (2011) 152003, [arXiv:1107.1164].

[202] G. Ferrera, M. Grazzini, and F. Tramontano, *Higher-order QCD effects for associated WH production and decay at the LHC*, *JHEP* **04** (2014) 039, [arXiv:1312.1669].

[203] W. Astill, W. Bizon, E. Re, and G. Zanderighi, *NNLOPS accurate associated HW production*, *JHEP* **06** (2016) 154, [arXiv:1603.01620].

[204] J. M. Campbell, R. K. Ellis, and C. Williams, *Associated production of a Higgs boson at NNLO*, *JHEP* **06** (2016) 179, [arXiv:1601.00658].

[205] G. Ferrera, G. Somogyi, and F. Tramontano, *Associated production of a Higgs boson decaying into bottom quarks at the LHC in full NNLO QCD*, *Phys. Lett. B* **780** (2018) 346–351, [arXiv:1705.10304].

[206] M. L. Ciccolini, S. Dittmaier, and M. Kramer, *Electroweak radiative corrections to associated WH and ZH production at hadron colliders*, *Phys. Rev. D* **68** (2003) 073003, [hep-ph/0306234].

[207] A. Denner, S. Dittmaier, S. Kallweit, and A. Muck, *Electroweak corrections to Higgs-strahlung off W/Z bosons at the Tevatron and the LHC with HAWK*, *JHEP* **03** (2012) 075, [arXiv:1112.5142].

[208] F. Granata, J. M. Lindert, C. Oleari, and S. Pozzorini, *NLO QCD+EW predictions for HV and HV +jet production including parton-shower effects*, *JHEP* **09** (2017) 012, [arXiv:1706.03522].

[209] R. Frederix, S. Frixione, V. Hirschi, D. Pagani, H.-S. Shao, and M. Zaro, *The automation of next-to-leading order electroweak calculations*, *JHEP* **07** (2018) 185, [arXiv:1804.10017].

[210] **LEP, ALEPH, DELPHI, L3, OPAL, LEP Electroweak Working Group, SLD Electroweak Group, SLD Heavy Flavor Group** Collaboration, The SLD Electroweak Group, *A Combination of preliminary electroweak measurements and constraints on the standard model*, hep-ex/0312023.

[211] A. Falkowski, M. Gonzalez-Alonso, A. Greljo, D. Marzocca, and M. Son, *Anomalous Triple Gauge Couplings in the Effective Field Theory Approach at the LHC*, *JHEP* **02** (2017) 115, [arXiv:1609.06312].

[212] J. De Blas, G. Durieux, C. Grojean, J. Gu, and A. Paul, *On the future of Higgs, electroweak and diboson measurements at lepton colliders*, *JHEP* **12** (2019) 117, [arXiv:1907.04311].

[213] J. Ellis, C. W. Murphy, V. Sanz, and T. You, *Updated Global SMEFT Fit to Higgs, Diboson and Electroweak Data*, *JHEP* **06** (2018) 146, [arXiv:1803.03252].

[214] R. S. Gupta, A. Pomarol, and F. Riva, *BSM Primary Effects*, *Phys. Rev. D* **91** (2015), no. 3 035001, [arXiv:1405.0181].

[215] **LHC Higgs Cross Section Working Group** Collaboration, D. de Florian et al., *Handbook of LHC Higgs Cross Sections: 4. Deciphering the Nature of the Higgs Sector*, arXiv:1610.07922.

[216] J. D. Wells and Z. Zhang, *Effective theories of universal theories*, *JHEP* **01** (2016) 123, [arXiv:1510.08462].

[217] I. Maksymyk, C. P. Burgess, and D. London, *Beyond S, T and U*, *Phys. Rev. D* **50** (1994) 529–535, [hep-ph/9306267].

[218] R. Barbieri, A. Pomarol, R. Rattazzi, and A. Strumia, *Electroweak symmetry breaking after LEP-1 and LEP-2*, *Nucl. Phys. B* **703** (2004) 127–146, [hep-ph/0405040].

[219] R. Contino, D. Marzocca, D. Pappadopulo, and R. Rattazzi, *On the effect of resonances in composite Higgs phenomenology*, *JHEP* **10** (2011) 081, [arXiv:1109.1570].

[220] D. Pappadopulo, A. Thamm, R. Torre, and A. Wulzer, *Heavy Vector Triplets: Bridging Theory and Data*, *JHEP* **09** (2014) 060, [arXiv:1402.4431].

[221] A. Thamm, R. Torre, and A. Wulzer, *Future tests of Higgs compositeness: direct vs indirect*, *JHEP* **07** (2015) 100, [arXiv:1502.01701].

[222] A. Efrati, A. Falkowski, and Y. Soreq, *Electroweak constraints on flavorful effective theories*, *JHEP* **07** (2015) 018, [arXiv:1503.07872].

[223] G. Panico, A. Pomarol, and M. Riembau, *EFT approach to the electron Electric Dipole Moment at the two-loop level*, *JHEP* **04** (2019) 090, [arXiv:1810.09413].

[224] F. U. Bernlochner, C. Englert, C. Hays, K. Lohwasser, H. Mildner, A. Pilkington, D. D. Price, and M. Spannowsky, *Angles on CP-violation in Higgs boson interactions*, *Phys. Lett. B* **790** (2019) 372–379, [arXiv:1808.06577].

[225] A. Biekötter, R. Gomez-Ambrosio, P. Gregg, F. Krauss, and M. Schönherr, *Constraining SMEFT operators with associated $h\gamma$ production in weak boson fusion*, *Phys. Lett. B* **814** (2021) 136079, [arXiv:2003.06379].

[226] F. Bishara, R. Contino, and J. Rojo, *Higgs pair production in vector-boson fusion at the LHC and beyond*, *Eur. Phys. J. C* **77** (2017), no. 7 481, [arXiv:1611.03860].

[227] M. Cacciari, F. A. Dreyer, A. Karlberg, G. P. Salam, and G. Zanderighi, *Fully Differential Vector-Boson-Fusion Higgs Production at Next-to-Next-to-Leading Order*, *Phys. Rev. Lett.* **115** (2015), no. 8 082002, [arXiv:1506.02660]. [Erratum: Phys.Rev.Lett. 120, 139901 (2018)].

[228] J. J. Sakurai and J. Napolitano, *Modern Quantum Mechanics*. Quantum physics, quantum information and quantum computation. Cambridge University Press, 10, 2020.

[229] A. Bilal, *Lectures on Anomalies*, arXiv:0802.0634.

[230] S. Pokorski and K. Sakurai, *Goldstone boson decays and chiral anomalies*, 5, 2021. arXiv:2105.04877.

[231] S. Weinberg, *The quantum theory of fields. Vol. 2: Modern applications*. Cambridge University Press, 8, 2013.

[232] M. E. Peskin and D. V. Schroeder, *An Introduction to quantum field theory*. Addison-Wesley, Reading, USA, 1995.

[233] J. Preskill, *Gauge anomalies in an effective field theory*, *Annals Phys.* **210** (1991) 323–379.

[234] S. Pokorski, *GAUGE FIELD THEORIES*. Cambridge University Press, 2005.

[235] A. Zee, *Quantum field theory in a nutshell*. 2003.

[236] D. Kabat, *Anomalies and Bose symmetry*, arXiv:1911.06529.

[237] O. Cata, W. Kilian, and N. Kreher, *Gauge anomalies in the Standard-Model Effective Field Theory*, arXiv:2011.09976.

[238] G. 't Hooft, C. Itzykson, A. Jaffe, H. Lehmann, P. K. Mitter, I. M. Singer, and R. Stora, eds., *Recent Developments in Gauge Theories. Proceedings, Nato Advanced Study Institute, Cargese, France, August 26 - September 8, 1979*, vol. 59, 1980.

[239] E. Dudas, Y. Mambrini, S. Pokorski, and A. Romagnoni, *(In)visible Z-prime and dark matter*, *JHEP* **08** (2009) 014, [arXiv:0904.1745].

[240] J. Wess and B. Zumino, *Consequences of anomalous Ward identities*, *Phys. Lett.* **37B** (1971) 95–97.

[241] P. Anastasopoulos, M. Bianchi, E. Dudas, and E. Kiritsis, *Anomalies, anomalous U(1)'s and generalized Chern-Simons terms*, *JHEP* **11** (2006) 057, [hep-th/0605225].

[242] Q. Bonnefoy, E. Dudas, and S. Pokorski, *Axions in a highly protected gauge symmetry model*, *Eur. Phys. J. C* **79** (2019), no. 1 31, [arXiv:1804.01112].

[243] S. L. Adler, *Axial vector vertex in spinor electrodynamics*, *Phys. Rev.* **177** (1969) 2426–2438.

[244] J. Bell and R. Jackiw, *A PCAC puzzle: $\pi^0 \to \gamma\gamma$ in the σ model*, *Nuovo Cim. A* **60** (1969) 47–61.

[245] E. Witten, *Global Aspects of Current Algebra*, *Nucl. Phys.* **B223** (1983) 422–432.

[246] D. J. Gross and R. Jackiw, *Effect of anomalies on quasirenormalizable theories*, *Phys. Rev. D* **6** (1972) 477–493.

[247] C. Bouchiat, J. Iliopoulos, and P. Meyer, *An Anomaly Free Version of Weinberg's Model*, *Phys. Lett. B* **38** (1972) 519–523.

[248] L. E. Ibanez, *Grand Unification, Supersymmetry, Superstrings: An Introduction to Physics Beyond the Standard Model*, *NATO Sci. Ser. B* **204** (1990) 59–115.

[249] Q. Bonnefoy, L. Di Luzio, C. Grojean, A. Paul, and A. N. Rossia, *The anomalous case of axion EFTs and massive chiral gauge fields*, *JHEP* **07** (2021) 189, [arXiv:2011.10025].

[250] F. Feruglio, *A Note on Gauge Anomaly Cancellation in Effective Field Theories*, *JHEP* **03** (2021) 128, [arXiv:2012.13989].

[251] I. G. Irastorza and J. Redondo, *New experimental approaches in the search for axion-like particles*, *Prog. Part. Nucl. Phys.* **102** (2018) 89–159, [arXiv:1801.08127].

[252] L. Di Luzio, M. Giannotti, E. Nardi, and L. Visinelli, *The landscape of QCD axion models*, *Phys. Rept.* **870** (2020) 1–117, [arXiv:2003.01100].

[253] R. D. Peccei and H. R. Quinn, *CP Conservation in the Presence of Instantons*, *Phys. Rev. Lett.* **38** (1977) 1440–1443.

[254] R. Peccei and H. R. Quinn, *Constraints Imposed by CP Conservation in the Presence of Instantons*, *Phys. Rev. D* **16** (1977) 1791–1797.

[255] S. Weinberg, *A New Light Boson?*, *Phys. Rev. Lett.* **40** (1978) 223–226.

[256] F. Wilczek, *Problem of Strong p and t Invariance in the Presence of Instantons*, *Phys. Rev. Lett.* **40** (1978) 279–282.

[257] A. Hebecker, S. Leonhardt, J. Moritz, and A. Westphal, *Thraxions: Ultralight Throat Axions*, *JHEP* **04** (2019) 158, [arXiv:1812.03999].

[258] A. Belyaev, G. Cacciapaglia, H. Cai, G. Ferretti, T. Flacke, A. Parolini, and H. Serodio, *Di-boson signatures as Standard Candles for Partial Compositeness*, *JHEP* **01** (2017) 094, [arXiv:1610.06591]. [Erratum: JHEP 12, 088 (2017)].

[259] G. Cacciapaglia, G. Ferretti, T. Flacke, and H. Serodio, *Revealing timid pseudo-scalars with taus at the LHC*, *Eur. Phys. J. C* **78** (2018), no. 9 724, [arXiv:1710.11142].

[260] G. Cacciapaglia, G. Ferretti, T. Flacke, and H. Serôdio, *Light scalars in composite Higgs models*, *Front. in Phys.* **7** (2019) 22, [arXiv:1902.06890].

[261] H. Georgi, D. B. Kaplan, and L. Randall, *Manifesting the Invisible Axion at Low-energies*, *Phys. Lett. B* **169** (1986) 73–78.

[262] J. Steinberger, *On the Use of subtraction fields and the lifetimes of some types of meson decay*, *Phys. Rev.* **76** (1949) 1180–1186.

[263] J. Quevillon and C. Smith, *Axions are blind to anomalies*, *Eur. Phys. J. C* **C79** (2019), no. 10 822, [arXiv:1903.12559].

[264] I. Brivio, M. B. Gavela, L. Merlo, K. Mimasu, J. M. No, R. del Rey, and V. Sanz, *ALPs Effective Field Theory and Collider Signatures*, *Eur. Phys. J. C* **77** (2017), no. 8 572, [arXiv:1701.05379].

[265] N. Bizot and M. Frigerio, *Fermionic extensions of the Standard Model in light of the Higgs couplings*, *JHEP* **01** (2016) 036, [arXiv:1508.01645].

[266] G. G. Raffelt, *Astrophysical axion bounds*, *Lect. Notes Phys.* **741** (2008) 51–71, [hep-ph/0611350].

[267] J. Quevillon and C. Smith, *Baryon and lepton number intricacies in axion models*, *Phys. Rev. D* **102** (6, 2020) 075031, [arXiv:2006.06778].

[268] F. Feruglio, *The Chiral approach to the electroweak interactions*, *Int. J. Mod. Phys. A* **8** (1993) 4937–4972, [hep-ph/9301281].

[269] M. Bauer, M. Neubert, and A. Thamm, *Collider Probes of Axion-Like Particles*, *JHEP* **12** (2017) 044, [arXiv:1708.00443].

[270] S. Rajpoot and M. A. Samuel, *Evidence for the Fourth Generation?*, *Mod. Phys. Lett. A* **3** (1988) 1625–1627.

[271] S. F. King, *A Minimal four family model*, *Phys. Lett. B* **281** (1992) 295–299.

[272] O. Eberhardt, G. Herbert, H. Lacker, A. Lenz, A. Menzel, U. Nierste, and M. Wiebusch, *Impact of a Higgs boson at a mass of 126 GeV on the standard model with three and four fermion generations*, *Phys. Rev. Lett.* **109** (2012) 241802, [arXiv:1209.1101].

[273] O. Matsedonskyi, G. Panico, and A. Wulzer, *On the Interpretation of Top Partners Searches*, *JHEP* **12** (2014) 097, [arXiv:1409.0100].

[274] A. De Simone, O. Matsedonskyi, R. Rattazzi, and A. Wulzer, *A First Top Partner Hunter's Guide*, *JHEP* **04** (2013) 004, [arXiv:1211.5663].

[275] R. Slansky, *Group Theory for Unified Model Building*, *Phys. Rept.* **79** (1981) 1–128.

[276] E. Witten, *An SU(2) Anomaly*, *Phys. Lett. B* **117** (1982) 324–328.

[277] T. Cohen, X. Lu, and Z. Zhang, *Functional Prescription for EFT Matching*, *JHEP* **02** (2021) 228, [arXiv:2011.02484].

[278] M. Dine, W. Fischler, and M. Srednicki, *A Simple Solution to the Strong CP Problem with a Harmless Axion*, *Phys. Lett. B* **104** (1981) 199–202.

[279] A. Zhitnitsky, *On Possible Suppression of the Axion Hadron Interactions. (In Russian)*, *Sov. J. Nucl. Phys.* **31** (1980) 260.

[280] G. C. Branco, P. M. Ferreira, L. Lavoura, M. N. Rebelo, M. Sher, and J. P. Silva, *Theory and phenomenology of two-Higgs-doublet models*, *Phys. Rept.* **516** (2012) 1–102, [arXiv:1106.0034].

[281] R. Franceschini, G. F. Giudice, J. F. Kamenik, M. McCullough, F. Riva, A. Strumia, and R. Torre, *Digamma, what next?*, *JHEP* **07** (2016) 150, [arXiv:1604.06446].

[282] M. Bauer, M. Heiles, M. Neubert, and A. Thamm, *Axion-Like Particles at Future Colliders*, *Eur. Phys. J.* **C79** (2019), no. 1 74, [arXiv:1808.10323].

[283] Gfitter, "Constraints on the oblique parameters and related theories." http://project-gfitter.web.cern.ch/project-gfitter/Oblique_Parameters/.

[284] A. Djouadi, *The Anatomy of electro-weak symmetry breaking. I: The Higgs boson in the standard model*, *Phys. Rept.* **457** (2008) 1–216, [hep-ph/0503172].

[285] **ATLAS** Collaboration, G. Aad et al., *Combined measurements of Higgs boson production and decay using up to* 80 fb^{-1} *of proton-proton collision data at* $\sqrt{s}$ = *13 TeV collected with the ATLAS experiment*, *Phys. Rev. D* **101** (2020), no. 1 012002, [arXiv:1909.02845].

[286] M. Cepeda et al., *Report from Working Group 2: Higgs Physics at the HL-LHC and HE-LHC*, *CERN Yellow Rep. Monogr.* **7** (2019) 221–584, [arXiv:1902.00134].

[287] I. F. Ginzburg, M. Krawczyk, and P. Osland, *Potential of photon collider in resolving SM like scenarios*, *Nucl. Instrum. Meth. A* **472** (2001) 149–154, [hep-ph/0101229].

[288] J. F. Gunion and H. E. Haber, *The CP conserving two Higgs doublet model: The Approach to the decoupling limit*, *Phys. Rev. D* **67** (2003) 075019, [hep-ph/0207010].

[289] P. M. Ferreira, J. F. Gunion, H. E. Haber, and R. Santos, *Probing wrong-sign Yukawa couplings at the LHC and a future linear collider*, *Phys. Rev. D* **89** (2014), no. 11 115003, [arXiv:1403.4736].

[290] **ATLAS** Collaboration, *A combination of measurements of Higgs boson production and decay using up to* 139 fb^{-1} *of proton–proton collision data at* $\sqrt{s}$ = *13 TeV collected with the ATLAS experiment*, .

[291] T. Yamagata, Y. Takamori, and H. Utsunomiya, *Search for anomalously heavy hydrogen in deep sea water at 4000-m*, *Phys. Rev. D* **47** (1993) 1231–1234.

[292] L. Di Luzio, R. Gröber, J. F. Kamenik, and M. Nardecchia, *Accidental matter at the LHC*, *JHEP* **07** (2015) 074, [arXiv:1504.00359].

[293] C. F. Berger, L. Covi, S. Kraml, and F. Palorini, *The Number density of a charged relic*, *JCAP* **10** (2008) 005, [arXiv:0807.0211].

[294] S. Burdin, M. Fairbairn, P. Mermod, D. Milstead, J. Pinfold, T. Sloan, and W. Taylor, *Non-collider searches for stable massive particles*, *Phys. Rept.* **582** (2015) 1–52, [arXiv:1410.1374].

[295] E. Del Nobile, R. Franceschini, D. Pappadopulo, and A. Strumia, *Minimal Matter at the Large Hadron Collider*, *Nucl. Phys. B* **826** (2010) 217–234, [arXiv:0908.1567].

[296] A. D. Martin, W. J. Stirling, R. S. Thorne, and G. Watt, *Parton distributions for the LHC*, *Eur. Phys. J. C* **63** (2009) 189–285, [arXiv:0901.0002].

[297] **CMS** Collaboration, V. Khachatryan et al., *Search for long-lived charged particles in proton-proton collisions at* $\sqrt{s}$ = *13 TeV*, *Phys. Rev. D* **94** (2016), no. 11 112004, [arXiv:1609.08382].

[298] T. Ma, B. Zhang, and G. Cacciapaglia, *Doubly Charged Lepton from an Exotic Doublet at the LHC*, *Phys. Rev. D* **89** (2014), no. 9 093022, [arXiv:1404.2375].

[299] C. Vafa and E. Witten, *Restrictions on Symmetry Breaking in Vector-Like Gauge Theories*, *Nucl. Phys. B* **234** (1984) 173–188.

[300] L. Michaels and F. Yu, *Probing new $U(1)$ gauge symmetries via exotic $Z \to Z'\gamma$ decays*, *JHEP* **03** (2021) 120, [arXiv:2010.00021].

[301] C. G. Callan, Jr. and J. A. Harvey, *Anomalies and Fermion Zero Modes on Strings and Domain Walls*, *Nucl. Phys. B* **250** (1985) 427–436.

[302] F. Feruglio, A. Masiero, and L. Maiani, *Low-energy effects of heavy chiral fermions*, *Nucl. Phys. B* **387** (1992) 523–561.

[303] A. Masiero, *On effective Lagrangians with heavy chiral fermions*, *Nucl. Phys. Proc. Suppl.* **29BC** (1992) 102–113.

[304] K. Fujikawa, *Path Integral for Gauge Theories with Fermions*, *Phys. Rev. D* **D21** (1980) 2848. [Erratum: Phys. Rev.D22,1499(1980)].

[305] H. Elvang and Y.-t. Huang, *Scattering Amplitudes*, arXiv:1308.1697.

[306] D. Maitre and P. Mastrolia, *S@M, a Mathematica Implementation of the Spinor-Helicity Formalism*, *Comput. Phys. Commun.* **179** (2008) 501–574, [arXiv:0710.5559].

[307] J. Kuczmarski, *SpinorsExtras - Mathematica implementation of massive spinor-helicity formalism*, 6, 2014. arXiv:1406.5612.

[308] G. Cullen, M. Koch-Janusz, and T. Reiter, *Spinney: A Form Library for Helicity Spinors*, *Comput. Phys. Commun.* **182** (2011) 2368–2387, [arXiv:1008.0803].

[309] J. Elias Miró, J. Ingoldby, and M. Riembau, *EFT anomalous dimensions from the S-matrix*, *JHEP* **09** (2020) 163, [arXiv:2005.06983].

[310] P. Baratella, C. Fernandez, and A. Pomarol, *Renormalization of Higher-Dimensional Operators from On-shell Amplitudes*, *Nucl. Phys. B* **959** (2020) 115155, [arXiv:2005.07129].

[311] P. Baratella, C. Fernandez, B. von Harling, and A. Pomarol, *Anomalous Dimensions of Effective Theories from Partial Waves*, *JHEP* **03** (2021) 287, [arXiv:2010.13809].

[312] Z. Bern, J. Parra-Martinez, and E. Sawyer, *Nonrenormalization and Operator Mixing via On-Shell Methods*, *Phys. Rev. Lett.* **124** (2020), no. 5 051601, [arXiv:1910.05831].

[313] Z. Bern, J. Parra-Martinez, and E. Sawyer, *Structure of two-loop SMEFT anomalous dimensions via on-shell methods*, *JHEP* **10** (2020) 211, [arXiv:2005.12917].

[314] M. Jiang, T. Ma, and J. Shu, *Renormalization Group Evolution from On-shell SMEFT*, *JHEP* **01** (2021) 101, [arXiv:2005.10261].

[315] H. Elvang, *Bootstrap and Amplitudes: A Hike in the Landscape of Quantum Field Theory*, arXiv:2007.08436.

[316] T. Cohen, H. Elvang, and M. Kiermaier, *On-shell constructibility of tree amplitudes in general field theories*, *JHEP* **04** (2011) 053, [arXiv:1010.0257].

[317] R. Britto, F. Cachazo, and B. Feng, *New recursion relations for tree amplitudes of gluons*, *Nucl. Phys. B* **715** (2005) 499–522, [hep-th/0412308].

[318] R. Britto, F. Cachazo, B. Feng, and E. Witten, *Direct proof of tree-level recursion relation in Yang-Mills theory*, *Phys. Rev. Lett.* **94** (2005) 181602, [hep-th/0501052].

[319] Q. Bonnefoy, E. Gendy, and C. Grojean, *Positivity bounds on Minimal Flavor Violation*, *JHEP* **04** (2021) 115, [arXiv:2011.12855].

[320] J. M. Cornwall, D. N. Levin, and G. Tiktopoulos, *Derivation of Gauge Invariance from High-Energy Unitarity Bounds on the s Matrix*, *Phys. Rev. D* **10** (1974) 1145. [Erratum: Phys.Rev.D 11, 972 (1975)].

[321] C. E. Vayonakis, *Born Helicity Amplitudes and Cross-Sections in Nonabelian Gauge Theories*, *Lett. Nuovo Cim.* **17** (1976) 383.

[322] B. W. Lee, C. Quigg, and H. B. Thacker, *Weak Interactions at Very High-Energies: The Role of the Higgs Boson Mass*, *Phys. Rev. D* **16** (1977) 1519.

[323] M. S. Chanowitz and M. K. Gaillard, *The TeV Physics of Strongly Interacting W's and Z's*, *Nucl. Phys. B* **261** (1985) 379–431.

[324] N. Christensen and B. Field, *Constructive standard model*, *Phys. Rev. D* **98** (2018), no. 1 016014, [arXiv:1802.00448].

[325] Y. Shadmi and Y. Weiss, *Effective Field Theory Amplitudes the On-Shell Way: Scalar and Vector Couplings to Gluons*, *JHEP* **02** (2019) 165, [arXiv:1809.09644].

[326] G. F. S. Alves, E. Bertuzzo, and G. M. Salla, *An on-shell perspective on neutrino oscillations and non-standard interactions*, arXiv:2103.16362.

[327] A. Falkowski, G. Isabella, and C. S. Machado, *On-shell effective theory for higher-spin dark matter*, *SciPost Phys.* **10** (2021) 101, [arXiv:2011.05339].

[328] T. Ma, J. Shu, and M.-L. Xiao, *Standard Model Effective Field Theory from On-shell Amplitudes*, arXiv:1902.06752.

[329] G. Durieux and C. S. Machado, *Enumerating higher-dimensional operators with on-shell amplitudes*, *Phys. Rev. D* **101** (2020), no. 9 095021, [arXiv:1912.08827].

[330] G. Durieux, T. Kitahara, C. S. Machado, Y. Shadmi, and Y. Weiss, *Constructing massive on-shell contact terms*, *JHEP* **12** (2020) 175, [arXiv:2008.09652].

[331] Z.-Y. Dong, T. Ma, and J. Shu, *Constructing on-shell operator basis for all masses and spins*, arXiv:2103.15837.

[332] R. Contino, C. Grojean, M. Moretti, F. Piccinini, and R. Rattazzi, *Strong Double Higgs Production at the LHC*, *JHEP* **05** (2010) 089, [arXiv:1002.1011].

[333] M. E. Peskin, *Simplifying Multi-Jet QCD Computation*, in *13th Mexican School of Particles and Fields*, 1, 2011. arXiv:1101.2414.